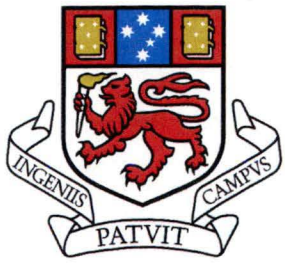

UNIVERSITY
OF TASMANIA

Synthetic and Theoretical Studies of Lanthanide Imide and Alkene Complexes

Damien Stringer, B.Sc.(Hons)

A thesis submitted in fulfilment of the requirements for the degree of

Doctor of Philosophy

School of Chemistry,
University of Tasmania
July 2009

This thesis contains no material which has been accepted for the award of any other degree or diploma in any university, and contains no copy or paraphrase material previously presented by another person, except where due reference is made in the text.

This thesis may be made available for loan and limited copying in accordance with the Copyright Act, 1968

Damien N. Stringer
July 2009

Acknowledgements

I would firstly like to thank my principal supervisor Dr Michael Gardiner for his tuition throughout my candidature. His guidance and encouragement has been essential to the completion of this work, and I am sincerely grateful for his assistance. I am also thankful for the assistance from my co-supervisor Prof. Brian Yates, whose guidance through the theoretical component of my project has been of great assistance.

Thank you to Dr Craig Forsyth and Dr Matthias Hilder, Monash University, for X-ray crystallography services. Thanks also to Dr Noel Davies and particularly Dr Thomas Rodemann, Central Science Laboratory, Univeristy of Tasmania for GC-MS and microanalytic studies, respectively.

I would also like to thank my co-workers from the Gardiner group throughout my candidature, particularly Mr Adam James and Mr Bryce Lockhart-Gillet whose friendship has made the journey through this project much easier. Mr Adam James is also acknowledged for his assistance with X-ray crystallography studies.

The completion of this project would not have been possible without the support of my family and friends, and I am eternally grateful for their support and encouragement throughout my studies. Particular thanks are extended to my parents for their endless love and support.

Finally, I would like to specially thank my wife Penny, whose love, support, patience and encouragement throughout my candidature has been invaluable.

For Mum and Dad,

for whom nothing has ever been too much.

Abstract:

This thesis describes the synthetic and theoretical investigations of lanthanide imide complexes stabilised by the N,N'-deprotonated *meso*-octaethyl-*trans*-dioxaporphyrinogen ligand, of relevance to lanthanide mediated dinitrogen fixation. Also described are the synthesis of dibenzotropylidene based ligands and subsequent Group 1 metal complexes as pre-cursors for lanthanide complexes bearing alkene interactions, of relevance to lanthanide based catalytic alkene polymerisation.

Chapter 1 introduces nitrogen fixation in both biological and synthetic systems and includes a review of strategic ligand design in organolanthanide chemistry.

The synthesis, characterisation and reactivity of macrocyclic lanthanide complexes bearing auxiliary halide, azo and amide ligands as intermediates in the synthesis of macrocyclic lanthanide imides are described in Chapters 2-4. The KI incorporating macrocyclic samarium(II) complex, $[\{(C_6H_5Me)K(Et_8N_2O_2)Sm(\mu\text{-}I)\}_2]$ and the macrocyclic samarium(III) bromide, $[\{(Et_8N_2O_2)Sm(\mu\text{-}Br)\}_2]$ were prepared from metathetical exchange reactions, whilst the macrocyclic samarium(III) iodide, $[\{(Et_8N_2O_2)Sm(\mu\text{-}I)\}_2]$ was prepared *via* oxidation of $[\{(C_6H_5Me)K(Et_8N_2O_2)Sm(\mu\text{-}I)\}_2]$.

The macrocyclic azo complexes $[Et_8N_2O_2Sm\{\eta^2\text{-}N_2(Mes)_2\}]$ and $[(Et_8N_2O_2)Sm(\eta^2\text{-}N_2Ph_2)]$ were prepared *via* redox processes from $[\{(C_6H_5Me)K(Et_8N_2O_2)Sm(\mu\text{-}I)\}_2]$ and characterised from X-ray diffraction and NMR spectroscopic studies. The macrocyclic amides $[(THF)_2K(Et_8N_2O_2)Sm(N(H)Mes)_2]$, $[\{\text{-}\mu\text{-}\eta^1\text{:}\eta^3\text{-}(N(H)Mes)K(Et_8N_2O_2)SmN(H)Mes\}_n]$, $[(Et_8N_2O_2)Sm\{N(H)(C_6H_2\text{-}2,4,6\text{-}t\text{-}Bu)\}]$ and $[\{(Et_8N_2O_2)SmN(H)Mes]$ were synthesised from $[\{(Et_8N_2O_2)Sm(\mu\text{-}I)\}_2]$ *via* metathetical exchange reactions and their subsequent reactivity with a number of Group 1 metal bases was investigated. The desired α-deprotonation of the amides to yield an imide complex was not observed.

A comprehensive analysis of the bonding within the model macrocyclic imide $[K(H_8N_2O_2)SmN(CH_3)]$ and pre-cursor amide $[(H_8N_2O_2)SmN(H)CH_3]$ is presented in Chapter 5, along with a thermodynamic analysis of synthetic methods for imide formation from high-level density functional theory calculations. The samarium-based *d* orbitals were found to be important in stabilising the imide moiety, and were also found to exhibit strong interactions with the macrocyclic ligand.

Synthetic studies of various dibenzotropylidene (trop) functionalised ligands are presented in Chapter 6. The synthesis and characterisation of the novel dibenzotropylidene ligands derived from deprotonation of tropN(H)-*t*-Bu, tropacacH, tropNsalOH and tropNsal‡OH are described. Subsequent metallation of tropN(H)-*t*-Bu and tropNsal‡OH gave the lithium complexes $[(tropN(t\text{-}Bu)Li)_2OEt_2]$, $[(tropNsal^{\ddagger}OLi)_2]$ and $[\{tropN(H)C(n\text{-}Bu)sal^{\ddagger}OLi\}_2]$. Further reactivity studies of these complexes in various reactions, including metathetical exchangea aimed at preparing lanthanide complexes, revealed instability in the tropylidene-heteroatom bond, which restricted the use of the tropylidene framework in organolanthanide studies.

Contents

Appendices

Abbreviations:

Å	Angström, 10^{-10} m
acacH	acetylacetone
ADF	Amsterdam Density Functional
Anal.	Microanalysis
Ar	aryl
bipy	bipyridine
B3LYP	Becke 3-Parameter (Exchange), Lee, Yang and Parr
B3PW91	Becke exchange, Perdew–Wang 91 correlation
t-Bu	tertiary-butyl
n-Bu	normal-butyl
Calcd.	Calculated
C_5H_5	cyclopentadienyl
C_5Me_5	pentamethylcyclopentadienyl
COT	cyclooctatetraendiyl
18-crown-6	1,4,7,10,13,16-hexaoxacyclooctadecane
Ct	centroid
d	doublet
$DACH_2$	4,13-diaza-18-crown-6
DFT	Density Functional Theory
Et	ethyl
$Et_8N_4H_4$	*meso*-octaethylporphyrinogen
$Et_8N_4Me_2H_2$	*trans-N,N'*-dimethyl-*meso*-octaethylporphyrinogen
$Et_8N_2O_2H_2$	*meso*-octaethyl-*trans*-dioxaporphyrinogen
$Et_8N_2Ph_2H_2$	*meso*-octaethyl-*trans*-diphenyleneporphyrinogen
Et_2O	diethyl ether
GC-MS	gas chromatography-mass spectrometry
gCOSY	gradient correlation spectroscopy
gHMBC	gradient heteronuclear multiple bond correlation
gHMQC	gradient heteronuclear multiple quantum correlation
c-hex	cyclohexyl
$H_8N_2O_2$	*trans*-dioxaporphyrinogen

L	ligand
Ln	lanthanide
M	metal
m	multiplet
Me	methyl
$Me_8N_2O_2H_2$	*meso*-octamethyl-*trans*-dioxaporphyrinogen
Mes	2,4,6-trimethylbenzyl
MPA	Mulliken Population Analysis
MW	Molecular Weight
NBO	Natural Bond Order
NMR	nuclear magnetic resonance
NOESY	nuclear overhauser effect spectroscopy
Ph	phenyl
Ph_4N_4	*meso*-tetraphenylporphyrin
ppm	parts per million
q	quartet
R	alkyl, aryl
RDAD	*N,N'*-disubstituted-1,4-diazabuta-1,3-diene
RECP	Relativistic Effective Core Potential
s	singlet
SDD	Stuttgart-Dresden
t	triplet
tert	tertiary
THF	tetrahydrofuran
trop	5H-dibenzo[a,d]cycloheptene
$P_2N_2H_2$	PhP{$CH_2SiMe_2N(H)SiMe_2CH_2$}$_2$PPh
salO	$C(C_6H_4)$-2-O
sal^{t}O	$C(C_6H_2)$-2-O-3,5-*t*-Bu)
TMEDA	*N,N,N',N'*-tetramethylethylenediamine
TMS	trimethylsilyl
VDD	Voronoi Deformation Density
ZORA	zeroth order regular approximation
δ	chemical shift

Chapter 1. Introduction to dinitrogen and lanthanide chemistry.

1.1. Nitrogen Fixation.

1.1.1. Introduction to nitrogen fixation.

The demand for chemically accessible nitrogen by man since the early 20th century has far outstripped biology's capacity to fix atmospheric nitrogen to ammonia. Necessarily, studies of synthetic chemical fixation were undertaken and resulted in the discovery by Fritz Haber of the first patented catalytic method to chemically fix nitrogen as ammonia, which was commercialised in 1910 by Carl Bosch.[1] The Haber-Bosch process, as it is now commonly known, fixes nitrogen *via* the use of high pressures of nitrogen and hydrogen over a heterogeneous Fe catalyst. The Haber-Bosch process has remained the primary synthetic means for the fixation of nitrogen to ammonia and now contributes half of the total required nitrogen input to world agriculture. Because of the high pressure and temperature demands of the process, 1 % of the world's total energy supply is consumed to satisfy society's nitrogen demands.[2]

1.1.2. Biological nitrogen fixation.

Biologically, nitrogen is fixed by a limited group of microbes at atmospheric pressures and temperatures by the nitrogenase enzyme. The contrast in energy requirements between the Haber-Bosch process and biological nitrogen fixation has resulted in significant research focus over the last 50 years to understand the nitrogen fixation mechanism within the nitrogenase enzyme.[3] Through studies of this nature, four different nitrogenase enzymes have been characterised,[4] with varying metal co-factors present, containing Fe in each case and either Mo or V depending on the bio-availability of each metal to the microbe.[4a,5] The exploratory studies of the nitrogenase enzyme have been influential in determining the metals that have been studied for chemical nitrogen fixation by synthetic methods.

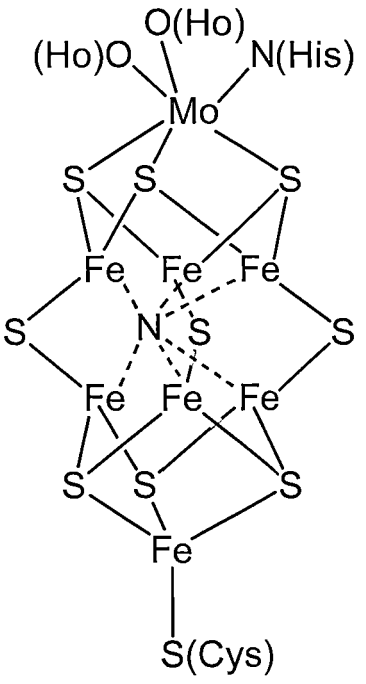

Figure 1.1. Model of the FeMo cofactor of nitrogenase adapted from Smith.[2] Ho = Homocitrate, His = Histamine, Cys = Cysteine

1.1.3. Synthetic transition metal mediated nitrogen fixation.

Allen and Senoff isolated the first dinitrogen complex of a transition metal, $[Ru(NH_3)_5(N_2)]^{2+}$ (**I**), in 1965 from the aqueous reaction of hydrazine with ruthenium trichloride, and since this initial discovery, transition metal complexes displaying promise for achieving nitrogen fixation have been reported in abundance.[7] Early attempts of nitrogen fixation at a single metal centre focused on the use of Mo(0) and W(0) species. Through this early work, the Chatt cycle for nitrogen fixation was proposed, which included the identification of several key intermediates in the catalytic nitrogen fixation cycle, including $M(N_2)$, M–N=NH, M=N–NH_2, M≡N, M=NH, M–NH_2 and $M(NH_3)$ species. However, catalytic activity was not observed.[8]

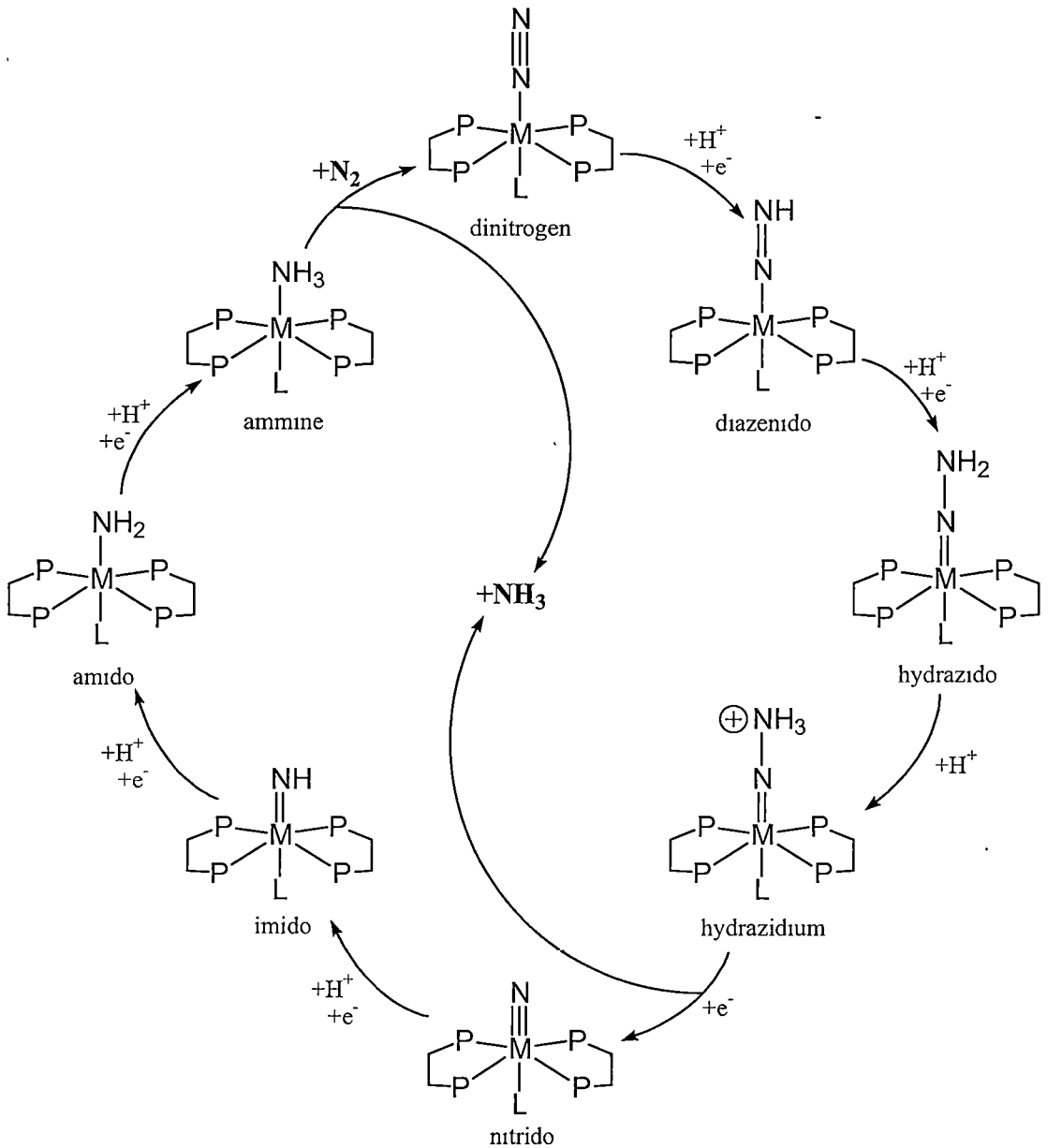

Figure 1.2. Chatt cycle for dinitrogen fixation at a single metal centre adapted from MacKay.[9]

Following decades of research into transition metal dinitrogen chemistry, the first catalytic reductions of N_2 to NH_3 have recently been reported.[10] Of these, only that of Schrock has been rationalised *via* the characterisation of a number of intermediate species. The Mo HIPT system studied by Schrock, Figure 1.3, was observed to involve several of the key intermediates proposed in the Chatt cycle from the 1960's, and a catalytic cycle based on the characterised intermediate species has been

proposed. The Mo centre within the cycle ranges in oxidation states from Mo^{III} to Mo^{VI}.

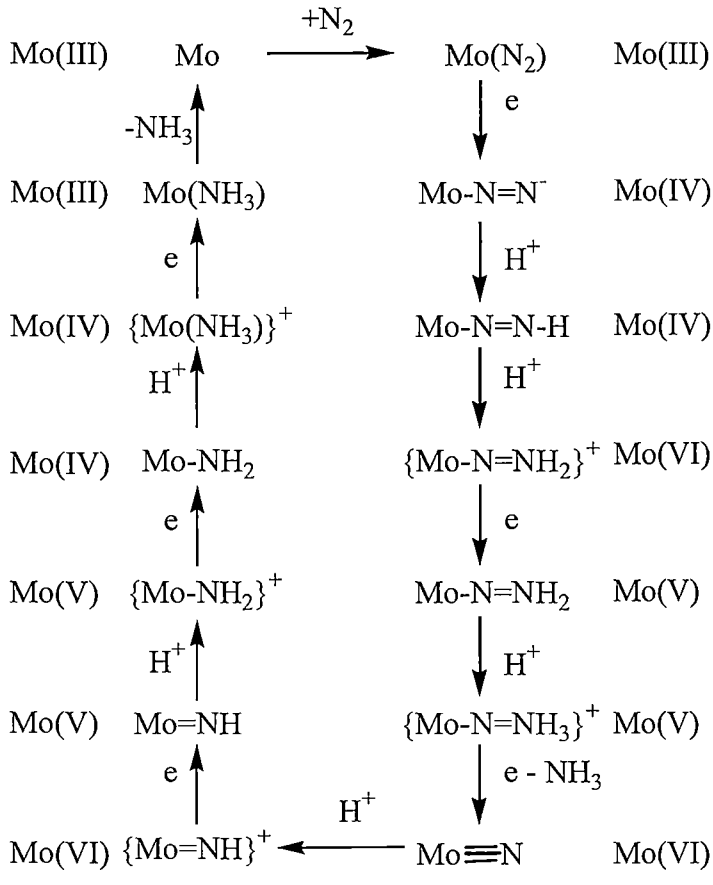

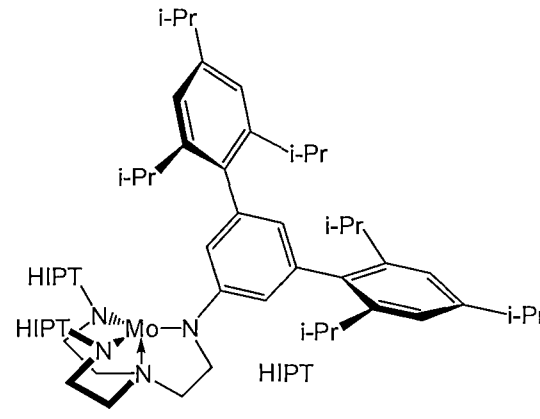

(II)

Figure 1.3. Schrock catalytic cycle for the Mo HIPT system.[10]

The liberated $NH_3(g)$ in the Schrock cycle has been shown to inhibit catalysis as it competes with N_2 for the vacant coordination site on [MoHIPT]. Furthermore, it is proposed that the activity of other transition metals such as W, Fe or V for N_2 fixation with the HIPT system will be less than that observed for Mo.[8b] Studies of bi-metallic systems, with alternative mechanisms to the Chatt cycle, have also had some success.[11]

Dinitrogen cleavage to yield a molybdenum nitride complex was observed for the Mo(III) trisamide species, $[Mo(NRAr)_3]$, (R = $C(CD_3)_2CH_3$, **(III)** Ar = 3,5-$(Me)_2C_6H_3$, **(IV)**), whereby two $[Mo(NRAr)_3]$ molecules cooperatively reduced the N_2 moiety without the need for the first three intermediate species in the Chatt cycle. The reduction of N_2 was observed to be stoichiometric, with catalytic activity not observed.[11] Theoretical studies of this system have yielded detailed mechanistic knowledge.[12]

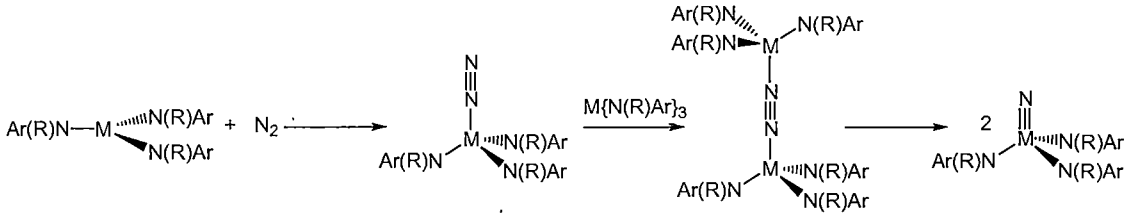

Scheme 1.1. Mechanism for N_2 cleavage by the MoN(R)Ar system.

Recent studies of Group 4 metal compounds have yielded a number of activated nitrogen species which have exhibited reactivity with carbon containing molecules, as well as hydrogen, though a catalytic system has yet to be found.[13]

1.1.4. N_2 bonding modes.

Nitrogen complexes of the transition metals have historically exhibited end-on bonding to one or more metal centres. Typically, weak activation of the N≡N bond is observed for end-on bound nitrogen molecules with single metal centres, such as the Schrock Mo(HIPT) system.[14] In 1998, Evans reported the synthesis of a novel side-on bound dinitrogen complex of decamethylsamarocene, $[(C_5Me_5)_2Sm(\mu_2\text{-}N_2)]$, (**V**), as shown in Figure 1.4.[15] Whilst little activation of the dinitrogen bond was observed in this case (based on the N-N bond length), the possibility that side-on bound dinitrogen complexes could be synthesised led to renewed efforts utilising other metals to replicate the side-on bonding mode. This indeed led to the isolation of side-on bound dinitrogen complexes of other lanthanides, actinides, and the transition metals, Zr, Nb, Ta, Hf and Os.[14] From these studies, it has been shown that the side-on bonding mode can result in quite variable dinitrogen activation, ranging from weakly (N≡N bonds) to strongly (N=N and N-N bonds) activated species, as shown in Table 1.1.

N_2 Binding Mode	Weak Activation	Strong Activation
End-on mononuclear	M—N≡N	
End-on dinuclear	M—N≡N—M	M=N—N=M
Side-on dinuclear	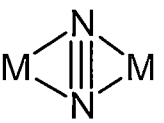	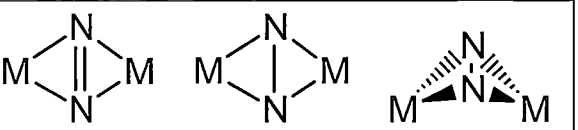
Side-on/End-on dinuclear		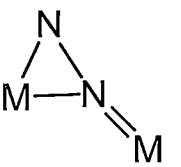

Table 1.1. N_2 activation according to bonding mode, adapted from Fryzuk.[14]

1.1.5. Lanthanide mediated dinitrogen reduction.

The novel planar side-on N_2 binding mode exhibited by $[(C_5Me_5)_2Sm)_2N_2]$, (**V**), coupled with the reducing power of the Sm^{II}/Sm^{III} redox couple suggested that further studies utilising lanthanide based reducing agents may reveal insights into dinitrogen reduction chemistry.[16]

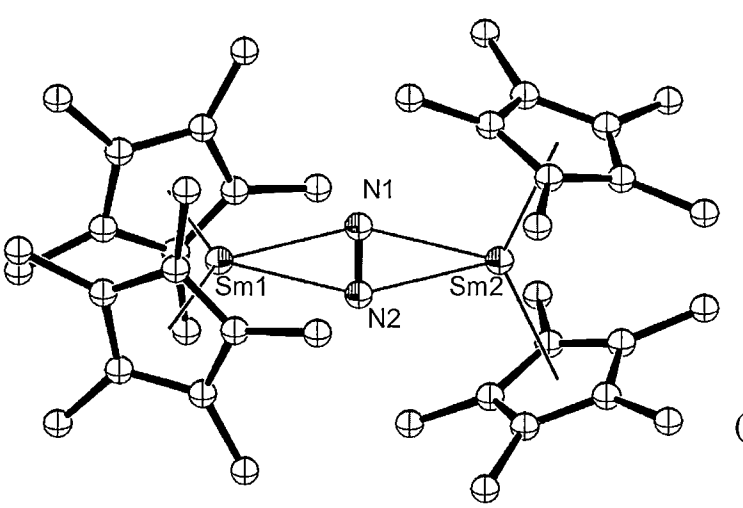

(**V**)

Figure 1.4. Molecular structure of side-on bound dinitrogen decamethylsamarocene complex **V**.[15] Figure generated from CCDC obtained coordinates. Atoms of arbitrary size. H atoms omitted for clarity.

Subsequent studies have resulted in the formation of several Sm mediated reduced dinitrogen species, and led to the extension of dinitrogen reduction chemistry to the

majority of the remaining divalent lanthanides.[17] In each case, the Ln(II) centre contributes one electron to the reduction of the dinitrogen bond, most often resulting in a bimetallic complex bridged by a dianionic reduced dinitrogen ligand, as shown for $[(C_5Me_5)_2Sm)_2N_2]$, (V). Gambarotta reported the cooperative reduction of dinitrogen by four Sm(II) centres bound to macrocyclic porphyrinogen ligands resulted in a tetraanionic reduced $(N_2)^{4-}$ species $[\{(hex_4N_4)_2Sm_3Li_2\}(\mu^3\text{-}N_2)\{Li(THF)_2\}\cdot THF]$, (**VI**), shown in Figure 1.5, whereby the fourth samarium atom involved in the reduction formed the samarium(III) macrocyclic by-product, $[(c\text{-}hex_4N_4)Sm(Cl)\{(Li(THF))_3(\mu^3\text{-}Cl)\}]$, (**VII**).[18] Such strongly reduced species do not occur frequently from Ln(II) based reductions, as a number of metal centres are required to cooperatively reduce the dinitrogen substrate. Catalytic dinitrogen reduction systems utilising lanthanide metals are more commonly postulated to involve an external electron source.

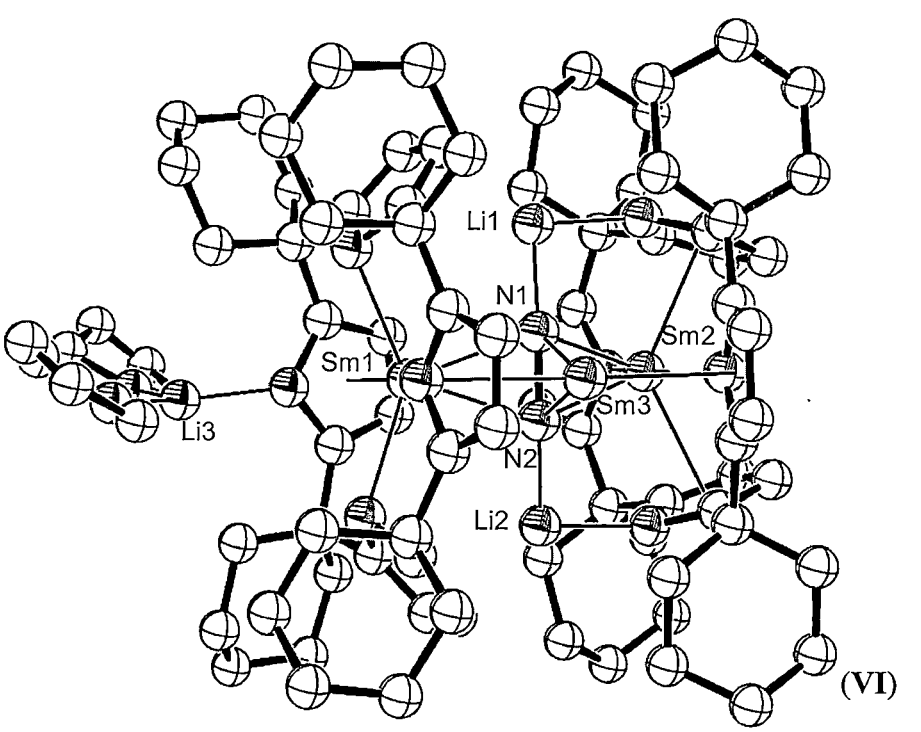

Figure 1.5. Strongly reduced $(N_2)^{4-}$ species in $[\{(c\text{-}hex_4N_4)_2Sm_3Li_2\}(\mu^3\text{-}N_2)\{Li(THF)_2\}.THF]$, (**VI**). Figure generated from CCDC obtained coordinates. Atoms of arbitrary size. H atoms are omitted for clarity.

Gambarotta has also reported the synthesis of a four electron reduced N_2 samarium porphyrinogen complex, $[\{(THF)_2Li(Et_8N_4)Sm\}_2(N_2Li_4)]$, (**VIII**), which utilised Li

as the electron source for the reduction, with reduction of the nitrogen fragment occurring at the Sm centre.[19] Complexes of this nature suggest that external electron sources may enable metals without widely accessible oxidation states such as the lanthanides to achieve N_2 fixation without the need for high oxidation states of the metal catalyst, as observed for Mo in the Schrock cycle. Lanthanide mediated dinitrogen reduction utilising an external electron source has since been reported for the entire lanthanide series excepting Eu and Yb.[20] The lanthanide centre in each case was supported by bis(trimethylsilyl)amide ligands as shown for the Gd example shown in Figure 1.6.

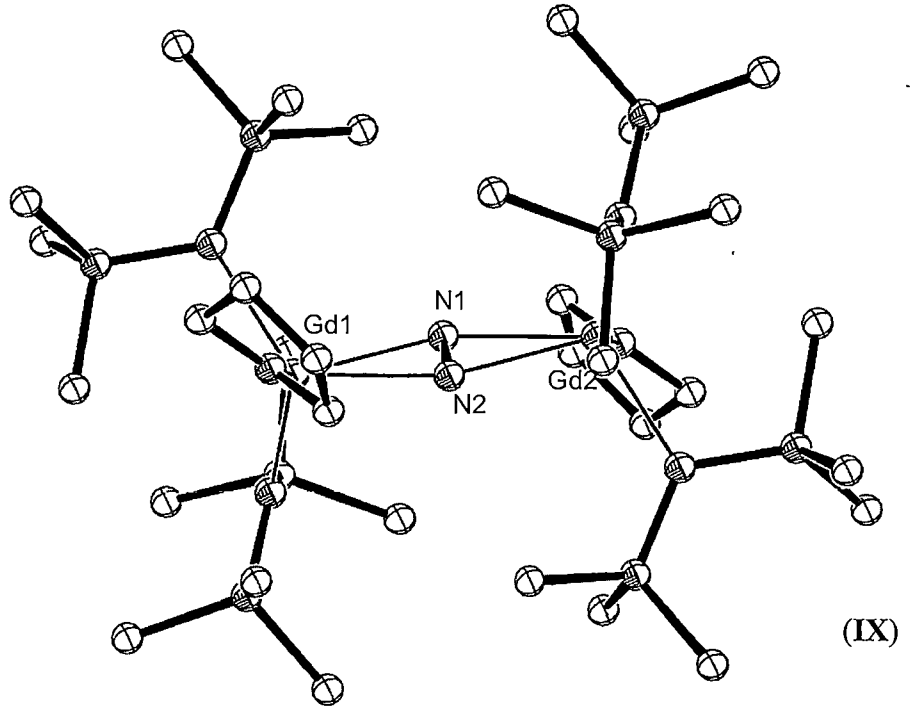

Figure 1.6. Reduced dinitrogen Gd complex, $[\{Gd(N(SiMe_3)_2)_2THF\}_2N_2]$, **(IX)**.[20b] Disorder in one TMS group is not shown. Figure generated from CCDC obtained coordinates. Atoms of arbitrary size. H atoms omitted for clarity.

The reactivity of Ln(III)/M mixtures with dinitrogen, coupled with Ln(II) dinitrogen reduction chemistry has shown the readiness with which the initial N_2 reduction step can be undertaken by organolanthanide species. Studies of other N_2 fixation intermediates of the lanthanide elements have been limited, however a number of the key intermediates proposed in the Chatt cycle have been observed.

1.1.6. Intermediate complexes in lanthanide mediated nitrogen fixation.

Organolanthanide complexes containing a dinitrogen moiety are limited primarily to those of anionic $(N_2)^{n-}$, n = 2, 4, species from dinitrogen reduction,[15-20] and reduced azobenzene compounds, $(RNNR)^{n-}$, n=1, 2, reviewed further in Chapter 3. An unsubstituted hydrazido complex, $[\{(C_5Me_5)Sm\}_4(NHNH)_2(NHNH_2)_4(NH_3)_2]$, (**X**), synthesised from the reaction of $[(C_5Me_5)_2Sm]$, (**XI**) with excess hydrazine has been reported,[21] as has the generation of a dimetallated Sm hydrazine complex, $[\{(C_5Me_5)_2Sm\}_2(\mu\text{-}\eta^2\text{:}\eta^2\text{-}HNNH)]$, (**XII**) from the reaction of $[\{(C_5Me_5)_2Sm(\mu\text{-}H)\}_2]$, (**XIII**) with hydrazine.[16] Protonation of hydrazine complex **XII** led to the isolation of the neutral hydrazine adduct, $[(C_5Me_5)_2Sm(THF)(H_2NNH_2)][BPh_4]$, (**XIV**).[22] Further discussion of these dinitrogen containing complexes appears in Chapter 3.

Lanthanide amine and amide compounds have been reported in abundance. However, imide species, which are amide precursors in the Schrock and Chatt cycles, have been reported sparingly in the literature.[23-27]

Attempts to isolate a terminal lanthanide imide complex have as yet been unsuccessful. Schumman *et. al.* reported the isolation of tetranuclear Sm(III), (**XV**) and Yb(III), (**XVI**) complexes containing an imide ligand from the reduction of azobenzene by $(naphthalene)Ln(THF)_n$.[23] The serendipity with which the imide fragment in **XV** and **XVI** was synthesised has been common in the other limited number of imide syntheses.[24-27]

Xie *et. al.* have reported a series of μ_4-imido clusters of Gd, (**XVII**), Er, (**XVIII**) and Dy, (**XIX**) from the reaction of $Me_2Si(C_9H_7)(C_2B_{10}H_{11})$ with 4 equivalents of $NaNH_2$, followed by treatment with 1 equiv of $LnCl_3$.[24]

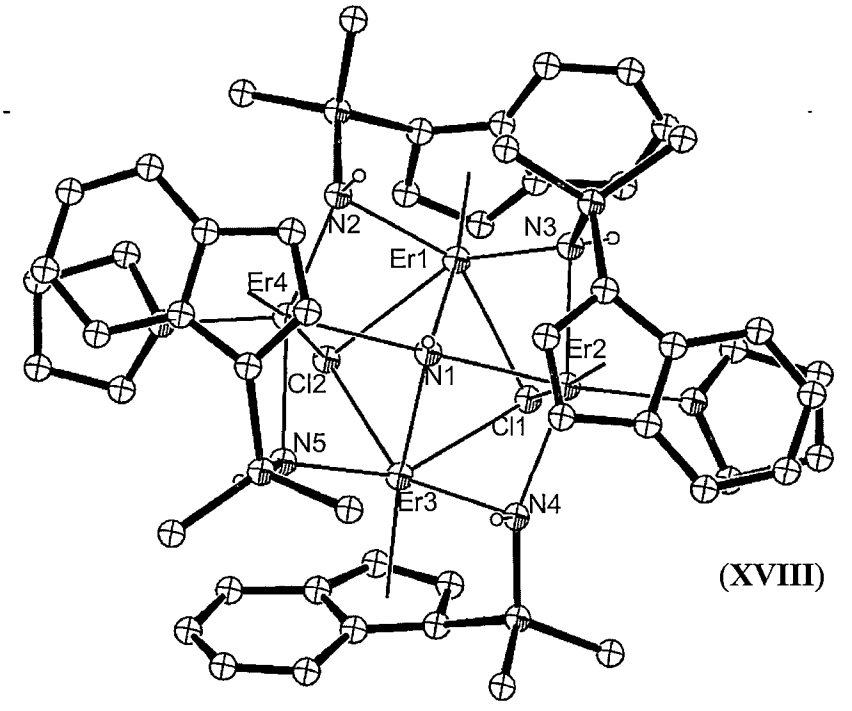

(XVIII)

Figure 1.7. Erbium imide cluster **XVIII**.[24b] Figure generated from CCDC obtained coordinates. Atoms of arbitrary size. Non-nitrogen H atoms are omitted for clarity.

Hou *et. al.* have reported the isolation of imide complexes *via* the addition of Ln-H units across the C≡N bond in benzonitrile. The resulting methylene imide fragment formed a Ln_4N_4 cubane core.[25] Gordon *et. al* synthesised a bis(μ^2-imido) complex $[(\mu\text{-ArN})\text{Sm}\mu\text{-NHAr})(\mu\text{-Me})\text{AlMe}_2]_2$, (**XX**), (Ar = 2,6-(*i*-Pr)$_2$C$_6$H$_3$) *via* the reaction of $[\text{Sm}(\mu\text{-NHAr})(\text{NHAr})_2]_2$, (**XXI**), with $AlMe_3$.[26] In this instance, two equivalents of $AlMe_3$ deprotonated the precursor amide moiety and a further two equivalents were incorporated into the dimeric complex to sterically shield the lanthanide centres. A similar approach has been used by Xie *et. al.* to yield mixed amido-imido-ytterbium complexes *via* deprotonation of $[(i\text{-Pr}_2\text{C}_6\text{H}_3\text{NH})_2\text{Yb}(\mu\text{-N(H)-}i\text{-Pr}_2\text{C}_6\text{H}_3)_2\text{Na(THF)}]$, (**XXII**) with *n*-BuLi. A complex heterometallic Yb, Na, Li cluster, (**XXIII**) resulted.[27]

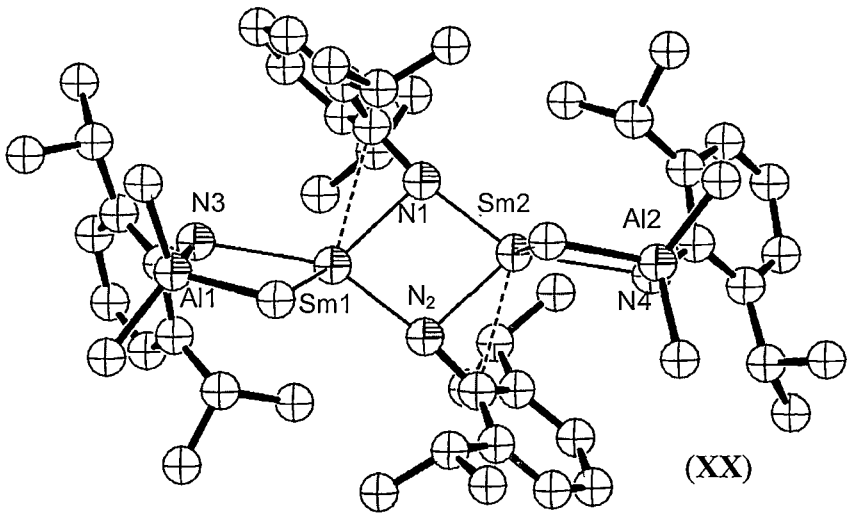

Figure 1.8. $AlMe_3$ retained, nitrogen bridged samarium imide complex **XX**. Figure generated from CCDC obtained coordinates. Atoms of arbitrary size. H atoms omitted for clarity.[26]

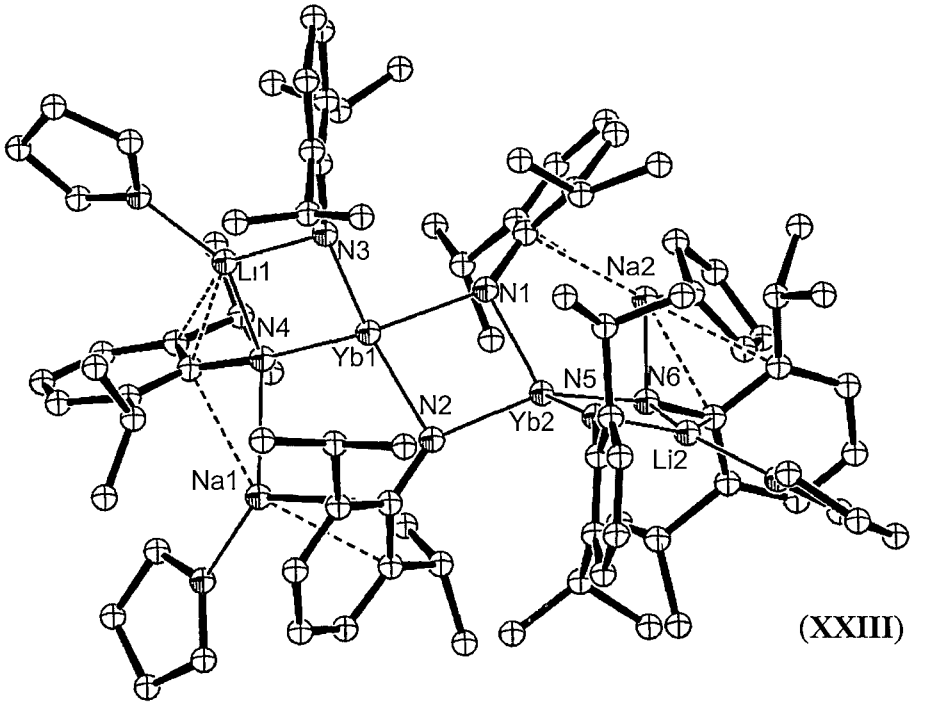

Figure 1.9. Ytterbium imide complex **XXIII** resulting from deprotonation by *n*-BuLi.[27] Figure generated from CCDC obtained coordinates. Atoms of arbitrary size. H atoms are excluded for clarity. Amido H atoms on N3 and N5 were inferred but were not located.

In each of the reported imido syntheses to date, the final outcome could not have been easily predicted. However, the isolation of these complexes has led to the prediction that organolanthanide complexes containing bulky non-participating ligands and mixed anilido-alkyl ligands should yield imido complexes in a directed manner.[28]

1.2. Strategic ligand design in organolanthanide chemistry.

1.2.1. General comment on ligand design.

The design of bulky non-participative ligands is essential in organolanthanide chemistry to ensure that stable, soluble complexes result. Mono-nuclearity is particularly desirable for solubility and reactivity considerations. Historically, bulky cyclopentadienyl ligands have satisfied these requirements for the lanthanide elements and, subsequently, the chemistry of these systems has been well explored and reviewed elsewhere.[29] Organolanthanide complexes of this nature typically display bent metallocene structures allowing further chemistry to occur on the vacant face of the lanthanide centre.

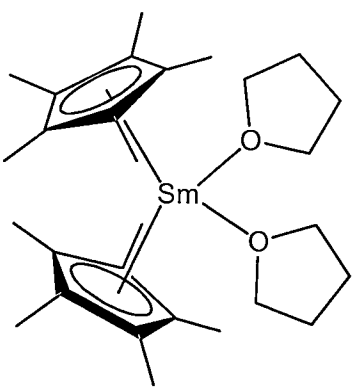

(XXIV)

Figure 1.10. Decamethylsamarocene, $[(C_5Me_5)_2Sm(THF)_2]$, (**XXIV**), a representative cyclopentadienyl lanthanide complex.[30]

Whilst cyclopentadienyl lanthanide complexes have been dominant in establishing reactivity trends within the lanthanide elements, alternative ligand sets have been sought to broaden the chemical understanding of the lanthanide metals.

1.2.2. Introduction to non-cyclopentadienyl ligands.

Non-cyclopentadienyl stabilised mono-nuclear organolanthanide complexes generally incorporate sterically demanding ligands in order to prevent the unwanted

aggregation of the lanthanide centres. Steric bulk is generally achieved *via* the use of substituted –π-bound ligands, or through bulky substituents surrounding a σ-bound centre. Both methodologies are discussed in the following review. In the latter case, σ-bonding to lanthanide centres is achieved through both carbon and heteroatoms.

1.2.3. σ- alkyl and aryl complexes.

Homoleptic alkyl and aryl complexes of the lanthanides have proven challenging to isolate, with initial reports of these species relying on indirect evidence to support their existence.[31] Following the isolation of the first neutral homoleptic alkyl compound, $[La\{C(H)(SiMe_3)_2\}_3]$, (**XXV**),[32] however, a number of structurally authenticated, stable complexes of this type have been reported.

Lanthanide (III) σ-alkyl compounds are dominated by those containing the stabilising bulky trimethylsilyl functional group. The monometallic species of this type often form trigonal structures.[33]

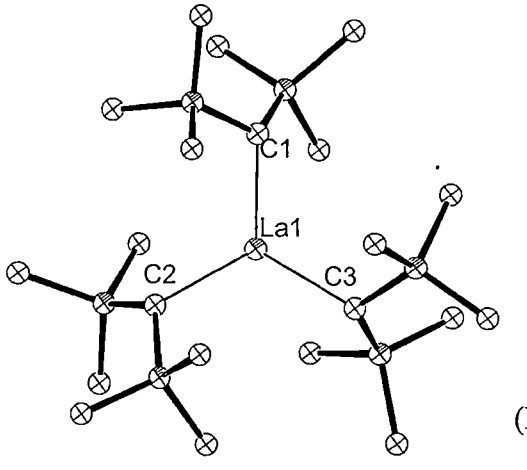

(**XXV**)

Figure 1.11. The first neutral homoleptic lanthanide alkyl complex, $[La\{C(H)(SiMe_3)_2\}_3]$, (**XXV**). Figure generated from CCDC obtained coordinates. Atoms of arbitrary size. H atoms omitted for clarity.[32]

Alkyl complexes not bearing trimethylsilyl groups are very limited: Schumann reported the synthesis of $[Lu(t\text{-}Bu)_4]Li(TMEDA)_2]$, (**XXVI**), in 1986,[34] and Niemeyer has reported $[Yb(CH_2\text{-}t\text{-}Bu)_3(THF)_2]$, (**XXVII**) from the reaction of Yb metal with neopentyl iodide in 2000.[35]

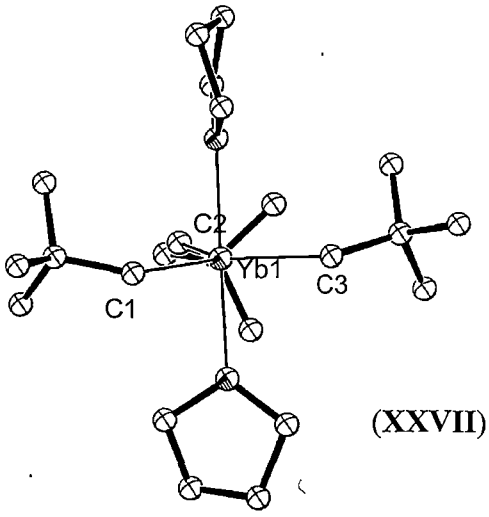

(XXVII)

Figure 1.12. Ttrimethylsilyl free lanthanide alkyl complex, $[Yb(CH_2\text{-}t\text{-}Bu)_3(THF)_2]$, (**XXVII**). Figure generated from CCDC obtained coordinates. Atoms of arbitrary size. H atoms and disorder in one *t*-Bu group omitted for clarity.

Trimethylsilyl substitution has also been important in isolating the few reported stable Ln(II) alkyl species,[36] such as $[Yb\{C(SiMe_3)_3\}_2]$, (**XXVIII**), the first solvent free Ln(II) alkyl complex.[36a]

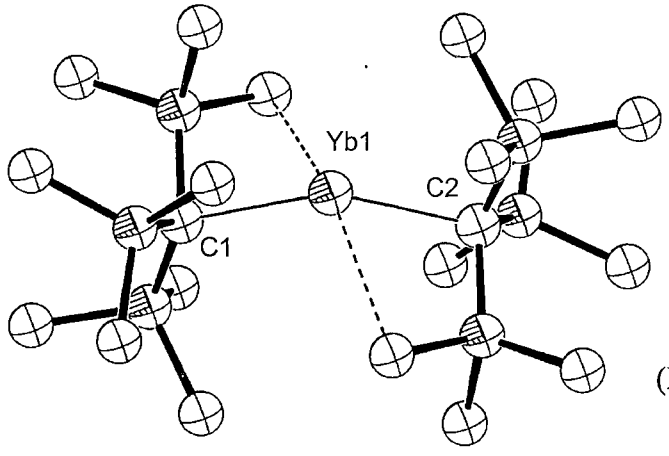

(XXVIII)

Figure 1.13. The first solvent free homoleptic lanthanide(II) alkyl complex, $[Yb\{C(SiMe_3)_3\}_2]$, (**XXVIII**). Figure generated from CCDC obtained coordinates. Atoms of arbitrary size. H atoms omitted for clarity.

Monometallic σ-aryl complexes are also quite limited. 2,6-disubstituted aryl ligands have had some success, whereby steric bulk at the 2 and 6 positions help stabilise the lanthanide centre.[37]

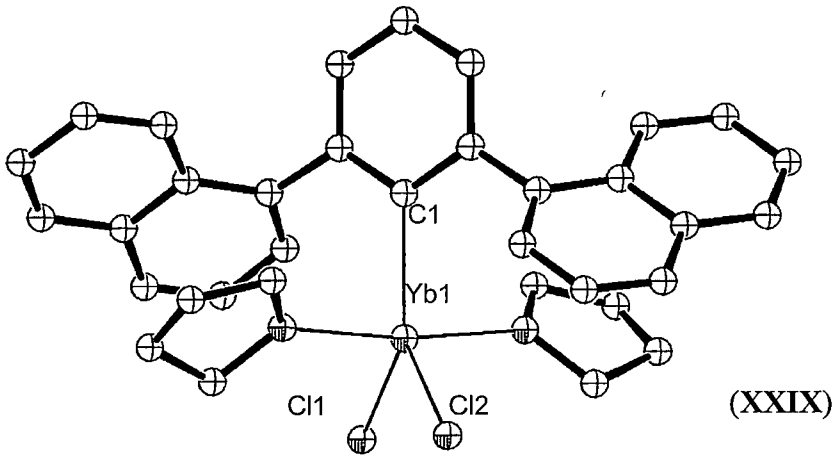

(XXIX)

Figure 1.14. Typical 2,6-substituted lanthanide aryl complex, [Yb(C_6H_3-2,6-$C_{10}H_7$)Cl_2], (**XXIX**). Figure generated from CCDC obtained coordinates. Atoms of arbitrary size. H atoms omitted for clarity.[37i]

Recently, the first structural characterisation of a Ln(II) σ-aryl compound was achieved utilising the Dpp ligand (Dpp=2,6-$Ph_2C_6H_3$).

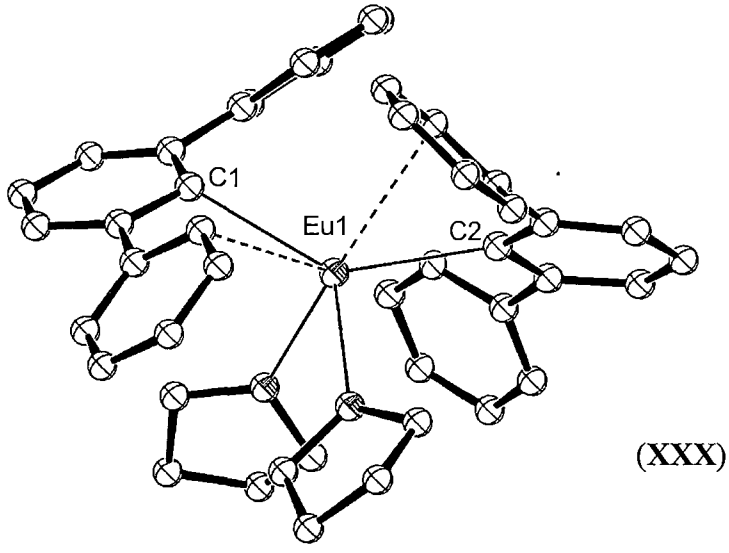

(XXX)

Figure 1.15. The first lanthanide(II) aryl complex, [Eu(2,6-$(Ph)_2C_6H_3$)$(THF)_2$], (**XXX**). Atoms are shown with arbitrary radii. H atoms, disorder in one THF molecule, and one THF molecule of crystallisation are omitted for clarity.[37g]

Deacon has also successfully characterised a range of Ln(II) complexes utilising the perfluoroaryl ligand, C_6F_5.[37k]

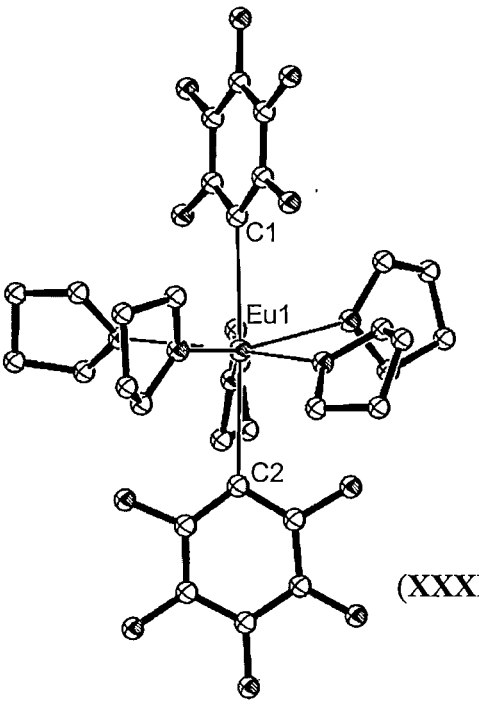

(XXXI)

Figure 1.16. Perfluoroaryl europium(II) complex, $[Eu(C_6F_5)_2(THF)_5]$, (**XXXI**). Figure generated from CCDC obtained coordinates. Atoms of arbitrary size. H atoms and disorder in one THF molecule are omitted for clarity.

1.2.4 π-bound non-aromatic ligands.

Non-aromatic π-bound organolanthanide complexes are restricted predominantly to allyl and pentadienyl ligands. Substituted allyl ligands have resulted in a number of well-defined complexes forming, often utilising bulky trimethylsilyl groups, with η^3 bonding favoured.[38]

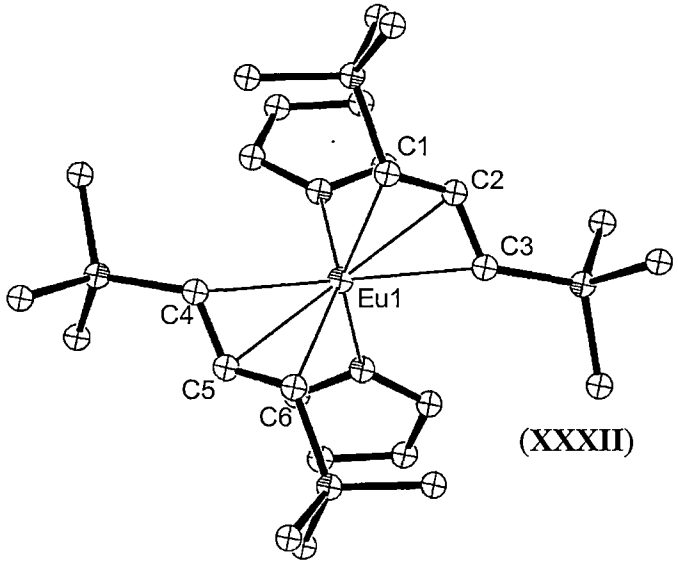

(XXXII)

Figure 1.17. Europium(II) allyl complex, $[Eu(\eta^3\text{-}C_3H_3\text{-}1,3\text{-}SiMe_3)_2(THF)_2]$, (**XXXII**). Figure generated from CCDC obtained coordinates. Atoms of arbitrary size. H atoms are omitted for clarity.[38c]

Similarly to the allyl case, azaallyl ligands employing 1,3-bis(trimethylsilyl) substitution have been shown to be successful in stabilising both Ln(II) and Ln(III) complexes. η^3 bonding is again favoured.

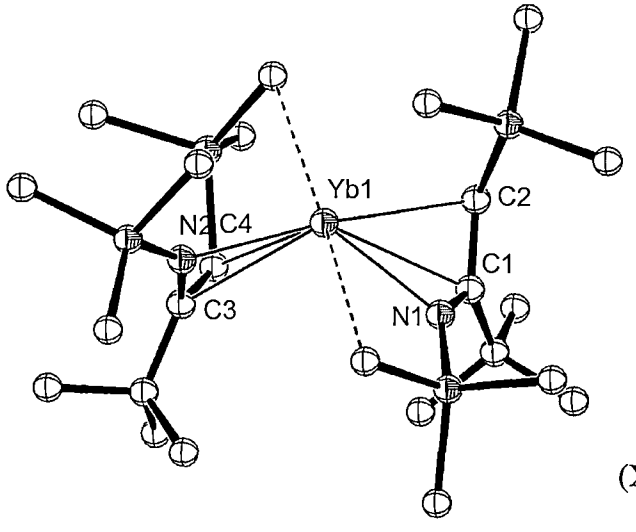

(XXXIII)

Figure 1.18. Azaallyl Yb(II) complex, $[Yb\{N(SiMe_3)C(t\text{-}Bu)CHSiMe_3\}_2]$, (**XXXIII**). Figure generated from CCDC obtained coordinates. Atoms of arbitrary size. H atoms and one of the two independent molecules in the asymmetric unit are omitted for clarity.[39a]

In the pentadienyl case, steric bulk is incorporated through 2,4-disubstitution, which has permitted the isolation of bis -(pentadienyl) lanthanides,[40] and homoleptic [Ln(C_7H_{11})$_3$] species,[41] though a monometallic mono(pentadienyl) derivative is yet to be crystallographically authenticated. Generally, an η^5 bonding mode is observed for the pentadienyl ligand, however, flexibility in the bonding mode of the ligand is possible, as shown in the homoleptic Ln(C_7H_{11})$_3$ species, where Ln = Lu. In this instance, the ligand was observed to adopt an η^3 bonding mode for one of the ligands in order to fit around the relatively small coordination sphere of the metal.[41b]

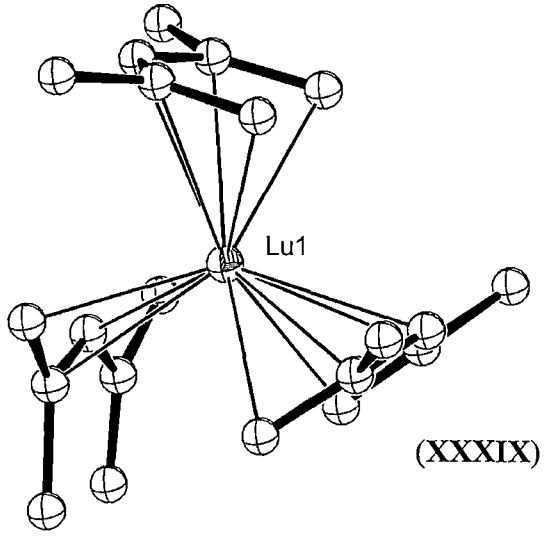

(XXXIX)

Figure 1.19. Lutetium pentadienyl complex, [Lu(η^5-2,4-(Me)$_2C_5H_5$)$_2$(η^3-2,4-(Me)$_2C_5H_5$)], (**XXXIX**). Figure generated from CCDC obtained coordinates. Atoms of arbitrary size. H atoms are omitted for clarity.[41b]

1.2.5. π-bound aromatic ligands.

Non-cyclopentadienyl π-bound aromatic systems are dominated by complexes containing cyclooctatetraenyl (COT) ligands and N containing heterocyclic ligands. Reports of monometallic divalent cyclooctatetraenyl complexes are limited, due to the ready formation of polymeric structures with limited solubility.[31] A monomeric cyclooctatetraenyl Yb(II) compound has been crystallographically authenticated by solubilising with pyridine.[42] Two crystallographically authenticated bis(cyclooctatetraenyl) lanthanide(II) compounds with two external countercations have also been reported.[43]

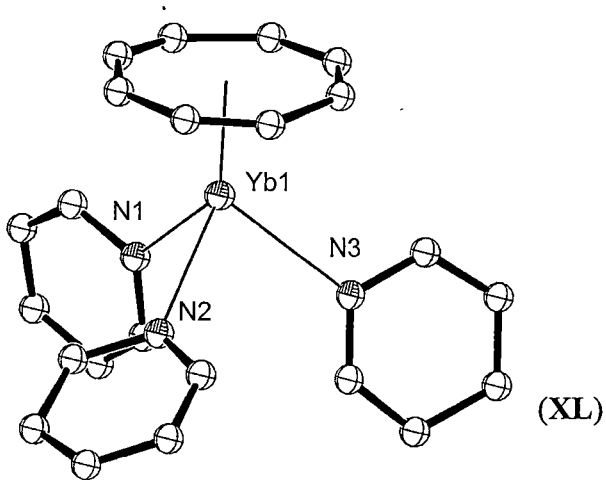

(XL)

Figure 1.20. Ytterbium(II) cyclooctatetraenyl complex, $[Yb(COT)(NC_5H_5)_3]$, (**XL**). Figure generated from CCDC obtained coordinates. Atoms of arbitrary size. H atoms, one of the two independent molecules from the asymmetric unit and two benzene molecules of crystallisation are omitted for clarity.

Compared to their divalent counterparts, trivalent lanthanide cyclooctatetraenyl complexes have been reported in relative abundance. Both mono- and bis(cyclooctatetraenyl) lanthanide(III) complexes are common, with either an auxiliary ligand such as a halide present in the former case,[44] as shown for $[Tm(COT)I(THF)_2]$, (**XLI**) in Figure 1.21,[44j] or an external countercation present in the latter.[45] Bis(cyclooctatetraenyl) complexes generally exhibit linear COT-Ln-COT bonding to form regular sandwich complexes as shown in Figure 1.22 for $[Ce(COT)_2][K(O(CH_2CH_2OCH_3)]$, (**XLII**).[45c] Cerium(IV) bis(cyclooctatetraenyl) complexes have also been reported, with regular sandwich structures resulting.[46]

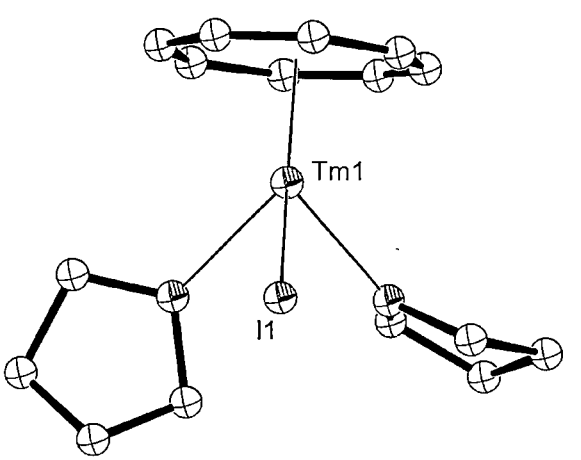

(XLI)

Figure 1.21. Mono(cyclooctatetraenyl) thulium(III) iodide complex, $[Tm(COT)I(THF)_2]$, (**XLI**). Figure generated from CCDC obtained coordinates.

Atoms of arbitrary size. H atoms and one of the two independent molecules in the asymmetric unit are omitted for clarity.[44j]

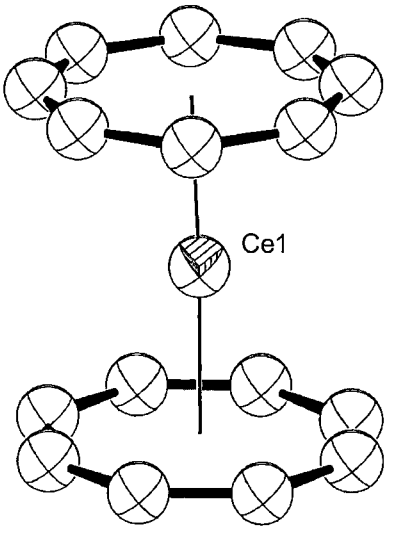

(XLII)

Figure 1.22. The first crystallographically authenticated lanthanide bis(cyclooctatetraenyl) complex, $[Ce(COT)_2][K(O(CH_2CH_2OCH_3)]$, (**XLII**). Figure generated from CCDC obtained coordinates. Atoms of arbitrary size. H atoms and the $[K\{O(CH_2CH_2OCH_3\}]$ ion are not shown for clarity.[45c]

1.2.6. Complexes of N and P containing heterocycles.

Nitrogen containing heterocycles have also found use in stabilising lanthanide(II) and (III) complexes. In this instance, pyrrolide, dipyromethanide, pyrazolate and macrocyclic pyrrolide based ligands have been most successful. Binding modes ranging from η^1 through to η^5 are observed.

Complexes of pyrrolide itself, or substituted pyrrolyl ligands are very limited. Yb and Eu complexes of mixed pyrrolide/pyrrole ligands and ammonia have only recently been reported.[47] Di-substitution of the pyrrole moiety at the 2 and 5 positions by either methyl or *t*-butyl groups have led to the isolation of mixed lanthanide/s-Block complexes of Nd, Sm and Yb. In the latter case, the bonding mode of the ligand was influenced by the retained alkali metal.[48]

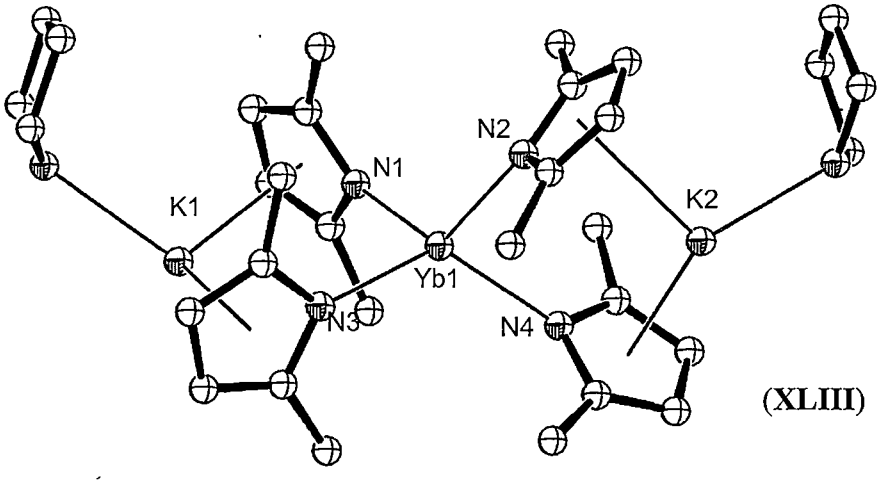

(XLIII)

Figure 1.23. Alkali metal retaining ytterbium(II) pyrrolide complex, [Yb(NC_4H_2-2,5-$CH_3)_4${K(THF)}$_2$], (**XLIII**). Figure generated from CCDC obtained coordinates. Atoms of arbitrary size. H atoms are omitted for clarity.[48b]

t-Butyl substitution has also led to two well-defined η^5-bound Yb and Sm complexes, [(2,5-(t-Bu)$_2C_4H_4N$)$YbCl_2THF_2$], (**XLIX**) and [(C_4H_4N-2,5-*t*-Bu)Sm(COT)THF], (**L**).[49]

Analogous to the chemistry of pyrrole, phosphorous containing heterocycles employing steric bulk through 2,5-disubstitution are capable of forming stable mononuclear lanthanide compounds. Both Ln(II)[50] and Ln(III)[51] species have been isolated, including well-defined solvent free systems such as [Tm(2,5-(*t*-Bu)$_2$-3,4-(Me)$_2PC_4)_2$], (**LI**), shown in Figure 1.24.[50a]

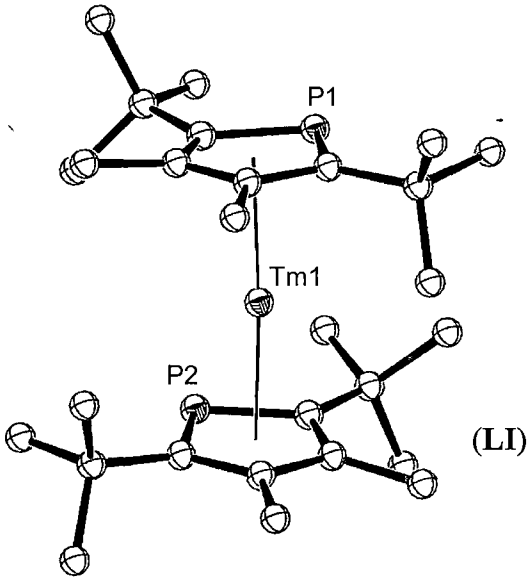

(LI)

Figure 1.24. Thulium(II) phospholyl complex, $[Tm(2,5\text{-}(t\text{-}Bu)_2\text{-}3,4\text{-}(Me)_2PC_4)_2]$, (**LI**). Figure generated from CCDC obtained coordinates. Atoms of arbitrary size. H atoms and two of the three independent molecules in the asymmetric unit are omitted for clarity.[50e]

Lanthanide pyrazolate complexes have been reported in abundance relative to pyrrolide compounds. In this instance, 3,5-di-substitution with either Ph or *t*-Bu groups has resulted in the greatest success, with η^2 coordination favoured,[52] as shown in Figure 1.25, though η^5 bonding has also been observed.[53] The number of pyrazolate ligands bound to the metal centre varies from 1 to 4 with other neutral ligands satisfying the coordination sphere of the metal. Alkali metal retention as shown in Figure 1.26 is also observed in some instances.

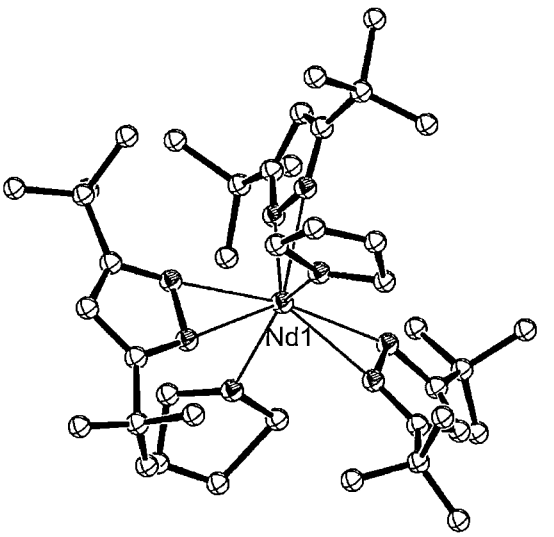

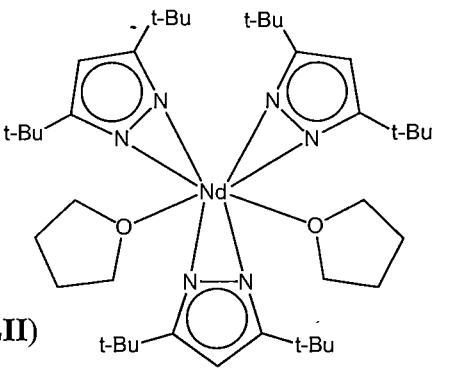

(LII)

Figure 1.25. Neodymium(III) tris(pyrazolate) complex, [Nd(2,5-(*t*-Bu)$_2$N$_2$C$_3$)$_3$(THF)$_2$], (**LII**). Figure generated from CCDC obtained coordinates. Atoms of arbitrary size. H atoms are omitted for clarity.[52k]

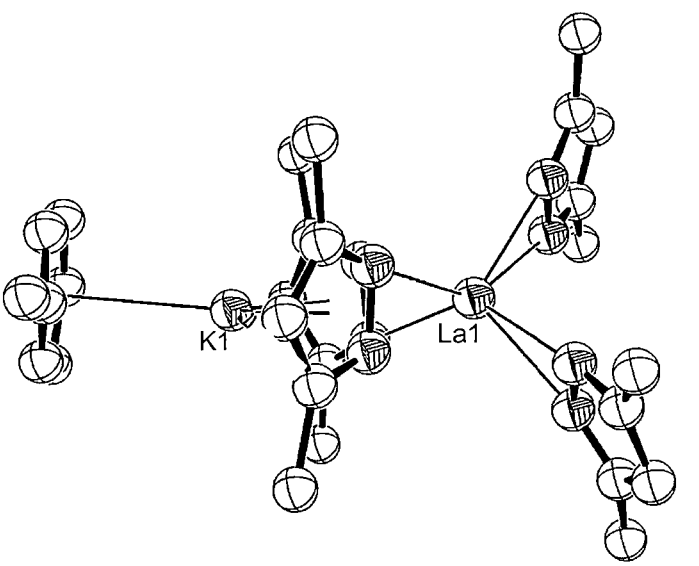

(LIII)

Figure 1.26. Group . 1 alkali metal retained tetrapyrazolate La compound, [(C$_6$H$_5$Me)K(μ-C$_3$N$_2$-3,5-*t*-Bu)$_2$La(C$_3$N$_2$-3,5-*t*-Bu)$_2$], (**LIII**). Figure generated from CCDC obtained coordinates. Atoms of arbitrary size. H atoms, two toluene molecules of crystallisation, disorder in the molecule and Me groups from the *t*-Bu substituents omitted for clarity. [52d]

The hydrotris(pyrazolyl)borate anion, and variants thereof have been extensively investigated, with stable, mononuclear lanthanide complexes often observed. Both

Ln(II) and Ln(III) complexes have been characterised, with up to 3 hydrotris(pyrazolyl)borate anions bound to each metal centre.[54]

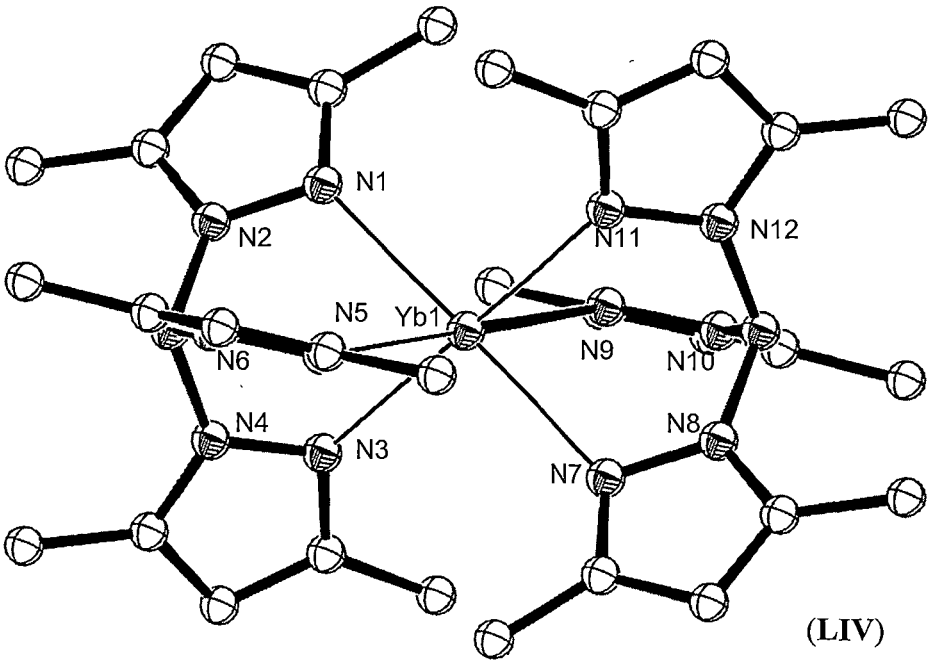

(LIV)

Figure 1.27. Ytterbium(II) hydrotris(pyrazolyl)borate, [Yb{(2,4-$(Me)_2N_2C_3H)_3BH\}_2$], (**LIV**).[55] Figure generated from CCDC obtained coordinates. Atoms of arbitrary size. H atoms are omitted for clarity.

Dipyromethanide dianion ligands have also been successful in stabilising lanthanide centres. Substitution with bulky groups such as Et, Ph and cyclohexyl at the bridging carbon centre have allowed numerous polynuclear dipyrrolylmethane lanthanide complexes to be isolated. However, Gambarotta has reported the synthesis of the only two mononuclear lanthanoid dipyrrolylmethane complexes, [$\{Et_2C(C_4H_4N)_2)_3Tm{\cdot}3K{\cdot}3C_6H_5Me$], (**LV**),[56] though this complex resulted from the unprecedented cleavage of a macrocyclic ligand precursor, and [$(THF)_4Na_2\{Ph_2C(C_4H_4N)_2\}_2Yb$], (**LVI**).[57] Both of these complexes retain alkali metal counter-cations to form the resulting neutral complex.

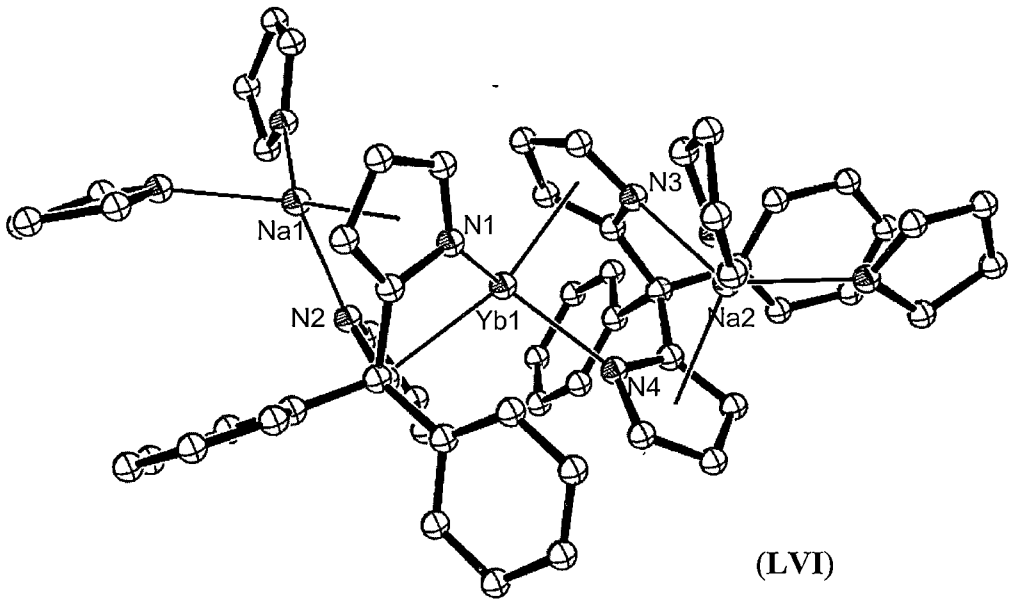

(LVI)

Figure 1.28. Sodium incorporated ytterbium dipyrromethane complex $[(THF)_4Na_2\{Ph_2(C_4H_4N)_2C\}_2Yb]$, (**LVI**). Atoms are shown with arbitrary radii. H atoms are omitted for clarity.[57]

1.2.7 Macrocyclic pyrrole based ligands.

Macrocyclic pyrrolide ligands have also been successful in stabilising lanthanide metals within the cavity of the macrocycle. In this instance, N-deprotonated porphyrinogen ligands bearing substituents at the *meso*- carbon atoms to resist ligand oxidation to porphyrins, have had most success. Both ethyl and cyclohexyl substitution has been employed, with the metal most often bound to the ligand in an $\eta^5{:}\eta^1{:}\eta^5{:}\eta^1$- bonding fashion. Complexes of this nature have exhibited strong dinitrogen reduction capabilities, as discussed above (in Section 1.1.5.). Typically, tetraanionic ligands are observed, necessitating the incorporation of counter-cation species external to the macrocyclic cavity.[58]

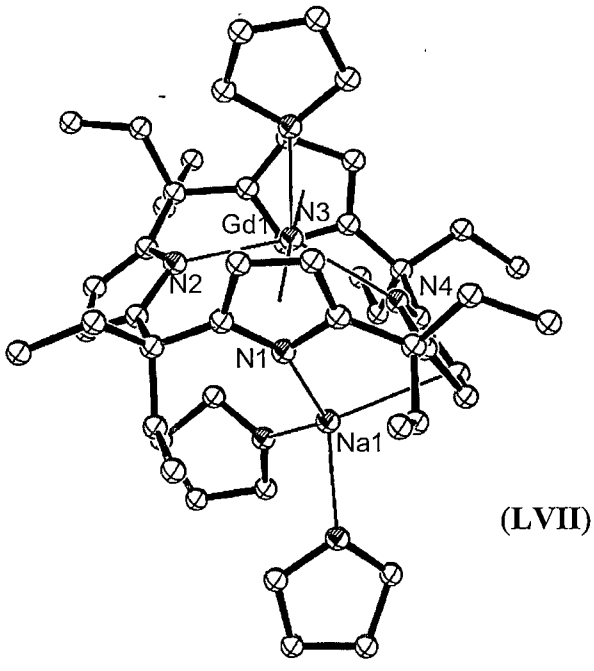

(LVII)

Figure 1.29. Sodium incorporating gadolinium(III) *meso*-octaethylporphyinogen complex, $[(THF)_2Na(Et_8N_4)Gd(THF)]$, (**LVII**). Figure generated from CCDC obtained coordinates. Atoms of arbitrary size. H atoms and disorder in two THF molecules is not shown for clarity.[58b]

Modification of the porphyrinogen ligand *via* pyrrole *N,N'*-dimethylation or substitution of two pyrrolyl units by furanyl units has led to dianionic ligands which do not require alkali metal counter-cations to produce neutral complexes.[59] In the latter case, novel C–H activation was observed as a result of counter-cation stabilisation in the base of the macrocyclic cavity, which will be discussed further in Chapter 4.

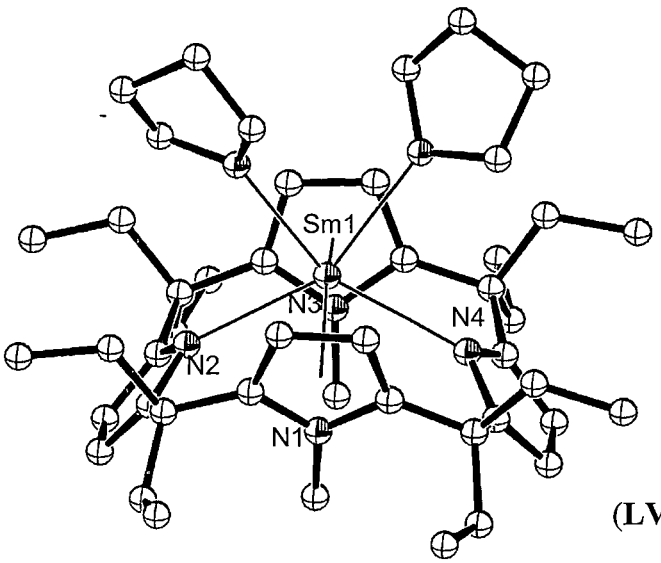

(LVIII)

Figure 1.30. Group 1 metal free modified porphyinogen samarium(III) complex, $[(Et_8N_4Me_2)Sm(THF)_2]$, (**LVIII**). Atoms of arbitrary size. H atoms are omitted for clarity.[59b]

1.3. Project Outline.

Following the isolation of $[\{(C_5Me_5)_2Sm\}_2N_2]$, (**V**), and subsequent reduced dinitrogen lanthanide species, it is apparent that organolanthanide systems may possess the necessary reducing capabilities to achieve nitrogen fixation. However, before this is to be achieved, a thorough understanding of the chemistry of the required nitrogen fixation intermediate species must be developed. Analogous to the studies of transition metal nitrogen fixation intermediates which were undertaken throughout the latter part of the last century, directed syntheses of organolanthanide nitrogen compounds is of current interest. Of the key intermediates identified in the Schrock cycle, a number of lanthanide mono- and dinitrogen containing ligand complexes have yet to be observed. Lanthanide amide compounds are prevalent throughout the literature, however no reports of a terminal lanthanide imide compound have been made. The targeted synthesis of a terminal lanthanide imide species, stabilised by a macrocyclic porphyrinogen ligand, of interest as a key intermediate in nitrogen fixation, in addition to the novel functional group nature of this species, provides the basis for the research reported in this thesis.

In addition to the targeted synthesis of a terminal lanthanide imide species, a study of lanthanide-alkene interactions utilising tropylidene based ligands provides the basis for a secondary project discussed in Chapter 6.

1.4. References

1. a) Haber, F.; van Oordt, G. *Z. Anorg. Chem.* **1905**, *43*, 111,
   b) Haber, F. *Naturwissenschaften* **1922**, *10*, 1041,
   c) Haber, F. *Naturwissenschaften* **1923**, *11*, 339.
2. Smith, B.E. *Science* **2002**, *297*, 1654.
3. Barney, B.M.; Lee, H.I.; Dos Santos, P.C.; Hoffman, B.M.; Dean, D.R.; Seefeldt, L.C. *Dalton Trans.* **2006**, 2277.
4. a) Eady, R.R. *Chem. Rev.* **1996**, *96*, 3013,
   b) Ribbe, M.; Gadkari, D.; Meyer, O. *J. Biol. Chem.* **1997**, *42*, 26627,
   c) Burgess, B.K.; Lowe, D.J. *Chem. Rev.* **1996**, *96*, 2983.
5. a) Smith, B. E. *Adv. Inorg. Chem.* **1999**, *47*, 159,
   b) Rehder, D. *Coord. Chem. Rev.* **1999**, *182*, 297.
6. Allen, A.D.; Senoff, C.V. *J. Chem. Soc., Chem. Commun.* **1965**, 621.
7. a) Chatt, J.; Dilworth, J. R.; Richards, R. L. *Chem. Rev.* **1978**, *78*, 589,
   b) Hidai, M. Coord. *Chem. Rev.* **1999**, *185*, 99,
   c) Fryzuk, M. D.; Johnson, S. A. *Coord. Chem. Rev.* **2000**, *200*, 379,
   d) Barriere, F. *Coord. Chem. Rev.* **2003**, *236*, 71,
   e) Allen, A. D.; Harris, R. O.; Loescher, B. R.; Stevens, J. R.; Whiteley, R. N. *Chem. Rev.* **1973**, *73*, 11,
   f) Richards, R. L. *Coord. Chem. Rev.* **1996**, *154*, 83.
8. a) Chatt, J.; Pearman, A.J.; Richards R.L. *Dalton Trans.* **1977**, 1852,
   b) Schrock, R.R. *Acc. Chem. Res.* **2005**, *38*, 955.
9. MacKay, B.A.; Fryzuk, M.D. *Chem. Rev.* **2004**, *104*, 385.
10. a) Shilov, A.E. *Russ.Chem.Bull., Int.Ed.* **2003**, *52*, 2555,
    b) Yandulov, D. V.; Schrock, R. R. *Science* **2003**, *301*, 76.
11. a) Laplaza, C.E.; Cummins, C.C. *Science* **1995**, *268*, 861,
    b) Laplaza, C.E.; Johnson, M.J.A.; Peters, J.C.; Odom, A.L.; Kim, E.; Cummins, C.C.; George, G.N.; Pickering, I.J.
    J. Am. Chem. Soc. **1996**, *118*, 8623,
    c) Laplaza, C.E.; Johnson, A.R.; Cummins, C.C.
    J. Am. Chem. Soc. **1996**, *118*, 709.
12. a) Christian, G.; Stranger, R.; Yates, B.F.; Cummins C.C.
    Dalton Trans. **2007**, 1939,

b) Christian, G.; Stranger, R.; Yates, B.F.; Cummins C.C.
Dalton Trans. **2008**, 338.

13. a) Ohki, Y.; Fryzuk, M.D. *Angew. Chem., Int. Ed.* **2007**, *46*, 3180,
b) Fryzuk, M.D.; Love, J.B.; Rettig, S.J.; Young, V.G.
Science **1997**, *275*, 1445.
14. MacLachlan, E.A.; Fryzuk, M.D. *Organometallics* **2006**, *25*, 1530.
15. Evans, W.J.; Ulibarri, T.A.; Ziller, J.W. *J. Am. Chem. Soc.* **1988**, *110*, 6877.
16. Evans, W.J.; Kociok Köhn, G.; Leong, V.S.; Ziller, J.W.
Inorg. Chem. **1992**, *31*, 3592.
17. Evans, W.J.; Zucchi, G.; Ziller, J.W. *J. Am. Chem. Soc.* **2003**, *125*, 10.
18. Guan, J.; Dubé, T.; Gambarotta, S.; Yap, G.P.A.
Organometallics, **2000**, *19*, 4820.
19. Jubb, J.; Gambarotta, S. *J. Am. Chem. Soc.* **1994**, *116*, 4417.
20. a) Evans, W.J.; Lee, D.S. Ziller, J.W. Kaltsoyannis, N.
J. Am. Chem. Soc. **2006**, *128*, 14176,
b) Evans, W.J.; Lee, D.S.; Rego, D.B.; Perotti, J.M.; Kozimor, S.A.K.;
Moore, E.K.; Ziller, J.W. *J. Am. Chem. Soc.* **2004**, *126*, 14574,
c) Evans, W.J.; Lee, D.S.; Lie, C.; Ziller, J.W.
Angew. Chem. Int. Ed. **2004**, *43*, 5517,
d) Evans, W.J.; Lee, D.S.; Johnston, M.A.; Ziller, J.W.
Organometallics **2005**, *24*, 6393.
21. Wang, K.G.; Stevens, E.D.; Nolan, S.P. *Organometallics* **1992**, *11*, 1011.
22. Evans, W.J.; Kociok Köhn, G.; Ziller, J.W.
Angew. Chem., Int. Ed. Engl. **1992**, *31*, 1081.
23. a) Emel'Yanova, N.S.; Bochkarev, M.N.; Schumann, H.; Loebel, J.; Esser, L.
Koord. Khim. **1994**, *20*, 789,
b) Trifonov, A.A.; Bochkarev, M.N.; Schumann, H; Loebel, J. *Angew. Chem., Int. Ed. Engl.* **1991**, *30*, 1149.
24. a) Xie, Z.; Wang, S.; Yang, Q.; Mak, T. *Organometallics* **1999**, *18*, 1578,
b) Wang, S.; Yang, Q.; Mak, T. Xia, Z. *Organometallics* **1999**, *18*, 5511.
25. Cui, D.; Nishiura, M.; Hou, Z. *Angew. Chem. Int. Ed.* **2005**, *44*, 959.
26. Gordon, J.C.; Giesbrecht, G.R.; Clark, D.L.; Hay, P.J.; Keogh, D.W.; Poli, R.; Scott, B.L.; Watkin, J.G. *Organometallics* **2002**, *21*, 4726.
27. Chan, H.S.; Li, H.W.; Xie, Z. *J. Chem. Soc., Chem. Commun.* **2002**, 652.

28. Giesbrecht, G.R.; Gordon, J.C. *Dalton Trans.* **2004**, 2387.

29. a) Okuda, J.; Arndt, S.; Beckerle, K.; Hultzsch, K.C.; Voth, P.; Spaniol, T.P. *Organometallic Catalysts and Olefin Polymerization* **2001**, 156,
b) Bombieri, G.; Paolucci, G. *Handbook on the Physics and Chemistry of Rare Earths* **1998**, *25*, 265,
c) Lappert, M.F.; Singh, A.; *J. Organomet. Chem.* **1982**, *239*, 133-141,
d) Evans, W.J. *J. Organomet. Chem.* **2002**, *652*, 61.

30. Evans, W.J.; Grate, J.W.; Choi, H.W.; Bloom, I.; Hunter, W.E.; Atwood, J.L. *J. Am. Chem. Soc.* **1985**, *107*, 941.

31. Edelmann, F.T.; Freckmann, D.M.M.; Schumann, H. *Chem. Rev.* **2002**, *102*, 1851.

32. Hitchcock, P.B.; Lappert, M.F.; Smith, R.G.; Bartlett, R.A.; Power, P.P. *J. Chem. Soc., Chem. Commun.* **1988**, 1007.

33. a) Avent, A.G.;.Caro, C.F; Hitchcock, P.B.; Lappert, M.F.; Li, Z.; Wei, X.H. *Dalton Trans.* **2004**, 1567,
b) Niemeyer, M. *Acta Crystallogr,* **2001**, *E57*, m553,
c) Schumann, H.; Freckmann, D.M.M.; Dechert, S.
Z. Anorg. Allg. Chem. **2002**, *628*, 2422,
d) Schaverien, C.J.; van Mechelen, J.B. *Organometallics* **1991**, *10*, 1704,
e) Arndt, S.; Zeimentz, P.M., Spaniol, T.P.; Okuda, J.; Honda, M. Tatsumi, K. *Dalton Trans.* **2003**, 3622,
f) Herbrich, T.; Thiele, K.H.; Thewalt, U.
Z. Anorg. Allg. Chem. **1996**, 622, 1609,
g) Atwood, J.L.; Hunter, W.E.; Rogers, R.D.; Holton, J.; McMeeking, J.; Pearce, R.; Lappert, M.F. *J. Chem. Soc., Chem. Commun.* **1978**, 140.

34. Schumann, H.; Genthe, W.; Hahn, E.; Pickardt, J.; Schwarz, H.; Eckart, K. *J. Organomet. Chem.* **1986**, *306*, 215.

35. Niemeyer, M. *Z. Anorg. Allg. Chem.* **2000**, *626*, 1027.

36. a) Harder, S. *Angew. Chem., Int.Ed.* **2004**, *43*, 2714,
b) Qi, G; Nitto, Y.; Saiki, A.; Tomohiro, T.; Nakayama, Y.; Yasuda, H. *Tetrahedron* **2003**, *59*, 10409,
c) Hitchcock, P.B. Khvostov, A.V.; Lappert, M.F.
J. Organomet. Chem. **2002**, *663*, 263,
d) Clegg, W.; Eaborn, C.; Izod, K.; O'SHaughnessy, P.O.; Smith, J.D.

Angew.Chem.,Int.Ed. **1997**, *36*, 2815,

e) Eaborn, C.; Hitchcock, P.B.; Izod, K.; Lu, Z.R.; Smith, J.D. *Organometallics* **1996**, *15*, 4783.

37. a) Rabe, G.W.; Zhang-Presse, M.; Reiderer, F.A.; Yap, G.P.A. *Inorg. Chem.* **2003**, *42*, 3527,

b) Niemeyer, M. *Acta Crystallogr,* **2001**, *E57*, m578,

c) Rabe, G.W.; Zhang-Presse, Riederer, F.A.; Golen, J.A.; Incarvito, C.D.; Rheingold, A.L. *Inorg. Chem.* **2003**, *42*, 7587,

d) Ihara, E.; Adachi, Y.; Yasuda, H.; Hashimoto, H.; Kanehisa, N.; Kai, Y. *J. Organomet. Chem.***1998**, *569*, 147,

e) Cotton, S.A.; Hart, F.A.; Hursthouse, M.B.; Welch, A.J. *J. Chem. Soc., Chem. Commun.* **1972**, 1225,

f) Rabe, G.W.; Strissel, C.S.; Liable-Sands, L.M.; Concolino, T.E.; Rheingold, A.L. *Inorg. Chem.* **1999**, *38*, 3446,

g) Heckmann, G.; Niemeyer, M. *J. Am. Chem. Soc.* **2000**, *122*, 4227,

h) Rabe, G.W.; Bérubé, C.D.; Yap, G.P.A.; Lam, K.C.; Concolino, T.E.; Rheingold, A.L. *Inorg. Chem.* **2002**, *41*, 1446,

i) Rabe, G.W.; Bérubé, C.D.; Yap, G.P.A. *Inorg. Chem.* **2001**, *40*, 2682,

j) Rabe, G.W.; Rhatigan, B.; Golen, J.A.; Rheingold, A.L. *Acta Crystallogr.* **2003**, *E59*, m99,

k) Forsyth, C.M.; Deacon, G.B. *Organometallics* **2000**, *19*, 1205.

38. a) Woodman, T.J.; Schormann, M.; Hughes, D.L.; Bochmann, M. *Organometallics* **2004**, *23*, 2972,

b) Kuehl, C.J.; Simpson, C.K.; John, K.D.; Sattelberger, A.P.; Carlson, C.N.; Hanusa, T.P. *J. Organomet. Chem.* **2003**, *683*, 149,

c) Simpson, C.K.; White, R.E.; Carlson, C.N.; Wrobleski, D.A.; Kuehl, C.J.; Croce, T.A.; Steele, I.M.; Scott, B.L.; Young, V.G. Junior; Hanusa, T.P.; Sattelberger, A.P.; John, K.D. *Organometallics* **2005**, *24*, 3685,

d) Taube, R.; Windisch, H.; Weisenborn, H.; Hemling, H.; Schumann, H. *J. Organomet. Chem.* **1997**, *548*, 229,

e) Wu, W.; Chen, M.; Zhou, P. *Organometallics* **1991**, *10*, 98,

f) Taube, R; Maiwald, S; Sieler, J. *J. Organomet. Chem.* **2001**, *621*, 327.

39. a) Hitchcock, P. B.; Lappert, M. F.; Tian, S. *J. Organomet. Chem.* **1997**, *549*, 1,

b) Caro, C. F.; Lappert, M. F.; Merle, P. G.
Coord. Chem. Rev. **2001**, *219*, 605.

40. a) Weng, W.; Kunze, K.; Arif, A.M.; Ernst, R.D.
Organometallics **1991**, *10*, 3643,
b) Kunze, K.; Arif, A.M.; Erns, R.D. *Bull. Soc. Chim. Fr.* **1993**, *130*, 708,
c) Baudry, D.; Nief, F.; Ricard, L. *J. Organomet. Chem.* **1994**, *482*, 125.
41. a) Ninghai, H.; Lixin, G.; Zhongsheng, J.; Wenqi, C. *Wuji Huaxue Xuebao(Chin. J. Inorg. Chem.)* **1989**, *5*, 107,
b) Schumann, H.; Dietrich, A. *J. Organomet. Chem.* **1991**, *401*, C33,
c) Zhang, S.; Chui, D.; Cheng, J.; Jin, J; Hu, N; Chen, W.; Liu, J. *Yingyong Huaxue (Chin. J. Appl. Chem.)* **2001**, *18*, 330,
d) Qiu, X.; Lio, J. *Chin. J. Chem.* **1991**, *9*, 10,
e) Zielinski, M.B.; Drummond, D.K.; Iyer, P.S.; Leman, J.T.; Evans, W.J.
Organometallics **1995**, *14*, 3724.
42. Wayda, A.L.; Mukerji, I.; Dye, J.L.; Rogers, R.D.
Organometallics **1987**, *6*, 1328.
43. a) Kinsley, S.A.; Streitwieser, A. Junior; Zalkin, A.
Acta Crystallogr, **1986**, *C42*, 1092,
b) Evans, W.J.; Schreeve, J.L.; Ziller, J.W. *Polyhedron* **1995**, *14*, 2945.
44. a) Kilimann, U.; Schafer, M.; Herbst-Irmer, R.; Edelmann, F.T. *J. Organomet. Chem.* **1994**, *469*, C10,
b) Cendrowski-Guillaume, S.M.; Nierlich, M.; Lance, M.; Ephritikhine, M.
Organometallics **1998**, *17*, 786,
c) Mashima, K.; Takaya, H. *Tetrahedron Lett.* **1989**, *30*, 3697,
d) Fedushkin, I.L.; Bochkarev, M.N.; Dechert, S.; Schumann, H.
Chem. Eur. J. **2001**, *7*, 3558,
e) Visseaux, M.; Nief, F.; Ricard, L. *J. Organomet. Chem.* **2002**, *647*, 139.
45. a) Wetzel, T.G.; Dehnen, S.; Roesky, P.W. *Organometallics* **1999**, *18*, 3835,
b) Kinsley, S.A.; Streitweiser, A. Junior; Zalkin, A.
Organometallics **1985**, *4*, 52,
c) Hodgson, K.O.; Raymond, K.N. *Inorg. Chem.* **1972**, *11*, 3030,
d) Boussie, T.R.; Eisenberg, D.C.; Rigsbee, J.; Streitweiser, A. Junior; Zalkin, A. *Organometallics* **1991**, *10*, 1922,
e) Kilimann, U.; Schafer, M.; Herbst-Irmer, R.; Edelmann, F.T.

J. Organomet. Chem. **1994**, *469*, C15,

f) Poremba, P.; Reissmann, U.; Noltemeyer, M.; Schmidt, H.G.; Bruser, W.; Edelmann, F.T. *J. Organomet. Chem.* **1997**, *544*, 1,

g) Anfang, S.; Seybert, G.; Harms, K.; Geiseler, G.; Massa, W.; Dehnicke, K. *Z. Anorg. Allg. Chem.* **1998**, *624*, 1187,

h) Rabe, G.W.; Zhang-Presse, M.; Golen, J.A.; Rheingold, A.L. *Acta Crystallogr,* **2003**, *E59*, m255,

i) Jizhu, J.; Zhongsheng, J.; Gecheng, W.; Wenqi, C.; Yin, Z. *Wuji Huazue Xuebao (Chin. J. Inorg. Chem.)* **1993**, *9*, 326.

46. a) Boussie, T.R.; Eisenberg, D.C.; Rigsbee, J.; Streitweiser, A. Junior; Zalkin, A. *Organometallics* **1991**, *10*, 1922,

b) Kilimann, U.; Herbst-Irmer, R.; Stalke, D.; Edelmann, F.T. *Angew. Chem., Int. Ed. Engl.* **1994**, *33*, 1618,

c) Kurras, E.; Kruger, C. *Private Communication* **2004**, CCDC 256935.

47. a) Quitmann, C.C.; Muller-Buschbaum, K. *Z. Anorg. Allg. Chem.* **2004**, *630*, 2422,

b) Quitmann, C.C., Muller-Buschbaum, K. *Z. Kristallogr.* **2005**, *220*, 158.

48. a) Schumman, H.; Winterfeld, J.; Hemling, H.; Kuhn, N. *Chem. Ber.* **1993**, *126*, 2657,

b) Ganesan, M.; Derube, C.D.; Gambarotta, S.; Yap, G.P.A. *Organometallics* **2002**, *21*, 1707.

49. a) Schumann, H.; Rosenthal, E.C.E.; Winterfeld, J.; Kociok-Kohn, G. *J. Organomet. Chem.* **1995**, *495*, 12,

b) Schumann, H.; Rosenthal, E.C.E.; Winterfeld, J.; Weimann, R.; Demtschuk, J. *J. Organomet. Chem.* **1996**, *507*, 287.

50. a) Nief, F.; de Borms, B.T.; Ricard, L.; Carmichael, D. *Eur. J. Inorg. Chem.* **2005**, 637,

b) Nief, F.; Ricard, L.; Mathey, F. *Polyhedron* **1993**, *12*, 19,

c) Nief, F.; Ricard, L.; Mathey, F. *J. Organomet. Chem.* **1994**, *464*, 149,

d) Nief, F.; Turcitu, D.; Ricard, L. *J. Chem. Soc., Chem. Commun.* **2002**, 1646,

e) Turcitu, D.; Nief, F.; Ricard, L. *Chem. Eur. J.* **2003**, *9*, 4916.

51. a) Nief, F.; Riant, P.; Ricard, L.; Desmurs, P.; Baudry-Barbier, D. *Eur. J. Inorg. Chem.* **1999**, 1041,

b) Barbier-Baudry, D.; Heiner, S.; Kubicki, M.M.; Vigier, E.; Visseaux, M.; Hafid, A. *Organometallics* **2001**, *20*, 4207.

52. a) Pfeiffer, D.; Ximba, B.J.; Liable-Sands, L.M.; Rheingold, A.L.; Heeg, M.J.; Coleman, D.M.; Schlegel, H.B.; Kuech, T.F.; Winter, C.H. *Inorg. Chem.* **1999**, *38*, 4539,
b) Quitman, C.C.; Muller-Buschbaum, K. *Z. Anorg. Allg. Chem.* **2005**, 631, 1191,
c) Deacon, G.B.; Delbridge, E.E.; Skelton, B.W.; White, A.H. *Eur. J. Inorg. Chem.* **1999**, 751,
d) Deacon, G.B.; Delbridge, E.E.; Evans, D.J.; Harika, R.; Junk, P.C.; Skelton, B.W.; White, A.H. *Chem. Eur. J.* **2004**, *10*, 1193,
e) Deacon, G.B.; Delbridge, E.E.; Skelton, B.W.; White, A.H. *Angew. Chem. Int. Ed.* **1998**, *37*, 2251,
f) Deacon, G.B.; Delbridge, E.E.; Fallon, G.D.; Jones, C.; Hibbs, D.E.; Hursthouse, M.B.; Skelton, B.W.; White, A.H. *Organometallics* **2000**, *19*, 1713,
g) Deacon, G.B.; Forsyth, C.M.; Wilkinson, D.L. *Chem. Eur. J.* **2001**, *7*, 1784
h) Deacon, G.B.; Delbridge, E.E.; Skelton, B.W.; White, A.H. *Eur. J. Inorg. Chem.* **1998**, 543,
i) Cosgriff, J.E.; Deacon, G.B.; Gatehouse, B.M. *Aust. J. Chem.* **1993**, *46*, 1881,
j) Deacon, G.B.; Forsyth, C.M.; Junk. P.C. *Eur. J. Inorg. Chem.* **2005**, 817,
k) Cosgriff, J.E.; Deacon, G.B.; Gatehouse, B.M.; Hemling, H.; Schumann, H. *Angew. Chem., Int. Ed. Engl.* **1993**, *32*, 874.

53. Quitman, C.C.; Muller-Buschbaum, K. *Z. Naturforsch., B:Chem. Sci.* **2004**, *59*, 562.

54. Marques, N.; Sella, A.; Takats, J. *Chem. Rev.* **2002**, *102*, 2137.

55. Hillier, A.C.; Zhang, X.W̃.; Maunder, G.H.; Liu, S.Y.; Eberspacher, T.A.; Metz, M.V.; McDonald, R.; Domingos, Â.; Marques, N.; Day, V.W.; Sella, A.; Takats, J. *Inorg. Chem.* **2001**, *40*, 5106.

56. Korobkov, I.; Aharonian, G.; Gambarotta, S.; Yap, G.P.A. *Organometallics* **2002**, *21*, 4899.

57. Dubé, T.; Freckman, D.; Conoci, S.; Gambarotta, S.; Yap, G.P.A. *Organometallics* **2000**, *19*, 209.

58. a) Campazzi, E.; Solari, E.; Scopelliti, R.; Floriani, C.
J. Chem. Soc., Chem. Commun. **1999**, 1617,
b) Campazzi, E.; Solari, E.; Scopelliti, R.; Floriani, C.
Inorg. Chem. **1999**, *38*, 6240,
c) Dubé, T.; Gambarotta, S.; Yap, G.P.A.
Angew. Chem., Int. Ed. Engl. **1999**, *38*, 1432,
d) Dubé, T.; Guan, J.; Gambarotta, S.; Yap, G.P.A.
Chem. Eur. J. **2001**, *7*, 374,
e) Campazzi, E.; Solari, E.; Floriani, C.; Scopelliti, R.
J. Chem. Soc., Chem. Commun. **1998**, 2603,
f) Jubb, J.; Gambarotta, S. *J. Am. Chem. Soc.* **1994**, *116*, 4477,
g) Korobkov, I.; Aharonian, G.; Gambarotta, S.; Yap, G.P.A.
Organometallics **2002**, *21*, 4899.
59. a) Davies, N.W.; Frey, A.S.P.; Gardiner, M.G.; Wang, J.
J. Chem. Soc., Chem. Commun. **2006**, 4853,
b) Wang, J.; Dick, A.K.J.; Gardiner, M.G.; Yates, B.F.; Peacock, E.J.;
Skelton, B.W.; White, A.H. *Eur. J. Inorg. Chem.* **2004**, 1992,
c) Wang, J.; Amos, R.I.J.; Frey, A.S.P.; Gardiner, M.G.; Cole, M.L.; Junk,
P.C. *Organometallics* **2005**, *24*, 2259,
d) Wang, J.; Gardiner, M.G.; Skelton, B.W.; White, A.H.
Organometallics **2005**, *24*, 815,
e) Frey, A.S.P.; Gardiner, M.G.; Stringer, D.N.; Yates, B.F.
Organometallics **2007**, *26*, 1299.

Chapter 2. Syntheses of macrocyclic lanthanide complexes

2.1. Introduction to macrocyclic lanthanide complexes

2.1.1. Overview of macrocyclic lanthanide chemistry

The utilisation of macrocyclic ligand frameworks in lanthanide chemistry has been well reported and reviewed elsewhere for inorganic systems,[1] with applications in such areas as luminescence,[2] NMR spectroscopy shift reagents and MRI contrast agents.[3] However, reports of organometallic macrocyclic lanthanide compounds are far less abundant in the literature. Organometallic macrocyclic lanthanide complexes typically employ multi-dentate donor atom functionalised ligands such as deprotonated azacrown ethers, calixarenes, porphyrins and porphyrinogens, with both σ- and π- bonding observed, though σ- bonding is most common.

2.1.2. Macrocyclic non-pyrrole lanthanide complexes.

Azacrown ethers have been reported in relative abundance as ligands for coordination compounds, however their use as deprotonated ligands in organolanthanide chemistry has been limited to one report of the Yb(II), (**LIX**), Ce(III), (**LX**), and Sm(III), (**LXI**), complexes of the deprotonated diazacrown ether 4,13-diaza-18-crown-6 ($DACH_2$), (**LXII**). Each complex was synthesised *via* metallation of the macrocyclic ligand with the lanthanide amide precursors, $[Ce\{N(SiMe_3)_2\}_3]$, (**LXIII**), $[Sm\{N(SiMe_3)_2\}_2]$, (**LXIV**), and $[Yb\{N(SiMe_3)_2\}_2]$, (**LXV**), to yield the isostructural Ce and Sm mononuclear complexes, $[Ln(DAC)\{N(SiMe_3)_2\}]$, and the trinuclear Yb complex, $[\{(\{Me_3Si\}_2N)Yb(\mu\text{-}DAC)\}_2Yb]$, (**LIX**). The trivalent $[Sm(DAC)\{N(SiMe_3)_2\}]$, (**LXI**) complex, resulting from the reaction of $DACH_2$ with the divalent amide **LXIV** was thought to result from reduction of a $DACH_2$ N-H bond[4]

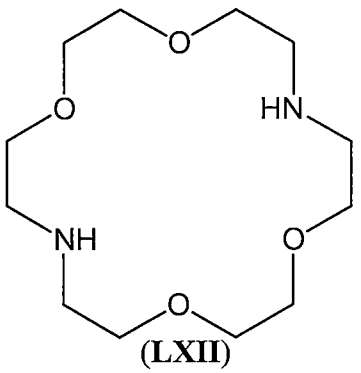

(LXII)

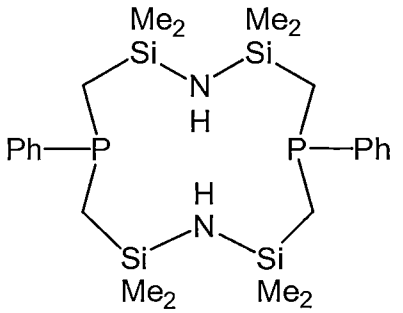

(LXVI)

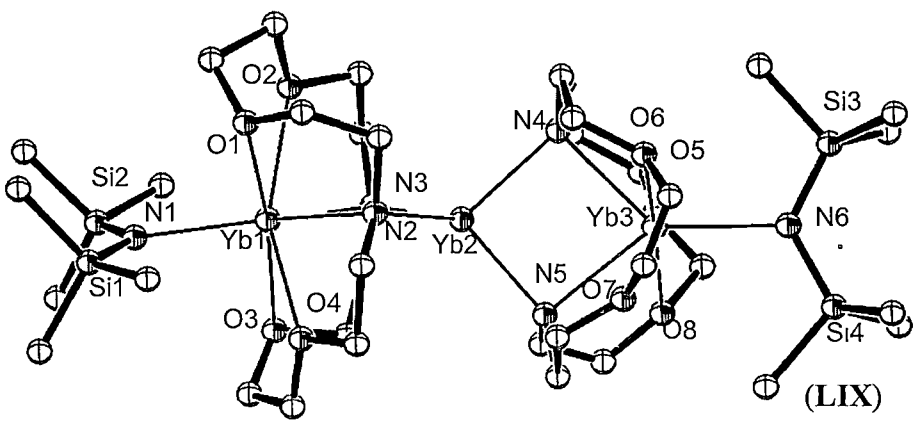

(LIX)

Figure 2.1. Representations of the $DACH_2$ and $P_2N_2H_2$ ligands (top) and the molecular structure of the Yb DAC trinuclear complex, $[\{(\{Me_3Si\}_2N)Yb(\mu\text{-}DAC)\}_2Yb]$, (**LIX**) (bottom). Figure generated from CCDC obtained coordinates. Atoms of arbitrary size. H atoms are omitted for clarity.

Analogous to the synthesis of the azacrown ether complexes, **LIX-LXI**, the mixed bis(amidophosphane) ligand, $PhP\{CH_2SiMe_2N(H)SiMe_2CH_2\}_2PPh$, ($P_2N_2H_2$), (**LXVI**), has also been used to synthesise the lanthanide complexes $[\{(P_2N_2)M\}_2(\mu\text{-}Cl)_2]$, where M = Sm, (**LXVII**), Ho, (**LXVIII**), Yb, (**LXIX**), Lu, (**LXX**).[5] The macrocyclic lanthanide complexes were synthesised *via* metathetical exchange reactions involving the dilithiated macrocycle and the corresponding metal trichloride. For M = Lu, an X-ray crystal structure determination was undertaken, revealing a chloride bridged dimeric Lu(III) species, (**LXX**).

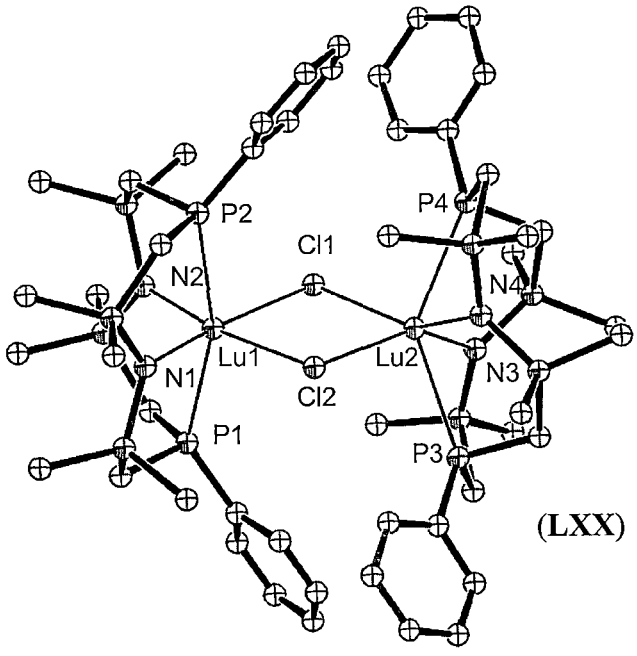

(LXX)

Figure 2.2. Molecular structure of the chloride bridged dimeric Lu macrocyclic complex **LXX**. Figure generated from CCDC obtained coordinates. Atoms of arbitrary size. H atoms are omitted for clarity.

2.1.3. Lanthanide complexes of metallated calix[4]arene ligands.

Similar to the utilisation of macrocyclic crown ethers and their related derivatives, calixarene ligands have been well studied with respect to their lanthanide coordination chemistry. Non-aqueous lanthanide complexes employing calixarene ligands form lanthanide aryloxide complexes when deprotonated through the phenolic oxygen atoms. Due to the relative ease with which the phenolic O atoms may be deprotonated, the synthesis of such organolanthanide complexes typically involves either direct metallation of the calixarene ligand through redox processes involving lanthanide(II) reagents or proton abstraction using lanthanide amide reagents. The most widely used calixarene ligand applied to lanthanide chemistry are those based on *para-t*-butylcalix[4]arene, (**LXXI**) which may be substituted at one or more O atom positions to give tetra-, tri-, di-, or mono- anionic ligands when deprotonated through the remaining hydroxyl group(s).[6] When bound to lanthanide elements, calix[4]arene ligands in non-aqueous complexes have always adopted a cone conformation, with 4 η^1- O interactions.

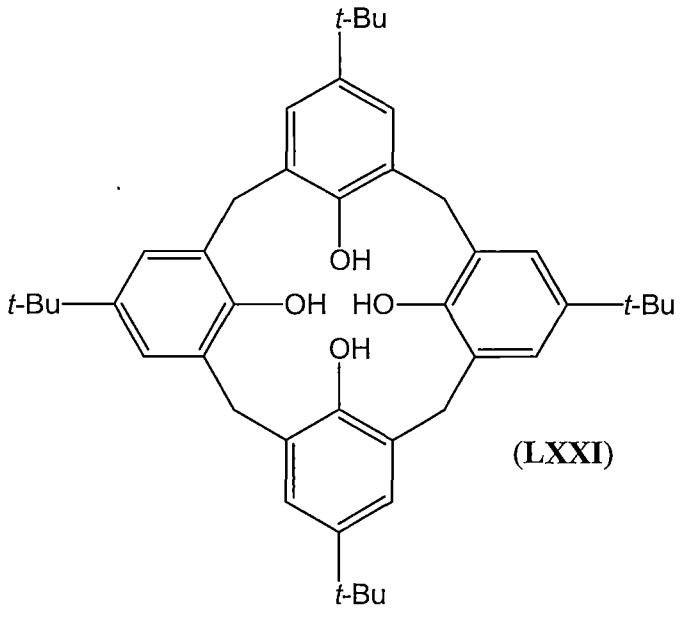

(LXXI)

Figure 2.3. *para-t*-butylcalix[4]arene, (**LXXI**).

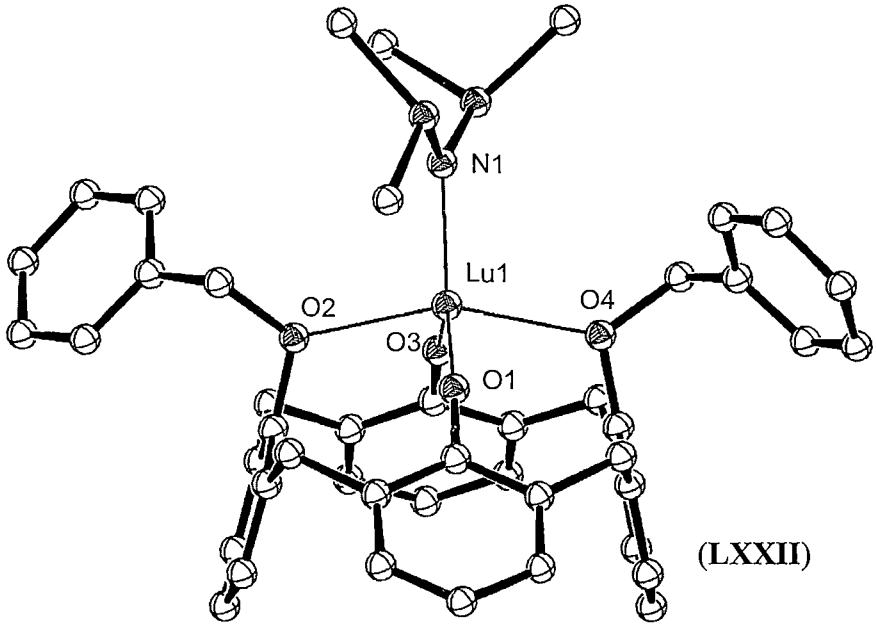

(LXXII)

Figure 2.4. Molecular structure of a benzylated calix[4]arene Lu amide **LXXII** which exhibits the typical cone conformation observed in lanthanide complexes of calix[4]arene ligands.[7] Figure generated from CCDC obtained coordinates. Atoms of arbitrary size. H atoms are omitted for clarity.

Lanthanide calix[4]arene complexes bearing halide substituents resulting from the reaction of lanthanide halide precursors with calix[4]arene ligands are limited to a monomeric thullium(III) iodide, (**LXXIII**),[6a] and a chloride bridged samarium(III) dimer (**LXXIV**) based on deprotonated *trans*-O,O′-dimethyl substituted *t*-

butylcalix[4]arene, as shown in Figure 2.5.[6b] Whilst the Lewis base solvent in each complex is different (Et_2O for Tm, THF for Sm), the observed tendency for aggregation in the samarium case is consistent with the larger atomic radii of samarium.

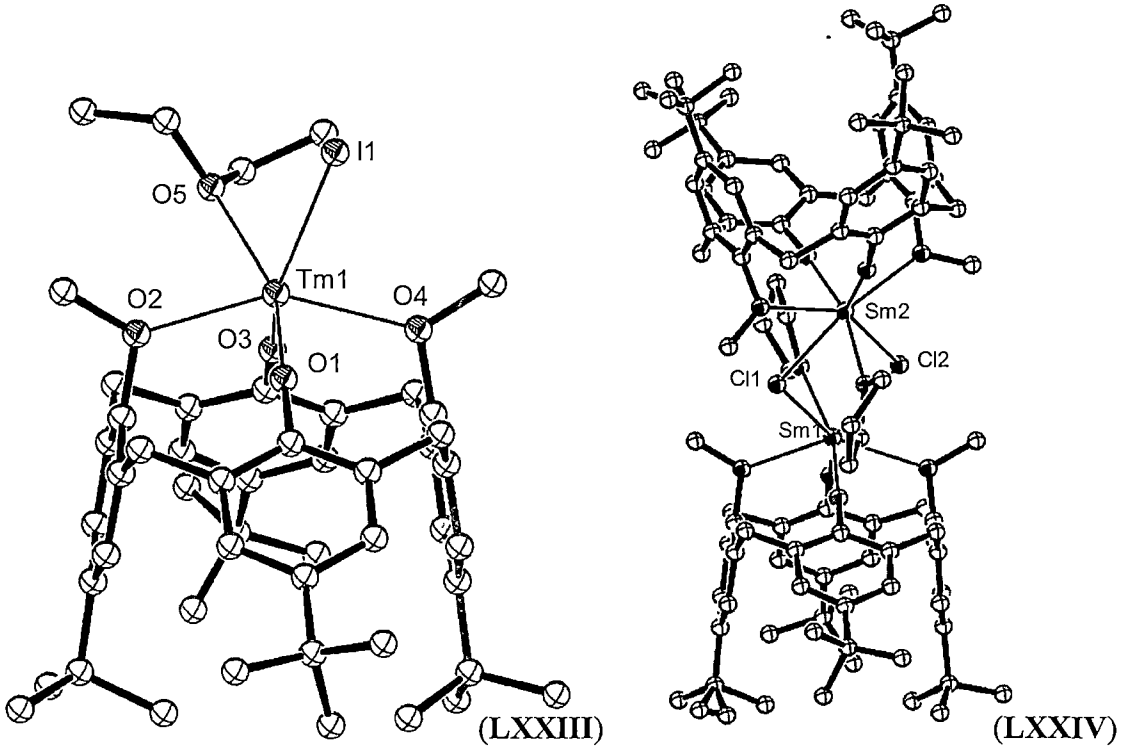

Figure 2.5. Molecular structures of the calixarene lanthanide halide complexes, (**LXXIII**) and (**LXXIV**). Figure generated from CCDC obtained coordinates. Atoms of arbitrary size. H atoms are omitted for clarity.

2.1.4. Lanthanide complexes of pyrrolide containing macrocycles.

Porphyrin complexes of the lanthanides are also dominated by inorganic coordination compounds, which have been extensively investigated, typically forming anionic sandwich complexes, with η^1 interactions forming between a lanthanide centre and the nitrogen atoms of doubly deprotonated porphyrins.[8] The larger size of the lanthanides prevents the metal centres from binding within the plane of the porphyrin as observed for smaller transition metals such as Fe. Despite the extensive research into lanthanide porphyrin coordination complexes, few reports of non-aqueous organometallic species have been made. Investigation into lanthanide based near-infrared luminescent complexes have yielded a number of porphyrin complexes differing from the typical sandwich structure, such as the mixed

tetra(pyrazolyl)borate porphyrin complex, $[(Ph_4N_4)Yb\{(N_2C_3H_3)_3BH\}]$, (**LXXV**) shown in Figure 2.6.[9]

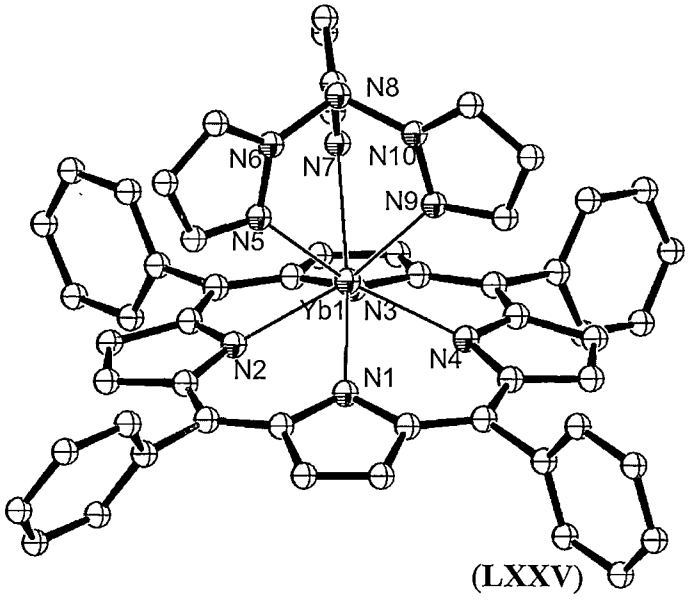

(**LXXV**)

Figure 2.6. Mixed porphyrin/tetra(pyrazolyl)borate ytterbium complex, $[(Ph_4N_4)Yb\{(N_2C_3H_3)_3BH\}]$, (**LXXV**). Figure generated from CCDC obtained coordinates. Atoms of arbitrary size. H atoms are omitted for clarity.

As discussed in Section 1.2.7., metallated macrocyclic porphyrinogen ligands have been successfully employed as ligands for the synthesis of organolanthanide reagents in both +2 and +3 oxidation states. Synthetic methods for the formation of lanthanide porphyrinogen complexes predominantly involve metathetical exchange reactions between the metallated ligand and lanthanide halide species, yielding lanthanide(II) and (III) complexes of varying structural motifs, often featuring the retention of Group I metal cations and halide anions.

The binding of metallated porphyrinogen ligands to lanthanide elements has been shown to relate to the ubiquitous lanthanocene systems, with the pyrrolide anions present within the macrocyclic ligands capable of binding to lanthanide centres through η^5, η^3 or η^1 interactions, similar to that observed for cyclopentadienyl systems.[10] Typically, metallated porphyrinogens bind to lanthanide centres through an η^5: η^1: η^5: η^1 bonding motif and adopt the 1,3-alternate macrocyclic conformation.

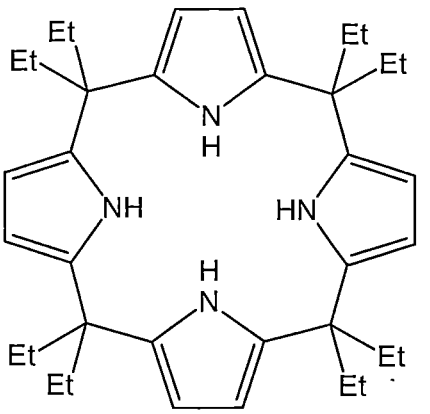

Figure 2.7. *meso*-octaethylporphyrinogen, ($Et_8N_4H_4$), (**LXXVI**).

The reaction of the sodium salt of *meso*-octaethylporpyrinogen, [$Et_8N_4Na_4(THF)_3$], (**LXXVII**) with lanthanide trichlorides gave lanthanide(III) complexes of the macrocycle which retained a sodium counter-ion in the macrocyclic cavity giving bimetallic complexes which were monomeric when solvated by THF, as shown in Figure 1.29 in Section 1.2.7. for [$(THF)_2Na(Et_8N_4)Gd(THF)$], (**LVII**), or dimeric in the presence of dioxane,[10] as shown in Figure 2.8, below, for [{(η^5: η^1: η^5: η^1-Et_8N_4)Nd(DME)}Na(dioxane)1.5], (**LXXVIII**). The sodium incorporated monomeric and dimeric structures of the lanthanide complexes of *meso*-octaethylporphyrinogen shown are typical of the organolanthanide complexes of tetra-anionic porphyrinogen ligands, exhibiting the typical η^5: η^1: η^5: η^1 bonding motif and adopting the 1,3-alternate macrocyclic conformation.[11]

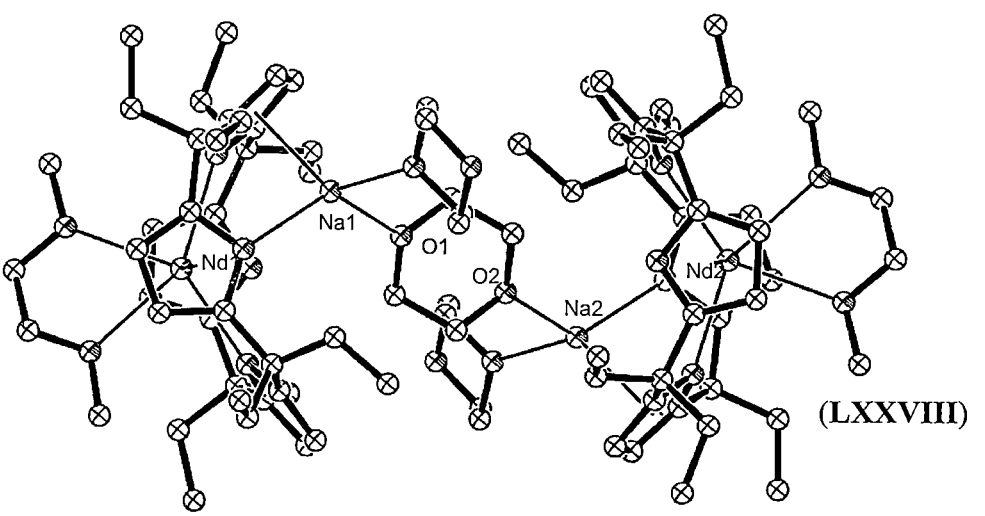

(**LXXVIII**)

Figure 2.8. Structure of the dioxane bridged *meso*-octaethylporphyrinogen lanthanide complex [{(η^5: η^1: η^5: η^1-Et_8N_4)Nd(DME)}-η^3-Na(dioxane)1.5], (**LXXVIII**). Figure generated from CCDC obtained coordinates. Atoms of arbitrary size.

The incorporation of two lanthanide(III) centres in the macrocyclic cavity of tetrametallated *meso*-octaethylporphyrinogen resulted from the reaction of $SmCl_3(THF)_3$ with half an equivalent of the tetra-lithiated porphyrinogen, yielding the disamarium(III) halide complex $[(Et_8N_4)Sm_2\{(\mu\text{-}Cl)_2[Li(THF)_2]\}_2]$, (**LXXIX**).[11g]

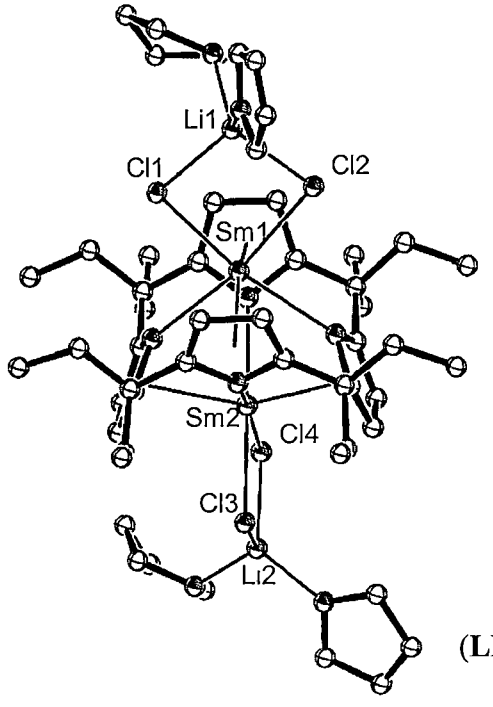

(**LXXIX**)

Figure 2.9. Molecular structure of the macrocyclic disamarium(III) halide complex, $[(Et_8N_4)Sm_2\{(\mu\text{-}Cl)_2[Li(THF)_2]\}_2]$, (**LXXIX**). Figure generated from CCDC obtained coordinates. Atoms of arbitrary size. H atoms are omitted for clarity.

Lanthanide(II) complexes of tetrametallated porphyrinogens are less abundant than lanthanide(III) complexes, though a number have been reported. Bimetallic samarium(II) complexes of porphyrinogen ligands have been prepared from metathetical exchange reactions between SmI_2 and Group 1 salts of the macrocycle, as well as from reduction of trivalent Sm(III) complexes, and deprotonation by $[Sm\{N(SiMe_3)_2\}_2]$, (**LXIV**). The resulting bimetallic Sm(II) complexes formed alkali metal and halide free motifs,[11g,12] with the Sm centres adopting $\eta^5{:}\eta^1{:}\eta^5{:}\eta^1$ interactions within opposite ends of the macrocyclic cavity, as shown in Figure 2.10. Mononuclear alkali metal and halide incorporating samarium(II) complexes have also been isolated from similar synthetic methods, as shown in Figure 2.11.[11g,h]

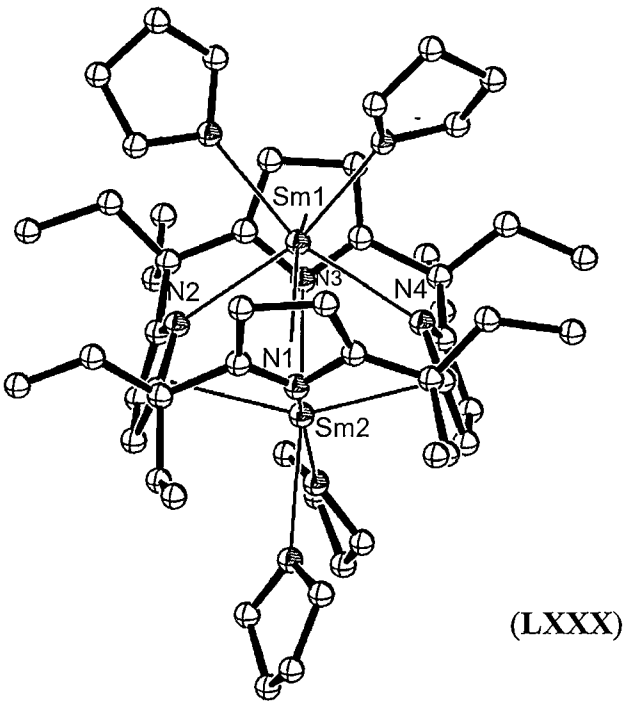

(LXXX)

Figure 2.10. Molecular structure of the bimetallic alkali metal and halide free samarium(II) porphyrinogen complex, $[(Et_8N_4)\{Sm(THF)\}_2]$, (**LXXX**). Figure generated from CCDC obtained coordinates. Atoms of arbitrary size. H atoms are omitted for clarity.

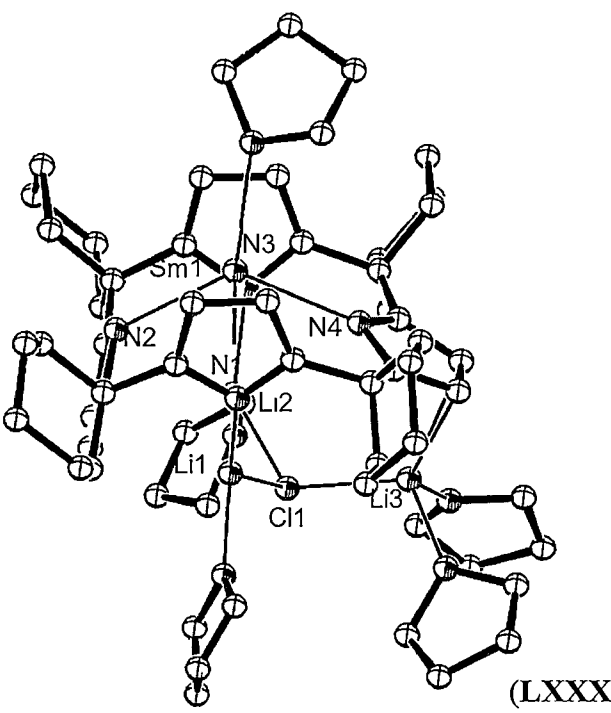

(LXXXI)

Figure 2.11. Structure of the samarium(II) porphyrinogen complex, $[\{(THF)Li\}_2(c\text{-}hex_4N_4)Sm(THF)(\mu^3\text{-}Cl)Li(THF)_2]$ (**LXXXI**), which retains Li and Cl ions.[11h] Figure generated from CCDC obtained coordinates. Atoms of arbitrary size.

Recent modifications of the porphyrinogen ligand in our research group through *N,N'*-dimethylation, or *trans*-difuran substitution gave the macrocycles *trans-N,N'*-dimethyl-*meso*-octaethylporphyrinogen, ($Et_8N_4Me_2H_2$), (**LXXXII**) and *meso*-octaethyl-*trans*-dioxaporphyrinogen, ($Et_8N_2O_2H_2$), (**LXXXIII**), which, when deprotonated, gave dianionic ligands utilised in organolanthanide syntheses. The reaction of the potassium salt of the *N,N'* dimethylated porphyrinogen, $[(Et_8N_4Me_2)K_2(THF)_2]_n$, (**LXXXIV**) with samarium diiodide, gave the corresponding halide free Sm(II) macrocyclic complex $[(Et_8N_4Me_2)Sm(THF)_2]$, (**LVIII**), as shown in Figure 1.30, Section 1.2.7. Oxidation of this compound with *t*-butylchloride gave the corresponding samarium(III) macrocyclic chloride complex, $[\{(Et_8N_4Me_2)Sm(\mu\text{-}Cl)\}_2]$, (**LXXXV**), which exhibited a halide bridged dimeric structure, as shown in Figure 2.12.[13] Most lanthanide complexes of both metallated modified porphyrinogens exhibit the typical 1,3-alternate macrocyclic conformation and $\eta^5{:}\eta^1{:}\eta^5{:}\eta^1$ binding mode, common to the N_4^{4-} porphyrinogens. η^5 Interactions were observed to involve the neutral pyrrolyls in ($Et_8N_4Me_2$) by necessity of the *N*-methyl substituents limiting the macrocyclic conformation, also shown in Figure 2.12.

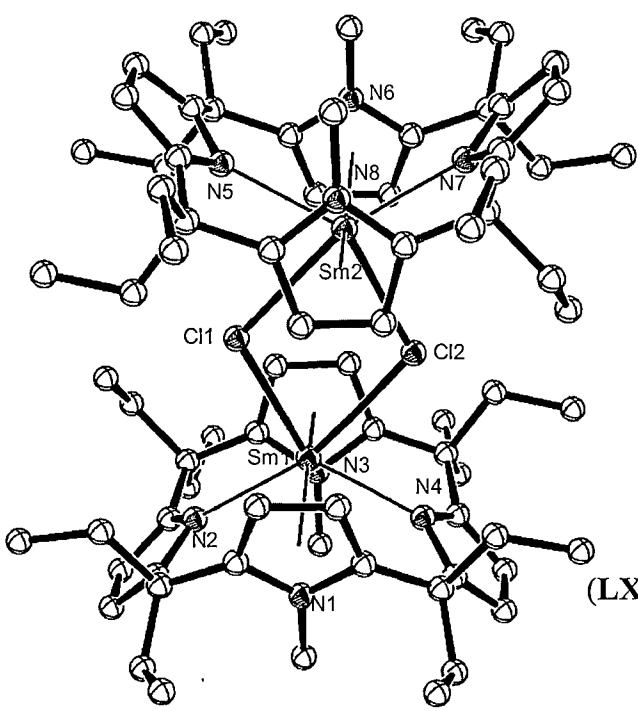

(**LXXXV**)

Figure 2.12. Molecular structure of $[\{(Et_8N_4Me_2)Sm\text{-}\mu\text{-}Cl\}_2]$, (**LXXXV**). Atoms are shown with arbitrary radii. H atoms are omitted for clarity.

The reaction of the THF solvate of the potassium salt of the difuran substituted macrocycle, $[(Et_8N_2O_2)K_2(THF)_4]$, (**LXXXVI**), with samarium diiodide gave the green divalent samarium complex $[(THF)_2K(Et_8N_2O_2)Sm(\mu\text{-}I)\}_2]$, (**LXXXVII**), which retained KI through binding of the K centre to the base of the macrocyclic cavity and iodide by forming bridging interactions to the samarium centres. The macrocyclic ligand in **LXXXVII** also exhibited a 1,3-alternate macrocyclic conformation and $\eta^5{:}\eta^1{:}\eta^5{:}\eta^1$ binding mode as shown in Figure 2.13.[14] In this instance, the conformational restraints imposed by the *N*-methyl substituents of $(Et_8N_4Me_2)$ were not applicable, and the binding mode of the macrocycle was reversed such that η^5 interactions were observed to involve the pyrrolides, whilst the furanyl O atoms exhibited η^1 bonding to the samarium centre.

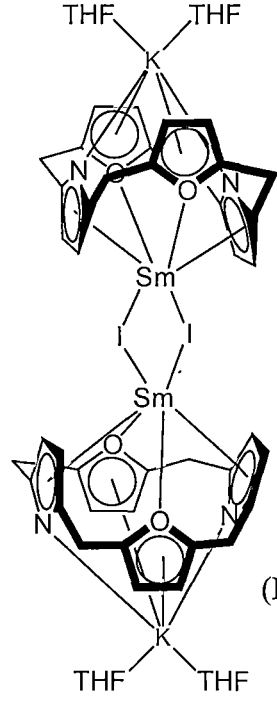

(LXXXVII)

Figure 2.13. Schematic representation of the samarium(II) *meso*-octaethyl-*trans*-dioxaporphyrinogen $[(THF)_2K(Et_8N_2O_2)Sm(\mu\text{-}I)\}_2]$ (**LXXXVII**).

The dipotassium precursor $[(Et_8N_2O_2)K_2(THF)_4]$, (**LXXXVI**), used in the synthesis of **LXXXVII** was prepared *via* metallation of *meso*-octaethyl-*trans*-dioxaporphyrinogen, (**LXXXIII**) through the two pyrrolyl N-H atoms using potassium metal. Recrystallisation of **LXXXVI** from TMEDA gave crystals suitable for X-ray diffraction studies determined to be $[(Et_8N_2O_2)K_2(TMEDA)_2]$,

(**LXXXVIII**) which also exhibited a 1,3-alternate macrocyclic conformation, as shown in Figure 2.14.[15]

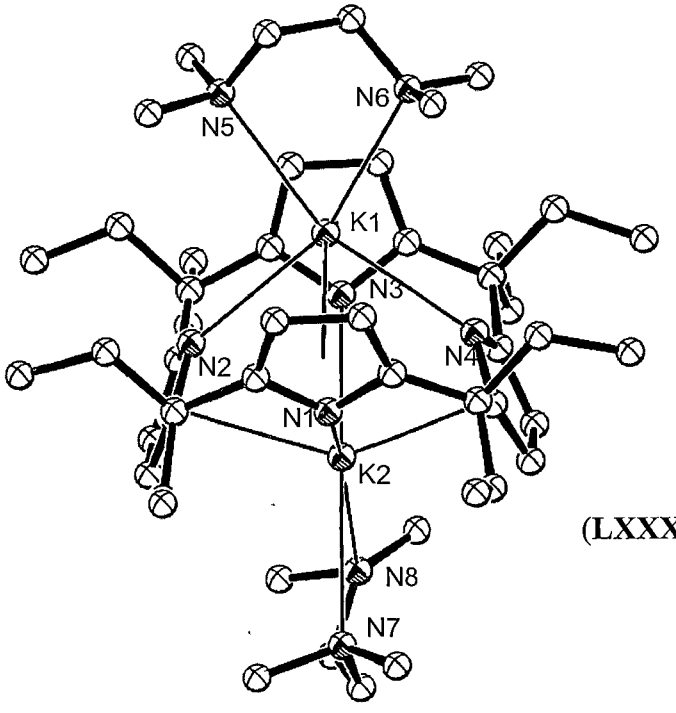

(**LXXXVIII**)

Figure 2.14. Structure of the dipotassium salt of deprotonated *meso*-octaethyl-*trans*-dioxaporphyrinogen, $[(Et_8N_2O_2)K_2(TMEDA)_2]$, (**LXXXVIII**). Atoms are shown with arbitrary radii. H atoms are omitted for clarity.

Prior to the reported synthesis of $[(Et_8N_2O_2)K_2(TMEDA)_2]$, (**LXXXVIII**) the only reports of metallations of *trans*-dioxaporphyrinogens, utilised NaH and *n*-BuLi for the octamethyl analogue, *meso*-octamethyl-*trans*-dioxaporphyrinogen, ($Me_8N_2O_2H_2$), (**LXXXIX**). For the sodium case, a single crystal X-ray structure determination was carried out, revealing a dianionic ligand, deprotonated through both pyrrolide N atoms, adopting a flattened partial cone conformation, to give $[(Me_8N_2O_2)\{Na(DME)\}_2]$, (**XC**), as shown in Figure 2.15.[16a] The observed conformational change is enforced by the smaller radii of sodium versus potassium, and results in an $\eta^5:\eta^1:\eta^1:\eta^1$ binding mode.

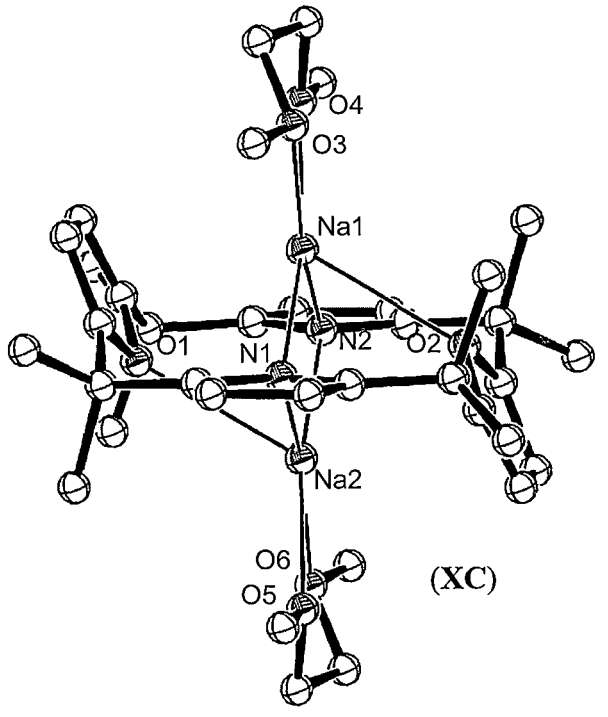

Figure 2.15. Molecular structure of the disodiated *meso*-octamethyl-*trans*-dioxaporphyrinogen $[(Me_8N_2O_2)\{Na(DME)\}_2]$, (**XC**). Figure generated from CCDC obtained coordinates. Atoms of arbitrary size. H atoms are omitted for clarity.

Reaction of **XC** with the transition metal halide $[CoCl_2(THF)_{1.5}]$, (**XCI**), gave the corresponding cobalt(II) complex $[(Me_8N_2O_2)Co(THF)_2]$, (**XCII**), which exhibited a flattened 1,3-alternate macrocyclic conformation with an $\eta^1{:}\eta^1{:}\eta^1{:}\eta^1$ binding mode.[16a]

Results and Discussion:

2.2. Synthesis of samarium(II) macrocyclic complexes.

2.2.1. Synthesis of *meso*-octaethyl-*trans*-dioxaporphyinogen, ($Et_8N_2O_2H_2$), (**1**).

The synthesis of the macrocyclic ligand *meso*-octaethyl-*trans*-dioxaporphyrinogen, ($Et_8N_2O_2H_2$), (**1**), was achieved using a modified '3 + 1' approach based on the previously reported synthesis of the analogous *meso*-methyl substituted macrocycle, *meso*-octamethyl-*trans*-dioxaporphyrinogen, (**LXXXIX**),[14,16] and shown in Scheme 2.1.

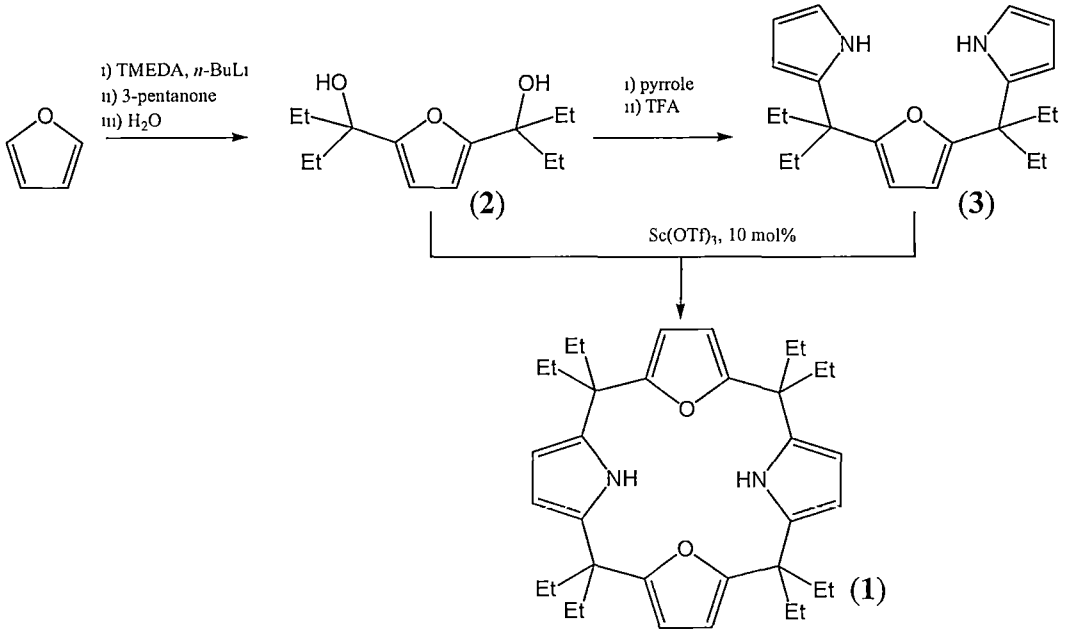

Scheme 2.1. Synthesis of *meso*-octaethyl-*trans*-dioxaporphyrinogen, ($Et_8N_2O_2H_2$), (**1**).

The diol, 2,5-bis(hydroxydiethylmethyl)furan, (**2**), was prepared *via* the deprotonation of furan at the 2 and 5 positions by 2.5 molar equivalents of *n*-BuLi followed by reaction with 3-pentanone and quenching with water. Previous studies by the author demonstrated the poor yield of the analogous dimethyl diol, (**4**), used in the synthesis of *meso*-octamethyl-*trans*-dioxaporphyrinogen, (**LXXXIX**) when acetone was used in place of pentanone, as a result of proton exchange from acetone to the dilithiated furan.[17] Consequently pentanone, which ultimately gives *meso*-octaethyl-*trans*-dioxaporphyrinogen, (**1**), was used in the diol synthesis.

Condensation of diol **2** with pyrrole in the presence of trifluoroacetic acid gave the tricyclic compound 2,5-bis{(2′-pyrrolyl)diethylmethyl}furan, (**3**) in 45 % yield. Condensation of tricycle **3** with diol **2** in the presence of $Sc(OTf)_3$ (10 mol %) then gave the desired macrocycle ($Et_8N_2O_2H_2$), (**1**), in 50 % isolated yield, comparable to the highest reported yield of the final '3 + 1' reaction of the analogous *meso*-methyl substituted macrocycle, *meso*-octamethyl-*trans*-dioxaporphyrinogen, (**LXXXIX**), of 46%.[16c]

The yield of the final '3 + 1' condensation reaction represents a 10-fold increase as compared to the 5 % yield of ($Et_8N_2O_2H_2$), (**1**) obtained using boron trifluoride diethyl etherate as the acid catalyst as for the synthesis of the *meso*-methyl macrocycle **LXXXIX**, and represents a 2.5-fold increase as compared to the previous optimal synthesis of the macrocycle which used trifluoracetic acid as the catalyst to give **1** in 20 % yield.[14] The use of a solution of the mild Lewis acid catalyst $Sc(OTf)_3$ in MeCN in place of trifluoroacetic acid in toluene resulted in an increase in yield to 40 % when a similar batch reaction was attempted. When the reaction conditions were altered such that a mixture of diol **2** and tricycle **3** were added *via* syringe pump to a solution of $Sc(OTf)_3$ in MeCN, a further increase in yield to 50 % was observed, presumably due to the effective high dilution of the diol, **2** and tricycle, **3**, favouring the formation of the target macrocycle.

2.2.2. Synthesis of samarium(II) complexes of ($Et_8N_2O_2H_2$), (**1**).

The synthesis of the dipotassium salt of the dioxaporphyrinogen was achieved according to a previously reported method.[14] Potassium metal was added to a solution of **1** in toluene, liberating $H_2(g)$ and giving [{$(Et_8N_2O_2)K_2(C_6H_5Me)$}$_n$], (**5**) in 66 % isolated yield after concentration *in vacuo* and crystallisation at –17 °C, as shown in Scheme 2.2.

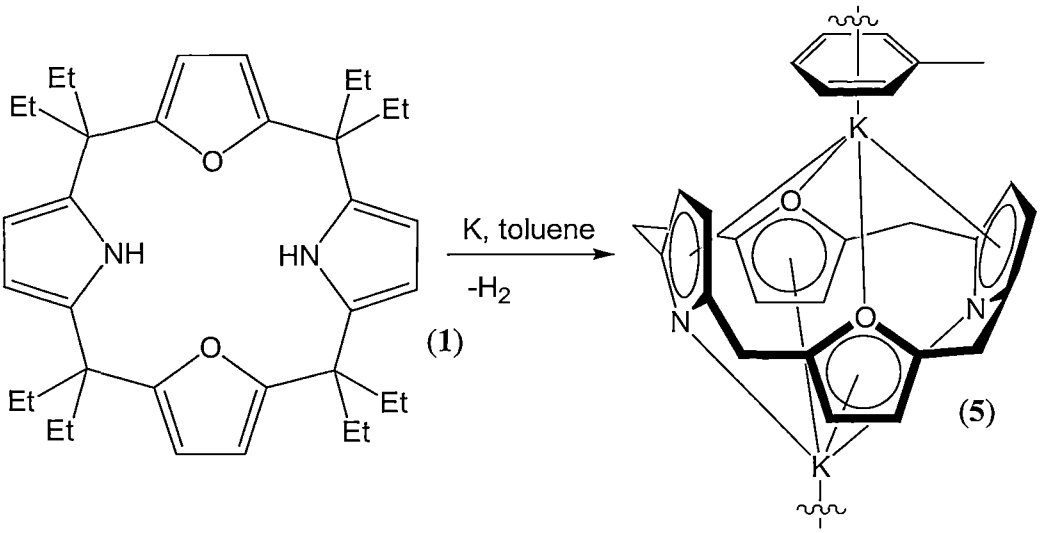

Reaction 2.1. Synthesis of $[\{(Et_8N_2O_2)K_2(C_6H_5Me)\}_n]$, (**5**). *Meso*-ethyl groups in **5** are omitted for clarity.

Full characterisation of $[\{(Et_8N_2O_2)K_2(C_6H_5Me)\}_n]$, (**5**), including a single crystal X-ray diffraction study has previously been studied.[18] $[\{(Et_8N_2O_2)K_2(C_6H_5Me)\}_n]$, (**5**) was found to exhibit a rare $\mu:\eta^6:\eta^6$- bridging toluene molecule linking potassium centres of each monomeric dipotassium macrocycle molecule, resulting in a polymeric structure.

The reaction of the white dipotassium salt of the *meso*-octaethyl-*trans*-dioxaporphyrinogen ligand, **5**, with a blue THF solution of samarium diiodide yields the previously reported green KI incorporated divalent samarium species $[\{(THF)_2K(Et_8N_2O_2)Sm(\mu\text{-}I)\}_2]$, (**6**).[14] When dried *in vacuo* and recrystallised from toluene, the THF adduct, **6**, reacts to form the brown toluene adduct of the divalent samarium complex, $[\{(C_6H_5Me)K(Et_8N_2O_2)Sm(\mu\text{-}I)\}_2]$, (**7**) as shown in Scheme 2.3.

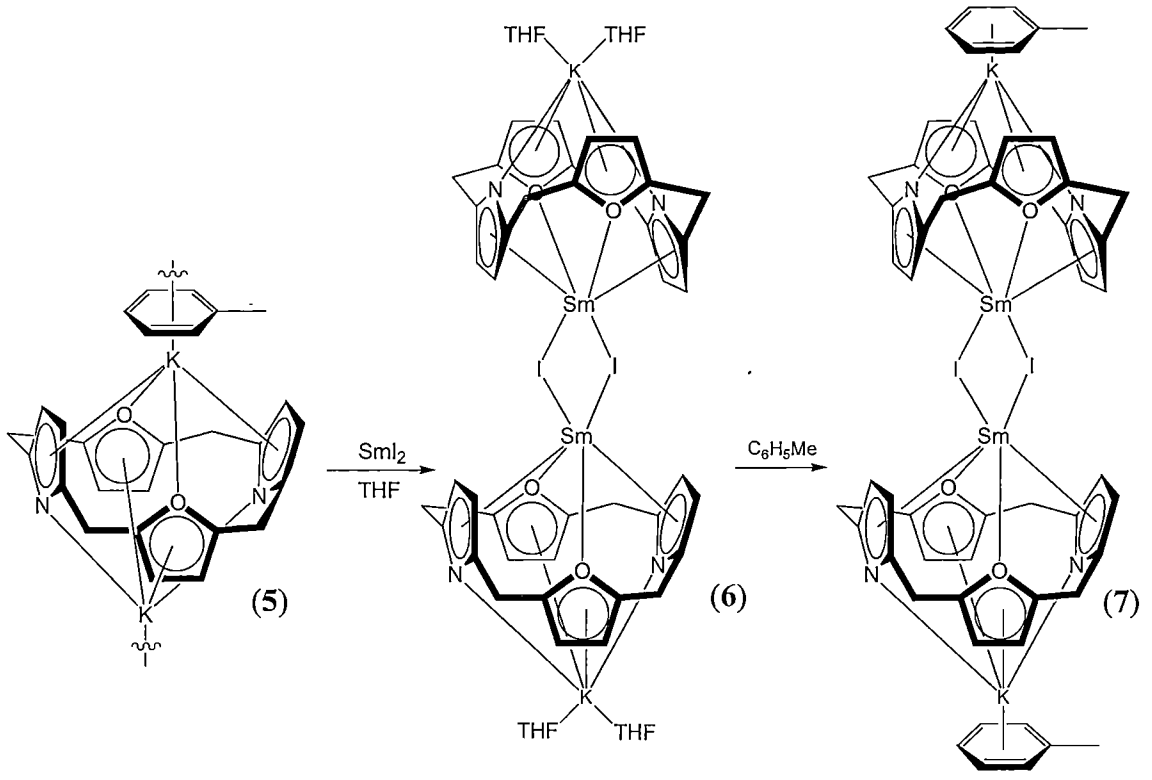

Scheme 2.2. Synthesis of $[\{(C_6H_5Me)K(Et_8N_2O_2)Sm(\mu\text{-}I)\}_2]$, (**7**). *Meso*-ethyl groups are omitted for clarity.

The reaction of the samarium(II) THF adduct, **6**, with toluene occurs instantaneously despite its poor solubility which results in a heterogenous reaction mixture. The resulting crystalline brown solid, $[\{(C_6H_5Me)K(Et_8N_2O_2)Sm(\mu\text{-}I)\}_2]$, (**7**), also exhibits extremely poor solubility in aromatic and aliphatic solvents, preventing ^{1}H and ^{13}C NMR spectroscopic characterisation. However, it is moderately soluble in THF, returning to a green solution of $[\{(THF)_2K(Et_8N_2O_2)Sm(\mu\text{-}I)\}_2]$, (**6**). Despite the distinct colour changed observed upon addition of toluene to the THF adduct, **6**, $[\{(C_6H_5Me)K(Et_8N_2O_2)Sm(\mu\text{-}I)\}_2]$, (**7**) retains KI, without yielding the targeted KI free samarium(II) species, $[(Et_8N_2O_2)Sm(C_6H_5Me)_n]$, (**8**). The incorporated KI in **7** was also unable to be removed by the addition of 18-crown-6. Consequently, $[\{(C_6H_5Me)K(Et_8N_2O_2)Sm(\mu\text{-}I)\}_2]$, (**7**), was not used directly in further reactivity studies, rather the more convenient THF adduct, **6** was used throughout this thesis. The proposed structural details of $[\{(C_6H_5Me)K(Et_8N_2O_2)Sm(\mu\text{-}I)\}_2]$, (**7**) were confirmed *via* a single crystal X-ray diffraction study. Microanalytic data was also consistent with the proposed structure.

The molecular structure of [{(C_6H_5Me)K($Et_8N_2O_2$)Sm(μ-I)}$_2$], (**7**) exhibits a dimeric structure with two samarium centres bridged by two iodide anions. Two potassium cations balance the charge of the iodide anions, and reside in the base of the macrocyclic cavity of each doubly deprotonated porphyrinogen ligand. The coordination sphere of each potassium cation is completed with an η^6- bound toluene molecule, as shown above in Scheme 2.2.

2.2.3. Molecular structure of [{(C_6H_5Me)K($Et_8N_2O_2$)Sm(μ-I)}$_2$], (**7**).

Brown crystals of [{(C_6H_5Me)K($Et_8N_2O_2$)Sm(μ-I)}$_2$].3(C_6H_5Me), (**7**), suitable for single crystal X-ray diffraction studies were grown from a suspension of **7** in toluene, left at 100 °C in a sealed tube for 5 days. The crystals were found to belong to the monoclinic space group, $P2_1/m$ (No. 11), a = 14.126(4), b = 26.129(9), c = 14.212(10) Å, β = 91.02(4) °, with 2 dimeric molecules in the unit cell. The asymmetric unit consisted of one half of a molecule of [{(C_6H_5Me)K($Et_8N_2O_2$)Sm(μ-I)}$_2$], (**7**), and three toluene molecules of crystallisation. The positions of the pyrrolide N atoms and furanyl O atoms were unambiguously determined *via* significant differences in the refinement model when their positions were transposed. The structure of **7** is shown below in Figures 2.16 and 2.17.

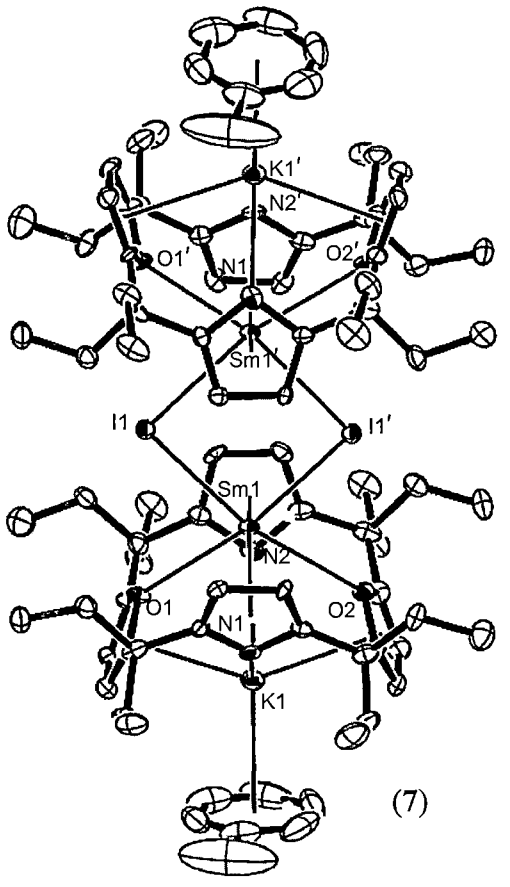

(7)

Figure 2.16. Molecular structure of the samarium(II) toluene adduct, **7**, with thermal ellipsoids drawn at the 20 % level of probability. H atoms and three toluene molecules of crystallisation have been omitted for clarity.

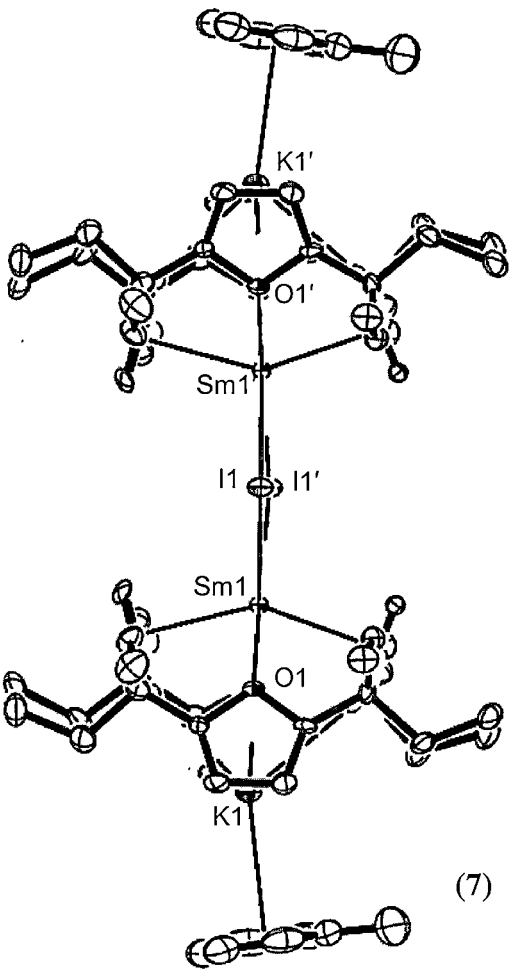

(7)

Figure 2.17. Side view of the molecular structure of **7** with thermal ellipsoids drawn at the 20 % level of probability. H atoms and three toluene molecules of crystallisation have been omitted for clarity.

In the interpretation of the structure of **7** and subsequent macrocyclic lanthanide complexes, the binding of the macrocyclic ligand to the lanthanide centre is analysed *via* comparison of the relative angles of the least squares planes defined by the pyrrolide and furanyl rings to the least squares plane defined by the four *meso*-C atoms, as shown in Figure 2.18. The distances of the η^5- interactions between the macrocycle and metal centres are measured between the metal centre and the centroids of the furanyl and pyrrolide rings.

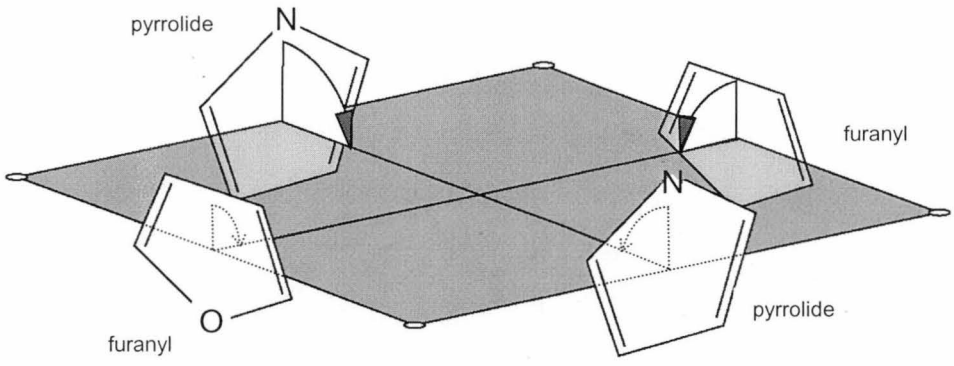

Figure 2.18. Least squares plane defined by the macrocyclic *meso*-C atoms, used to interpret the binding characteristics of the deprotonated *meso*-octaethyl-*trans*-dioxaporphyrinogen ligand, **1**.

$[\{(C_6H_5Me)K(Et_8N_2O_2)Sm(\mu\text{-}I)\}_2]$, (**7**), adopts a dimeric form in the solid state with two iodide centres bridging both of the samarium centres, which are each bound to the macrocyclic ligand through an η^5:η^1:η^5:η^1 bonding mode. The macrocycle exhibits the typical 1,3-alternate conformation previously observed for lanthanide complexes of this ligand.[14] Two potassium centres, capped by toluene molecules *via* η^6- interactions reside in the base of each macrocyclic cavity, with η^5: η^1: η^5: η^1 binding to the macrocycle. η^1- binding between the samarium centres and the O atoms of the furanyl rings features, whilst η^5- interactions are observed between the pyrrolide rings and the samarium centres. For the potassium centres, η^1- binding is observed to the pyrrolide N atoms, with η^5- interactions to the furanyl rings. The η^1-Sm–O(furanyl) interactions occur at a distance of 2.952(6) and 2.990(6) Å, which is significantly longer than typical Sm-O(furan) Lewis base interactions such as the Sm-O(THF) interactions in $[(Et_8N_4)\{Sm(THF)\}_2]$ (**LXXX**) and $[\{(THF)Li\}_2(c\text{-}hex_4N_4)Sm(THF)(\mu^3\text{-}Cl)Li(THF)_2]$ (**LXXXI**), which measure 2.63_4 and 2.61_3 Å respectively.[11g-h] The Sm–η^5 (pyrrolide) interactions of 2.66_5 and 2.66_3 Å are shorter than those of the dinuclear Sm(II) complex of the *meso*-octaethylporphyrinogen complex, $[(Et_8N_4)\{Sm(THF)_2\}_2]$, (**LXXX**), shown in Figure 2.10 in Section 2.1.4 of 2.76_8 Å,[11g] but are similar to those of the LiCl incorporating samarium(II) complex of the tetracyclohexylporphyrinogen, $[\{(THF)Li\}_2(c\text{-}hex_4N_4)Sm(THF)(\mu^3\text{-}Cl)Li(THF)_2]$, (**LXXXI**), as shown in Figure 2.11. in section 2.1.4, of 2.64_9 and 2.66_6 Å.[11h] The furanyl ring tilt angles of **7** of 69.6_9 and 70.5_7 ° are significantly smaller

than the pyrrolide tilt angles of 109.5_0 and 108.8_5 °, as a consequence of the η^5:η^1:η^5:η^1 bonding mode and 1,3-alternate macrocyclic conformation. The Ct(pyrrolide)-Sm-Ct(pyrrolide) angle in **7** of 146.3_1 ° is comparable to that of $[(Et_8N_4)\{Sm(THF)_2\}_2]$, (**LXXX**) of 149.4_3 °.[11g]

The μ:η^1- Sm–I interactions of 3.3195(12) and 3.2909(13) Å are marginally shorter than those of the iodide bridged pentamethylcyclopentadienyl samarium(II) complex $[\{(C_5Me_5)Sm(\mu\text{-}I)(THF)_2\}_2]$, (**XCIII**), of 3.356(2) and 3.459(2),[19] and the iodide bridged samarium(II) amide complex $[\{(Me_3Si)_2NSm(\mu\text{-}I)(DME)(THF)\}_2]$, (**XCIV**), of 3.3414(9) and 3.3553 (9) Å,[20] despite the higher samarium coordination number in $[\{(C_6H_5Me)K(Et_8N_2O_2)Sm(\mu\text{-}I)\}_2]$, (**7**). The samarium-macrocycle and samarium-iodide interactions of **7** do not differ significantly from those observed in the molecular structure of $[\{(THF)_2K(Et_8N_2O_2)Sm(\mu\text{-}I)\}_2]$, (**6**).[14]

The potassium centres in $[\{(C_6H_5Me)K(Et_8N_2O_2)Sm(\mu\text{-}I)\}_2]$, (**7**), bind to the macrocycle in a reverse fashion compared to the samarium centres, with η^5 interactions to the furan rings, and σ binding to the pyrrolide nitrogen centres. The K–η^5(furanyl) interactions in **7** of 3.05_2 and 3.03_5 Å, are larger than those in the dipotassium complex, $[(Et_8N_2O_2)\{K(TMEDA)\}_2]$, (**LXXXVIII**), of 2.88_1 and 2.93_1 Å.[14] However, the σ K–N interactions in **7** of 2.914(8) and 2.930(7) Å are similar to those in $[(Et_8N_2O_2)\{K(TMEDA)\}_2]$, (**LXXXVIII**) of 2.952(4) and 2.898(4) Å, which is consistent with the smaller ionic radius of the samarium(III) centre compared to potassium in $[\{(C_6H_5Me)K(Et_8N_2O_2)Sm(\mu\text{-}I)\}_2]$, (**7**) enforcing a greater furanyl tilt angle in the macrocyclic ligand, as it seeks to maximise the η^1- Sm–O(furanyl) interactions. This is further demonstrated in a comparison of the furanyl tilt angles of $[\{(C_6H_5Me)K(Et_8N_2O_2)Sm(\mu\text{-}I)\}_2]$, (**7**) and $[(Et_8N_2O_2)\{K(TMEDA)\}_2]$, (**LXXXVIII**) of 69.6_9 and 70.5_7 ° for **7** and 67.56 and 67.72 ° for **LXXXVIII** respectively. The potassium-toluene centroid distance of **7** of 3.152_9 Å is slightly longer than that of the potassium incorporating tetra(pyrazolyl) samarium complex, $[(C_6H_5Me)K(\mu\text{-}C_3N_2\text{-}2,4\text{-}t\text{-}Bu)_2Sm(C_3N_2\text{-}2,4\text{-}t\text{-}Bu)]$, (**LIII**),[21] as shown in Figure 1.26 of Section 1.2.6 of 2.9_9 Å, presumably due to the higher potassium coordination number in $[\{(C_6H_5Me)K(Et_8N_2O_2)Sm(\mu\text{-}I)\}_2]$, (**7**). The cross-cavity samarium-potassium distance measures 3.89_5 Å. A summary of important bond lengths and angles for **7** is shown in Table 2.3.

2.3. Synthesis of samarium(III) complexes of ($Et_8N_2O_2$), (1).

2.3.1. Synthesis of [{($Et_8N_2O_2$)Sm(μ-I)}$_2$], (8).

The reaction of [{$(THF)_2K(Et_8N_2O_2)Sm(\mu\text{-}I)\}_2$], (6), with iodine in THF proceeds rapidly despite the heterogeneous nature of the reaction induced by the moderate solubility of **6**, giving the samarium(III) species [{$(Et_8N_2O_2)Sm(\mu\text{-}I)\}_2$], (**8**), in high yield (73 % isolated yield) as an orange solid, as shown in Reaction 2.2. The reaction mixture changes colour instantly from green to orange upon addition of 1 equivalent of iodine, and by titrimetric addition of the iodine solution, allows for a determination of the purity of the samarium(II) starting material, [{$(THF)_2K(Et_8N_2O_2)Sm(\mu\text{-}I)\}_2$], (**6**).

$$[\{(THF)_2K(Et_8N_2O_2)Sm(\mu\text{-}I)\}_2]\ (\mathbf{6}) \xrightarrow[THF]{I_2} [\{(Et_8N_2O_2)Sm(\mu\text{-}I)\}_2]\ (\mathbf{8})$$

Reaction 2.2. Synthesis of [{$(Et_8N_2O_2)Sm(\mu\text{-}I)\}_2$], (**8**).

The molecular structure of **8** was able to be confirmed *via* a single crystal X-ray structure determination. ^{1}H NMR spectroscopic analysis and microanalysis studies were also consistent with the proposed structure. [{$(Et_8N_2O_2)Sm(\mu\text{-}I)\}_2$], (**8**), exhibits poor solubility in most solvents, but is moderately soluble in THF. As a result, ^{13}C NMR spectroscopy was unable to be achieved.

[{$(Et_8N_2O_2)Sm(\mu\text{-}I)\}_2$], (**8**), has a dimeric, solvent free structure, featuring bridging iodide centres, with the base of the macrocyclic cavity free from any bound species. A three dimensional representation of **8** is shown in Figure 2.19.

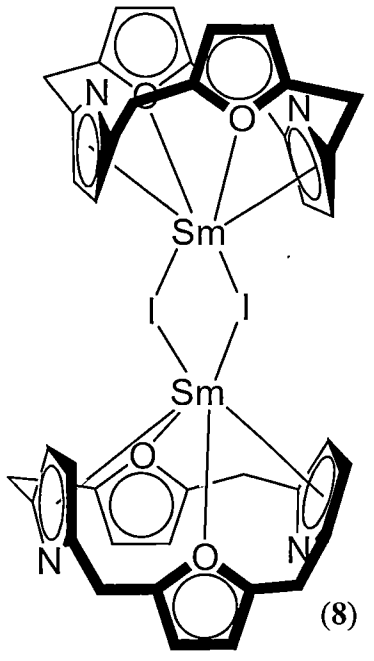

(8)

Figure 2.19. Three dimensional representation of the dimeric samarium(III) iodide $[\{(Et_8N_2O_2)Sm(\mu\text{-}I)\}_2]$, (**8**).

The ^1H NMR spectrum of **8** exhibited a range of broad proton resonances between 0 and 14 ppm, characteristic of the paramagnetic lanthanide centre. Full assignment of the proton resonances are summarised in Table 2.1 though the poor solubility of **8** prevented full assignment using 2D NMR techniques. Previous studies of lanthanide complexes of the dioxaporphyrinogen ligand have suggested that the chemical shift range observed in the ^1H NMR spectra is dependent on the presence or absence of Group 1 metal species in the base of the macrocyclic cavity.[22] A smaller chemical shift range was observed for macrocyclic complexes bearing two metal centres within the macrocyclic cavity (pyrrolide =CH ~ 7ppm), whilst larger chemical shifts were observed for complexes bearing only a lanthanide centre (pyrrolide =CH ~ 15 ppm). **8** exhibits a broader range of ^1H NMR resonances than the ^1H NMR spectrum of the sodium containing samarium(III) dioxaporphyrinogen $[(C_6H_5Me)Na(Et_8N_2O_2)Sm\{N(SiMe_3)Si(CH_3)_2(CH_2\}]$, (**XCV**),[22] of 0 to 7 ppm, which is consistent with the understanding that the binding of a Group 1 metal centre to the base of the macrocyclic cavity contracts the chemical shift range of the resulting ^1H NMR spectrum of the complex.

Resonance (ppm)	Assignment	Resonance (ppm)	Assignment
0.52	CH_3	3.36	CH_2
0.61	CH_2	4.97	=CH (pyr or fur)
1.69	$CH_3 + CH_2$	13.97	=CH (pyr or fur)
2.29	CH_2		

Table 2.1. ^{1}H NMR spectral data for [{($Et_8N_2O_2$)Sm(μ-I)}$_2$], (**8**), (THF-d^8, 299.905 MHz, 298 K).

2.3.2. Molecular structure of [{($Et_8N_2O_2$)Sm(μ-I)}$_2$], (**8**).

Orange crystals of [{($Et_8N_2O_2$)Sm(μ-I)}$_2$].2THF, and [{($Et_8N_2O_2$)Sm(μ-I)}$_2$].C_6H_6, suitable for single crystal X-ray diffraction studies were grown from a saturated THF solution of [{($Et_8N_2O_2$)Sm(μ-I)}$_2$], (**8**), left at 60 °C in a sealed tube for 7 days, and from a suspension of **8** in benzene left in a sealed tube at 100 °C for 10 days, respectively. The crystals from THF were found to belong to the triclinic spacegroup $P\bar{1}$, (No. 2), a = 13.5356(15), b = 15.2741(15), c = 20.139(2) Å, α = 87.247(4), β = 89.663(4), γ = 67.804(4) °, with 4 molecules in the unit cell, whilst the crystals from benzene were found to belong to the monoclinic space group, $C2/c$ (No. 15), a = 17.6141(3), b = 20.2278(5), c = 22.5253(6) Å, β = 111.725(1) °, also with 4 molecules in the unit cell. For the THF solvate, the asymmetric unit consisted of two independent halves of the molecule, lying on inversion centres, with two lattice THF molecules, whilst for the benzene solvate, the asymmetric unit consisted of one half of the molecule and one half of a lattice benzene molecule both residing on inversion centres. As for [{(C_6H_5Me)K($Et_8N_2O_2$)Sm(μ-I)}$_2$], (**7**), the positions of the pyrrolide N atoms and furanyl O atoms were unambiguously determined *via* significant differences in the refinement model when their positions were transposed. Further discussion of the molecular structure of [{($Et_8N_2O_2$)Sm(μ-I)}$_2$], (**8**), is based on the benzene derived crystals owing to the superior quality of the refinement. A comparison of the important bond lengths and angles for the two solvates is summarised in Table 2.2. The structure of **8** is shown below in Figures 2.20 and 2.21.

Distance (Å) / Angle (°)	*C*2/*c* benzene solvate	*P*$\bar{1}$ THF solvate
Sm(1)–O(fur)	2.660(4), 2.685(4)	2.661(12), 2.661(12)
Sm(2)–O(fur)		2.639(12), 2.677(13)
I(1)–Sm(1)#1	3.2006(5)	3.2160(14)
I(2)-Sm(2)#2		3.2328(14)
O(1)-Sm(1)-O(2)	122.20(13)	123.2(4)
O(3)-Sm(2)-O(4)		121.8(4)
Sm(1)-I(1)-Sm(1)#1	101.973(14)	102.84(4)
Sm(2)#2-I(2)-Sm(2)		103.07(4)

Table 2.2. Comparison of distances and angles of the benzene and THF solvates of **8**.

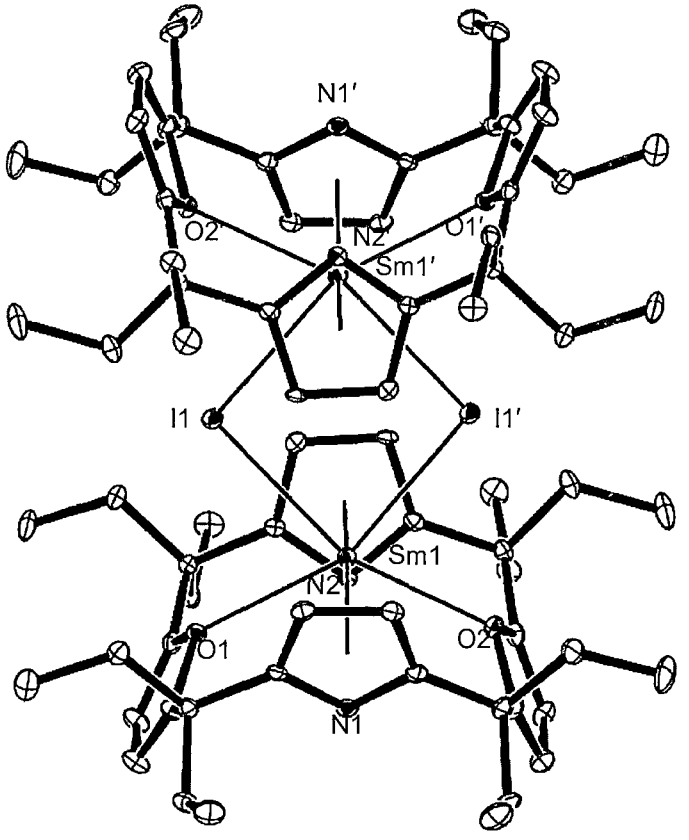

Figure 2.20. Molecular structure of **8** with thermal ellipsoids drawn at the 20 % level of probability. H atoms and the benzene molecule of crystallisation are not shown for clarity.

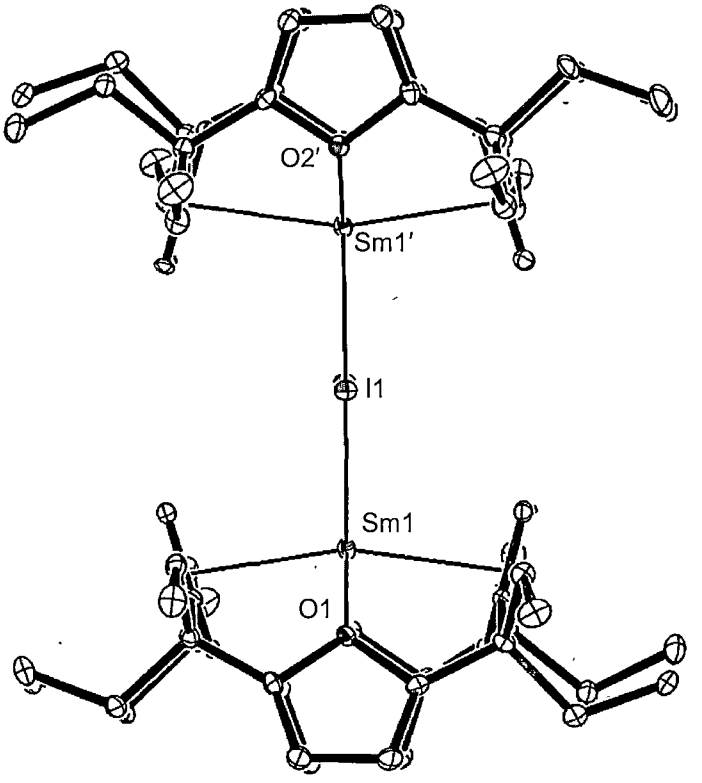

Figure 2.21. Side view of the molecular structure of **8** with thermal ellipsoids drawn at the 20 % level of probability. H atoms and the benzene molecule of crystallisation are not shown for clarity.

The samarium(III) centres in $[\{(Et_8N_2O_2)Sm(\mu\text{-}I)\}_2]$, (**8**) reside more deeply within the macrocyclic cavity of the porphyrinogen ligand than in the samarium(II) precursor $[\{(C_6H_5Me)K(Et_8N_2O_2)Sm(\mu\text{-}I)\}_2]$, (**7**), whilst also maintaining shorter bond lengths to the iodide ligands, which is consistent with the smaller ionic radius for the +3 oxidation state of the metal. The η^1 Sm–O(furanyl) interactions measure 2.660(4) and 2.685(4) Å, which is significantly shorter than those in **7** of 2.952(6) and 2.990(6) Å. Similarly, the Sm–η^5(pyrrolide) interactions are significantly shorter in **8** than in **7** with distances of 2.51_9 and 2.53_0 Å (for **8**) and 2.66_5 and 2.66_3 Å (for **7**), respectively. The η^5(pyrrolide) interactions in **8** are also shorter than those of the LiCl incorporating disamarium(III) *meso*-octaethylporphyrinogen $[(Et_8N_4)Sm_2\{(\mu\text{-}Cl)_2[Li(THF)_2]\}_2]$, (**LXXIX**), shown in Figure 2.9, Section 2.1.4, of 2.62_0 and 2.64_6 Å. The relative difference in binding depth of the samarium centres within **8** and **7** also results in substantial differences in the furanyl O-Sm-O angles of 122.20(13) and 110.6_3 °.

As for $[\{(C_6H_5Me)K(Et_8N_2O_2)Sm(\mu\text{-}I)\}_2]$, (**7**), the pyrrolide ring angles of $[\{(Et_8N_2O_2)Sm(\mu\text{-}I)\}_2]$, (**8**), with the *meso* plane of 106.3_2 and 107.4_4 °, are substantially larger than the furanyl ring angles of 62.5_3 and 70.1_2 °, as a consequence of the η^5(pyrrolide) and η^1(furanyl) bonding motifs. The furanyl ring tilt angles of **8** are smaller than those of **7** of 69.6_9 and 70.5_7 °, resulting from the η^5 interaction with the potassium centre in **7**, which pulls the furanyl rings closer to the potassium centre and increases the ring tilt angles. The increased furanyl tilt angle in **7** compared to **8** is also observed in the large shortening of the Sm-O(furanyl) interactions in **8** discussed above. The *meso*- C atoms of **8** lie closer to the least squares planes defined by each of the furanyl rings as compared to the pyrrolide rings, with average deviations from the respective planes of 0.092_4 and 0.21_8 Å, respectively. This is consistent with the pyrrolide rings being pulled into the macrocyclic cavity towards the samarium centre to maximise the η^5 interactions with the samarium centre, as shown below in Figure 2.22.

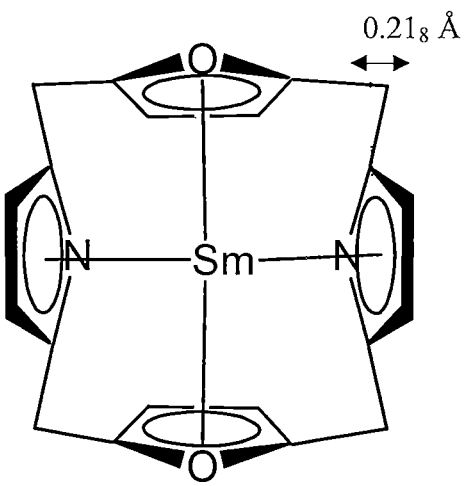

Figure 2.22 Representative top view of $[\{(Et_8N_2O_2)Sm(\mu\text{-}I)\}_2]$, (**8**) demonstrating the *meso*-C deformation from the pyrrolide rings.

The Sm–I interactions in **8**, which measure 3.2006(5) and 3.1990(5) Å, are also expectedly shorter than those observed in the samarium(II) precursor $[\{(C_6H_5Me)K(Et_8N_2O_2)Sm(\mu\text{-}I)\}_2]$, (**7**) of 3.3195(12) and 3.2909(13) Å, but are comparable to those of the only other reported iodide bridged samarium(III) dimeric complex, $[\{Me_2Si(C_5Me_4)(PC_6H_2\text{-}t\text{-}Bu_3\text{-}2,4,6)Sm(\mu\text{-}I)(THF)\}_2]$, (**XCVI**), which exhibited bridging Sm–I interactions of 3.1037(7) and 3.2299(7) Å.[23] A comparison

of the important bond lengths and angles of $[\{(C_6H_5Me)K(Et_8N_2O_2)Sm(\mu\text{-}I)\}_2]$, (**7**), and $[\{(Et_8N_2O_2)Sm(\mu\text{-}I)\}_2]$, (**8**), is summarised in Table 2.3.

Distance (Å)/Angle (°)	**7**	**8**
Sm–O	2.952(6), 2.990(6)	2.660(4), 2.685(4)
Sm–N	2.863(7), 2.865(7)	2.603(5), 2.624(5)
Sm–η^5(pyrrolide)	2.66_5, 2.66_3	2.51_9, 2.53_0
Sm–I	3.3195(12), 3.2909(13)	3.2006(5), 3.1990(5)
Sm···K	3.89_6	-
$\eta^5(pyr)_1$-Sm-$\eta^5(pyr)_2$	146.3_2	163.2_5
N_1-Sm-N_2	96.6(2)	109.22(16)
O_1-Sm-O_2	110.61(18)	122.20(13)
Sm–I–Sm	93.95(4), 95.02(5)	101.973(14)
pyrrolide tilt angle	109.5_0, 108.8_5	106.3_2, 107.4_2
furanyl tilt angle	69.6_9, 70.5_7	62.5_3, 70.1_2

Table 2.3. Summary of important bond distances and angles for the samarium(II) and (III) complexes, $[\{(C_6H_5Me)K(Et_8N_2O_2)Sm(\mu\text{-}I)\}_2]$, (**7**) and $[\{(Et_8N_2O_2)Sm(\mu\text{-}I)\}_2]$, (**8**), (benzene solvate).

2.3.3. Synthesis of $[\{(Et_8N_2O_2)Sm(\mu\text{-}Br)\}_2]$, (**9**).

The reaction of the white dipotassium salt of the *meso*-octaethyl-*trans*-dioxaporphyrinogen ligand $[\{(Et_8N_2O_2)K_2(C_6H_5Me)\}_n]$, (**5**) with $SmBr_3$ in THF gave the orange samarium(III) macrocyclic complex $[\{(Et_8N_2O_2)Sm(\mu\text{-}Br)\}_2]$, (**9**), in 67% isolated yield, as shown in Reaction 2.3.

$$[\{(Et_8N_2O_2)K_2(C_6H_5Me)\}_n]\ \textbf{(5)} \xrightarrow[THF]{SmBr_3} [\{(Et_8N_2O_2)Sm(\mu\text{-}Br)\}_2]\ \textbf{(9)}$$

Reaction 2.3. Synthesis of $[\{(Et_8N_2O_2)Sm(\mu\text{-}Br)\}_2]$, (**9**).

The low solubility of $SmBr_3$ results in a heterogenous reaction mixture, which slowly reacts over a period of 36 hours at 50 °C to give orange crystals of $[\{(Et_8N_2O_2)Sm(\mu\text{-}Br)\}_2]$, (**9**), in conjunction with a large amount of white solid, presumed to be KBr.

The synthesis of **9** from $[\{(Et_8N_2O_2)K_2(C_6H_5Me)\}_n]$, (**5**) and $SmBr_3$ represents the first direct method for the synthesis of a lanthanide(III) complex of the metallated *meso*-octaethyl-*trans*-dioxaporphyinogen ligand. Previously, the oxidation of a lanthanide(II) intermediate species was required. This lead result offers promise for the extension of related lanthanide chemistry of the metallated dioxaporphyinogen ligand across the entire lanthanide series, beyond those which have an accessible +2 oxidation state.

$[\{(Et_8N_2O_2)Sm(\mu\text{-}Br)\}_2]$, (**9**), exhibits very poor solubility in a range of solvents including THF, toluene and 40-60 °C petroleum spirits, preventing NMR characterisation of the complex. As a result, the more soluble samarium(III) iodide complex, $[\{(Et_8N_2O_2)Sm(\mu\text{-}I)\}_2]$, (**8**), was used preferentially in further reactivity studies. The molecular structure of $[\{(Et_8N_2O_2)Sm(\mu\text{-}Br)\}_2]$, (**9**) was able to be determined *via* a single crystal X-ray diffraction study. The proposed formulation also gave a satisfactory microanalysis. A three dimensional representation of the molecular structure of **9** is shown in Figure 2.23.

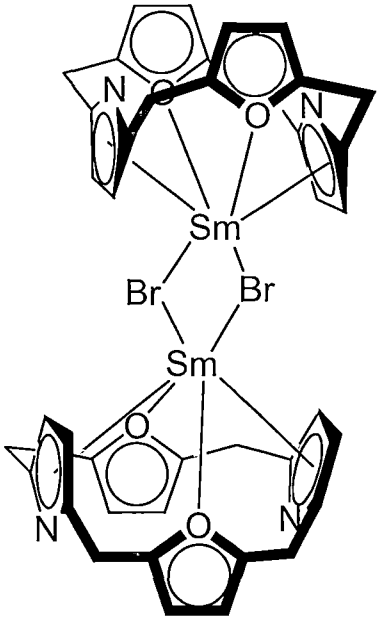

Figure 2.23. Three dimensional representation of the molecular structure of the samarium(III) bromide complex $[\{(Et_8N_2O_2)Sm(\mu\text{-}Br)\}_2]$, (**9**).

2.3.4. Molecular structure of $[\{(Et_8N_2O_2)Sm(\mu\text{-}Br)\}_2]$, (**9**).

Crystals of $[\{(Et_8N_2O_2)Sm(\mu\text{-}Br)\}_2]\cdot 2THF$, (**9**), suitable for single crystal X-ray diffraction studies were grown from the reaction mixture of

$[\{(Et_8N_2O_2)K_2(C_6H_5Me)\}_n]$, (**5**), and $SmBr_3$ let stand at 50 °C for 48 hours. The crystals were found to belong to the monoclinic space group, *C*2/*c*, (No. 15), a = 17.6497(15), b = 19.9677(14), c = 22.4222(15) Å, β = 112.783(4) °, with four molecules in the unit cell. The asymmetric unit consisted of one half of the molecule of $[\{(Et_8N_2O_2)Sm(\mu\text{-}Br)\}_2]$, (**9**), lying on an inversion centre and one THF molecule of crystallisation. Carbon and hydrogen atoms in **9** were refined isotropically due to poor anisotropic modelling which did not significantly reduce the value of R. The derived molecular structure of **9** is shown in Figure 2.24.

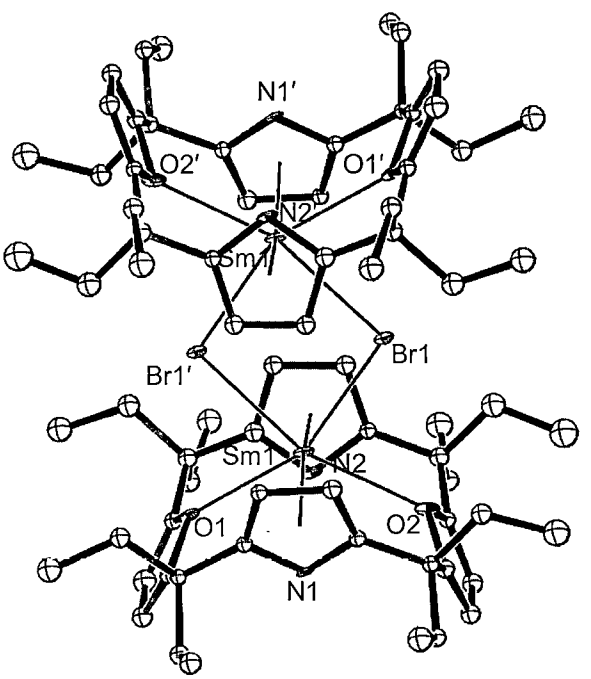

Figure 2.24. Molecular structure of the bromide bridged samarium(III) macrocyclic complex, $[\{(Et_8N_2O_2)Sm(\mu\text{-}Br)\}_2]$, (**9**). Thermal ellipsoids are drawn at the 20 % level of probability. H atoms and the THF molecule of crystallisation are omitted for clarity.

$[\{(Et_8N_2O_2)Sm(\mu\text{-}Br)\}_2]$, (**9**), forms a halide bridged dimeric structure, analogous to $[\{(Et_8N_2O_2)Sm(\mu\text{-}I)\}_2]$, (**8**). The lanthanide centre is bound to the macrocyclic ligand through a similar $\eta^5{:}\eta^1{:}\eta^5{:}\eta^1$ bonding motif, with an analogous 1,3-alternate macrocyclic conformation. The Sm-O (furanyl) and Sm η^5-pyrrolide interactions in **9** of 2.670(8) and 2.687(8) Å (furanyl) and 2.50_3 and 2.49_6 Å (pyrrolide) are similar to those in **8**, of 2.660(4) and 2.685(4) Å (furanyl) and 2.51_9 and 2.53_0 Å (pyrrolide), respectively.

The bridging Sm–Br interactions in $[\{(Et_8N_2O_2)Sm(\mu\text{-}Br)\}_2]$, (**9**), exhibit similar bond lengths of 2.9578(15) and 3.008(2) Å. However, the two monomeric components are slightly offset from one another in order to minimise steric congestion between the macrocyclic ligands, as shown in the space-filling representation of the molecular structure in Figure 2.24. This contrasts with the molecular structure of $[\{(Et_8N_2O_2)Sm(\mu\text{-}I)\}_2]$, (**8**), and $[\{(Et_8N_4Me_2)Sm(\mu\text{-}Br)\}_2]$, (**XCVII**)[24] which do not exhibit significant offset of the monomeric components. For the iodide bridged complex, **8**, the lack of lanthanide offset can be rationalised as resulting from the larger bridging iodide centres providing greater separation between the samarium centres, as shown in the space-filling representation in Figure 2.24, and observed in the longer Sm–I contacts of 3.2006(5) Å. In the bromide bridged complex of the $Et_8N_4Me_2$ ligand, $[\{(Et_8N_4Me_2)Sm(\mu\text{-}Br)\}_2]$, (**XCVII**), the binding depth of the lanthanide centre within the macrocyclic ligand is smaller, resulting in a greater distance between each macrocycle, and negating the need for an offset bridging interaction, despite exhibiting only marginally longer Sm–Br interactions of 3.0354(11) Å.[24] However, the chloride and bromide bridged samarium(III) complexes of the related *trans-N,N'*-dimethyl and *trans*-diphenyl ($Et_8N_2Ph_2H_2$) macrocycles, $[\{(Et_8N_4Me_2Sm(\mu\text{-}Cl)\}_2]$, (**LXXXV**)[14] and $[\{(Et_8N_2Ph_2Sm(\mu\text{-}Br)\}_2]$, (**XCVIII**)[25] exhibit similar lanthanide offset to $[\{(Et_8N_2O_2)Sm(\mu\text{-}Br)\}_2]$, (**9**), consistent with the smaller bridging halide centres enforcing shorter lanthanide (and hence macrocycle) distances. A comparative summary of the important bond lengths and angles of $[\{(Et_8N_2O_2)Sm(\mu\text{-}Br)\}_2]$, (**9**), $[\{(Et_8N_2O_2)Sm(\mu\text{-}I)\}_2]$, (**8**), and $[\{(Et_8N_4Me_2)Sm(\mu\text{-}Cl)\}_2]$, (**LXXXV**) is shown in Table 2.4.

Distance/Angle	(**9**)	(**8**)	(**LXXXV**)
Sm–O(N) (Å)	2.670(8), 2.687(8)	2.660(4), 2.685(4)	2.4879(16), 2.5378(16)
Sm–N (Å)	2.629(9), 2.637(9)	2.603(5), 2.624(5)	
Sm–η^5(pyrrolide) (Å)	2.50_3, 2.49_6	2.51_9, 2.53_0	2.63_8, 2.62_8
Sm–X (Å)	2.9578(15), 3.008(2)	3.2006(5), 3.1990(5)	2.9290(5), 2.7511(5)
Sm···Sm (Å)	4.71_4	4.97_2	4.65_6
$\eta^5(pyr)_1$-Sm-$\eta^5(pyr)_2$ (°)	161.2_5	163.2_5	162.3_3
N_1-Sm-N_2 (°)	108.0(3)	109.22(16)	
$O(N)_1$-Sm-$O(N)_2$ (°)	120.3(2)	122.20(13)	119.16(5)
Sm–X–Sm (°)	104.39(4)	101.973(14)	110.077(16)
Pyrrolide/NMe tilt (°)	106.5_7, 105.0_4	106.3_2, 107.4_2	102.9_7, 101.9_1
Furanyl/η^1-pyrrolide tilt (°)	69.6_6, 61.4_4	62.5_3, 70.1_2	46.8_4, 43.5_4

Table 2.4. Summary of important bond lengths and angles for the halide bridged macrocyclic samarium(III) complexes $[\{(Et_8N_2O_2)Sm(\mu\text{-}Br)\}_2]$, (**9**), $[\{(Et_8N_2O_2)Sm(\mu\text{-}I)\}_2]$, (**8**), and $[\{(Et_8N_4Me_2Sm(\mu\text{-}Cl)\}_2]$, (**LXXXV**).

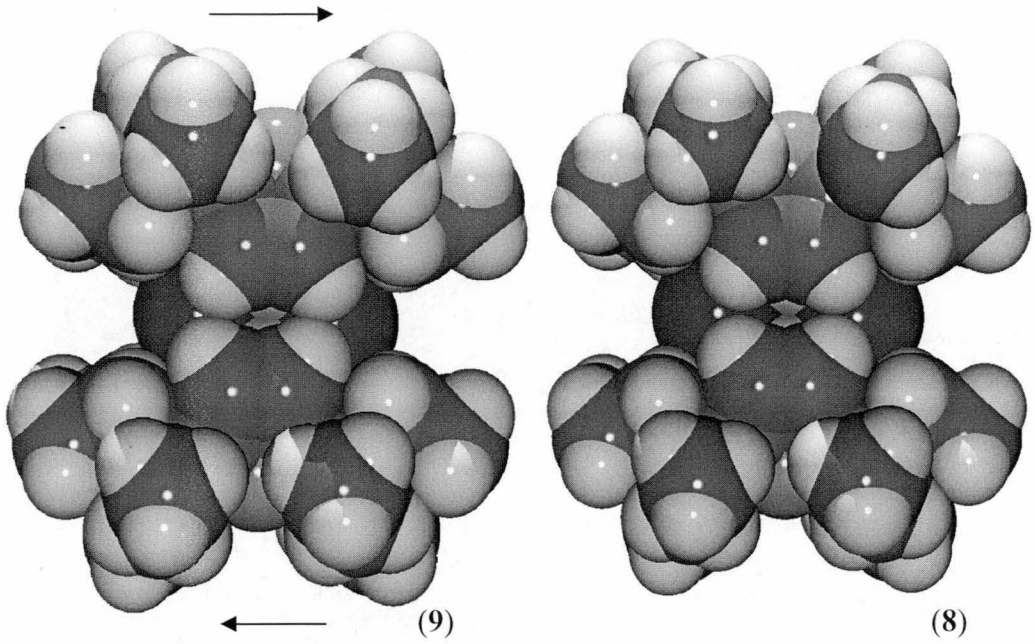

Figure 2.24. Space-filling representations of the molecular structure of the bromide (left) and iodide (right) bridged samarium(III) complexes, $[\{(Et_8N_2O_2)Sm(\mu\text{-}Br)\}_2]$, (**9**) and $[\{(Et_8N_2O_2)Sm(\mu\text{-}I)\}_2]$, (**8**).

2.4. Experimental

2,5-bis(hydroxydiethylmethyl)furan, (**2**)

2 was prepared according to a modified literature procedure.[14]

n-BuLi (312 mL, 1.6 M in hexanes, 0.5 mol) was added to a stirred solution of furan (12.7 g, 0.20 mol) in a mixture of 40-60 °C petroleum spirits (100 mL) and TMEDA (70 ml, 0.50 mol) under nitrogen at a temperature of 0 °C. The resulting mixture was refluxed for half an hour and then let cool to room temperature before 3-pentanone (49.6 mL, 0.50 mol) was added dropwise and the solution stirred for a further 2 hours at room temperature. Water, (9 mL,0.50 mol) was added dropwise to the mixture, which was stirred for a further hour. The resulting suspension was filtered, and the solid extracted three times with diethyl ether (3 x 100 mL). The petroleum spirit and diethyl ether solutions were combined and washed with a saturated aqueous solution of NaCl before being dried over Na_2CO_3. Solvent was then removed *via* rotary evaporation and the crude product recrystallised from a solution of diethyl ether and petroleum spirit (1:2 v/v) to give **2** as a pure white crystalline solid (20 g, 45 %).

^{1}H NMR (C_6D_6, 299.905 MHz, 25 °C, ppm): δ 0.78 (t, ^3J = 7.5 Hz, 12H, CH_3), 1.72 (m, 8H, CH_2), 1.92 (broad, s, 2H, OH), 6.00 (s, 2H, fur CH).

2,5-bis{(2'-pyrrolyl)diethylmethyl}furan, (**3**)

3 was prepared according to a modified literature procedure.[14]

Trifluoracetic acid (1.68 g, 1.1 ml, 14.8 mmol) was added to a stirred solution of 2,5-bis(hydroxydiethylmethyl)furan, (**2**), (9.6 g, 40 mmol) and pyrrole (10.0 g, 148 mmol) in degassed absolute ethanol (50 mL) under nitrogen. The resulting mixture was refluxed for six hours before ethanol and excess pyrrole were removed *via* rotary evaporation and the resulting dark grey oil was dissolved in diethyl ether. The resulting solution was then washed three times each with saturated aqueous solutions of $NaHCO_3$ and NaCl before being dried over Na_2CO_3. Solvent was then removed *via* rotary evaporation to give a concentrated ethereal solution of **3**, which upon cooling to -17 °C gave **3** as a pure grey crystalline solid (6.0 g, 45 %).

^{1}H NMR (C_6D_6, 299.905 MHz, 25 °C, ppm): 0.69 (t, ^3J = 7.5 Hz, 12H, CH_3), 1.81 (m, 8H, CH_2), 5.82, (s, 2H, fur CH), 6.09 (m, 2H, pyr CH), 6.25 (m, 2H, pyr CH), 6.33 (m, 2H, pyr CH).

Meso-octaethyl-*trans*-dioxaporphyrinogen, $Et_8N_2O_2H_2$, (**1**)

To a stirred acetonitrile (75 mL) solution of $Sc(OTf)_3$ (0.25 g, 0.5 mmol) at 75 °C, was added an acetonitrile (100 mL) solution of 2,5-bis{(2'-pyrrolyl)diethylmethyl}furan, (**3**), (1.55 g, 4.6 mmol) and 2,5-bis(hydroxydiethylmethyl)furan, (**2**), (1.57 g, 6.5 mmol) at a controlled rate of 0.4 mL/min *via* a syringe pump. The stirred solution was then let cool to room temperature and stirred for a further 62 hours. Acetonitrile was then removed *in vacuo* to leave a crude cream coloured solid product, which was washed with methanol to remove any unreacted 2,5-bis(hydroxydiethylmethyl)furan, (**2**). Re-crystallisation of the crude solid from a 40-60 °C petroleum spirit/toluene solution (5:1, v/v) yielded a pure white crystalline product (1.55 g, 62 %).

^{1}H NMR ($CDCl_3$, 299.905 MHz, 25 °C, ppm): δ 0.61 (t, 24H, CH_3), 1.82 (m, 16H, CH_2), 5.78 (d, 4H, pyr CH), 6.08 (s, 4H, fur CH), 6.57 (broad, s, 2H, NH).

(C_6D_6, 299.905 MHz, 25 °C, ppm): δ 0.64 (t, 24H, CH_3), 1.70 (m, 8H, CH_2), 1.93 (m, 8H, CH_2), 5.88 (d, 8H, pyr and fur CH), 6.69 (broad, s, 2H, NH).

$[\{(Et_8N_2O_2)K_2(toluene)\}_n]$, (**5**)

5 was prepared according to a modified literature procedure.[14]

To a stirred solution of ($Et_8N_2O_2H_2$), (**1**), (5.0 g, 9.2 mmol) in toluene (70 mL) was added potassium metal (0.90 g, 23 mmol) before the solution was heated to 60 °C for 9 hours. The solution at 60 °C was then cannula filtered and left to cool to room temperature 3 hours before being further cooled to – 17 °C for 48 hours yielding white crystals of $[\{(Et_8N_2O_2)K_2(toluene)\}_n]$, (**5**), (4.9 g, 6.1 mmol, 66 %).

^{1}H NMR (C_6D_6, 299.905 MHz, 25 °C, ppm): δ 0.76 (m, 24H, CH_3), 1.79 (m, 16H, CH_2), 2.07 (s, 3H, toluene-CH_3), 5.71 (s, 4H, fur/pyr CH), 5.95 (s, 4H, fur/pyr CH), 7.02-7.10 (m, 5H, toluene-Ar-CH).

$[(THF)_2K(Et_8N_2O_2)Sm(\mu\text{-}I)\}_2]$, (**6**)

6 was prepared according to a modified literature procedure.[14]

To a stirred solution of $[(Et_8N_2O_2)K_2(toluene)_2]$, (**5**), (4.8 g, 6.0 mmol) in THF (50 mL) was added dropwise, a solution of samarium diiodide (0.1 M in THF, 51 mL, 5.0 mmol). The green solution was stirred overnight before being heated to 50 °C and filtered from a white solid (presumably KI). The filtrate was then concentrated *in vacuo* and cooled to -17 °C overnight to give a pure green product, (4.5 g, 75 %).

$[(C_6H_5Me)K(Et_8N_2O_2)Sm(\mu\text{-}I)\}_2]$, (**7**)

To a flask containing $[(THF)_2K(Et_8N_2O_2)Sm(\mu\text{-}I)\}_2]$, (**6**), (0.05 g, 0.025 mmol) was added toluene (5 mL) before the flask was heated to 60 °C for 3 hours. Solvent was then removed *via* cannula to give **7** as a pure micro-crystalline brown solid (0.04 g, 77 %). Crystals of **7** suitable for single crystal X-ray diffraction studies were grown from a toluene suspension of **7** heated at 100 °C for 7 days.

Anal. Calcd: C, 57.67; H, 6.19; N, 2.69 (MW 2080.72 $C_{100}H_{128}I_2K_2N_4O_4Sm_2$),
Found: C, 57.04; H, 6.28; N, 2.60

$[\{(Et_8N_2O_2)Sm(\mu\text{-}I)\}_2]$, (**8**)

To a stirred solution of $[(THF)_2K(Et_8N_2O_2)Sm(\mu\text{-}I)\}_2]$, (**6**), (2.0 g, 1.0 mmol) in THF (100 mL) was added dropwise, a solution of iodine (0.30 g 1.2 mmol) in THF (35 mL), until the colour of the solution changed from green to orange (at 29 mL). The resulting solution was then cannula filtered at 50 °C from a white precipitate (presumably KI) before the filtrate was cooled to –17 °C overnight to yield **8** as a pure orange solid (1.20 g, 73 %)

Anal. Calcd: C, 52.86; H, 5.91; N, 3.42 (MW 1636.09 $C_{72}H_{96}I_2N_4O_4Sm_2$),
Found: C, 52.23; H, 6.18; N, 2.96

^{1}H NMR (THF-d^8, 299.905 MHz, 25 °C, ppm): δ 0.52 (s, 24H, CH_3), 0.61 (m, 8H, CH_2), 1.69 (broad, s, 32H, CH_3 and CH_2), 2.29 (broad, s, 8H, CH_2), 3.36 (broad, s, 8H, CH_2), 4.97, (s, 8H, CH pyr/fur), 13.97 (broad, s, 8H, CH pyr/fur).

$[\{(Et_8N_2O_2)Sm(\mu\text{-}Br)\}_2]$, (**9**)

To a flask containing $[\{(Et_8N_2O_2)K_2(toluene)\}_n]$, (**5**), (0.20 g, 0.25 mmol) and $SmBr_3$ (0.1 g, 0.25 mmol) was added THF (10 mL) and the mixture heated without stirring at 60 °C for 36 hours. The resulting orange crystals were separated from a white precipitate (presumably KBr) *via* suspension of the white solid in THF with stirring and separation *via* cannula to give $[\{(Et_8N_2O_2)Sm(\mu\text{-}Br)\}_2]$, (**9**), as an orange crystalline solid (0.13 g, 67 %).

Anal. Calcd: C, 54.96; H, 6.14, N, 3.56 (MW 1542.09 $C_{72}H_{96}Br_2N_4O_4Sm_2$), + 2 %w/w KBr
Found: C, 54.98; H, 5.77; N, 3.41

2.5. References

1. a) Bombieri, G. *J. Alloys Compd.* **1997**, *249*, 76.
   b) Alexander, V. *Chem. Rev.* **1995**, *95*, 273.
2. Brunet, E.; Juanes, O.; Rodriguez-Ubis, J. C. *Curr. Chem. Biol.* **2007**, *1*, 11.
3. a) Piguet, C.; Geraldes, C.F.G.C. *Handbook on the Physics and Chemistry of Rare Earths* **2003**, *33*, 353,
   b) Sherry, A.D. *J. Alloys Compd.* **1997**, *249*, 153.
4. Lee, L.; Berg, D.J.; Bushnell, G.W. *Inorg. Chem.* **1994**, *33*, 5302.
5. Fryzuk, M.D.; Jafarpour, L.; Kerton, F.M.; Love, J.B.; Patrick, B.O.; Rettig, S.J. *Organometallics* **2001**, *20*, 1387.
6. a) Fedushkin, I.L.; Weydert, M.; Fagin, A.A.; Nefedov, S.E.; Eremenko, I.L.; Bochkarev, M.N.; Schumann H. *Z. Naturforsch., B:Chem.Sci* **1999**, *54*, 466,
   b) Guyllernot, G.; Solari, E.; Rizzoli, C.; Scopelliti, R.; Floriani, C. *Private Communication* **2004**, CCDC 167446,
   c) Guyllernot, G.; Solari, E.; Rizzoli, C.; Scopelliti, R.; Floriani, C. *Private Communication* **2004**, CCDC 167447,
   d) Gottfriedsen, J.; Dorokhin, D. *Z. Anorg. Allg. Chem.* **2005**, *631*, 2928.
7. Estler, F.; Herdtweck, E.; Anwander, R.; *J. Chem. Soc., Dalton Trans.* **2002**, 3088.
8. Bian, Y.; Jiang, J.; Tao, Y.; Choi, M. T. M.; Li, R.; Ng, A. C. H.; Zhu, P.; Pan, N.; Sun, X.; Arnold, D. P.; Zhou, Z.-Y.; Li, H.-W.; Mak, T. C. W.; Ng, D. K. P. *J. Am. Chem. Soc.* **2003**, *125*, 12257.
9. Foley, T.J.; Harrison, B.S.; Knefely, A.S.; Abboud, K.A.; Reynolds, J.R.; Schanze, K.S.; Boncella J.M. *Inorg. Chem.* **2003**, *42*, 5023.
10. Campazzi, E.; Solari, E.; Scopelliti, R.; Floriani, C. *Inorg. Chem.* **1999**, *38*, 6240.
11. a) Campazzi, E.; Solari, E.; Scopelliti, R.; Floriani, C. *Chem. Commun.* **1999**, 1617,
    b) Dubé, T.; Gambarotta, S.; Yap, G.P.A. *Angew. Chem. Int. Ed.* **1999**, *38*, 1432,
    c) Dubé, T.; Guan, J.; Gambarotta, S.; Yap, G.P.A. *Chem. Eur. J.* **2001**, *7*, 374,
    d) Campazzi, E.; Solari, E.; Floriani, C.; Scopelliti, R.

Chem. Commun. **1998**, 2603,

e) Jubb, J.; Gambarotta, S. *J. Am. Chem. Soc.* **1994**, *116*, 4477,

f) Korobkov, I.; Aharonian, G.; Gambarotta, S.; Yap, G.P.A. *Organometallics* **2002**, *21*, 4899,

g) Dubé, T.; Gambarotta, S.; Yap, G.P.A. *Organometallics* **2000**, *19*, 817,

h) Dubé, T.; Gambarotta, S.; Yap, G.P.A. *Organometallics* **2000**, *19*, 121,

i) Guan, J.; Dubé, T.; Gambarotta, S.; Yap, G.P.A. *Organometallics* **2000** *19*, 4820.

12. Song, J.I.; Gambarotta, S. *Angew. Chem., Int. Ed. Engl.* **1995**, *34*, 2141.
13. Wang, J.; Dick, A.K.J.; Gardiner, M.G.; Yates, B.F.; Peacock, E.J.; Skelton, B.W.; White, A.H. *Eur. J. Inorg. Chem.* **2004**, 1992.
14. Wang, J. *Doctoral Dissertation* **2003**, School of Chemistry, University of Tasmania.
15. Wang, J.; Gardiner, M.G.; Peacock, E.J.; Skelton, B.W.; White, A.H. *Dalton Trans.* **2003**, 161.
16. a) Crescenzi, R.; Solari, E.; Floriani, F.; Chiesi-Villa, A.; Rizzoli, C. *Inorg. Chem.* **1996**, *35*, 2413,

    b) Yong-Sung, J.; Han-Je, K.; Phil-Ho, L.; Chang-Hee L. *Tetrahedron Letters* **2000**, *41*, 2919,

    c) Nagarajan, A.; Ka, J.W.; Lee, C.H. *Tetrahedron* **2001**, *57*, 7323.
17. Wang, J.; Stringer, D. N.; Gardiner, M. G.; Skelton, B. W.; White, A. H. *J. Organomet. Chem.* **2005**, *690*, 220.
18. Wang, J. Unpublished Results.
19. Evans, W.J.; Grate, J.W.; Choi, H.W.; Bloom, I.; Hunter, W.E.; Atwood, J.L. *J. Am. Chem. Soc.* **1985**, *107*, 941.
20. Evans, W.J.; Drummond, D.K.; Zhang, H.; Atwood, J.L. *Inorg. Chem.* **1988**, *27*, 575.
21. Deacon, G.B.; Delbridge, E.E.; Evans, D.J.; Harika, R.; Junk, P.C.; Skelton, B.W.; White, A.H. *Chem. Eur. J.* **2004**, *10*, 1193.
22. Wang, J.; Gardiner, M. G. *Chem. Commun.* **2005**, *12*, 1589.
23. Tardif, O.; Hou, Z.; Nishiura, M.; Koizumi, T.-a.; Wakatsuki, Y. *Organometallics* **2001**, *20*, 4565.
24. Wang, J. Unpublished Results.
25. Fisk, G. *Honours Thesis* **2007**, School of Chemistry, University of Tasmania.

Chapter 3. Lanthanide mediated reduction of N_2 containing species.

3.1. Introduction to lanthanide N_2 substrate reduction

3.1.1. Overview of lanthanide N_2 complexes.

Lanthanide complexes comprising of dinitrogen containing fragments are predominantly synthesised from redox processes utilising Ln(II) reagents. For the reduction of N_2 itself, complexes employing up to 4 Ln(II) species have been reported, as discussed in Section 1.1.5. However, for azobenzenes and further substituted dinitrogen containing substrates, such as hydrazines and azines, reduction is typically facilitated by a maximum of 2 Ln(II) species. Complexes of azobenzene and the products of the reduction of azobenzene account for the majority of lanthanide species containing a dinitrogen moiety.

3.1.2. Reduction of azo compounds.

The first reports of crystallographically authenticated reduced azobenzene complexes were made by Evans in the late 1980s.[1] The first complex in this series, $[\{(C_5Me_5)Sm\}_2(\mu\text{-}\eta^1\text{:}\eta^1\text{-}N_2Ph_2)]$, (**XCIX**), contained two samarium(III) centres, bridged by a *trans*-azobenzene moiety, which exhibited lengthening in the N-C(phenyl) bonds of the azobenzene unit without lengthening of the N=N bond. Agostic hydrogen interactions to the *ortho* phenyl hydrogen atoms were observed.

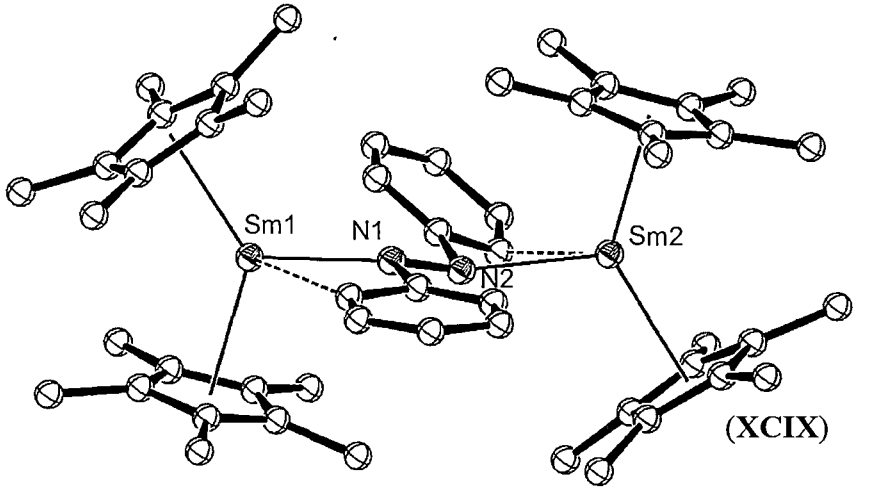

Figure 3.1. Molecular structure of $[\{(C_5Me_5)Sm\}_2(\mu\text{-}\eta^1\text{:}\eta^1\text{-}N_2Ph_2)]$, (**XCIX**). Figure generated from CCDC obtained coordinates. Atoms of arbitrary size. H atoms are omitted for clarity.[1a]

Both $[\{(C_5Me_5)Sm\}_2(\mu\text{-}\eta^1\text{:}\eta^1\text{-}N_2Ph_2)]$, (**XCIX**) and its 3-tolyl analogue, $[\{(C_5Me_5)Sm\}_2(3\text{-}Me\text{-}H_4C_6NNC_6H_4\text{-}3\text{-}Me)]$, (**C**), were found to exhibit reactivity with CO to form the corresponding *N,N'*-diarylphenoxamide ligands, which bridge each samarium centre through chelating N and O interactions to give $[\{C_5Me_5)_2Sm\}_2\{(PhN)CO\}_2]$, (**CI**), shown in Figure 3.2 and $[\{C_5Me_5)_2Sm\}_2\{[(3\text{-}MeC_6H_4N)(CO)\}_2]$, (**CII**) respectively.[1b]

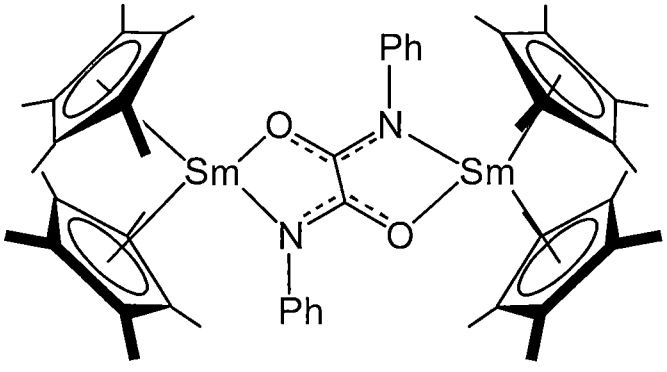

Figure 3.2. Representation of the structure of $[\{C_5Me_5)_2Sm\}_2\{(PhN)CO\}_2]$, (**CI**).[1b]

$[\{(C_5Me_5)Sm\}_2(PhNNPh)]$, (**XCIX**) was also found to undergo rearrangement in THF to give $[\{(C_5Me_5)Sm(THF)\}_2\{\mu\text{-}\eta^2\text{: }\eta^2\text{-}N_2Ph_2\}_2]$, (**CIII**), as shown in Reaction 3.1, which exhibited a much longer N=N bond length of 1.44(1) Å.[1b]

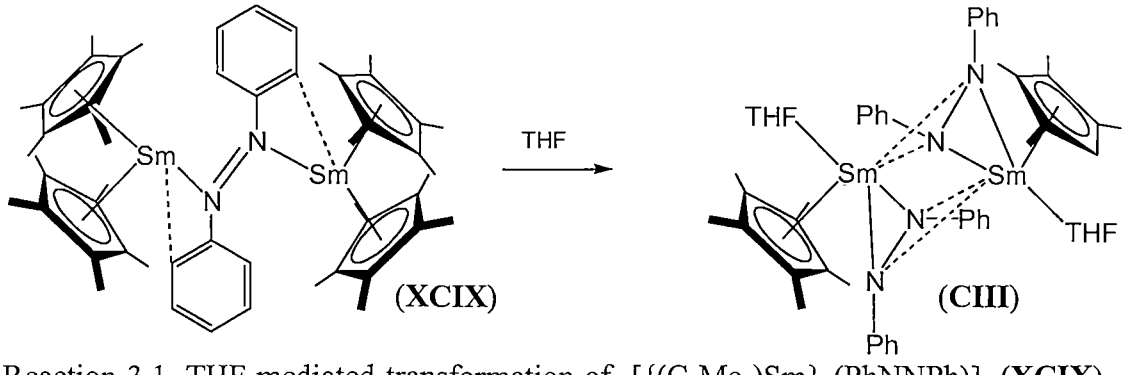

Reaction 3.1. THF mediated transformation of $[\{(C_5Me_5)Sm\}_2(PhNNPh)]$, (**XCIX**) to $[\{(C_5Me_5)Sm(THF)\}_2\{\mu\text{-}\eta^2\text{: }\eta^2\text{-}N_2Ph_2\}_2]$, (**CIII**).

Further studies on this azobenzene system allowed the isolation of the 1:1 *cis*-azobenzene complex $[(C_5Me_5)_2Sm(\eta^2\text{-}N_2Ph_2)(THF)]$, (**CIV**), shown in Figure 3.3. Efforts to synthesise the corresponding Yb analogue resulted in the isolation of the di-metallic ytterbium(III) species, $[(C_5H_5)(THF)Yb]_2[\mu\text{-}\eta^2\text{:}\eta^2\text{-}N_2Ph_2]_2$, (**CV**), which co-crystallised as a mixture with $[(C_5H_5)_3Yb(THF)]$, (**CVI**). The monometallic

samarium complex showed no reactivity with CO, but in contrast to the bimetallic case of **XCIX**, exhibited a lengthening of the N=N bond from 1.25 to 1.36 Å, without any change to the length of the N-C(phenyl) bonds.[1b]

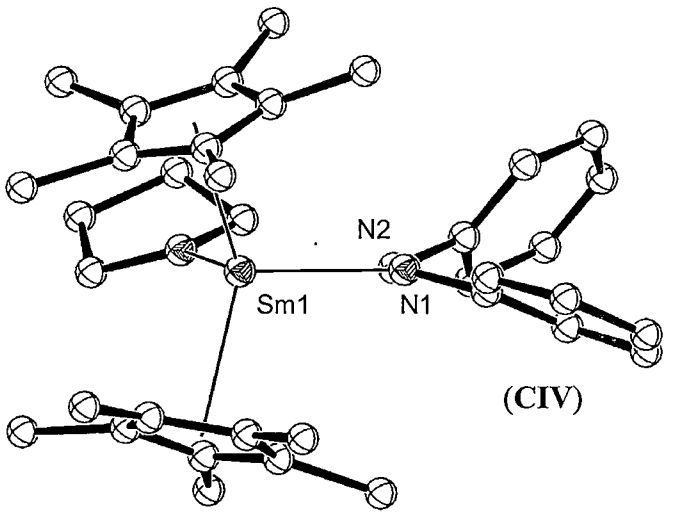

(CIV)

Figure 3.3. Molecular structure of $[(C_5Me_5)_2Sm(\eta^2\text{-PhNNPh})(THF)]$, (**CIV**). Figure generated from CCDC obtained coordinates. Atoms of arbitrary size. H atoms and one of the two independent molecules in the asymmetric unit are omitted for clarity.[1b]

Since the initial azobenzene reduction studies of Evans, a number of azobenzene lanthanide complexes have been reported. Bi-metallic systems are most common, with the azobenzene ligand bridging two lanthanide centres. However, a limited number of monometallic species have also been reported.

Five monometallic lanthanide η^2- azobenzene complexes have been reported, aside from those of Evans described above. The reaction of bis[hydrotris(3,5-dimethylpyrazolyl)borato]samarium(II), (**CVII**), with azobenzene gave the monometallic complex, $[Sm\{HB\text{-}(3,5\text{-}Me_2pz)_3\}_2(PhNNPh)]$, (**CVIII**), as shown in Figure 3.4.[2] The steric bulk of the hydrotris(3,5-dimethylpyrazolyl)borato ligand prevented further reduction by a second equivalent of the Sm(II) precursor complex, in contrast to the observed reactivity of the samarium C_5Me_5 system. The N=N bond exhibited similar lengthening to that observed for the decamethyl samarocene system, resulting in a bond length of 1.332(12) Å.

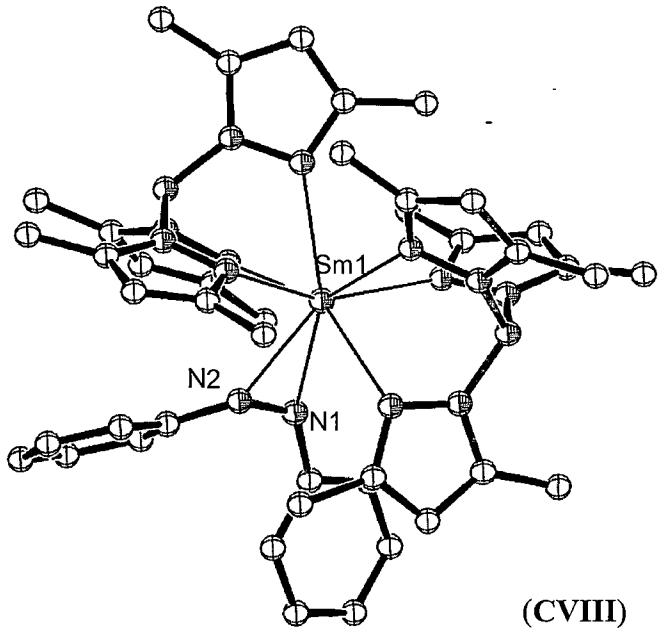

(CVIII)

Figure 3.4. Molecular structure of [Sm{HB-(3,5-Me_2pz)$_3$}$_2$(PhNNPh)], (**CVIII**). Figure generated from CCDC obtained coordinates. Atoms of arbitrary size. H atoms are omitted for clarity.

The divalent samarium aryloxide complex [Sm(OAr)$_2$(THF)$_3$], (**CIX**) (Ar = C_6H_2-*tert*-Bu_3-2,4,6) also formed a monometallic azobenzene complex, [Sm(OAr)$_2$(PhNNPh)], (**CX**), in which similar N=N bond lengthening to 1.358(11) Å was observed.[3] In this case, steric bulk did not appear to limit the reduction, as evident by the coordination of the THF molecules, as shown in Figure 3.5.

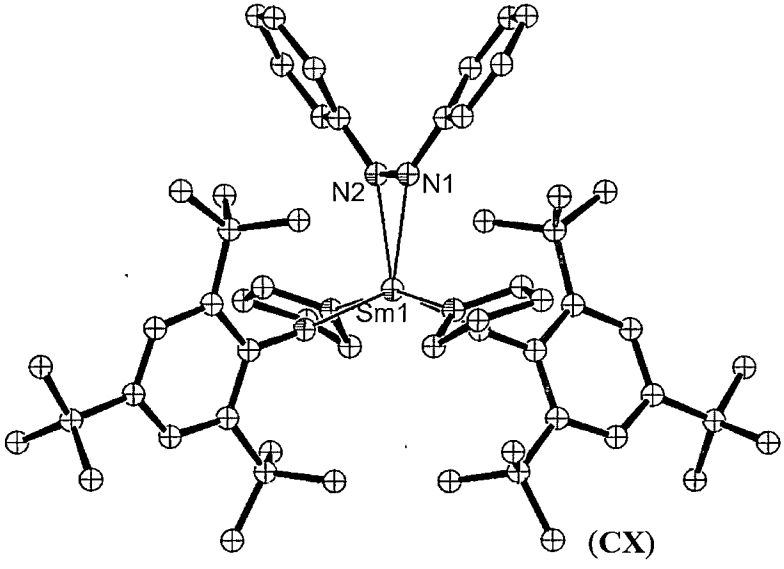

(CX)

Figure 3.5. Molecular structure of [Sm(OAr)$_2$(PhNNPh)], (**CX**).[3] Figure generated from CCDC obtained coordinates. Atoms of arbitrary size. H atoms and one diethyl ether molecule of crystallisation are omitted for clarity.

Reaction of the divalent complex $[(C_5Me_5)Sm(\mu\text{-}\eta^6\text{:}\eta^1\text{-}Ph)_2BPh_2]$, (**CXI**), with azobenzene gave $[(C_5Me_5)Sm\{(\eta^6\text{:}\eta^1\text{-}Ph)_2BPh_2\}(PhNNPh)]$, (**CXII**), which exhibited a strongly reduced N=N bond with a length of 1.435(5) Å,[4] which approaches the length of the N–N bond in hydrazine, as a consequence of the weaker electron donation from the $(BPh_4)^-$ moiety to the samarium(III) centre than in the analogous bispentamethylcyclopentadienyl complex, $[(C_5Me_5)_2Sm(\eta^2\text{-}PhNNPh)(THF)]$, (**CIV**), described earlier.

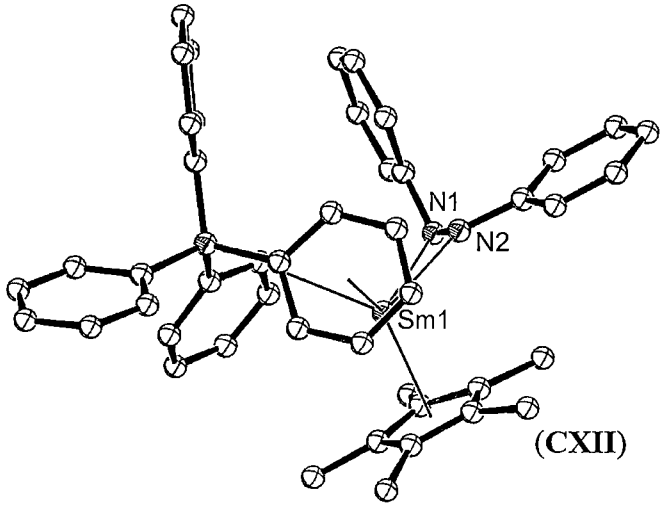

Figure 3.6. Molecular structure of $[(C_5Me_5)Sm\{(\eta^6\text{:}\eta^1\text{-}Ph)_2BPh_2\}(PhNNPh)]$, (**CXII**).[4] Figure generated from CCDC obtained coordinates. Atoms of arbitrary size. H atoms are omitted for clarity.

Thulium and samarium(II) complexes of 2,5-di-tert-butyl-3,4-dimethylphospholide also gave monometallic reduced azobenzene complexes as shown in Figure 3.7 for $[(PC_4\text{-}2,5\text{-}t\text{-}Bu\text{-}3,4\text{-}Me)_2Tm(PhNNPh)]$, (**CXIII**). Typical reduced bond lengths of 1.35 Å were observed in both complexes.[5]

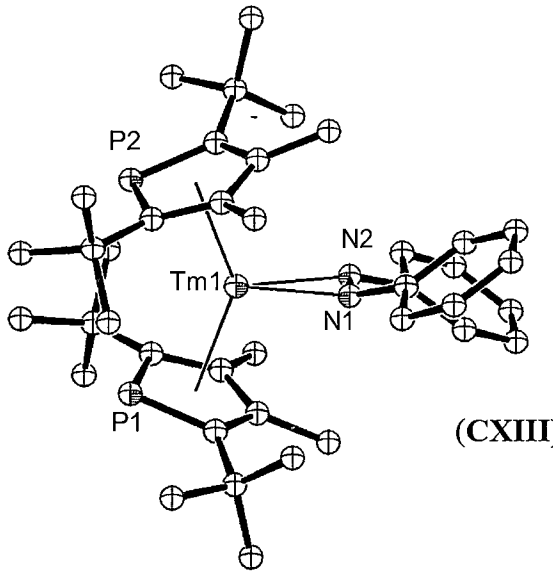

(CXIII)

Figure 3.7. Molecular structure of $[(PC_4\text{-}2,5\text{-}t\text{-}Bu\text{-}3,4\text{-}Me)_2Tm(PhNNPh)]$, **(CXIII)**.[5] Figure generated from CCDC obtained coordinates. Atoms of arbitrary size. H atoms are omitted for clarity.

Bi-metallic reduced azobenzene complexes exhibit more strongly reduced azobenzene fragments, with N=N bond lengths ranging between 1.44(1) Å to 1.48$_9$ Å as observed in $[\{(C_5Me_5)Sm(THF)\}_2\{\mu\text{-}\eta^2\text{:}\ \eta^2\text{-}N_2Ph_2\}_2]$, **(XCIX)**, and $[\{(C_5H_5)(THF)Lu\}_2\{\mu\text{-}\eta^2\text{:}\ \eta^2\text{-}N_2Ph_2\}_2]$, **(CXIV)**[6] respectively, except for $[\{(C_5Me_5)Sm\}_2(\mu\text{-}\eta^1\text{:}\eta^1\text{-}N_2Ph_2)]$, **(XCIX)** discussed above, which did not exhibit N=N lengthening. Most often, the reduced azobenzene ligand bridges the two lanthanide atoms in a $\mu\text{-}\eta^2\text{:}\eta^2$ bonding motif, such as in $[\{(C_5Me_5)Sm(THF)\}_2(\mu\text{-}\eta^2\text{:}\eta^2\text{-}N_2Ph_2)_2]$, **(XCIX)**, shown in Figure 3.8.[1b]

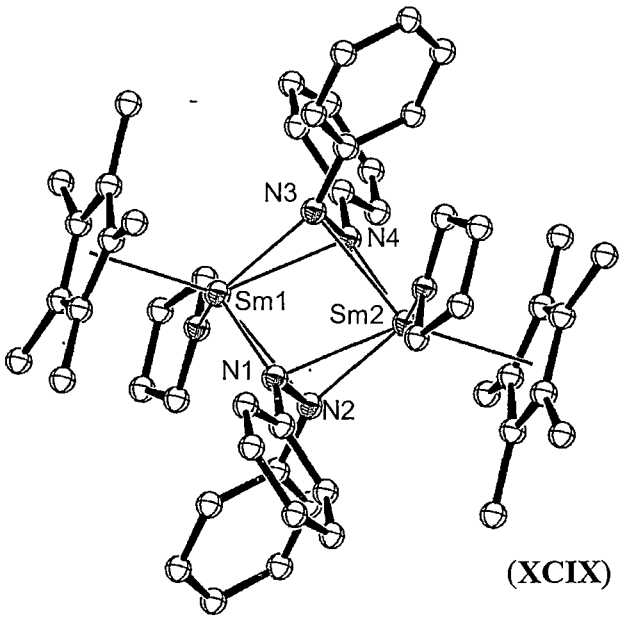

(XCIX)

Figure 3.8. Molecular structure of $[\{(C_5Me_5)Sm(THF)\}_2(\mu\text{-}\eta^2\text{:}\eta^2\text{-}N_2Ph_2)_2]$, (**XCIX**). Figure generated from CCDC obtained coordinates. Atoms of arbitrary size. H atoms are omitted for clarity.

Lanthanide(0) metal reagents have been used in the reduction of mixtures of PhNNPh/PhEEPh with the aim of cleaving the azo bond to give imido species. However bimetallic μ^2- bridged azo compounds resulted, with cleavage of the chalcogen bond observed.[7] Complexes of this nature, such as $[\{Ho(PhNNPh)(TePh)(C_6H_5N)\}_2]$, (**CXV**), shown in Figure 3.9 contained 2 dianionic reduced azo fragments distinct from the monoanionic reduction of azobenzene in $[\{(C_5Me_5)Sm(THF)\}_2(\mu\text{-}\eta^2\text{:}\eta^2\text{-}N_2Ph_2)_2]$, (**XCIX**).

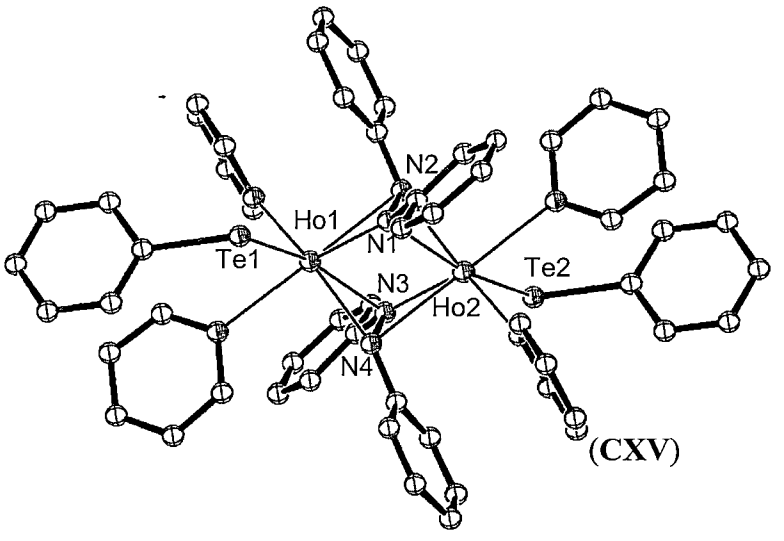

Figure 3.9. Molecular structure of $[\{Ho(PhNNPh)(TePh)(C_6H_5N)\}_2]$, (**CXV**). Figure generated from CCDC obtained coordinates. Atoms of arbitrary size. H atoms, two pyridine molecules of crystallisation and one of the two independent molecules in the asymmetric unit are omitted for clarity.

Azobenzene reductions utilising Ln(III) based reagents have also been reported recently. The reduced dinitrogen complexes such as $[\{(C_5Me_5)_2(THF)La\}_2(\mu\text{-}\eta^2\text{:}\eta^2\text{-}N_2)]$, (**CXVI**), facilitated the reduction of azobenzene to give the $\mu\text{-}\eta^2\text{:}\eta^2$ complex, $[\{(C_5Me_5)La(\mu\text{-}\eta^2\text{:}\eta^2\text{-}PhNNPh)(THF)\}_2]$, (**CXVII**). In this instance, the lanthanide(III) dinitrogen complex acts as a Lanthanide(II) synthon, *via* the liberation of the N_2^{2-} moiety as N_2 itself.[8]

3.1.3. Reduction of hydrazines.

Lanthanide mediated hydrazine reductions have been reported in limited cases. As described earlier in Section 1.1.6, reduction of an excess of hydrazine (NH_2NH_2) by $[(C_5Me_5)_2Sm]$, (**XI**), gave the tetranuclear complex, $[\{(C_5Me_5)Sm\}_4(NHNH)_2(NHNH_2)_4(NH_3)_2]$, (**X**).[9] Evans has also reported the dimetallation of hydrazine by either $[\{(C_5Me_5)_2Sm(\mu\text{-}H)\}_2]$, (**XIII**), and $[(C_5Me_5)_2Sm]$, (**XI**), to give $[\{(C_5Me_5)_2Sm\}_2(\mu\text{-}\eta^2\text{:}\eta^2\text{-}HNNH)]$, (**XII**).[10] Protonation of $[\{(C_5Me_5)_2Sm\}_2(\mu\text{-}\eta^2\text{:}\eta^2\text{-}HNNH)]$, (**XII**), by 2 equivalents of Et_3NHBPh_4 gave the bi-nuclear H_2NNH_2 complex, $[(C_5Me_5)_2Sm(THF)(H_2NNH_2)][BPh_4]$, (**XIV**).[11] The reactivity of hydrazines with the pentamethylcyclopentadienyl samarium systems is summarised in Scheme 3.1.

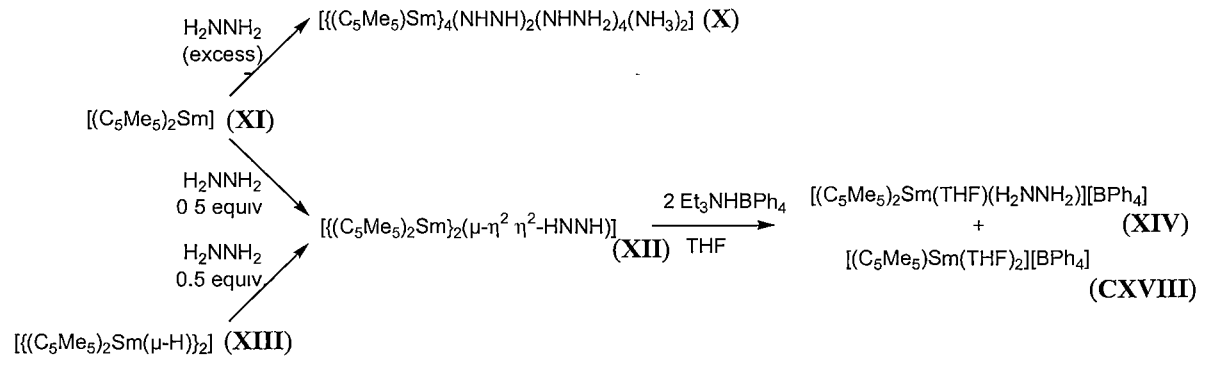

Scheme 3.1. Reactivity of hydrazine with samarium pentamethylcyclopentadienyl complexes.

Evans has also reported the reduction of diphenylhydrazine by $[(C_5Me_5)_2Sm(THF)_2]$, (**XXIV**) and $[(C_5Me_5)_2Sm]$, (**XI**) to yield the cleaved species $[(C_5Me_5)_2Sm(N(H)Ph)(THF)]$, (**CXIX**), and the non-cleaved THF adduct of the metallated species $[(C_5Me_5)_2Sm\{\eta^2\text{-}PhNHNPh\}(THF)]$, (**CXX**), shown in Figures 3.10 and 3.11, respectively.[10]

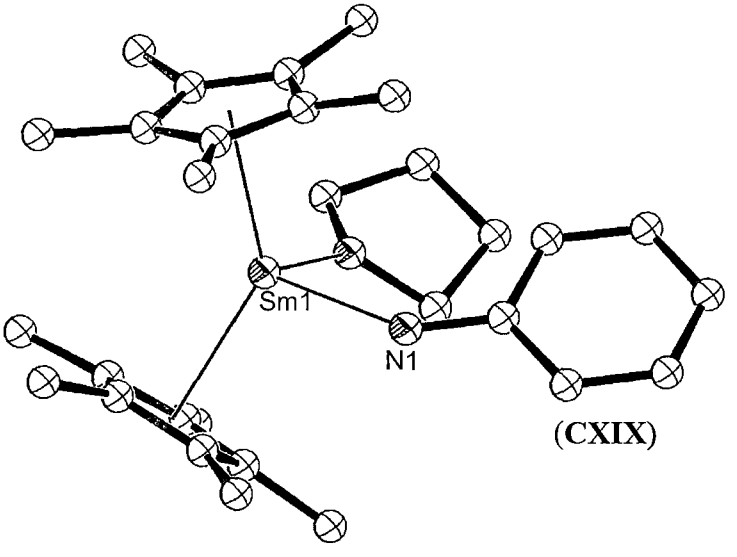

(**CXIX**)

Figure 3.10. Molecular structure of $[(C_5Me_5)_2Sm(N(H)Ph)(THF)]$, (**CXIX**). Figure generated from CCDC obtained coordinates. Atoms of arbitrary size. H atoms are omitted for clarity.

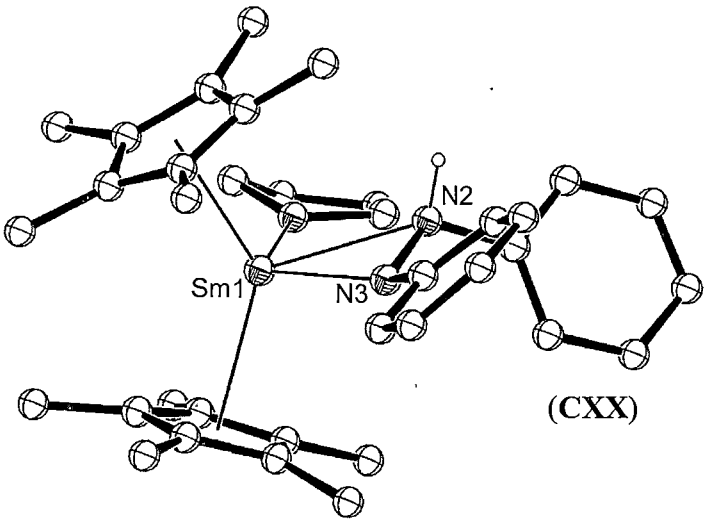

Figure 3.11. Molecular structure of $[(C_5Me_5)_2Sm\{\eta^2\text{-}PhNHNPh\}(THF)]$, (**CXX**). Figure generated from CCDC obtained coordinates. Atoms of arbitrary size. Non-hydrazine H atoms are omitted for clarity.

3.1.4. Reduction of azides.

No reports of the reaction of a lanthanide(II) reagent with an azide substrate have been made, though Niemeyer has utilised the bulky triazene, $Dmp(Tph)N_3^-$ (Dmp = 2,6-$Mes_2C_6H_3$ with Mes = 2,4,6-$Me_3C_6H_2$; Tph = 2-$TripC_6H_4$ with Trip = 2,4,6-*i*-$Pr_3C_6H_2$) to stabilise Eu(II), (**CXXI**), and Yb(II), (**CXXII**), complexes.[12]

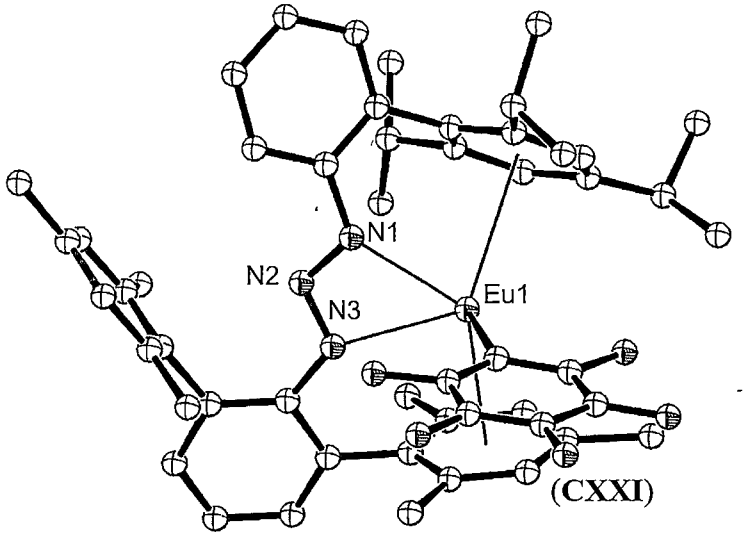

Figure 3.12. Molecular structure of $[Eu(Dmp(Tph)N_3)]$, (**CXXI**). Figure generated from CCDC obtained coordinates. Atoms of arbitrary size. H atoms are omitted for clarity.

Schumann has reported the synthesis of a samarium azide *via* reaction of the samarium(III) cyclopentadienyl $[(C_5H_5)_3Sm(THF)]$, (**CXXIII**), with LiN_3 to give $[Li(DME)_3][(C_5H_5)_3SmN_3Sm(C_5H_5)_3]$, (**CXXIV**).[13]

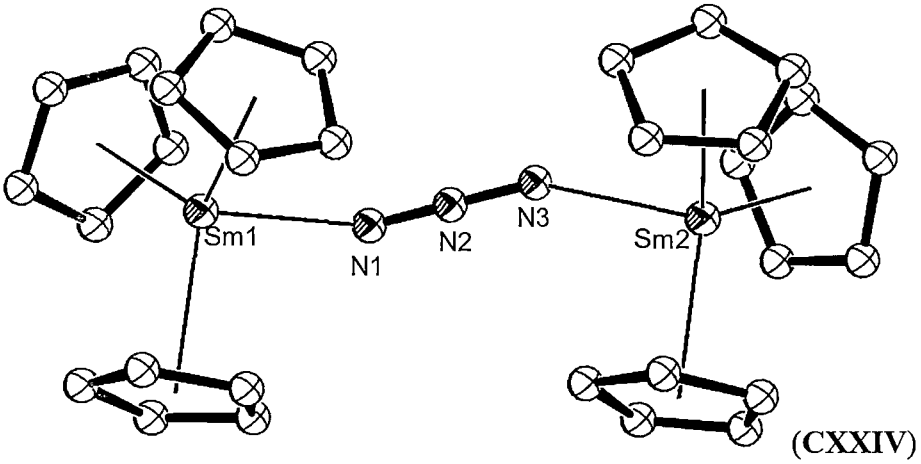

(**CXXIV**)

Figure 3.13. Molecular structure of $[Li(DME)_3][(C_5H_5)_3SmN_3Sm(C_5H_5)_3]$, (**CXXIV**). Figure generated from CCDC obtained coordinates. Atoms of arbitrary size. The $[Li(DME)_3]^+$ moiety and H atoms are omitted for clarity.

In contrast to their lack of use in lanthanide chemistry, azide substrates have been utilised frequently in transition metal chemistry to generate imido ligands *via* redox processes.[14] Similarly, since the first report of their use in 1985, where the trivalent uranium species, $[U(C_5H_4Me)_3(THF)]$, (**CXXV**) reductively cleaved PhN_3 to give the uranium(V) imide $[(C_5H_4Me)_3UNC_6H_5]$, (**CXXVI**),[15] their use in organoactinide chemistry has also yielded numerous imido complexes.[16]

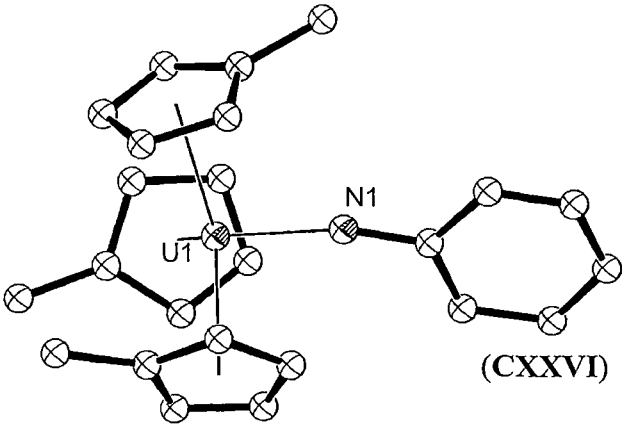

(**CXXVI**)

Figure 3.14. Molecular structure of $[U(C_5H_4Me),NC_6H_5]$, (**CXXVI**). Figure generated from CCDC obtained coordinates. Atoms of arbitrary size. H atoms are omitted for clarity.

3.1.5 Reduction of azines.

Studies of azine reductions by organolanthanide(II) reagents have been reported in limited cases. Evans reported the synthesis of $[\{(C_5Me_5)_2Sm\}_2\{\mu\text{-}\eta^3\text{:}\eta^3\text{-}(C_{12}H_8N_2)\}]$, (**CXXVII**), from the reduction of phenazine by $[(C_5Me_5)_2Sm]$, (**XI**). Allylic-type bonding between each Sm centre and the bridging dianionic phenazine ligand was observed, as shown in Figure 3.15, with Sm–N bond lengths of 2.360(2) Å.[17]

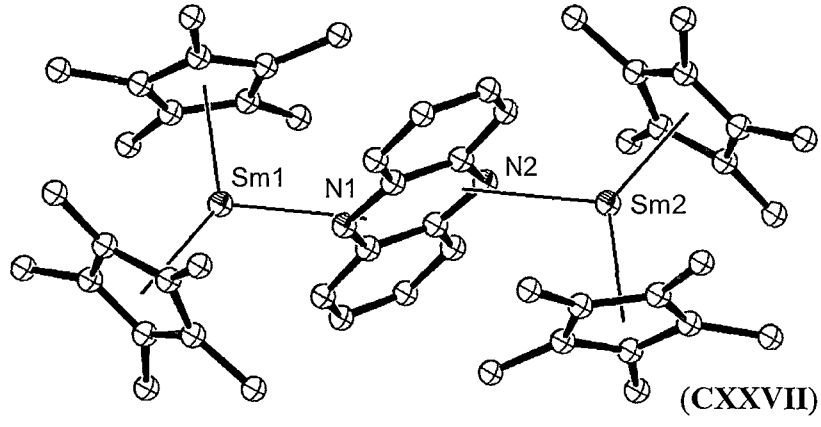

(CXXVII)

Figure 3.15. Molecular structure of $[\{(\eta^5\text{-}C_5Me_5)_2Sm\}_2\{\mu\text{-}\eta^3\text{:}\eta^3\text{-}(C_{12}H_8N_2)\}]$, (**CXXVII**). Figure generated from CCDC obtained coordinates. Atoms of arbitrary size. H atoms are omitted for clarity.

A lanthanum complex of phenazine has also been synthesised utilising the sterically induced reduction chemistry of the lanthanum(III) species, $[La(C_5Me_5)_3]$, (**CXXVIII**), to yield $[\{(C_5Me_5)_2La\}_2\{\mu\text{-}\eta^3\text{:}\eta^3\text{-}(C_{12}N_2H_8)\}]$, (**CXXIX**), which adopted a similar structure to $[\{(C_5Me_5)_2Sm\}_2\{\mu\text{-}\eta^3\text{:}\eta^3\text{-}(C_{12}H_8N_2)\}]$, (**CXXVII**).[18]

The reduction of benzaldehyde azine, (PhHC=NN=CHPh)) by $[(C_5Me_5)_2Sm(THF)_2]$, (**XXIV**), yielded a reductively coupled unsolvated dimeric complex, $[(C_5Me_5)_2Sm]_2[\mu,\eta^4\text{-}(PhCH=NNCHPh)_2]$, (**CXXIX**), as shown in Figure 3.16.[19]

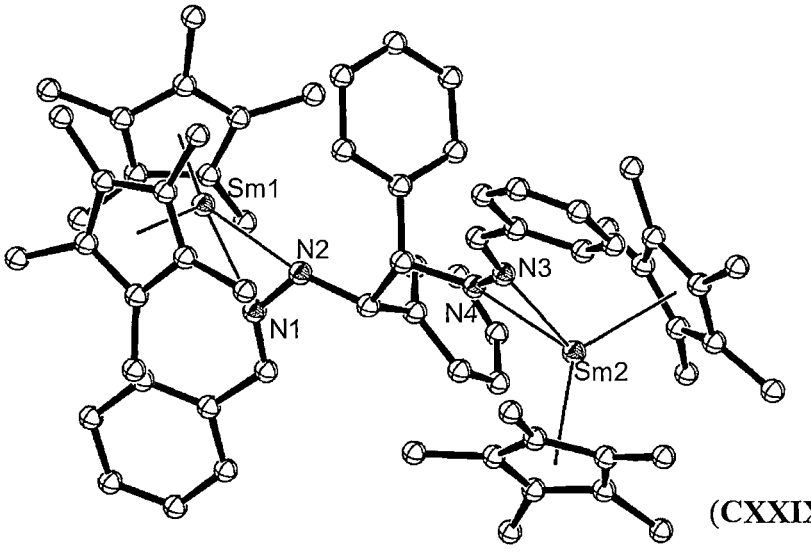

(CXXIX)

Figure 3.17. Molecular structure of $[(C_5Me_5)_2Sm]_2[\mu,\eta^2\text{-}(PhCH{=}NNCHPh)_2]$, (**CXXIX**). Figure generated from CCDC obtained coordinates. Atoms of arbitrary size. H atoms and disordered solvent molecules are omitted for clarity.

The reactivity of benzophenone azine by the actinide element uranium has been reported, yielding a bis(ketimido) complex. In this instance, KC_8 was used to prepare the U(III) species $[(C_5Me_5)_2UCl(KCl)]$, (**CXXX**), which functions as an equivalent to a U(II) reagent *via* auto-dissociation to give a mix of U(II) and U(IV) species,[20] that reacted with benzophenone azine to give the U(IV) bis(ketimido) $[(C_5Me_5)_2U(N{=}CPh_2)_2$, (**CXXXI**), as shown in Figure 3.18.[21]

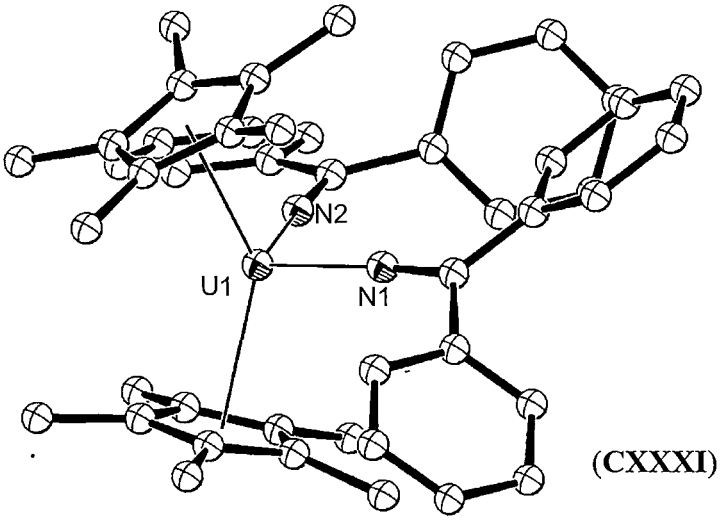

(CXXXI)

Figure 3.18. Molecular structure of $[(C_5Me_5)_2U(N{=}CPh_2)_2]$, (**CXXXI**) resulting from the reduction of benzophenone azine. Figure generated from CCDC obtained coordinates. Atoms of arbitrary size. H atoms and one of the two independent molecules of the asymmetric unit are omitted for clarity.

Previous studies into the reactivity of benzophenone azine by the samarium(II) macrocyclic complex, $[\{(THF)_2K(Et_8N_2O_2)Sm(\mu\text{-}I)\}_2]$, (**6**), have been undertaken by the author, yielding a mixture of products including the crystallographically authenticated $[(Et_8N_2O_2)Sm(\eta^2\text{-}NNC(Ph)_2)]$, (**CXXXII**).[22]

Results and Discussion:

3.2. Synthesis of macrocyclic samarium azo complexes

3.2.1. Synthesis of $[(Et_8N_2O_2)Sm\{\eta^2\text{-}N_2(Mes)_2\}]$, (**10**).

The reaction of the green, divalent samarium(II) complex $[\{(THF)_2K(Et_8N_2O_2)Sm(\mu\text{-}I)\}_2]$, (**6**), with azomesitylene, (**11**), in THF resulted in a dark green solution, which was filtered from a white precipitate, presumed to be the by-product of the reaction, KI. The dark green samarium(III) reduced azo complex · $[(Et_8N_2O_2)Sm\{\eta^2\text{-}N_2(Mes)_2\}]$, (**10**), was isolated as a crystalline solid from THF following concentration of the dark green solution *in vacuo*, as shown in Reaction 3.2.

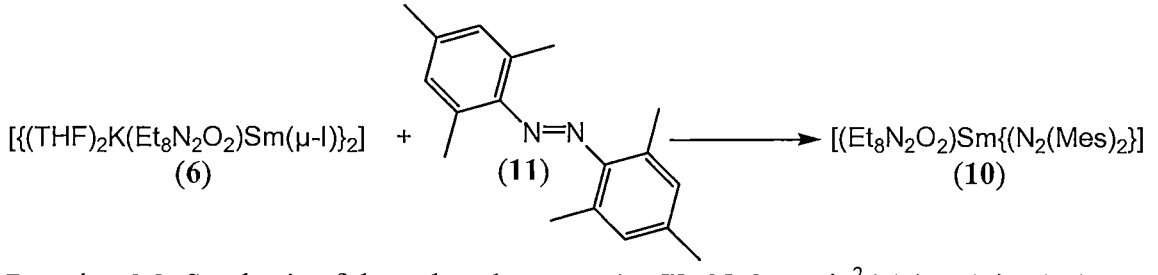

Reaction 3.2. Synthesis of the reduced azo species $[Et_8N_2O_2Sm\{\eta^2\text{-}N_2(Mes)_2\}]$, (**10**)

The reaction between $[\{(THF)_2K(Et_8N_2O_2)Sm(\mu\text{-}I)\}_2]$, (**6**), and azomesitylene, (**11**) occurs at a moderate rate, despite the low solubility of **6**, with the solution colour changing from light to dark green within half an hour of the addition of **11** to **6**. Removal of solvent *in vacuo* gave $[(Et_8N_2O_2)Sm\{\eta^2\text{-}N_2(Mes)_2\}]$, (**10**) as a dark green crystalline solid in 49 % isolated yield.

$[(Et_8N_2O_2)Sm\{\eta^2\text{-}N_2(Mes)_2\}]$, (**10**), exhibits high solubility in both THF and benzene, allowing the purity of the compound to be determined by ^1H NMR spectroscopy, with the proposed formulation also giving a satisfactory microanalysis. The radical anionic nature of the azomesitylene ligand, in conjunction with the

paramagnetic samarium(III) centre resulted in a wide chemical shift range in the ^1H NMR spectrum of the complex, with resonances occurring from –250 to 24 ppm.

The molecular structure of $[(Et_8N_2O_2)Sm\{\eta^2\text{-}N_2(Mes)_2\}]$, (**10**), was determined *via* a single crystal X-ray diffraction study, whilst ^1H NMR spectroscopic studies were consistent with the solid-state structure. **10** has a mononuclear solvent free structure with the samarium centre stabilised within the macrocyclic cavity. The samarium coordination sphere is completed with an η^2- interaction with the azomesitylene ligand. A three dimensional representation of **10** is shown in Figure 3.19. **10** represents the first report of a crystallographically authenticated reduced azomesitylene.

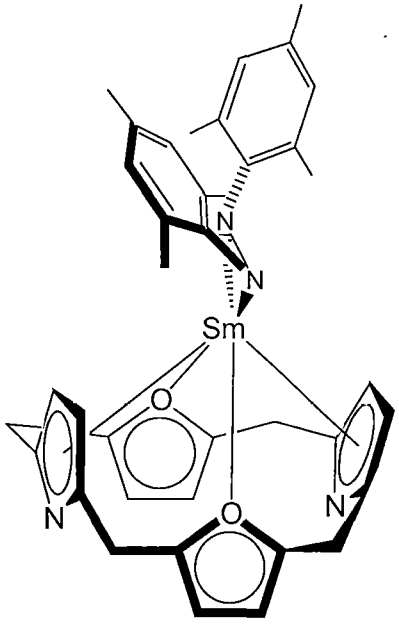

Figure 3.19. Three dimensional representation of $[(Et_8N_2O_2)Sm\{\eta^2\text{-}N_2(Mes)_2\}]$, (**10**). *Meso*-ethyl groups omitted for clarity.

$[(Et_8N_2O_2)Sm\{\eta^2\text{-}N_2(Mes)_2\}]$, (**10**) does not undergo further reduction upon addition of excess $[\{(THF)_2K(Et_8N_2O_2)Sm(\mu\text{-}I)\}_2]$, (**6**), in contrast to the reduction of azobenzene by $[(C_5Me_5)_2Sm(THF)_2]$, (**XXIV**). However, this result is to be expected given the steric bulk of the asomesitylene ligand.

3.2.2. Synthesis of $[(Et_8N_2O_2)Sm(\eta^2\text{-}N_2Ph_2)]$, (**12**).

The reaction of the green, divalent samarium(II) complex, $[\{(THF)_2K(Et_8N_2O_2)Sm(\mu\text{-}I)\}_2]$, (**6**), with azobenzene in THF gave a dark blue

coloured solution which was filtered from a white precipitate, presumed to be the by-product of the reaction, KI. Crystals of the dark blue samarium(III) reduced azo complex, $[(Et_8N_2O_2)Sm(\eta^2\text{-}N_2Ph_2)]$, (**12**) in good (78 % isolated) yield were obtained from a mixed solution of THF and benzene following concentration *in vacuo* as shown in Reaction 3.3.

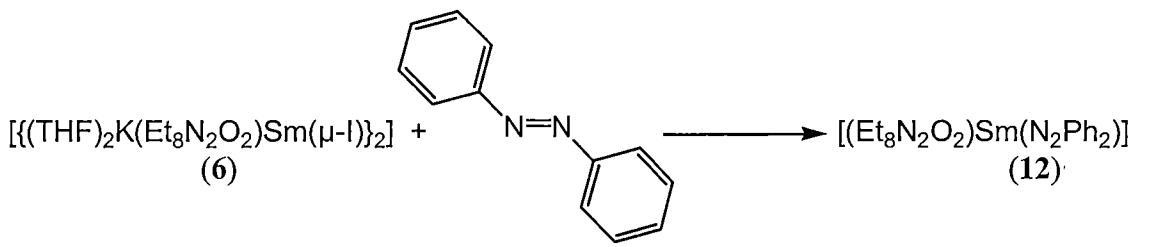

Reaction 3.3. Synthesis of the reduced azo macrocyclic lanthanide species $[(Et_8N_2O_2)Sm(\eta^2\text{-}N_2Ph_2)]$, (**12**)

Analogous to the reaction of $[\{(THF)_2K(Et_8N_2O_2)Sm(\mu\text{-}I)\}_2]$, (**6**) and azomesitylene, the reaction between **6** and azobenzene in THF or benzene occurs at a moderate rate, consuming all of the poorly soluble **6** to yield a dark blue solution of $[(Et_8N_2O_2)Sm(\eta^2\text{-}N_2Ph_2)]$, (**12**), within 30 minutes.

$[(Et_8N_2O_2)Sm(\eta^2\text{-}N_2Ph_2)]$, (**12**), is highly soluble in both THF and benzene, giving a dark blue solution in either case. The purity of **12** was confirmed through ^1H NMR spectroscopy, and microanalysis. Analogous to $[(Et_8N_2O_2)Sm\{\eta^2\text{-}N_2(Mes)_2\}]$, (**10**), the paramagnetic samarium(III) centre and reduced azobenzene radical anion in **12** cause a wide chemical shift range in the ^1H NMR spectrum of the complex, with resonances occurring from –260 to 21 ppm.

The molecular structure of $[(Et_8N_2O_2)Sm(\eta^2\text{-}N_2Ph_2)]$, (**12**), was able to be confirmed through single crystal X-ray diffraction. The molecular structure of **12** is analogous to that of $[(Et_8N_2O_2)\{\eta^2\text{-}N_2(Mes)_2\}]$, (**10**), forming a monomeric, solvent free structure with the samarium centre bound within the macrocyclic cavity of the porphyrinogen ligand, and the azobenzene unit completing the coordination sphere of the samarium centre with an η^2- bonding interaction through the two nitrogen centres. A schematic three dimensional representation of **12** is shown below in Figure 3.20.

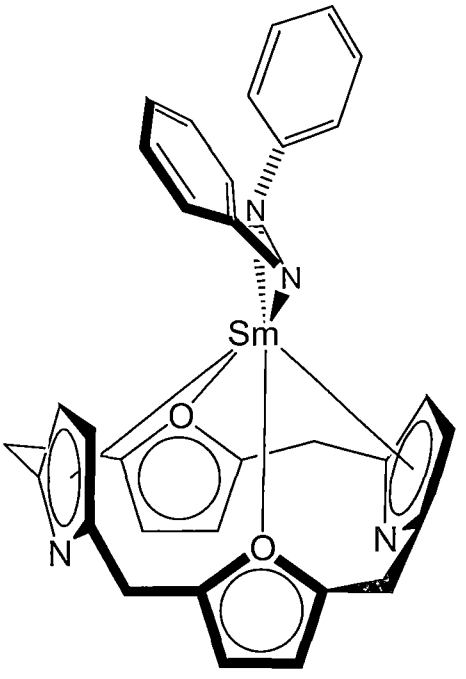

Figure 3.20. Three dimensional representation of $[(Et_8N_2O_2)Sm(\eta^2\text{-}N_2Ph_2)]$, (**12**). M*eso*-ethyl groups omitted for clarity.

3.2.3. NMR spectroscopy of macrocyclic samarium azo complexes.

The ^1H NMR spectra of both $[(Et_8N_2O_2)Sm\{\eta^2\text{-}N_2(Mes)_2\}]$, (**10**) and $[(Et_8N_2O_2)Sm(\eta^2\text{-}N_2Ph_2)]$, (**12**) exhibited wide chemical shift ranges due to the paramagnetic samarium(III) centres and radical azo anions. Full assignment of the ^{13}C NMR resonances was not possible due to these paramagnetic effects, however, partial assignment was achieved utilising gHMQC and gHMBC spectroscopic techniques. For both **10** and **12**, one of the two ^1H resonances attributed to the furanyl/pyrrolide CH centres exhibited significant de-shielding presumably resulting from the close proximity of the unpaired electron density of the azo ligand.

The ^1H NMR spectrum of $[(Et_8N_2O_2)Sm\{\eta^2\text{-}N_2(Mes)_2\}]$, (**10**), exhibits a loss of symmetry in the macrocyclic and mesityl ligands in the solution state compared to previous ^1H NMR spectroscopic studies of related compounds, from C_{2v} to C_2 symmetry, with no anti↔anti SmN_2 inversion observed, presumably as a result of the steric bulk of the *cis*-mesityl rings, preventing access to the intermediate syn SmN_2 geometry on the NMR time-scale, as shown in Figure 3.21. In contrast, $[(Et_8N_2O_2)Sm(\eta^2\text{-}N_2Ph_2)]$, (**12**) retains C_{2v} macrocyclic symmetry in the solution state suggesting that the *cis*-phenyl rings of the azobenzene moiety have a

sufficiently smaller steric bulk than the mesityl rings of **10** so as to allow ring inversion across the azo N–N bond on the NMR timescale.

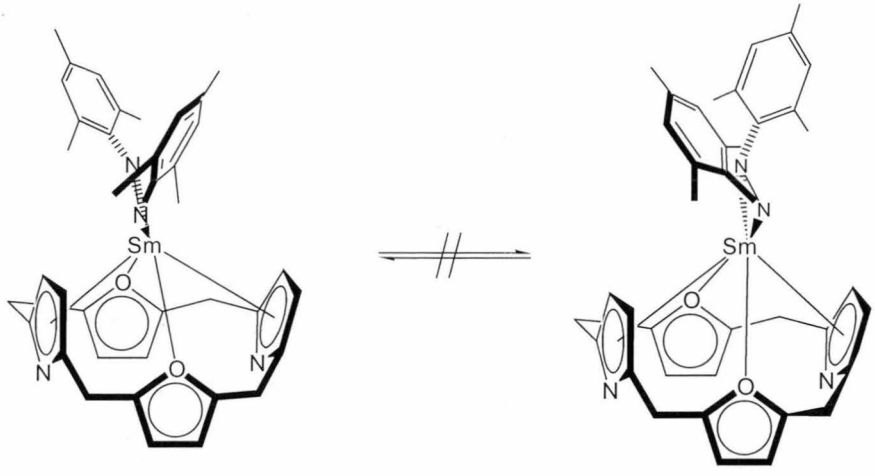

Figure 3.21. Mesityl ring inversion not observed for $[(Et_8N_2O_2)Sm\{\eta^2\text{-}N_2(Mes)_2\}]$, (**10**). *Meso*-ethyl substituents omitted for clarity.

Presumably, the *ortho*-methyl substituents of the mesityl rings in $[(Et_8N_2O_2)Sm\{\eta^2\text{-}N_2(Mes)_2\}]$, (**10**) exhibit significant steric interactions with the macrocyclic ligand, enforced by the proximity of each mesityl ring to each other. The steric interactions of the exterior methyl subsituents with the macrocyclic ligand, combined with the steric interactions between each mesityl ring therefore prevent the rotation of each aromatic ring required for ring inversion as shown in Figure 3.22.

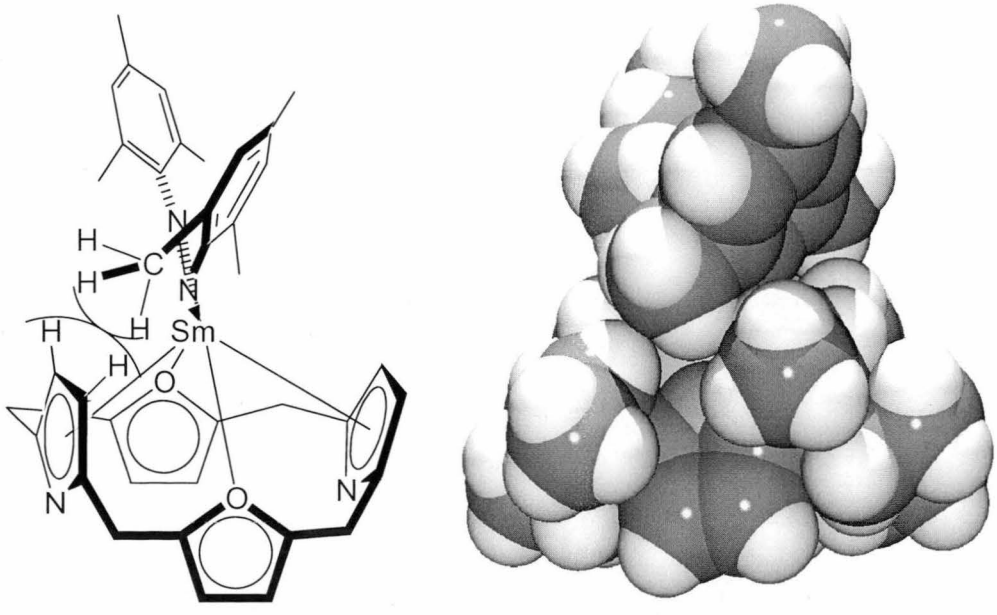

Figure 3.22. Representation of the macrocycle/mesityl steric interactions that prevent ring inversion in $[(Et_8N_2O_2)Sm\{\eta^2\text{-}N_2(Mes)_2\}]$, (**10**), (left) and spacefilling representation of **10** (right).

3.2.4. Molecular structure of $[(Et_8N_2O_2)Sm\{\eta^2\text{-}N_2(Mes)_2\}]$, (**10**)

Crystals of $[(Et_8N_2O_2)Sm\{\eta^2\text{-}N_2(Mes)_2\}]\cdot 2C_6H_5Me$, (**10**) suitable for single crystal X-ray diffraction studies were isolated from a toluene solution of **10** left to slowly evaporate at room temperature under nitrogen. The crystals were found to belong to the monoclinic space group, $P2_1/c$ (No. 14), a = 20.664(10), b = 12.824(11), c = 24.241(13) Å, with 6 molecules in the unit cell. The asymmetric unit consisted of one full molecule of $[(Et_8N_2O_2)Sm\{\eta^2\text{-}N_2(Mes)_2\}]$, (**10**) and two toluene molecules. The molecular structure of **10** is shown in Figure 3.23.

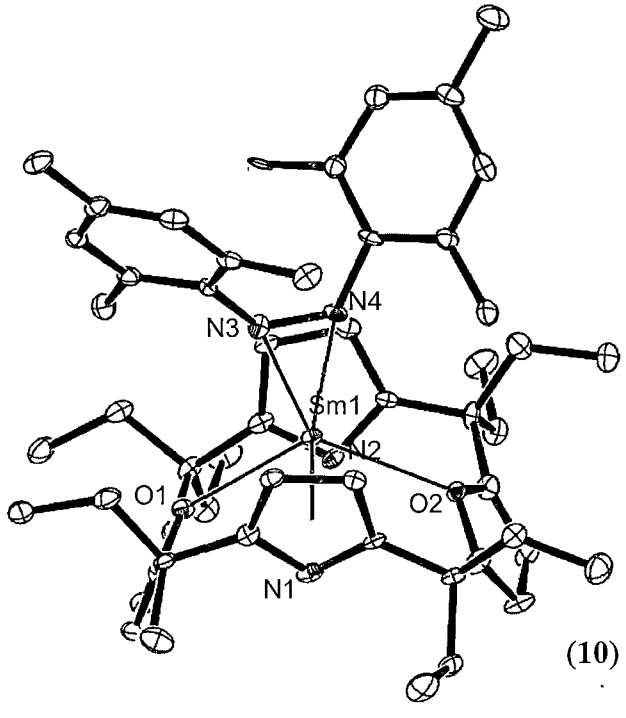

(**10**)

Figure 3.23. Molecular structure of $[(Et_8N_2O_2)Sm\{\eta^2\text{-}N_2(Mes)_2\}]$, (**10**). Thermal ellipsoids are shown at the 20 % level of probability. H atoms and two toluene molecules of crystallisation have been omitted for clarity.

As observed in previous samarium complexes of metallated *meso*-octaethyl-*trans*-dioxaporphyrinogen, the lanthanide centre in $[(Et_8N_2O_2)Sm\{\eta^2\text{-}N_2(Mes)_2\}]$, (**10**) is bound to the macrocycle through an $\eta^5{:}\eta^1\eta^5{:}\eta^1$ bonding motif, with the macrocycle adopting the 1,3-alternate conformation. The lanthanide centre is bound to the macrocycle through Sm–O (furanyl) interactions measuring 2.641(6) and 2.682(6) Å, and Sm–centroid (pyrrolide) interactions of 2.521_3 and 2.529_1 Å, which are consistent with previous samarium(III) complexes of the macrocyclic ligand, such as $[\{(Et_8N_2O_2)Sm(\mu\text{-}I)\}_2]$, (**8**), which exhibited Sm–O (furanyl) and Sm–centroid

(pyrrolide) interactions of 2.660(4) and 2.685(4) Å and 2.51_9 and 2.53_0 Å, respectively. The macrocyclic ligand in **10** exhibits significant buckling, with the furan and pyrrolide rings twisted with respect to the macrocyclic plane, as shown in Figure 3.24. This effect may also be observed in the average deviation of the *meso*-carbon centres from their least-squares plane of 0.32_9 Å, which is significantly larger than that observed in other macrocyclic samarium(III) complexes such as $[\{(Et_8N_2O_2)Sm(\mu\text{-}I)\}_2]$, (**8**), of 0.06_3 Å.

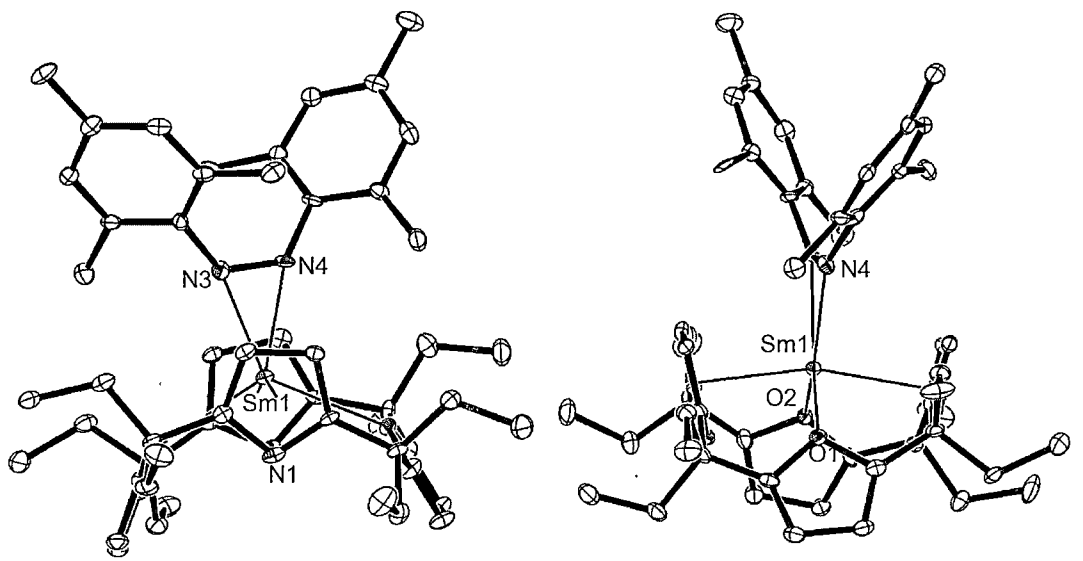

Figure 3.24. Molecular structure of $[(Et_8N_2O_2)Sm\{\eta^2\text{-}N_2(Mes)_2\}]$, (**10**). Side views demonstrating the buckling of the macrocyclic ligand. Thermal ellipsoids are shown at the 20 % level of probability. H atoms and two toluene molecules of crystallisation are omitted for clarity.

The azomesitylene ligand in $[(Et_8N_2O_2)Sm\{\eta^2\text{-}N_2(Mes)_2\}]$, (**10**), is bound to the lanthanide centre in a *cis* configuration, with the two mesitylene rings oriented above the binding groove available on the lanthanide centre resulting from the cavity of the macrocyclic ligand. The Sm–N (azomesitylene) interactions measure 2.366(7) and 2.344(8) Å, which are slightly shorter with those of $[\{(C_5Me_5)Sm\}_2(\mu\text{-}\eta^1\text{:}\eta^1\text{-}N_2Ph_2)]$, (**XCIX**) and $[Sm\{HB\text{-}(3,5\text{-}Me_2pz)_3\}_2(PhNNPh)]$, (**CVIII**), which both exhibited Sm–N interactions averaging 2.4_0 Å,[1,2] but are more similar to those of $[Sm(OAr)_2(PhNNPh)]$, (**CX**) which measured 2.37_2 Å.[3] The azomesitylene N–N bond length in **10** of 1.347(10) Å lies between the N=N bond length of free azomesitylene, 1.217(3) Å,[23] and the N–N bond length of diphenyl hydrazine, 1.45

Å[24] (dimesityl hydrazine structure has not yet been reported), as expected for the single electron reduced species, and is comparable to that observed in [Sm{HB-(3,5-$Me_2pz)_3\}_2$(PhNNPh)], (**CVIII**), of 1.332(12) Å. A summary of important bond lengths and angles for [$(Et_8N_2O_2)Sm\{\eta^2\text{-}N_2(Mes)_2\}$], (**10**) is presented in Table 3.1.

3.2.5. Molecular structure of [$(Et_8N_2O_2)Sm(\eta^2\text{-}N_2Ph_2)$], (**12**)

Crystals of [$(Et_8N_2O_2)Sm(\eta^2\text{-}N_2Ph_2)$], (**12**), suitable for X-ray diffraction studies were isolated from a concentrated THF/benzene solution left at room temperature for 72 hours. The crystals were found to belong to the triclinic space group, $P\bar{1}$ (No. 2), a = 14.024(7), b = 17.503(12), c = 18.348(10) Å, α = 80.86(4) β = 75.75(4), γ = 83.46(4) °, with four molecules of [$(Et_8N_2O_2)Sm(\eta^2\text{-}N_2Ph_2)$], (**12**) in the unit cell. The asymmetric unit consisted of two molecules of [$(Et_8N_2O_2)Sm(\eta^2\text{-}N_2Ph_2)$], (**12**), both of which possessed similar structural parameters, summarised in Table 3.1. The molecular structure of **12** is shown in Figures 3.25 and 3.26.

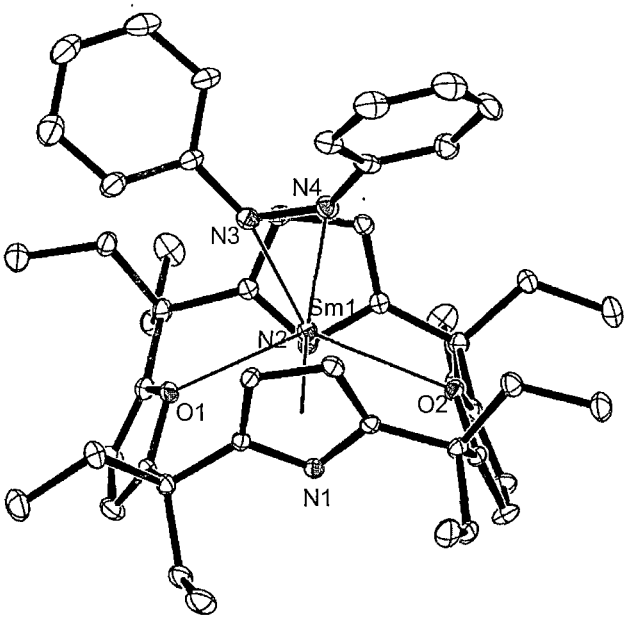

Figure 3.25. Molecular structure of one of the two molecules of [$(Et_8N_2O_2)Sm\{\eta^2\text{-}N_2(C_6H_5)_2\}$], (**12**), in the asymmetric unit. Thermal ellipsoids are drawn at the 20 % level of probability. H atoms are omitted for clarity.

[$(Et_8N_2O_2)Sm(\eta^2\text{-}N_2Ph_2)$], (**12**), forms a monomeric, solvent free structure in the solid state. As for previous lanthanide complexes of the *meso*-octaethyl-*trans*-dioxaporphyinogen ligand, the samarium centre in **12** is bound to the macrocyclic

ligand through an η^5:η^1:η^5:η^1 bonding motif, with the macrocycle adopting the 1,3-alternate conformation. The Sm–O (furanyl) and Sm–centroid (pyrrolide) distances in **12** which range from 2.619(3) – 2.675(3) and 2.496 – 2.511 Å, respectively, are consistent with previous Sm(III) complexes of the macrocycle, such as $[\{(Et_8N_2O_2)Sm(\mu\text{-}I)\}_2]$, (**8**), which exhibited Sm–O (furanyl) and Sm–centroid (pyrrolide) distances of 2.660(4) – 2.685(4) and 2.5_2 – 2.5_3 Å, respectively. Analogous to $[(Et_8N_2O_2)Sm\{\eta^2\text{-}N_2(Mes)_2\}]$, (**10**), **12** exhibits significant buckling of the macrocyclic ligand, observed in the average deviation of 0.32_3 and 0.26_7 Å for the *meso*- carbon atoms from the least squares planes of each macrocycle in the two independent molecules.

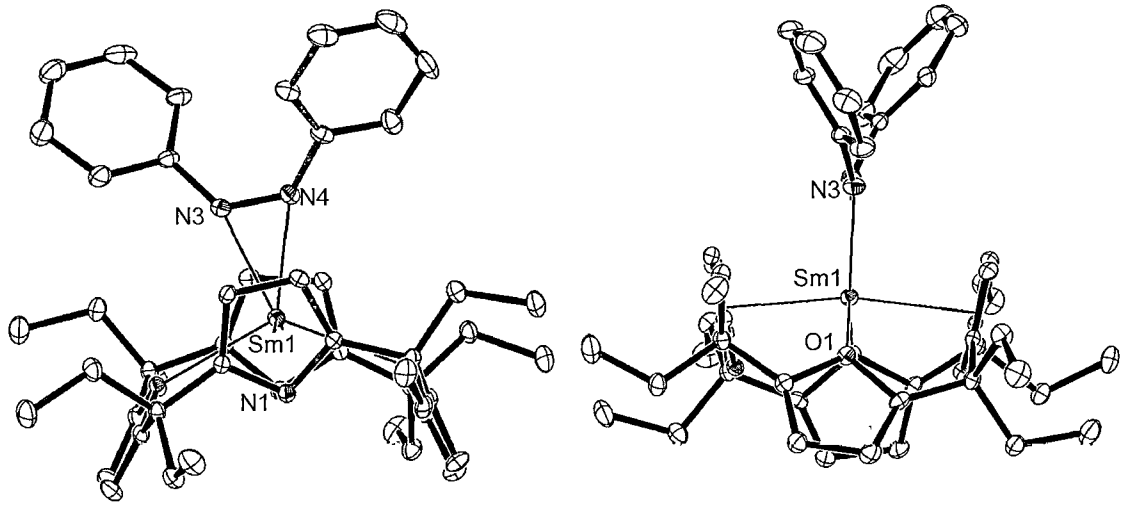

Figure 3.26. Side views of the molecular structure of $[(Et_8N_2O_2)Sm(\eta^2\text{-}N_2Ph_2)]$, (**12**). Thermal ellipsoids are drawn at the 20 % level of probability. H atoms are omitted for clarity.

The coordination sphere of the samarium(III) centre in $[(Et_8N_2O_2)Sm(\eta^2\text{-}N_2Ph_2)]$, (**12**), is completed with an η^2- interaction to the azobenzene moiety. The Sm–N (azobenzene) interactions measure between 2.337(3) – 2.375(4) Å, which are slightly shorter than those observed in $[(C_5Me_5)_2Sm\{\eta^2\text{-}N_2(C_6H_5)_2\}THF]$, (**CIV**) of 2.390(10) – 2.450(10) Å. The azobenzene N–N bond lengths in **12** of 1.345(4) and 1.360(5) Å are also comparable to those reported for $[(C_5Me_5)_2Sm\{\eta^2\text{-}N_2(C_6H_5)_2\}THF]$, (**CIV**) of 1.388(15) and 1.323(14) Å,[1b] which are consistent with a single electron reduction of azobenzene, lying between the 1.25 Å N=N distance of free azobenzene, and the 1.45 Å N–N bond length observed in diphenylhydrazine.[24]

Important bond lengths and angles for $[(Et_8N_2O_2)Sm\{\eta^2\text{-}N_2(Mes)_2\}]$, (**10**) and $[(Et_8N_2O_2)Sm(\eta^2\text{-}N_2Ph_2)]$, (**12**) are summarised in Table 3.1.

Distance (Å)/Angle (°)	**10**	**12** mol. A	**12** mol. B
Sm–O(fur)	2.641(6), 2.682(6)	2.619(3), 2.675(3)	2.644(3), 2.643(3)
Sm–N(pyr)	2.635(7), 2.639(8)	2.623(3), 2.619(3)	2.613(3), 2.628(3)
Sm–η^5(pyr)	2.52_1, 2.52_9	2.50_8, 2.49_6	2.51_2, 2.50_8
Sm–N(azo)	2.366(7), 2.344(8)	2.345(3), 2.354(3)	2.375(4), 2.337(3)
N–N(azo)	1.347(10)	1.345(4)	1.360(5)
$\eta^5(pyr)_1$-Sm-$\eta^5(pyr)_2$	163.1_3	167.9_3	167.9_0
N_1-Sm-N_2	110.2(2)	114.69(10)	114.22(10)
O_1-Sm-O_2	125.36(19)	129.70(8)	129.56(8)
Furanyl tilt	64.6_0, 64.0_3	69.3_2, 60.8_3	65.8_0, 61.8_7
Pyrrolide tilt	105.3_6, 105.6_3	102.4_8, 103.3_1	103.3_2, 103.1_7

Table 3.1. Summary of bond lengths and angles for the samarium(III) azo complexes, $[(Et_8N_2O_2)Sm\{\eta^2\text{-}N_2(Mes)_2\}]$, (**10**), and $[(Et_8N_2O_2)Sm(\eta^2\text{-}N_2Ph_2)]$, (**12**).

Despite the smaller steric bulk of the azobenzene substrate in $[(Et_8N_2O_2)Sm(\eta^2\text{-}N_2Ph_2)]$, (**12**), compared to the azomesityl substrate used in the formation of $[(Et_8N_2O_2)Sm\{\eta^2\text{-}N_2(Mes)_2\}]$, (**10**), the cooperative reduction of the azo unit by two samarium(II) centres to give a two electron reduced hydrazide species, analogous to that observed by Evans utilising $[(C_5Me_5)_2Sm(THF)_2]$, (**XXIV**),[1] was unable to be achieved. This result may be rationalised when the binding grooves of the samarium dioxaporphyrinogen and bis(pentamethylcyclopentadienyl) systems are compared, as shown in Figure 3.27. The steric congestion in **12** is shown in the space-filling representation of the molecule in Figure 3.28. In comparison, the singly reduced azobenzene complex bearing the bis(pentamethylcyclopentadienyl) ligand set, $[(C_5Me_5)_2Sm\{\eta^2\text{-}N_2(C_6H_5)_2\}THF]$, (**CIV**) possesses sufficient coordinative freedom to bind a THF ligand to the lanthanide centre, in addition to the azobenzene substrate. When two $[(C_5Me_5)Sm]$ units bind to the azobenzene ligand, the THF molecules are displaced, allowing the phenyl substituents to adopt a *trans*-

orientation. The bulk of the macrocyclic ligand in $[(Et_8N_2O_2)Sm(\eta^2\text{-}N_2Ph_2)]$, (**12**), does not allow a *trans*- azo ligand orientation and the differing reactivity trends of the samarium complexes of the bis(pentamethylcyclopentadienyl) and macrocyclic ligand sets can therefore be rationalised. Similarly, reduced azobenzene complexes bearing bulky auxiliary ligands such as the tris(pyrazolyl)borate ligand as discussed in Section 3.1.2 also exhibit monometallic reduced species.

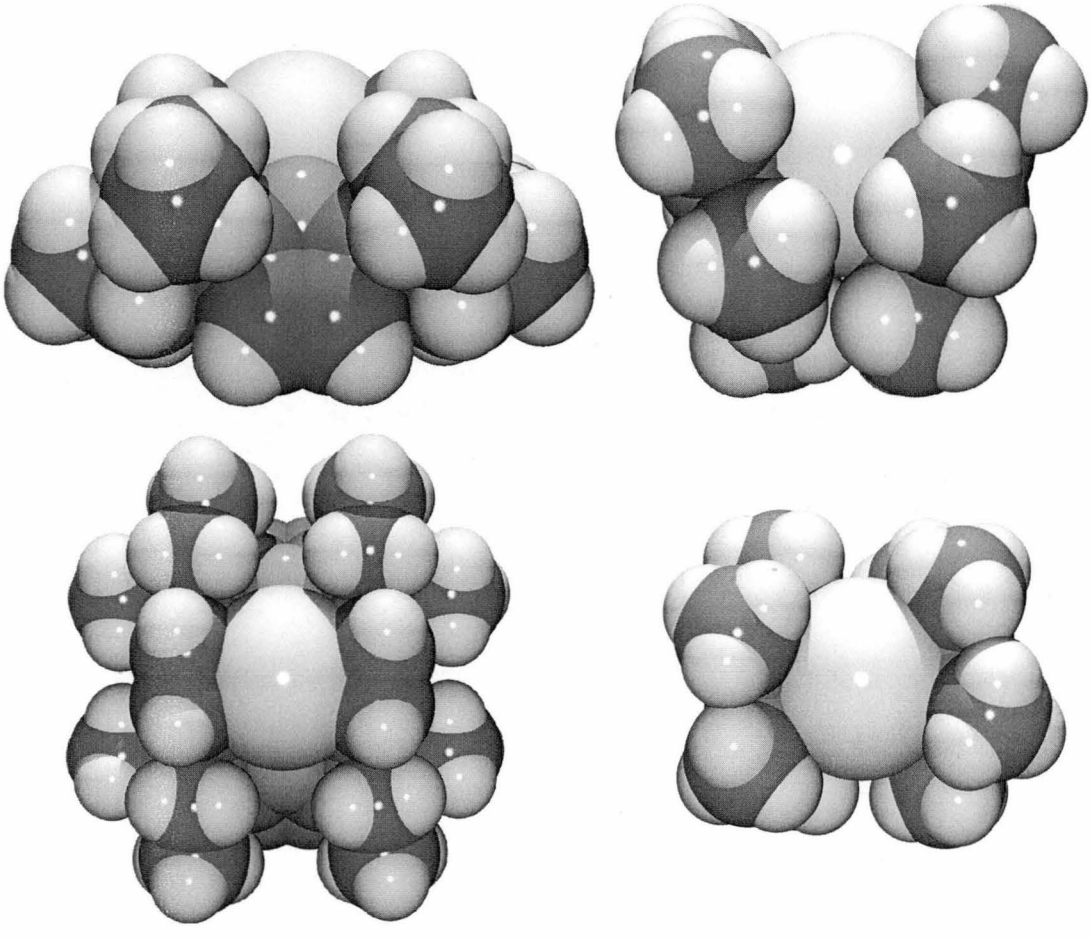

Figure 3.27. Comparative side and top space-filling representations of $[(Et_8N_2O_2)Sm]$ and $[(C_5Me_5)_2Sm]$, demonstrating the variation in binding grooves afforded by the two ligand sets. Figure generated with atomic coordinates from the asymmetric unit of $[\{(Et_8N_2O_2)Sm(\mu\text{-}I)\}_2]$, (**8**) for $[(Et_8N_2O_2)Sm]$ with the I atom omitted for clarity, and from CCDC obtained data of $[(C_5Me_5)_2Sm\ (THF)_2]$, (**XXIV**), for $[(C_5Me_5)_2Sm]$ with THF atoms omitted for clarity.

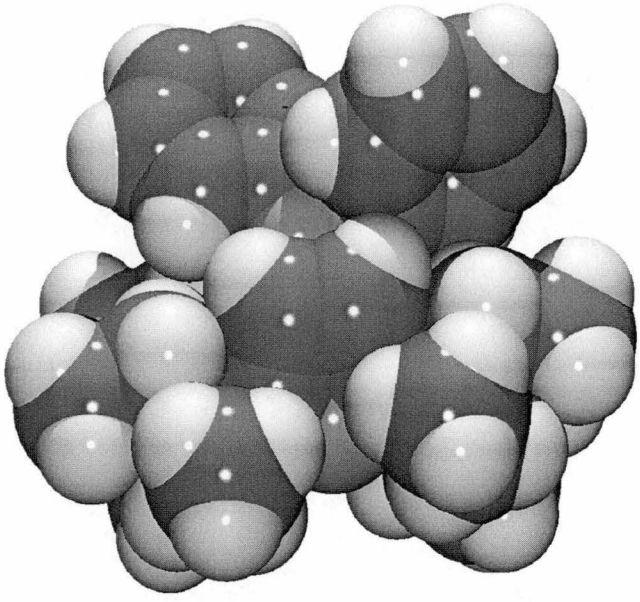

Figure 3.28. Space-filling representation of the reduced azobenzene macrocyclic samarium(III) complex, $[(Et_8N_2O_2)Sm(\eta^2\text{-}N_2Ph_2)]$, (**12**)

3.3. Further reductions of dinitrogen containing substrates utilising $[\{(THF)_2K(Et_8N_2O_2)Sm(\mu\text{-}I)\}_2]$, (6).

3.3.1. Reactivity of $[\{(THF)_2K(Et_8N_2O_2)Sm(\mu\text{-}I)\}_2]$, (**6**) with azides.

The reaction of the green divalent samarium complex $[\{(THF)_2K(Et_8N_2O_2)Sm(\mu\text{-}I)\}_2]$, (**6**) with mesityl azide, (**13**), in toluene resulted in the instantaneous bubbling of the solution, presumably liberating N_2. After 6 hours, the resulting red solution was filtered and solvent removed *in vacuo* to give a crude red solid. The reduction of the azide substrate was intended to give an imide complex, analogous to literature reports of transition metal azide reductions. Due to the possible incorporation of a counter-ion in the base of the macrocyclic cavity, a number of possible bridging or terminal imide structures are possible if the desired imidation reactivity is observed, as shown in Scheme 3.2.

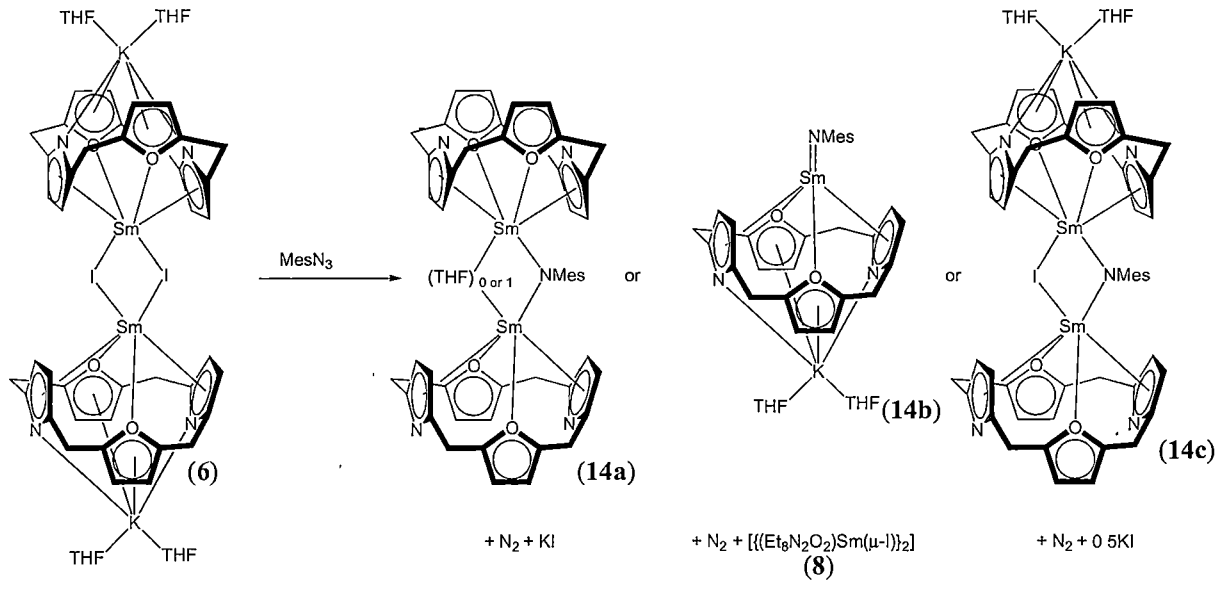

Scheme 3.2. Possible reactivity of the macrocyclic samarium(II) complex, $[\{(THF)_2K(Et_8N_2O_2)Sm(\mu\text{-}I)\}_2]$, (**6**) with $MesN_3$.

^1H NMR spectroscopy of the red solid indicated a complex mixture, which included paramagnetic compounds containing the dioxaporphyrinogen ligand, without a counter-ion in the base of the macrocyclic cavity based on ^1H NMR chemical shifts, see Section 2.3.1. Re-crystallisation of the red solid from toluene yielded a mixture of colourless crystals suitable for single crystal X-ray diffraction studies and an unidentified red precipitate. This revealed the colourless product to be the dipotassium macrocycle complex, $[\{(Et_8N_2O_2)K_2(toluene)\}_n]$, (**5**), presumably as a result of samarium displacement. Whilst the basis for samarium displacement in this instance is not clear, the stabilisation of the presumed imido nitrogen centre *via* further aggregation or reaction accompanied by the precipitation of the stable $[\{(Et_8N_2O_2)K_2(toluene)\}_n]$, (**5**), complex may be a driving force for the observed metal rearrangement. Attempts to characterise the red precipitate following re-crystallisation were unsuccessful. When the reaction of $[\{(THF)_2K(Et_8N_2O_2)Sm(\mu\text{-}I)\}_2]$, (**6**), with mesityl azide was carried out in THF, a large amount of an insoluble green solid precipitated in conjunction with an orange solid. The latter was identified by ^1H NMR spectroscopy as $[\{(Et_8N_2O_2)Sm(\mu\text{-}I)\}_2]$, (**8**). Upon heating, the green solid decomposed to an unknown insoluble white precipitate. Given the identification of $[\{(Et_8N_2O_2)Sm(\mu\text{-}I)\}_2]$, (**8**), from the reaction mixture, it is plausible that the green solid is a terminal macrocyclic lanthanide imide complex such as

$[(THF)_2K(Et_8N_2O_2)SmN(Mes)]$, (**14b**), as shown in Scheme 3.2. However the inherent poor crystallinity, solubility and stability of the green solid has prevented further characterisation.

3.3.2. Reactivity of $[\{(THF)_2K(Et_8N_2O_2)Sm(\mu\text{-}I)\}_2]$, (**6**) with hydrazines.

The reaction of the green divalent samarium(II) complex $[\{(THF)_2K(Et_8N_2O_2)Sm(\mu\text{-}I)\}_2]$, (**6**), with 1,2-diphenylhydrazine, (**15**) was attempted in THF, analogous to the reduction of 1,2-diphenylhydrazine by $[(C_5Me_5)_2Sm(THF)_2]$, (XXIV), which yielded $[(C_5Me_5)_2SmN(H)Ph(THF)]$, (**CXIX**), as discussed in Section 3.1.3. However, after prolonged heating at 50 °C, no reaction was evident.[10]

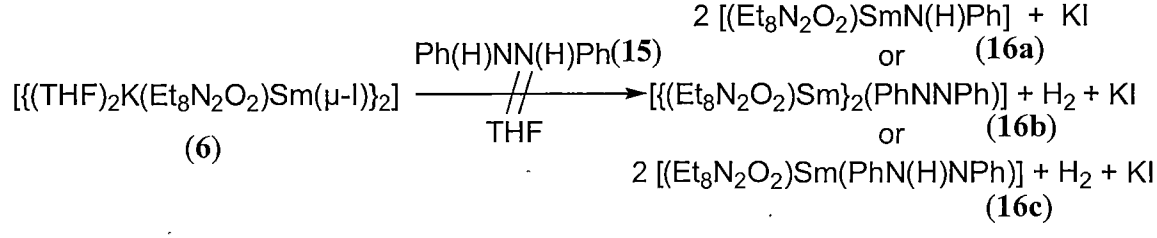

Scheme 3.3. Proposed reactivity of the macrocyclic samarium(II) complex, $[\{(THF)_2K(Et_8N_2O_2)Sm(\mu\text{-}I)\}_2]$, (**6**) with 1,2-diphenylhydrazine.

The observed lack of reactivity of $[\{(THF)_2K(Et_8N_2O_2)Sm(\mu\text{-}I)\}_2]$, (**6**), with 1,2-diphenylhydrazine contrasts with that observed by Evans for the samarium bis(pentamethylcyclopentadienyl) system, presumably resulting from the inability of the N atoms of the 1,2-diphenylhydrazine moiety to displace the bridging iodide atoms in $[\{(THF)_2K(Et_8N_2O_2)Sm(\mu\text{-}I)\}_2]$, (**6**), and allow electron transfer from the samarium(II) centre to the 1,2-diphenylhydrazine moiety.

3.4. Experimental

azomesitylene, (**11**)

11 was prepared according to a modified literature procedure.[25]

To a stirred solution of 2,4,6-trimethylaniline, (1.5 mL, 1.35 g, 10 mmol) and tetra-butylammonium bromide, (0.48 g, 1.5 mmol) in benzene (100 ml), $KMnO_4$ (4.52 g, 30 mmol) was added slowly in portions. The resulting purple solution was then stirred at room temperature for 7 hours before H_2O, (200 mL) was added. The bi-phasic suspension was then filtered, before the organic phase was separated and dried over sodium sulphate. Solvent was then removed *in vacuo*, before the crude orange solid was extracted with petroleum spirits and purified through a plug of silica gel. Cooling to -17 °C gave **11** as a pure red crystalline product (1.1 g, 83 %).

^{1}H NMR (C_6D_6, 299.905 MHz, 25 °C, ppm): δ 2.08 (s, 6H, *p*-CH_3), 2.43 (s, 12H, *o*-CH_3), 6.77 (s, 4H, Ar-H).

$[(Et_8N_2O_2)Sm\{N_2(Mes)_2\}]$, (**10**)

Toluene, (10 mL) was added to a flask containing $[\{(THF)_2K(Et_8N_2O_2)Sm(\mu\text{-}I)\}_2]$, (**6**), (0.20 g, 0.10 mmol) and azomesitylene, (**11**), (0.05 g, 0.19 mmol) before the suspension was stirred for 2 hours at room temperature before being let stand at room temperature overnight. The resulting dark green solution was then filtered from a white precipitate (presumably KI) and concentrated *in vacuo* and cooled to – 17 °C overnight to yield dark green crystals of **10** (0.09 g, 49 %).

^{1}H NMR (C_6D_6, 299.905 MHz, 25 °C, ppm): δ -247.69 (s, 6H, CH_3), -202.03 (s, 6H, CH_3) -196.52 (s, 6H, CH_3), -169.86 (s, 4H, *m*-CH), -164.35 (s, 2H, *m*-CH) -4.74 (dq(pseudo sextet), ^2J = 14.7 Hz, ^4J = 7.2 Hz, 2H, CH_2), -3.33 (dq, ^2J= 14.7 Hz ^4J = 7.2 Hz, 2H, CH_2), -1.03 (q, ^4J = 7.5 Hz, 12H, CH_3), -0.18 (dq, ^2J = 14.7 Hz, ^4J = 7.2 Hz, 2H, CH_2), 0.93 (t, ^3J = 7.5 Hz, 6H, CH_3), 1.28 (t, ^3J = 7.5 Hz, 6H, CH_3), 1.43 (dq, ^2J = 14.7 Hz, ^4J = 7.2 Hz, 2H, CH_2), 2.23 (dq, ^2J = 14.7 Hz, ^4J = 6.6 Hz, 2H, CH_2), 3.47 (dq, ^2J = 14.7 Hz, ^4J = 7.2 Hz, 2H, CH_2), 3.92 (dq, ^2J = 14.7 Hz, ^4J = 7.2 Hz, 2H, CH_2), 5.15 (d, ^2J = 3.6 Hz, 2H, fur/pyr CH), 5.58 (d, ^2J = 3.6 Hz, 2H, fur/pyr CH), 11.33 (s, 2H, fur/pyr CH), 23.65 (s, 2H, fur/pyr CH).

^{13}C{^{1}H} NMR (C_6D_6, 75.417 MHz, 25 °C, ppm): 5.20 (CH_3 (-1.03)), 7.84 (CH_3 (0.93)), 10.12 (CH_3 (1.28)), 59.18 (CH_2, (-0.18)), 63.24 (CH_2 (3.92)), 64.06 (CH_2 (1.43)), 77.98 (pyr or fur CH (11.33)), 95.90 (pyr or fur CH (23.65)), 108.08 (pyr or

fur CH (5.58)), 111.54 (pyr or fur CH (5.15)), 119.52 (pyr or fur CH (5.15)), 124.10 (pyr or fur CH (5.58)).

Anal. Calcd: C, 67.74; H, 7.37; N, 5.85 ($C_{54}H_{70}N_4O_2Sm$, MW 957.52 g/mol,)
Found: C, 67.81; H, 7.48; N, 5.70

$[(Et_8N_2O_2)Sm(N_2Ph_2)]$, (**12**)

Toluene (10 mL) was added to a flask containing $[\{(THF)_2K(Et_8N_2O_2)Sm(\mu\text{-}I)\}_2]$, (**6**), (0.25 g, 0.12 mmol) and freshly sublimed azobenzene (0.04 g, 0.22 mmol) before the suspension was stirred for 2 hours at room temperature, after which a dark blue precipitate had formed. THF (2 mL) was added, and the resulting solution was filtered from a white precipitate (presumably KI). The filtrate was then concentrated *in vacuo* and cooled to -17 °C to yield dark blue crystals of **12**, (0.15 g, 78 %).

^{1}H NMR (C_6D_6, 299.905 MHz, 25 °C, ppm): δ -259.65 (s, 4H, *o/m*-CH), -157.65 (s, 2H, *p*-CH), -149.41 (s, 4H, o/*m*-CH), -3.36 (m, 4H, CH_2), -1.06 (t, 12H, CH_3), 0.56 (m, 4H, CH_2), 1.07 (t, 12H, CH_3), 3.03 (m, 4H, CH_2), 3.21 (m, 4H, CH_2), 5.25 (s, 4H, pyr or fur CH), 20.65 (s, 4H, pyr or fur CH).

^{13}C{^{1}H} NMR (C_6D_6, 75.417 MHz, 25 °C, ppm): δ 7.24 (CH_3 (-1.06)), 8.10 (CH_3 (1.07)), 25.24 (*meso-C*CH_2), 35.08 (CH_2, (0.56)), 55.74 (CH_2, (3.03)), 66.98 (CH_2, 3.21), 105.02 (pyr or fur CH (20.65)), 110.80 (pyr or fur CH (5.25)), 122.86 (Ar-CH), 128.78 (Ar-CH), 151.98 (Ar-CH), 164.96 (Ar-*C*CH), 182.76 (α-C pyr or fur), 210.04 (α-C pyr or fur).

Anal. Calcd: C, 66.01; H, 6.69; N, 6.42 ($C_{48}H_{58}N_4O_2Sm$ MW 873.36)
Found: C, 66.12; H, 6.37; N, 6.14

mesityl azide, (**13**)

13 was prepared according to a modified literature procedure.[26]

To a stirred solution of 2,4,6-trimethylaniline (0.55 mL, 0.53 g, 3.9 mmol) in THF (7 mL), at 0 °C, was added a solution of concentrated HCl (1.6 mL) in water (14 mL). The resulting solution was then stirred at 0 °C for 15 minutes before a solution of $NaNO_2$ (0.54 g, 7.8 mmol) in water (6 mL) was added slowly, such that the temperature did not exceed 5 °C. The solution was then stirred at 0 °C for a further 15 minutes before urea was added until the solution was neutralised to pH 7.0. A solution of NaN_3 (0.60 g, 9.2 mmol) in water (6 mL) was then added and the solution stirred at room temperature for 1 hour. The mixture was then extracted 3 times with

diethyl ether (10 mL) and washed with a saturated solution of NaCl in water before being dried over Na_2SO_4. Diethyl ether was then removed *via* rotary evaporation and the crude oil was extracted in 40-60 °C petroleum spirits and run through a plug of silica gel before solvent was removed to give **13** as a pure yellow oil (0.50 g, 3.1 mmol, 79 %).

^{1}H NMR (C_6D_6, 299.905 MHz, 25 °C, ppm): δ 2.29 (s, 3H, *p*-CH_3), 2.36 (s, 6H, *o*-CH_3), 6.87 (s, 2H, Ar-CH).

1,2-diphenylhydrazine, (**15**)

15 was prepared according to a modified literature procedure.[27]

To a stirred solution of azobenzene (1.1 g, 6.0 mmol) in ethanol (150 mL), was added hydrazine hydrate (30 mL), before the solution was stirred at 60 °C for 3 hours. The resulting solution was poured into ice yielding **15** as a crude white solid, which was then recrystallised from 95 % ethanol (0.70 g, 63 %).

^{1}H NMR ($CDCl_3$, 299.905 MHz, 25 °C, ppm): δ 5.50 (broad, s, 2H, NH), 6.7-6.9 (m, 6H, Ar-CH), 7.1-7.2 (m, 4H, Ar-CH).

3.5. References

1. a) Evans, W.J.; Drummond, D.K.; Bott, S.G.; Atwood, J.L. *Organometallics* **1986**, *5*, 2389,
   b) Evans, W.J.; Drummond, D.K.; Chamberlain, L.R.; Doedens, R.J.; Bott, S.G.; Zhang, H.; Atwood, J.L. *J. Am. Chem. Soc.* **1988**, *110*, 4983.
2. Takats, J.; Zhang, X.W. *Organometallics* **1993**, *12*, 4286.
3. Yuan, F.; Liu, X. *Appl. Organometal. Chem.* **2005**, *19*, 877.
4. Evans, W.J.; Champagne, T.M.; Ziller, J.W. *Organometallics* **2007**, *26*, 1204.
5. Turcitu, D.; Nief, F.; Ricard, L. *Chem. Eur. J.* **2003**, *9*, 4916.
6. Roitershtein, D.M.; Lyssenko, K.A.; Belyakov, P.A.; Antipin, M.Y.; Petrov, E.S. *Izv.Akad.Navk SSSR (Russ. Chem. Bull.)* **1997**, 1667.
7. Kornienko, A.; Freedman, D.; Emge, T.J.; Brennan, J.G. *Inorg. Chem.* **2001**, *40*, 140.
8. Evans, W.J.; Lee, D.S.; Ziller, J.W.; Kaltsoyannis, N. *J. Am. Chem. Soc.* **2006**, 128, 14176-14184
9. Wang, K.G.; Stevens, E.D.; Nolan, S.P. *Organometallics* **1992**, *11*, 1011.
10. Evans, W.J.; Kociok-Köhn, G.; Leong, V.S.; Ziller, J.W. *Inorg. Chem.* **1992**, *31*, 3592.
11. Evans, W.J.; Kociok Köhn, G.; Ziller, J.W. *Angew. Chem., Int. Ed. Engl.* **1992**, *31*, 1081.
12. Hauber, S.O.; Niemeyer, M. *Inorg. Chem.* **2005**, *44*, 8644.
13. Schumann, H.; Janiak, C.; Pickardt, J. *J. Organomet. Chem.* **1988**, *349*, 117.
14. a) Zarubin, D.N.; Ustynuk, N.A. *Russ. Chem. Rev.* **2006**, 75, 671-707
    b) Edwards, N.Y.; Eikey, R.A.; Loring, M.I.; Abu-Omar, M.M. *Inorg. Chem.* **2005**, *44*, 3700.
15. Brennan, J.G.; Andenen, R.A. *J. Am. Chem. Soc.* **1985**, *107*, 514.
16. Warner, B.P.; Scott, B.L.; Burns, C.J. *Angew. Chem. Int. Ed.* **1998**, *37*, 959.
17. Evans, W.J.; Gonzales, S.L.; Ziller, J.W. *J. Am. Chem. Soc.* **1994**, *116*, 2600.
18. Evans, W.J.; Perotti, J.M.; Kozimor, S.A.; Champagne, T.M.; Davis, B.L.; Nyce, G.W.; Fujimoto, C.H.; Clark, R.D.; Johnston, M.A.; Ziller, J.W. *Organometallics* **2005**, *24*, 3916.
19. Evans, W.J.; Drummond, D.K. *J. Am. Chem. Soc.* **1989**, *111*, 3329.

20. Fagan, P.J.; Manriquez, J.M.; Marks, T.J.; Day, C.S.; Vollmer, S.H.; Day, V.W. *Organometallics* **1982**, *1*, 170.
21. Kiplinger, J.L.; Morris, D.E.; Scott, B.L.; Burns, C.J. *Organometallics* **2002**, *21*, 3073.
22. Stringer, D.N. *Honours Thesis* **2004**, School of Chemistry, University of Tasmania.
23. Gabe, E.J.; Wang, Y.; Barclay, L.R.C.; Dust, J.M. *Acta Crystallogr.* **1981**, *B37*, 978.
24. Allmann, R. in *The Chemistry of the Hydrazo, Azo, and Azoxy Groups*; Patai, S., Ed.; Wiley: New York, **1975**, Chapter 2
25. Hedayatullah, M.; Roger, A. *Bull. Soc. Chim. Belg.* **1993**, *102*, 59.
26. Murata, S.; Abe, S.; Tomioka, H. *J. Org. Chem.* **1997**, *62*, 3055.
27. Zhang, C.R.; Wang, Y.L. *Synth. Commun.* **2003**, *33*, 4205.

Chapter 4. Lanthanide amide chemistry.

4.1. Introduction to lanthanide amide complexes

4.1.1. Comment on lanthanide amide chemistry.

Substituted N donor amide ligands are prevalent throughout the literature, having found use in main group, transition metal and f-block chemistry. The incorporation of steric bulk on their complexes has been most important in directing the resulting chemistry and has allowed the investigation of many new classes of compounds. Due to the importance of these ligand types, particularly in main group and transition metal chemistry, they have been extensively reviewed elsewehere.[1]

Lanthanide complexes containing bulky amide ligands have similarly been reported in relative abundance in the literature. Initial studies concentrated on secondary amide compounds possessing steric bulk to form homoleptic complexes. Analogous to main group and transition metal amide complexes, lanthanide amide complexes have been active in key reactivity studies, such as dinitrogen fixation, as discussed in Section 1.1.5. Complexes bearing from 1 through to 4 amide ligands have been observed.

4.1.2 Lanthanide complexes of secondary amide ligands.

The bis(trimethylsilyl)amide ligand is the most abundant amide ligand in lanthanide chemistry, having first been reported in 1973 to stabilise a europium(III) centre in $[Eu\{N(SiMe_3)_2\}_3]$, (**CXXXIII**), as shown in Figure 4.1.[2] Since the isolation and characterisation of **CXXXIII**, lanthanide complexes bearing secondary amide ligands have been reported for metal oxidation states of +2, +3 and +4.[3]

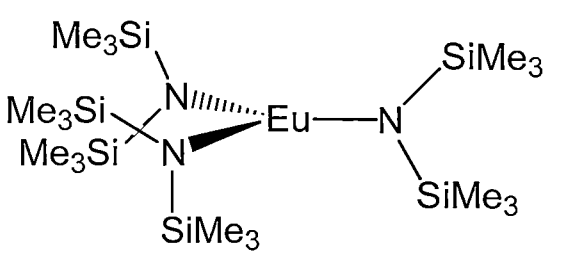

Figure 4.1. $[Eu\{N(SiMe_3)_2\}_3]$, (**CXXXIII**), the first lanthanide bis(trimethylsilyl)amide.

Aside from the bis(trimethylsilyl)amide ligand, a limited number of secondary amide ligands have been reported. Of these, diphenylamide complexes are most abundant, having first been reported in 1990 by Schumann who isolated $[Li(THF)_4][(C_5H_5)_2Lu(NPh_2)_2]$, (**CXXXIV**), shown in Figure 4.2, *via* proton abstraction from $HNPh_2$ by $[(C_5H_5)_2Lu(\mu\text{-}CH_3)_2Li(TMEDA)]$, (**CXXXV**).[4]

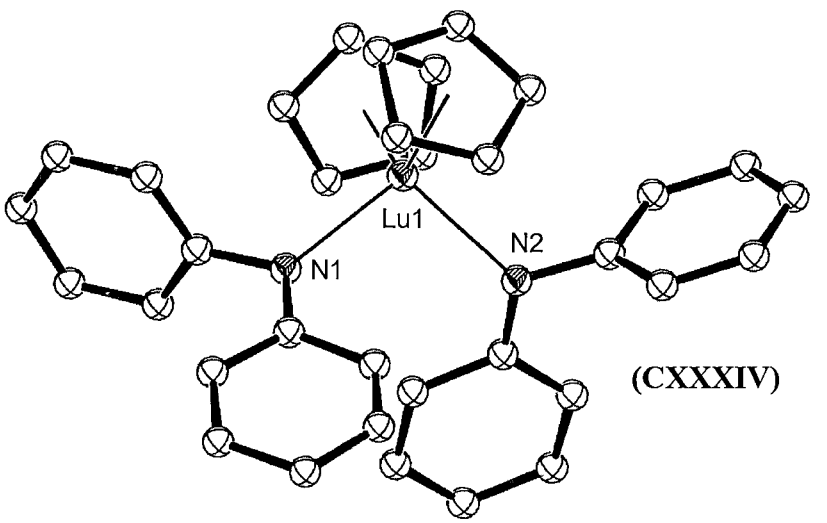

Figure 4.2. Molecular structure of $[(C_5H_5)_2Lu(NPh_2)_2][Li(THF)_4]$, (**CXXXIV**), the first lanthanide diphenylamide complex. Figure generated from CCDC obtained coordinates. Atoms of arbitrary size. H atoms, $[Li(THF)_4]^+$, and a disordered THF molecule of crystallisation are omitted for clarity.

Secondary amide ligands featuring both trimethylsilyl and aryl substituents have also been utilised to form stable lanthanide complexes. Metathetical exchange reactions were used to synthesise the first of this class of compound, $[Nd\{N(SiMe_3)(C_6H_3\text{-}2,6\text{-}i\text{-}Pr)\}_2Cl(THF)]$, (**CXXXVI**), shown in Figure 4.3, from the lithium amide and the corresponding neodymium trihalide.[5]

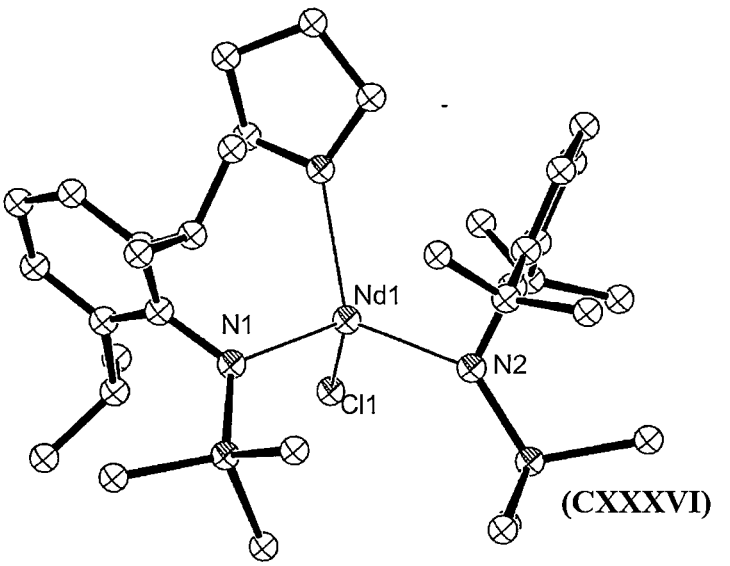

Figure 4.3. Molecular structure of [Nd{N(TMS)(C_6H_3-2,6-*i*-Pr)}$_2$Cl(THF)], (**CXXXVI**), the first mixed trimethylsilyl/aryl substituted lanthanide amide complex. Figure generated from CCDC obtained coordinates. Atoms of arbitrary size. H atoms and one disordered hexane molecule of crystallisation are omitted for clarity.

4.1.3. Lanthanide amide complexes bearing non-participative ligands.

Non-participative ligand sets such as the cyclopentadienyl ligand used in the synthesis of [Li(THF)$_4$][(C_5H_5)$_2$Lu(NPh_2)$_2$], (**CXXXIV**), above, have been used to form heteroleptic amide complexes containing only 1 or 2 amido ligands. Complexes utilising derivatives of the cyclopentadienyl and β-diketiminate ligand sets are most common. Of these, the cyclopentadienyl complexes were reported earliest, with the first such compound, [(C_5Me_5)Ce{N($SiMe_3$)$_2$}$_2$], (**CXXXVII**), as shown in Figure 4.4, being reported in 1989.[6]

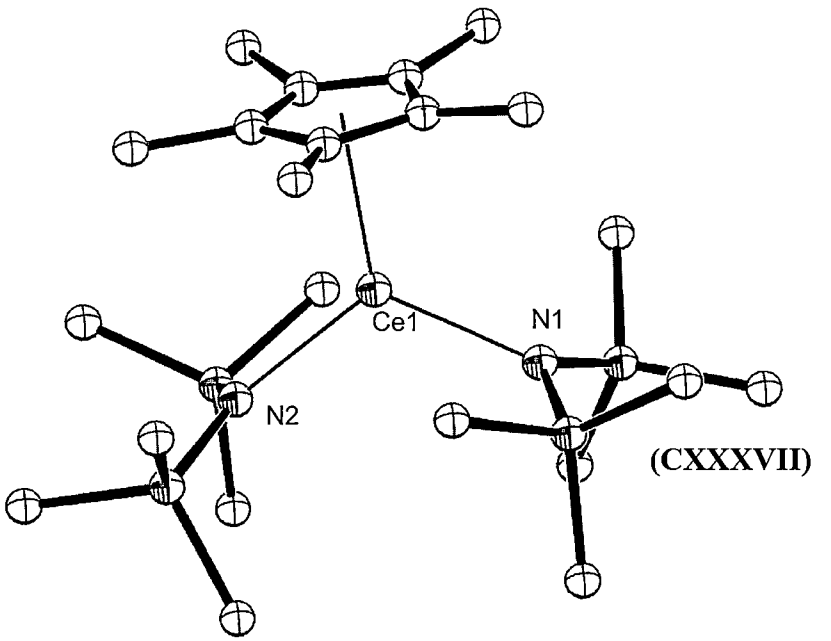

Figure 4.4. Molecular structure of $[(C_5Me_5)Ce\{N(SiMe_3\}_2)_2]$, (**CXXXVII**). Figure generated from CCDC obtained coordinates. Atoms of arbitrary size. H atoms are omitted for clarity.

Lanthanide secondary amide complexes bearing multidentate acyclic stabilising ligands, such as derivatives of the β-diketiminato ligand were first reported in 2001, with the synthesis of Sm, (**CXXXVIII**) and Nd, (**CXXXIX**) mono-bis(trimethylsilyl)amide complexes bearing the bis-5,5′-(1,3-propanediyldiimino)-2,2-dimethyl-4-hexen-3-onate ligand, as shown for the Sm case in Figure 4.5.[7] Since then, numerous complexes of secondary amido complexes utilising the β-diketiminato framework have been reported.[8]

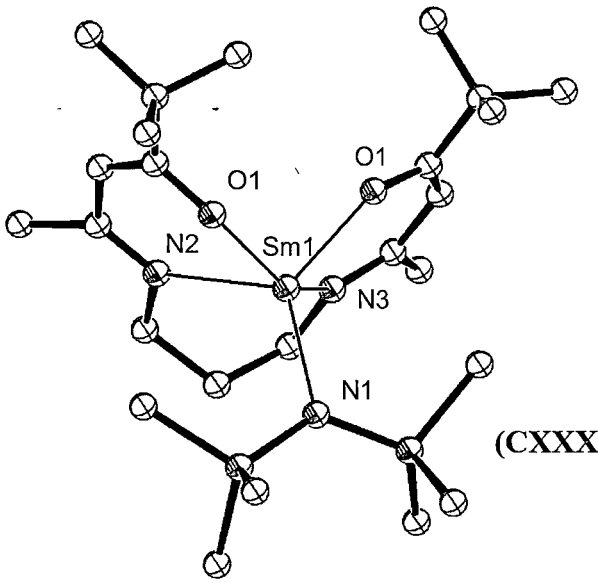

(CXXXVIII)

Figure 4.5. Molecular structure of $[Sm\{C_3H_6(NC_8H_{13}O)_2\}N(TMS)_2]$, (**CXXXVIII**). Figure generated from CCDC obtained coordinates. Atoms of arbitrary size. H atoms are omitted for clarity.[7]

Amide complexes employing cyclic multidentate ligands are limited to two complexes employing the modified porphyrinogen ligands, *meso*-octaethyl-*trans*-dioxaporphyrinogen, $[(Et_8N_2O_2)SmN(SiMe_3)_2]$, (**CXL**)[9] and *N,N'*-dimethyl-*meso*-octaethylporphyrinogen, $[(Et_8N_4Me_2)SmN(SiMe_3)_2]$, (**CXLI**).[10]

Both complexes resulted from metathetical exchange reactions of macrocyclic Sm(III) halide precursors with $NaN(SiMe_3)_2$, however, the furan substituted macrocyle exhibited further reactivity towards base resulting in γ-deprotonation to give $[(toluene)Na(Et_8N_2O_2)Sm\{N(SiMe_3)(Si(CH_3)_2CH_2)\}]$, (**XCV**) as a result of counter-cation stabilisation in the base of the macrocyclic cavity, as shown in Figure 4.6.

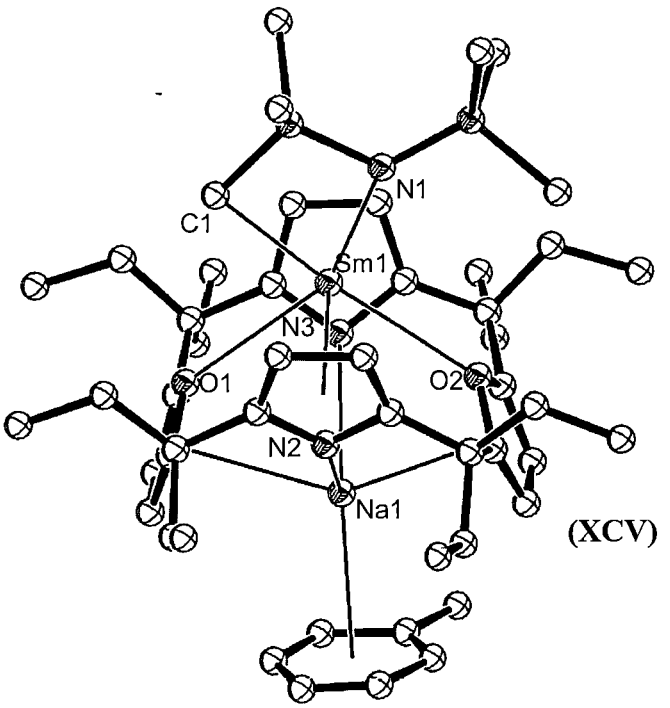

(XCV)

Figure 4.6. Molecular structure of [(toluene)Na($Et_8N_2O_2$)Sm{N($SiMe_3$)($Si(CH_3)_2CH_2$)}], (**XCV**). Atoms of arbitrary size. H atoms and one disordered toluene molecule of crystallisation are not shown for clarity.

The observed reactivity of [($Et_8N_2O_2$)SmN($SiMe_3$)$_2$], (**CXL**), towards excess base suggests that a primary lanthanide amide complex of the *meso*-octaethyl-*trans*-dioxaporphyrinogen ligand may also be susceptible to further deprotonation through the α-N-H proton to yield an imide species. This hypothesis is pursued in this chapter.

4.1.4. Overview of lanthanide complexes of primary amide ligands.

Primary amide ligands that only bear one bulky substituent have been reported for the lanthanides, though complexes featuring these ligands are far less abundant than their secondary amide counterparts. Evans reported the first primary amide complex, [(C_5Me_5)$_2$Sm(NHPh)], (**CXIX**), as shown in Figure 3.10., Section 3.1.3 from both the reduction of diphenylhydrazine, and proton abstraction from aniline. Studies of the formation of **CXIX** highlighted the possibility of N-N bond cleavage by lanthanide systems and subsequent H atom transfer – essential for any catalytic nitrogen fixation cycle.[11] The isolation of **CXIX** led to reactivity studies with KH,

$[(C_5Me_5)_2Sm(THF)]$, (**XXIV**) and $[(C_5Me_5)_2Sm]_2(\mu\text{-}H)_2]$, (**XIII**) in an attempt to deprotonate the amide ligand to yield an imide complex, however further reactivity was not observed. Since the isolation of $[(C_5Me_5)_2Sm(NHPh)(THF)]$, (**CXIX**), in 1992, numerous mono-, bis-, tris- and tetrakis-primary amide species have been reported. Incorporation of a strategically designed stabilising ligand can control the number of bound amide groups, resulting in mono- and bisamido- complexes.

4.1.5. Primary amide lanthanide complexes bearing cyclopentadienyl ligands.

Monoamide lanthanide complexes generally require auxiliary stabilising ligands to prevent aggregation of the metal centres. Typically, cyclopentadienyl ligands and derivatives thereof dominate the literature. Aryl amide compounds are most common and typically employ 2,6-disubstitution to control the coordination sphere of the metal.[12] Complexes containing a mix of cyclopentadienyl, amide and further ligands, such as $[(C_5Me_5)Lu(NHAr)(CH_2SiMe_3)(bipy)]$, (**CXLII**), (bipy = 2,2'-bipyridyl), as shown in Figure 4.7, are common.[12e] **CXLII** was found to undertake reactivity with CO, *via* insertion into a C-H bond of the (bipy) moiety following carbonylation of the alkyl group to yield $[(C_5Me_5)Lu(NHAr)\{OCH(CH_2SiMe_3)C_{10}H_7N_2\}]$, (**CXLIII**), as shown in Reaction 4.1.[12d]

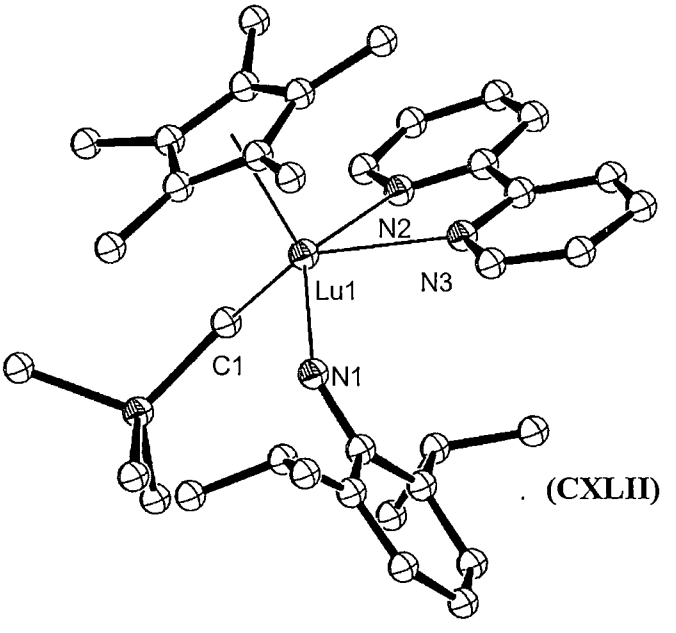

(CXLII)

Figure 4.7. Molecular structure of $[(C_5Me_5)Lu(NHAr)(CH_2SiMe_3)(bipy)]$, (**CXLII**). Figure generated from CCDC obtained coordinates. Atoms of arbitrary size. H atoms are omitted for clarity.

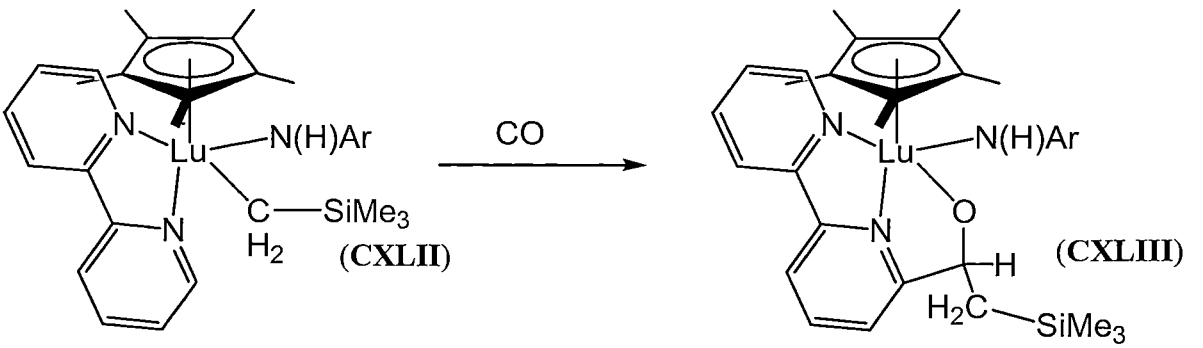

Reaction 4.1. CO insertion into $[(C_5Me_5)Lu(NHAr)(CH_2SiMe_3)(bipy)]$, (**CXLII**).

Recently, N-H bond activation of functionalised lanthanide primary amide compounds towards carbodiimides has been reported. Metathesis reactions were again employed to yield the precursor amide compounds, such as $[\{(C_5H_5)_2Yb[N(H)C_9H_6N]\}_2]$, (**CXLIV**), shown in Figure 4.8.[13] Reaction of **CXLIV** with carbodiimides, RN=C=NR, (R = Cy-hex, *i*-Pr), resulted in formal insertion of the carbodiimide into the amide N-H bond, as shown in Reaction 4.2 for the *i*-Pr case, yielding $[(C_5H_5)_2Yb\{\eta^1{:}\eta^2\text{-}i\text{-Pr-NC(N(H)-}i\text{-Pr)Nquinolyl}\}_2]$, (**CXLV**) .[13]

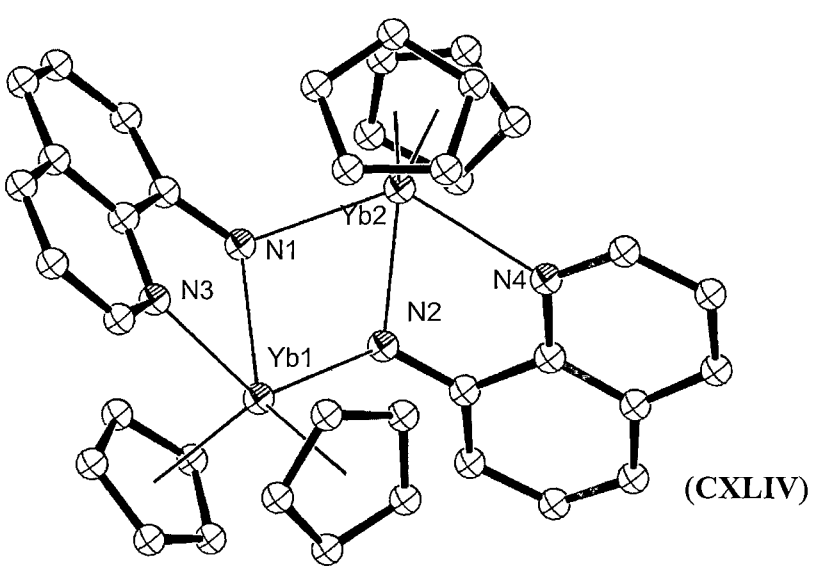

Figure 4.8. Molecular structure of $[\{Yb(C_5H_5)_2[N(H)C_9H_6N]\}_2]$, (**CXLIV**). Figure generated from CCDC obtained coordinates. Atoms of arbitrary size. H atoms and one of the two independent molecules of the asymmetric unit are not shown for clarity.

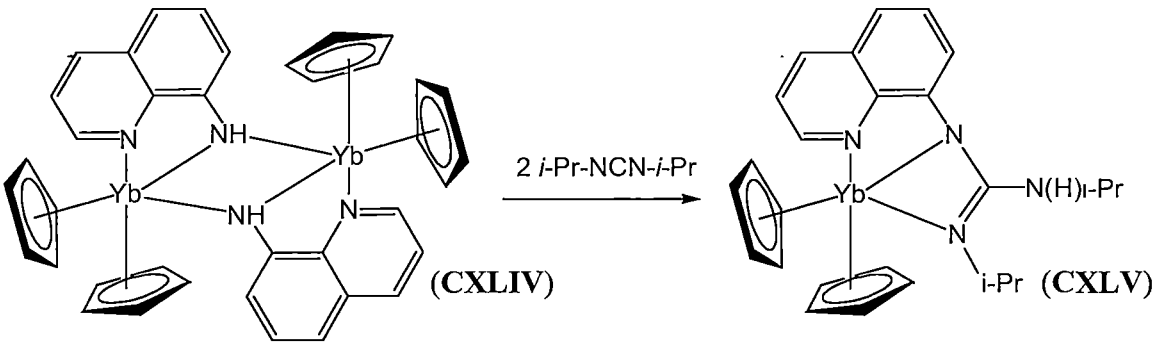

Reaction 4.2. Carbodiimide insertion into the amide N-H bond in $[\{(C_5H_5)_2Yb[N(H)C_9H_6N]\}_2]$, (**CXLIV**).

The reaction of $[(C_5Me_5)_2Sm(THF)_2]$, (**XXIV**), with $[K(NHC_6H_2\text{-}t\text{-}Bu_3\text{-}2,4,6)]$, (**CXLVI**), gave the corresponding Sm(II) monoamide complex $[(C_5Me_5)Sm[N(H)C_6H_2\text{-}t\text{-}Bu_3\text{-}2,4,6](\mu\text{-}C_5Me_5)K(THF)_2]$, (**CXLVII**), which was found to be active in styrene and ethylene polymerisation studies.[14]

$Ln(C_5H_5)_3$ complexes have also been successfully used to deprotonate pyrimidine compounds to yield the corresponding primary amides for Ln = Nd, (**CXLVIII**), Gd, (**CXLIX**), Dy, (**CL**) and Yb, (**CLI**), shown in Figure 4.9 for the Dy case. In each case, a dimeric complex resulted with two μ-$[2\text{-}N(H)\text{-}4,6\text{-}Me_2C_4N_2H_2]^-$ ligands bridging each Ln^{3+} centre. Further deprotonation of the amido nitrogen atoms was hoped for, but not achieved in this instance.[15]

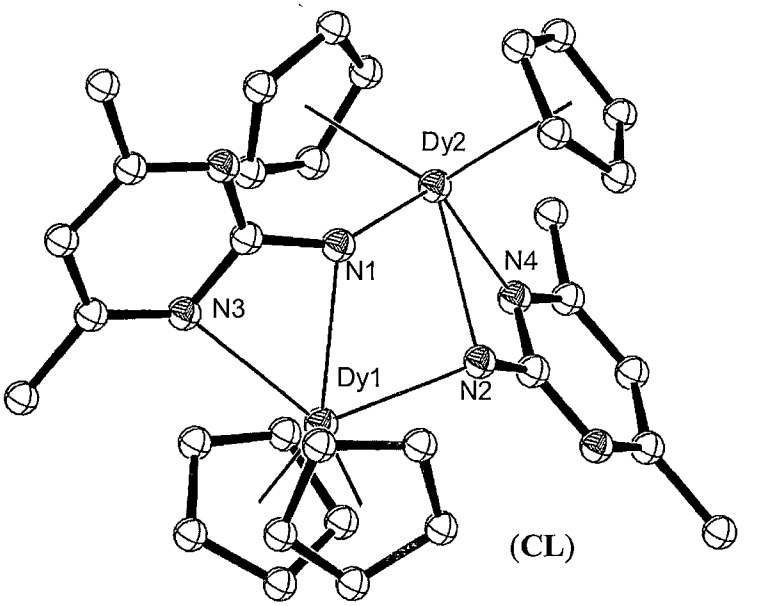

(CL)

Figure 4.9. Molecular structure of $[\{(C_5H_5)_2Dy[N(H)C_3H_2N_2\text{-}3,5\text{-}CH_3]\}_2]$, (**CL**). Figure generated from CCDC obtained coordinates. Atoms of arbitrary size. H atoms are omitted for clarity.

Substituted carboranyl-indenyl ligands possessing either an ether or tertiary amine side-arm have also been utilised to isolate primary amide lanthanide complexes of ytterbium $[\{\eta^5\text{:}\eta^1\text{:}\sigma\text{-}Me_2Si(C_9H_5CH_2\text{-}CH_2OMe)(C_2B_{10}H_{10})\}Yb(NHC_6H_3\text{-}2,6\text{-}i\text{-}Pr_2)(\mu\text{-}Cl)Li(THF)_3]$, (**CLII**), $[\{\eta^5\text{:}\ \eta^1\text{:}\sigma\text{-}Me_2Si(C_9H_5CH_2\text{-}CH_2NMe_2)(C_2B_{10}H_{10})\}Yb(NHC_6H_3\text{-}2,6\text{-}i\text{-}Pr_2)]$, (**CLIII**) and samarium, $[\{\eta^5\text{:}\eta^1\text{:}\sigma\text{-}Me_2Si(C_9H_5CH_2\text{-}CH_2NMe_2)(C_2B_{10}H_{10})\}Sm(\mu\text{-}NHC_6H_3\text{-}2,6\text{-}i\text{-}Pr_2)(\mu\text{-}Cl)Li\text{-}(THF)]$, (**CLIV**), were prepared *via* metathetical exchange of $Na\{N(H)C_6H_3\text{-}i\text{-}Pr_2\}$, (**CLV**) with the precursor lanthanide chloride complexes, and shown for **CLII** in Figure 4.10. No comment as to the reactivity of these complexes with base was reported.[16]

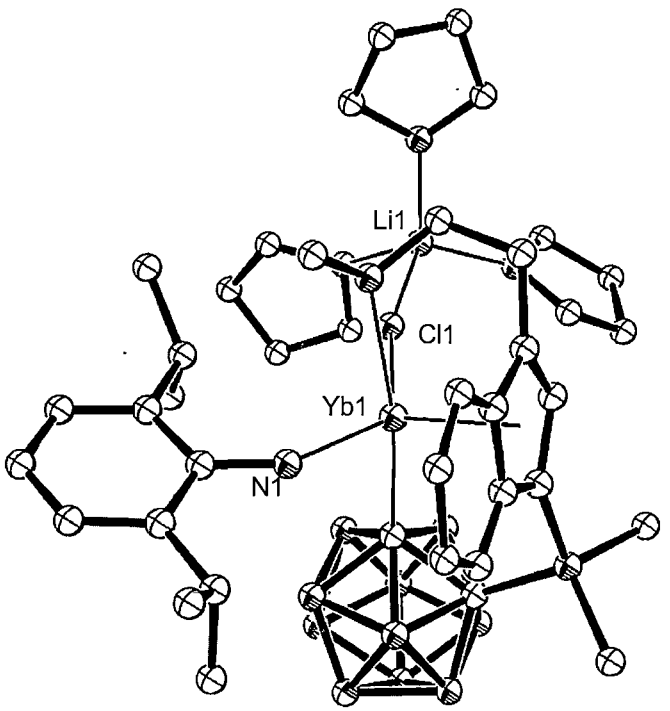

(CLII)

Figure 4.10. Molecular structure of $[\eta^5:\eta^1:\sigma\text{-}Me_2Si(C_9H_5CH_2\text{-}CH_2OMe)(C_2B_{10}H_{10})]Yb(NHC_6H_3\text{-}2,6\text{-}i\text{-}Pr_2)(\mu\text{-}Cl)Li(THF)_3]$, (**CLII**).[16a] Figure generated from CCDC obtained coordinates. Atoms of arbitrary size. H atoms are omitted for clarity.

4.1.6. Cyclopentadienyl free lanthanide primary amides.

Primary lanthanide amide complexes not bearing cyclopentadienyl ligands are almost exclusively limited to compounds without an auxiliary stabilising ligand. Consequently, complexes of this type generally bear three or four coordinated amide ligands.

Perfluoroarylamide ligands have been employed as ligands for homoleptic lanthanide amide complexes. In this instance, secondary Ln-F interactions were observed in the complex resulting from the reaction of $[Sm\{N(SiMe_3)_2\}_3]$, (**CLVI**), with pentafluoroaniline, $[Sm\{N(H)C_6F_5\}_3(THF)_3]$, (**CLVII**), shown in Figure 4.11.[17]

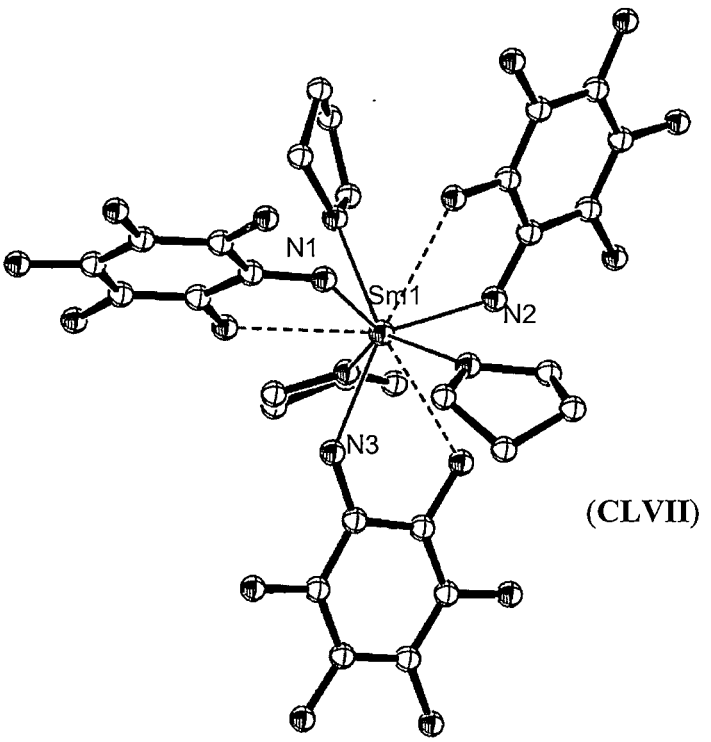

(CLVII)

Figure 4.11. Molecular structure of $[Sm\{N(H)C_6F_5\}_3(THF)_3]$, (**CLVII**). Figure generated from CCDC obtained coordinates. Atoms of arbitrary size. H atoms and one THF molecule of crystallisation are omitted for clarity.

Similar deprotonation methods were used to synthesise the La amide complex, $[\{La(N(H)C_6H_3\text{-}i\text{-}Pr_2)_3\}_2]$, (**CLVIII**), from the reaction of 2,6-diisopropylaniline with $[La\{N(SiMe_3)_2\}_3]$, (**CLIX**). The X-ray crystallographically authenticated dimer was shown to be fluxional in the solution state, with a monomer-dimer equilibrium present.[18]

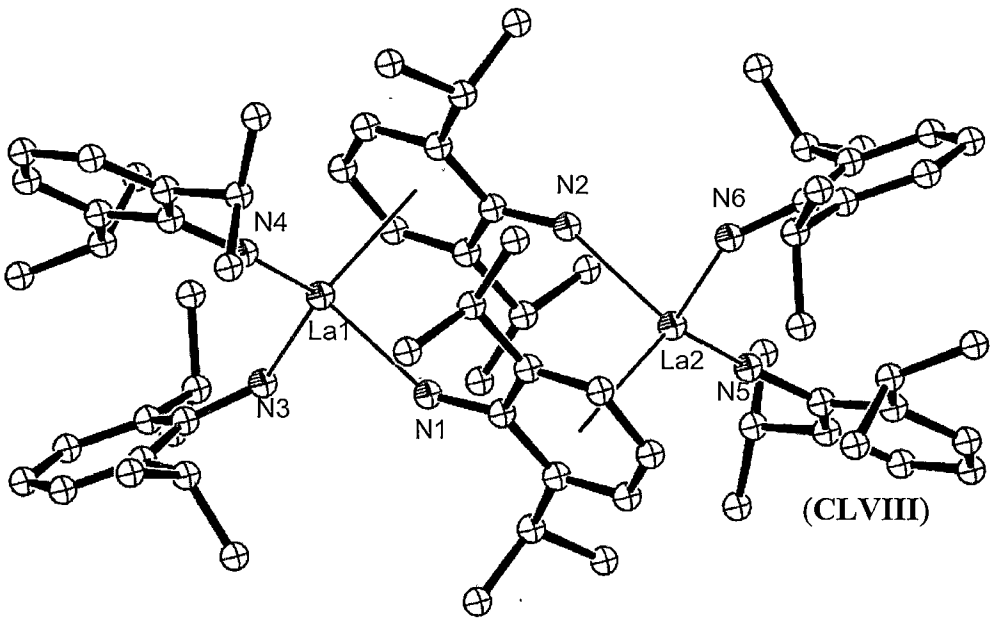

Figure 4.12. Molecular structure of $[\{La(N(H)C_6H_3\text{-}i\text{-}Pr_2)_3\}_2]$, (**CLVIII**). Figure generated from CCDC obtained coordinates. Atoms of arbitrary size. H atoms are omitted for clarity.

Arnold has reported the synthesis of the only primary amide complex featuring an auxiliary stabilising ligand other than the cyclopentadienyl ligand. In this instance, a β-diketiminato ligand was utilised, which gave the bis(amide) complex $[\{(2,6\text{-}i\text{-}Pr_2C_6H_3NC(Me)CHC(Me)NC_6H_3Pr_2\text{-}i\text{-}2,6\})Sm(N(H)C_6H_2\text{-}t\text{-}Bu_3\text{-}2,4,6)_2]$, (**CLX**) from a metathetical exchange reaction between $[\{\{2,6\text{-}i\text{-}Pr_2C_6H_3NC(Me)CHC(Me)NC_6H_3Pr_2\text{-}i\text{-}2,6\}SmCl_2\}_2(THF)]$, (**CLXI**) and $[KN(H)C_6H_2\text{-}t\text{-}Bu_3\text{-}2,4,6]$, (**CLXII**). **CLX** contains two amido units bound to the metal centre leading to a very sterically congested structure, as shown in Figure 4.13. No comment as to the reactivity of this complex with base was reported. [8e]

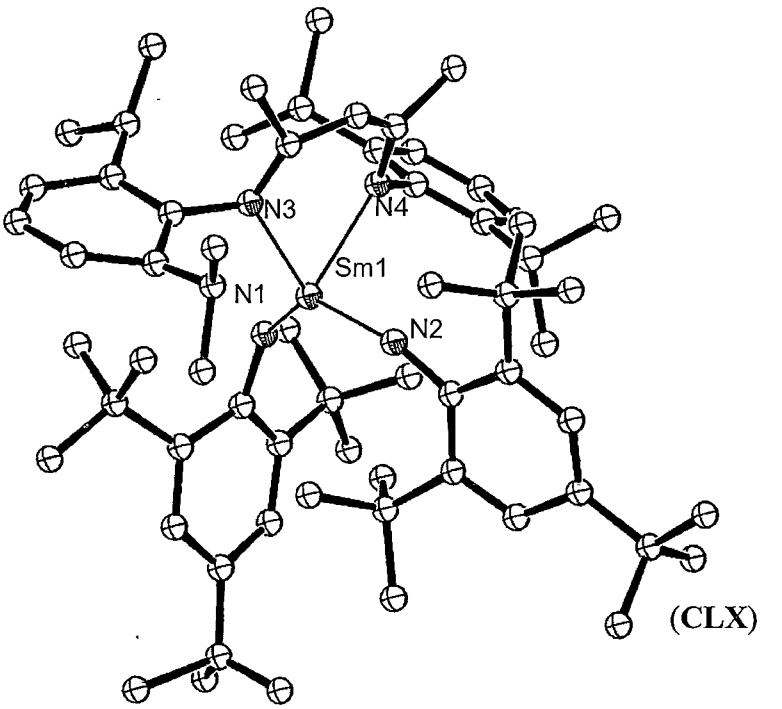

Figure 4.13. Molecular structure of [{(2,6-*i*-$Pr_2C_6H_3NC(Me)CHC(Me)NC_6H_3Pr_2$-*i*-2,6})$Sm(N(H)C_6H_2$-*t*-$Bu_3$-2,4,6)$_2$], (**CLX**). Figure generated from CCDC obtained coordinates. Atoms of arbitrary size. H atoms, one of the two independent molecules of the asymmetric unit, one hexane molecule of crystallisation and disorder within the molecule have been omitted for clarity.[8e]

Investigations into 2,6-disubstituted aryl ligands demonstrated the necessity for steric bulk in these positions to prevent dimerisation *via* bridging at the amido N position. *i*-propyl substitution resulted in stable mononuclear complexes, shown for [$Nd(NHC_6H_3iPr_2$-2,6)$_3(THF)_3$], (**CLXIII**) in Figure 4.14, whilst methyl substitution gave bimetallic species, as shown for [{$K(THF)_6$}$_2$][{$Sm(\mu$-$NHC_6H_3Me_2$-2,6)$(NHC_6H_3Me_2$-2,6)$_3$}$_2$], (**CLXIV**) in Figure 4.15.[19]

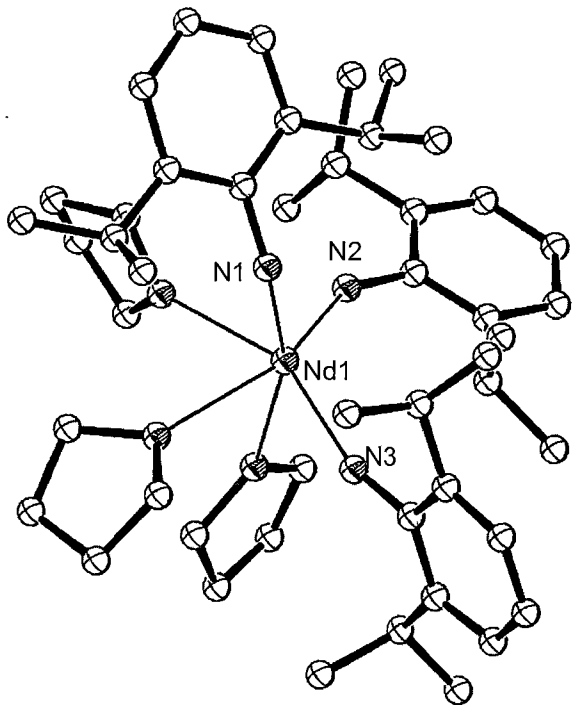

(CLXIII)

Figure 4.14. Molecular structure of $[Nd(NHC_6H_3iPr_2\text{-}2,6)_3(THF)_3]$, (**CLXIII**). Figure generated from CCDC obtained coordinates. Atoms of arbitrary size. H atoms and one THF molecule of crystallisation are omitted for clarity.

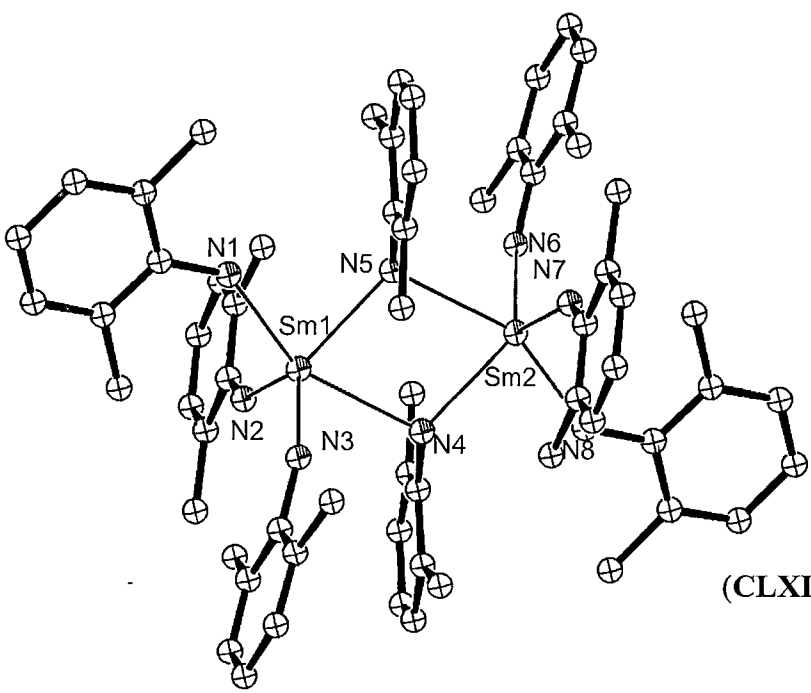

(CLXIV)

Figure 4.15. Molecular structure of $[\{K(THF)_6\}_2][\{Sm(\mu\text{-}NHC_6H_3Me_2\text{-}2,6)(NHC_6H_3\text{-}2,6\text{-}Me_2)_3\}_2]$, (**CLXIV**). Figure generated from CCDC obtained coordinates. Atoms of arbitrary size. H atoms, $[K(THF)_6]^+$, and one THF molecule of crystallisation are omitted for clarity.

The reactivity of the unsolvated powder $[Nd(NHC_6H_5)_3(KCl)_3]$, (**CLXV**), with base, $AlMe_3$, was also investigated, presumably in the hope of isolating an imide species.[19] In this instance, proton abstraction from one anilido N centre was observed, indeed yielding the heteroleptic mixed-metal cluster $[\{[Me_2Al(\mu\text{-}Me)_2]_2Nd(\mu_3\text{-}NC_6H_5)(\mu\text{-}Me)AlMe\}_2]$, (**CLXVI**), featuring a bridging imide ligand, as shown in Figure 4.16.

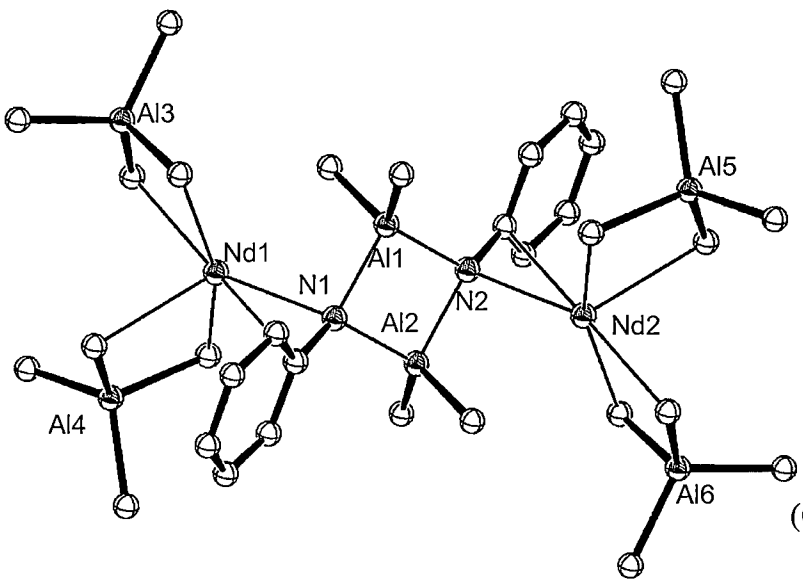

(**CLXVI**)

Figure 4.16. Molecular structure of $[\{[Me_2Al(\mu\text{-}Me)_2]_2Nd(\mu_3\text{-}NC_6H_5)(\mu\text{-}Me)AlMe\}_2]$, (**CLXVI**). Figure generated from CCDC obtained coordinates. Atoms of arbitrary size. H atoms are omitted for clarity.

Similarly, Gordon reported the synthesis of the bimetallic Sm amide $[Sm(\mu\text{-}NHC_6H_3\text{-}2,6\text{-}i\text{-}Pr_2)(NHC_6H_3\text{-}2,6\text{-}i\text{-}Pr_2]_2$, (**XXI**), shown in Figure 4.17, and investigated its reactivity with $AlMe_3$. In this instance, as described in Section 1.1.6., and shown in Figure 1.8, α-deprotonation was also successful giving the imide complex $[\{(\mu\text{-}ArN)Sm(\mu\text{-}NHAr)(\mu\text{-}Me)AlMe_2\}_2]$, (**XX**), that retained $AlMe_3$ to satisfy the coordination requirements of the lanthanide centres.[12h]

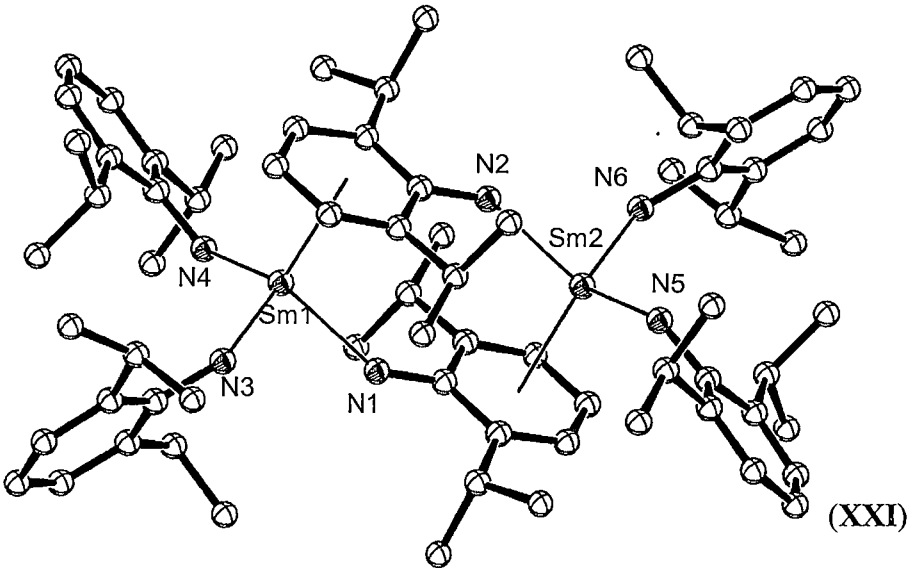

(XXI)

Figure 4.17. Molecular structure of [{Sm(μ-$NHC_6H_3iPr_2$-2,6)(NHC_6H_3-iPr_2-2,6)$_2$}$_2$], (**XXI**). Figure generated from CCDC obtained coordinates. Atoms of arbitrary size. H atoms are omitted for clarity.

Results and Discussion:

4.2. bis(amide) samarium(III) macrocyclic complexes.

4.2.1. Synthesis of $[(THF)_2K(Et_8N_2O_2)Sm\{N(H)Mes\}_2]$, (17), and $[\{\mu\text{-}\eta^1\text{:}\eta^3\text{-}\{N(H)Mes\}K(Et_8N_2O_2)SmN(H)Mes\}_n]$, (18).

The reaction of the orange samarium(III) dinuclear complex, $[\{(Et_8N_2O_2)Sm(\mu\text{-}I)\}_2]$, (8), with the potassium amide KN(H)Mes, (19), in THF gave a red solution, which was filtered from a white solid, presumed to be the by-product of the reaction, KI. Crystals of the samarium(III) bis(amide) $[(THF)_2K(Et_8N_2O_2)Sm\{N(H)Mes\}_2]$, (17), were isolated from the THF solution following concentration *in vacuo*. $[(THF)_2K(Et_8N_2O_2)Sm(N(H)Mes)_2]$, (17), may be recrystallised from benzene to give the polymeric, THF free bis(amide) $[\{\mu\text{-}\eta^1\text{:}\eta^3\text{-}\{N(H)Mes\}K(Et_8N_2O_2)SmN(H)Mes\}_n]$, (18), as shown below in Scheme 4.1.

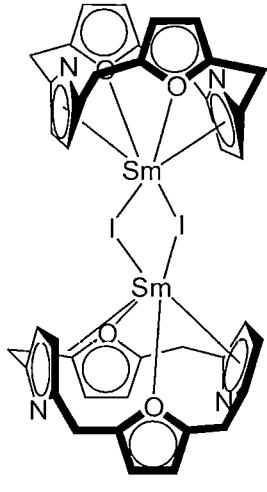

(8)

4 KN(H)Mes (19), THF

2 $[(THF)_2K(Et_8N_2O_2)Sm\{N(H)Mes\}_2]$ (17)

C_6H_6

2 $[\{\mu\text{-}\eta^1.\eta^3\text{-}\{N(H)Mes\}K(Et_8N_2O_2)SmN(H)Mes\}_n]$ (18)

Scheme 4.1 .Synthesis of the samarium(III) bis(amide) complexes $[(THF)_2K(Et_8N_2O_2)Sm\{N(H)Mes\}_2]$, (17), and $[\{\text{-}\mu\text{-}\eta^1\text{:}\eta^3\text{-}\{N(H)Mes\}K(Et_8N_2O_2)SmN(H)Mes\}_n]$, (18). *Meso*-ethyl groups in **8** omitted for clarity.

The poor solubility of the precursor samarium(III) reagent, $[\{(Et_8N_2O_2)Sm(\mu\text{-}I)\}_2]$, (8) results in a heterogeneous reaction mixture. Both amide complexes also exhibit poor solubility in non-Lewis base solvents but exhibit high solubility in THF, forming a dark red solution in each case resulting from the solvation of $[\{\mu\text{-}\eta^1\text{:}\eta^3\text{-}\{N(H)Mes\}K(Et_8N_2O_2)SmN(H)Mes\}_n]$, (18), by THF affording $[(THF)_2K(Et_8N_2O_2)Sm\{N(H)Mes\}_2]$, (17). If only two equivalents of KN(H)Mes, (19), are added to **8** in THF, **17** is still formed. However, a mixture of the

mono(amide) [$(Et_8N_2O_2)$Sm{N(H)Mes}], (**20**), the bis(amide) **17**, and unreacted [{$(Et_8N_2O_2)$Sm(μ-I)}$_2$], (**8**) results. The mono(amide) [$(Et_8N_2O_2)$Sm(N(H)Mes)], (**20**) exhibits high solubility in benzene and toluene. A full description of the mono(amide) **20**, including an alternative synthesis, is discussed later.

The proposed structural details of **17** and **18** were determined by single crystal X-ray diffraction. The proposed formulations also gave satisfactory microanalyses.

Both samarium bis(amide) complexes, [$(THF)_2$K$(Et_8N_2O_2)$Sm{N(H)Mes}$_2$], (**17**), and [{μ-η^1:η^3-{N(H)Mes}K$(Et_8N_2O_2)$SmN(H)Mes}$_n$], (**18**), of the metallated dioxaporphyrinogen macrocycle retain a potassium counter-ion in the base of the macrocyclic cavity resulting in formally neutral compounds. For **17**, no further association is observed as the coordination sphere of the potassium centre is completed by two THF molecules. For **18**, however, the absence of Lewis basic solvents results in an allyl-type bridging interaction between the potassium centre and the C2-C4 carbon centres of a mesityl substituent of an adjacent molecule in the solid state. In the presence of the Lewis basic solvent THF, the potassium counter-ion in the base of the macrocyclic cavity binds to two THF molecules rather than forming the μ-η^1:η^3 polymeric structure, resulting in a monomeric, heterodinuclear complex. Schematic three dimensional representations of both bis(amide) complexes are shown in Figure 4.18. ORTEP representations of the molecular structures appear later in Figures 4.19 – 4.21.

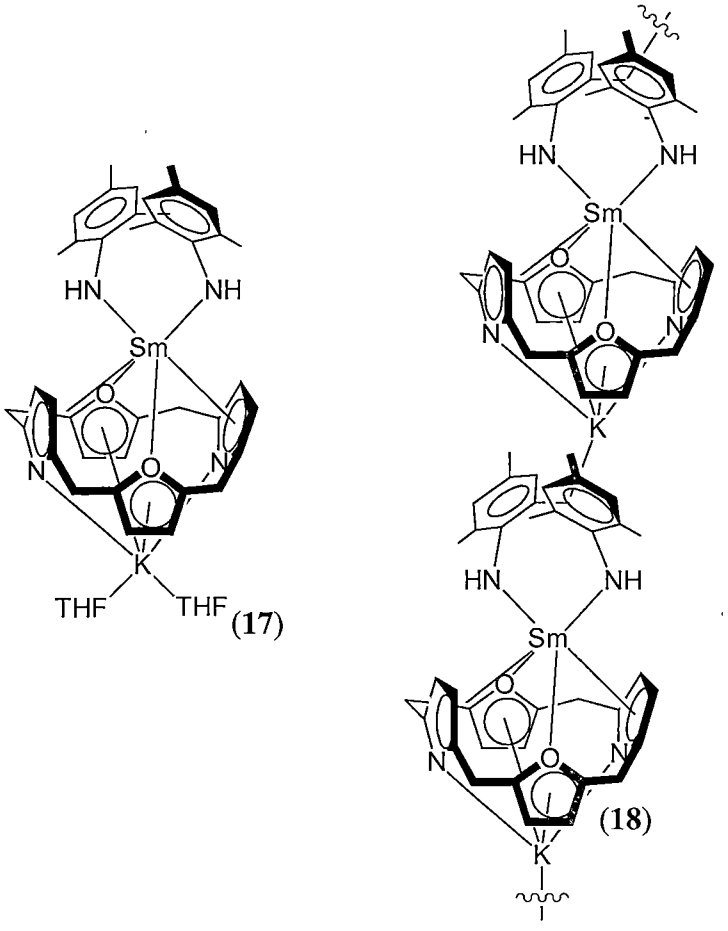

Figure 4.18. Three dimensional representations of the samarium(III) bis(amide) complexes, $[(THF)_2K(Et_8N_2O_2)Sm\{N(H)Mes\}_2]$, (**17**), and $[\{\mu\text{-}\eta^1\text{:}\eta^3\text{-}\{N(H)Mes\}K(Et_8N_2O_2)SmN(H)Mes\}_n]$, (**18**). *Meso*-ethyl groups omitted for clarity.

4.2.2. NMR spectroscopy of bis(amide) complexes.

The ^1H resonances in the NMR spectra of $[(THF)_2K(Et_8N_2O_2)Sm(N(H)Mes)_2]$, (**17**) , exhibit broad peak shapes within a contracted chemical shift range of –1.0 to 7.5 ppm at room temperature. As discussed in Section 2.3.1, previous studies of the samarium(III) bis(trimethylsilyl) amide derived complexes of the *meso*-octaethyl-*trans*-dioxaporphyrinogen ligand, $[(Et_8N_2O_2)SmN(SiMe_3)_2]$, (**CXL**) and $[(toluene)Na(Et_8N_2O_2)Sm\{N(SiMe_3)Si(Me_3)_2CH_2\}]$, (**XCV**) suggested that the incorporation of a counter-ion in the base of the macrocyclic cavity contracted the ^1H NMR spectrum of the complex. Subsequently, the observed chemical shift range of $[(THF)_2K(Et_8N_2O_2)Sm\{N(H)Mes\}_2]$, (**17**), is consistent with this understanding.

In contrast to the macrocyclic azomesitylene complex, $[(Et_8N_2O_2)Sm\{\eta^2\text{-}N_2(Mes)_2\}]$, (**10**), ^1H NMR spectroscopy of **17** revealed macrocyclic C_{2v} symmetry to be retained at room temperature. However, variable temperature ^1H NMR studies of **17** revealed fluxional processes, presumably involving the inversion of the mesityl substituents across the vertical macrocyclic mirror plane containing the pyrrolide N-centres, as discussed for **10**. Cooling to temperatures below –30 °C allowed this process to be resolved on the NMR timescale with the observation of the reduction of macrocyclic C_{2v} symmetry to C_2. The chemical shift range of **17** was also observed to broaden at lower temperatures, consistent with Curie-Weiss behaviour, as observed previously for macrocyclic complexes of porphyrinogen ligands.[10] The ^1H NMR resonances of **17** are summarised in Table 4.1.

Resonance (ppm)	Assignment	Resonance (ppm)	Assignment
-4.24	CH_2	2.51	CH_2
-2.62	CH_2	3.22	CH_2
-1.92	CH_2	3.86	CH_2
-1.25	*meso*-CH_3	5.02	CH_2
-0.24	*meso*-CH_3	7.10	fur/pyr CH
0.22	CH_2	7.18	fur/pyr CH
0.88	*meso*-CH_3	7.27	fur/pyr CH
1.64	*p*-CH_3	7.34	fur/pyr CH
2.22	*meso*-CH_3	9.92	*m*-CH
2.28	*o*-CH_3	10.21	*m*-CH
2.36	*o*-CH_3		

Table 4.1. ^1H NMR spectral data for $[(THF)_2K(Et_8N_2O_2)Sm\{N(H)Mes\}_2]$, (**17**). (THF-$d^8$, 299.905 MHz, 223 K)

4.2.3. Reactivity studies of $[(THF)_2K(Et_8N_2O_2)Sm\{N(H)Mes\}_2]$, (**17**), and $[\{\mu\text{-}\eta^1\text{:}\eta^3\text{-}\{N(H)Mes\}K(Et_8N_2O_2)SmN(H)Mes\}_n]$, (**18**).

The reactivity of $[(THF)_2K(Et_8N_2O_2)Sm\{N(H)Mes\}_2]$, (**17**), and $[\{\mu\text{-}\eta^1\text{:}\eta^3\text{-}\{N(H)Mes\}K(Et_8N_2O_2)SmN(H)Mes\}_n]$, (**18**), towards base was investigated in order to determine if α- proton abstraction from the amide N-H was possible, as shown in Scheme 4.2. Upon reaction with one equivalent of a range of bases, however, no evidence for α- proton abstraction was observed. The result, following prolonged reaction time, was metal displacement to yield $[\{(Et_8N_2O_2)K_2(\mu\text{-}\eta^6\text{:}\eta^6\text{-}C_6D_6)\}_n]$, (**5**), identified by ^1H NMR spectroscopy, as was noted for $[(toluene)Na(Et_8N_2O_2)Sm\{N(SiMe_3)(SiMe_2CH_2)\}]$, (**XCV**), upon prolonged exposure to excess base.

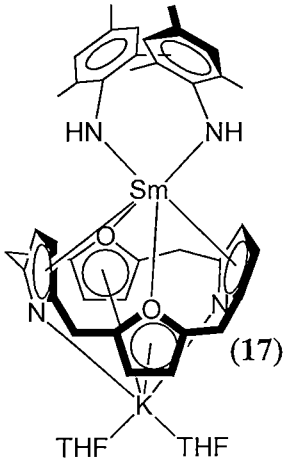

(**17**)

MR, THF → $[(THF)_xK(Et_8N_2O_2)Sm{=}NMes]$ + MN(H)Mes + RH
(**14b**)
MR=KH, LiMe

Scheme 4.2. Intended deprotonation of the samarium(III) bis(amide) $[(THF)_2K(Et_8N_2O_2)Sm\{N(H)Mes\}_2]$, (**17**). *Meso*-ethyl groups in **17** omitted for clarity.

Given the incorporation of the potassium ion in the base of the macrocyclic cavity of $[(THF)_2K(Et_8N_2O_2)Sm\{N(H)Mes\}_2]$, (**17**) and $[\{\mu\text{-}\eta^1\text{:}\eta^3\text{-}\{N(H)Mes\}K(Et_8N_2O_2)SmN(H)Mes\}_n]$, (**18**), the observed lack of α- proton abstraction with excess base may be rationalised. As discussed in Section 4.1, the samarium(III) bis(trimethylsilyl)amide $[(Et_8N_2O_2)SmN(SiMe_3)_2]$, (**CXL**), exhibited reactivity towards excess base and subsequently retained a counter-ion in the base of the macrocyclic cavity, forming the γ- deprotonated product, $[(C_6H_5Me)Na(Et_8N_2O_2)Sm\{N(SiMe_3)(SiMe_2CH_2)\}]$, (**XCV**). In comparison, the analogous bis(trimethylsilyl)amide samarium(III) complex of the *meso*-octaethyl-

trans-N,N'-dimethylporphyrinogen macrocycle $[(Et_8N_4Me_2)SmN(SiMe_3)_2]$, (**CXLI**), which lacks the ability to bind a counter-ion in the macrocyclic cavity, did not exhibit reactivity with excess base since the base of the macrocycle is not accessible due to the *N,N'*-dimethyl substituents. Consequently, the bis(amide) samarium(III) macrocycle complexes, $[(THF)_2K(Et_8N_2O_2)Sm\{N(H)Mes\}_2]$, (**17**) and $[\{\mu\text{-}\eta^1\text{:}\eta^3\text{-}\{N(H)Mes\}K(Et_8N_2O_2)SmN(H)Mes\}_n]$, (**18**), which already incorporate a counter-ion in the macrocylic cavity, cannot incorporate a second counter-ion following N-H deprotonation and did not exhibit deprotonation reactivity with base. These observations all suggest that counter-ion stabilisation within the macrocyclic cavity is an important driving force in achieving both the targeted α- proton abstraction of an amide N-H and the observed γ- deprotonation of $[(Et_8N_2O_2)SmN(SiMe_3)_2]$, (**CXL**).

The protonation of one amide unit using acid was also attempted in order to isolate the mono(amide) $[(Et_8N_2O_2)SmN(H)Mes]$, (**20**), through liberation of one equivalent of free amine, or the targeted imide, $[(THF)_xK(Et_8N_2O_2)Sm{=}NMes]$, (**14b**) and the conjugate acid of the amine, as shown in Scheme 4.3. However the addition of 1 equivalent of *p*-toluenesulfonic acid resulted in non-selective protonation of both the amide and macrocyclic ligands, yielding a complex mixture of protonated amine, macrocyclic ligand, $Et_8N_2O_2H_2$, (**1**), the starting bis(amide), $[(THF)_2K(Et_8N_2O_2)Sm\{N(H)Mes\}_2]$, (**17**), and the mono(amide) $[(Et_8N_2O_2)SmN(H)Mes]$, (**20**), identified by ^1H NMR spectroscopy.

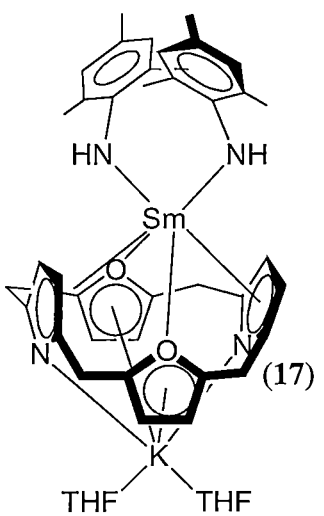

(**17**)

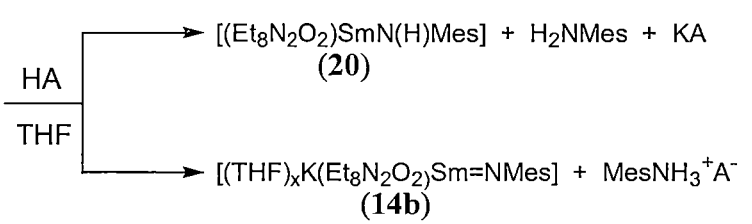

Scheme 4.3. Intended protonation of the samarium(III) bis(amide) complex, $[(THF)_2K(Et_8N_2O_2)Sm\{N(H)Mes\}_2]$, (**17**) to give a mono(amide) complex.

The observed importance of counter-ion stabilisation within the base of the macrocyclic cavity, and the lack of desired α- proton abstraction from the bis(amide) complexes, $[(THF)_2K(Et_8N_2O_2)Sm\{N(H)Mes\}_2]$, (**17**), and $[\{\mu\text{-}\eta^1\text{:}\eta^3\text{-}\{N(H)Mes\}K(Et_8N_2O_2)SmN(H)Mes\}_n]$, (**18**), suggest that for α- proton abstraction from a macrocyclic amide to occur, a mono(amide) complex free of a counter-ion in the base of the macrocyclic cavity is desired. Further attempts to isolate a macrocyclic mono(amide) complex utilising steric bulk and alternative metal amide substrates designed to favour the formation of mono(amide) complexes are discussed further in Section 4.3.

4.2.4. Molecular structure of $[(THF)_2K(Et_8N_2O_2)Sm\{N(H)Mes\}_2]$, (**17**).

Red crystals of $[(THF)_2K(Et_8N_2O_2)Sm\{N(H)Mes\}_2]$, (**17**), suitable for X-ray diffraction studies were grown from a concentrated THF solution left at room temperature overnight. The crystals were found to belong to the monoclinic space group *C*2/*c* (No. 15), a = 13.05400(10), b = 27.79010(10), c = 17.15130(10) Å, β = 100.2610(10) °, with 4 molecules in the unit cell. The asymmetric unit consisted of one half of a molecule of $[(THF)_2K(Et_8N_2O_2)Sm\{N(H)Mes\}_2]$, (**17**), and one half of a lattice THF molecule, residing on a C_2 symmetry site. The position of the pyrrolide N and furanyl O atoms were unambiguously determined *via* significant differences in the refinement model when their positions were transposed. The structure of **17** is shown in Figure 4.19.

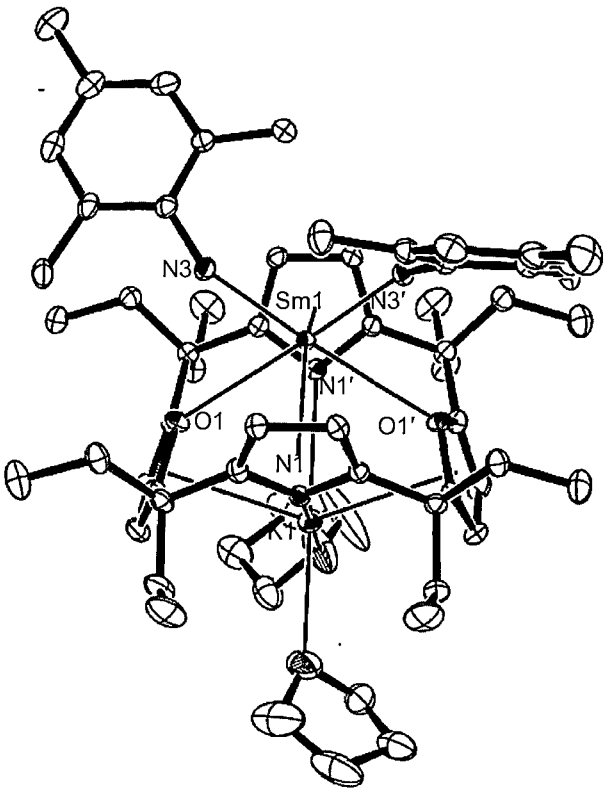

Figure 4.19: Molecular structure of $[(THF)_2K(Et_8N_2O_2)Sm\{N(H)Mes\}_2]$, (**17**) with thermal ellipsoids drawn at the 20 % level of probability. Protons and the THF molecule of crystallisation have been omitted for clarity.

$[(THF)_2K(Et_8N_2O_2)Sm\{N(H)Mes\}_2]$, (**17**), adopts a monomeric form in the solid state with the potassium cation in the base of the macrocyclic cavity capped by two THF molecules. The macrocyclic ligand binds to the samarium centre in the typical $\eta^5:\eta^1:\eta^5:\eta^1$ binding mode for this ligand, which exhibits the typical 1,3-alternate conformation observed in previous complexes. The complex exhibits η^1- interactions between the samarium atom and the oxygen atoms of the furanyl rings at a length of 3.036(2) Å, whilst the η^5 interactions between the samarium atom and the pyrrolide rings measure 2.63_5 Å. The samarium centre is bound to the two mesityl amide ligands through η^1 interactions with the amide nitrogen atoms at lengths of 2.327(1) Å. The potassium centre binds to the macrocyclic ligand in a reverse fashion to the samarium centre, with η^5 interactions between the potassium atom and the furanyl rings of the macrocycle, and η^1 interactions between the potassium atom and the pyrrolide N atoms. The η^5 K–Ct(furanyl) interactions measure 3.07_2 Å, whilst the η^1 K–N interactions measure 2.894(1) Å.

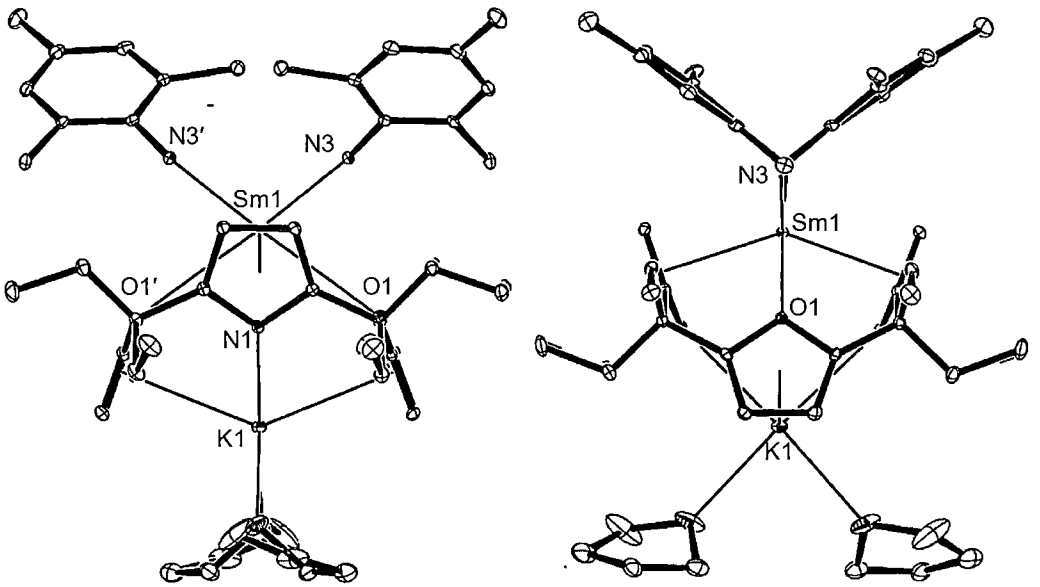

Figure 4.20. Side views of the molecular structure of $[(THF)_2K(Et_8N_2O_2)Sm(N(H)Mes)_2]$, (17). Thermal ellipsoids are shown at the 20 % level of probability. H atoms are omitted for clarity.

The η^5 and η^1 interactions between the samarium(III) centre and the macrocyclic ligand of 2.63_5 and 3.036(2) Å are significantly longer than those observed in the macrocyclic samarium(III) iodide $[\{(Et_8N_2O_2)Sm(-\mu\text{-}I)\}_2]$, (**8**), of 2.53_0 and 2.685(4) Å, respectively, presumably as a result of the binding of the potassium counter ion in the base of the macrocyclic cavity competing with the samarium(III) centre for coordination to the macrocycle. The pyrrolide and furanyl rings adopt similar tilt angles with respect to the *meso*- plane to **8** with angles of 69.9_5(furanyl) and 110.4_1(pyrrolide) ° for **17**, and 62.5_3 and 70.1_2 (furanyl) and 106.3_2 and 107.4_2 (pyrrolide) °, for **8**, which suggests that the shorter samarium-macrocycle interactions observed in **8** result from the samarium centre residing deeper within the macrocyclic cavity than in **17**. The cross-cavity Sm···K distance of 4.05_5 Å is significantly longer than the Sm···Na distance observed in $[(C_6H_5Me)Na(Et_8N_2O_2)Sm\{N(SiMe_3)(SiMe_2CH_2)\}]$, (**XCV**) of 3.884_1 Å, however the η^5 and η^1 interactions between the samarium centre and the macrocyclic ligand in both complexes are comparable, suggesting that the larger size of the potassium counter ion in **17** prevents it from binding as deeply within the macrocyclic cavity, whilst the binding mode of the samarium atom remains comparable. This is further

illustrated *via* a comparison of the η^5 and η^1 interactions of the samarium and potassium centres in **17** with those of the samarium and sodium centres in **XCV**, whereby the potassium bond lengths of **17** of 3.07_3 and 2.894(1) Å are longer than those in **XCV** of 2.99_4 and 2.787(3) Å, respectively, whilst the samarium interactions of **17**, of 2.63_5 and 3.036(2) Å are comparable to those of **XCV** of 2.61_8 and 3.046(2), respectively.

The Sm–N(amide) interactions of 2.327(1) Å are longer than those reported for the terminal amide interactions in the tris(amide) samarium(III) complex, [{Sm(μ-NHC_6H_3-*i*-Pr_2-2,6)(NHC_6H_3-*i*-Pr_2-2,6)$_2$}$_2$], (**XXI**), of 2.241(4) and 2.273(11) Å, and the γ-deprotonated samarium mono(amide) [$(C_6H_5Me)Na(Et_8N_2O_2)Sm${N(TMS)($SiMe_2CH_2$)}], (**XCV**), of 2.292(2) Å, but are shorter than the bridging μ-η^1:η^6 Sm-N(amide) interactions in [{Sm(μ-NHC_6H_3-*i*-Pr_2-2,6)(NHC_6H_3-*i*-Pr_2-2,6)$_2$}$_2$], (**XXI**), of 2.351(10) Å.

4.2.5. Molecular structure of [{μ-η^1:η^3-{N(H)Mes}K($Et_8N_2O_2$)SmN(H)Mes}$_n$], (**18**).

Red crystals of the Lewis base solvent free polymeric samarium(III) bis(amide), [{μ-η^1:η^3-{N(H)Mes}K($Et_8N_2O_2$)SmN(H)Mes}$_n$].C_6H_6, (**18**), suitable for X-ray diffraction studies were grown from a concentrated benzene solution left at room temperature overnight. The crystals were found to belong to the triclinic space group, $P\bar{1}$ (No. 2), a = 11.2292(4), b = 14.0261(5), c = 17.2912(6) Å, α = 86.629(1), β = 89.668(1), γ = 70.431(2) °, with 2 molecules in the unit cell. The asymmetric unit consisted of one molecule of [{μ-η^1:η^3-{N(H)Mes}K($Et_8N_2O_2$)SmN(H)Mes}$_n$], (**18**) ,and half a molecule of benzene. The position of the pyrrolide N and furanyl O atoms were unambiguously determined *via* significant differences in the refinement model when their positions were transposed. The derived structure of **18** is shown in Figures 4.21 and 4.23.

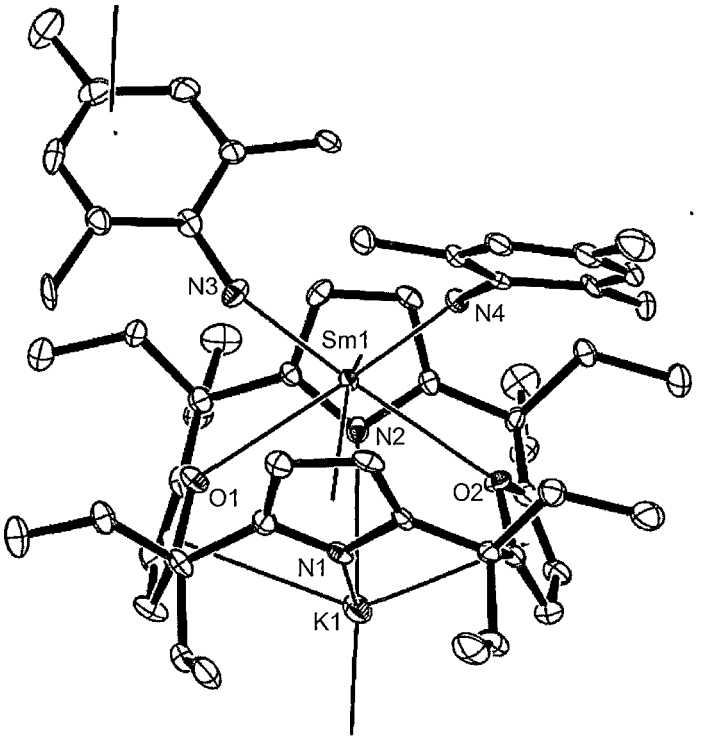

Figure 4.21. Molecular structure of $[\{\mu\text{-}\eta^1\text{:}\eta^3\text{-}(N(H)Mes)K(Et_8N_2O_2)SmN(H)Mes\}_n]$, (**18**), with thermal ellipsoids drawn at the 20 % level of probability. H atoms and the benzene molecule of crystallisation are omitted for clarity.

$[\{\mu\text{-}\eta^1\text{:}\eta^3\text{-}\{N(H)Mes\}K(Et_8N_2O_2)SmN(H)Mes\}_n]$, (**18**) exhibits a polymeric structure in the solid state with one mesityl amide forming a bridging $\mu\text{-}\eta^1\text{:}\eta^3$ interaction through the amide Sm-N bond and the potassium atom of the neighbouring monomeric unit. The bonding interactions between the macrocycle and both samarium and potassium atoms are of the same type as observed in $[(THF)_2K(Et_8N_2O_2)Sm\{N(H)Mes\}_2]$, (**17**). Consequently, the η^5 Sm–Ct(pyrrolide) interactions of 2.63_2 and 2.64_3 Å, and the η^1 Sm–O(furanyl) interactions of 2.944(6) and 3.092(6) Å are of a similar length as observed in **17** of 2.63_5 and 3.036(2) Å respectively. The asymmetry in the Sm–O interactions in **18** is likely due to the pseudo-*trans* terminal and bridging mesityl amide ligands, with the shorter (2.944(6) Å) bond *trans* to the bridging interaction. The furanyl and pyrrolide tilt angles of 67.7_0 and 69.7_8 ° (furanyl) and 109.1_0 and 111.2_5 ° (pyrrolide) are similar to those of 69.9_5 °° (furanyl) and 110.4_1° (pyrrolide) for **17**, suggesting that the bridging interaction does not significantly affect the macrocyclic binding mode. The cross-cavity Sm···K distance in **18** of 4.12_5 Å is marginally longer than the 4.05_5 Å

distance of **17**. Consequently, the potassium atom binds to the macrocycle through slightly longer pyrrolide nitrogen η^1 interactions of 2.941(5) and 2.939(5) Å and furanyl η^5 interactions of 3.13_4 and 3.05_9 Å, compared to 2.894(1) and 3.073(2) Å for **17**.

The Sm–N(amide) interactions measure 2.348(5) and 2.317(4) Å, with the larger bond length observed for the bridging amide ligand, as was observed for the tris(amide) dinuclear samarium(III) complex, [{Sm(μ-NHC_6H_3-*i*-Pr_2-2,6)(NHC_6H_3-*i*-Pr_2-2,6)$_2$}$_2$], (**XXI**), as discussed above. The K-C(mes) allyl-bridging interactions of 3.163(6), 3.228(6) and 3.518(7) Å are comparable to those in the allyl-bridged dimer [{Sm($C_3H_3(SiMe_3)_2)_3$[μ-K($THF)_2$]}$_2$], (**CLXVII**), of 3.115(5), 3.095(4) and 3.442(5) Å.[20] A comparison of important bond lengths and angles for the macrocyclic group 1 metal incorporated samarium amides [$(THF)_2$K($Et_8N_2O_2$)Sm{N(H)Mes}$_2$], (**17**), [{μ-η^1:η^3-{N(H)Mes}K($Et_8N_2O_2$)SmN(H)Mes}$_n$], (**18**) and [(C_6H_5Me)Na($Et_8N_2O_2$)Sm{N($SiMe_3$)($SiMe_2CH_2$)}], (**XCV**), is summarised in Table 4.2.

In order to accommodate both mesityl amide ligands in the coordination sphere of the samarium centre above the binding groove of the macrocycle, both amide ligands are tilted away from the centre of the molecule, with an interplanar angle between the plane of each mesityl ring of 91.5 °, which is slightly smaller than that of the monomeric bis(THF) solvate [$(THF)_2$K($Et_8N_2O_2$)Sm{N(H)Mes}$_2$], (**17**), of 95.7 °. In [{μ-η^1:η^3-{N(H)Mes}K($Et_8N_2O_2$)SmN(H)Mes}$_n$], (**18**), the allylic type bridging interaction between the potassium atom and the mesityl ring results in a deformation in the planarity of the bridging mesityl substituent with the *p*-methyl group bent below the least-squares plane of the mesityl ring through a distance of 0.2_4 Å, as shown in Figure 4.22. The bridging interaction also results in a loss of C_2 symmetry within the molecule as compared with [$(THF)_2$K($Et_8N_2O_2$)Sm{N(H)Mes}$_2$], (**17**).

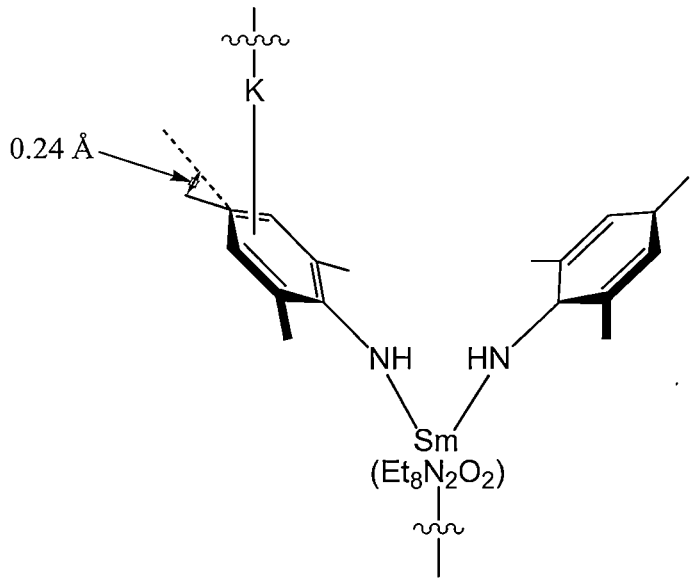

Figure 4.22. Deformation in planarity of the bridging mesityl ring in the polymeric bis(amide), [{μ-η^1:η^3-{N(H)Mes}K(Et$_8$N$_2$O$_2$)SmN(H)Mes}$_n$], (**18**).

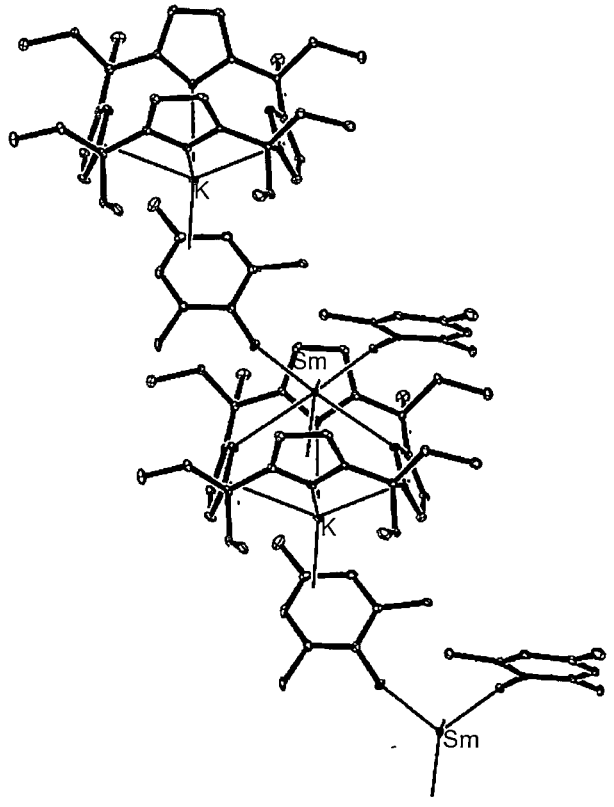

Figure 4.23. Extended structure of [{μ-η^1:η^3-{N(H)Mes}K(Et$_8$N$_2$O$_2$)SmN(H)Mes}$_n$], (**18**). Thermal ellipsoids are drawn at the 20 % level of clarity. H atoms are omitted for clarity.

Distance (Å)/Angle (°)	(17)	(18)	(XCV)
Sm–O(fur)	3.036(2)	2.944(5), 3.092(5)	3.046(2), 3.007(2)
Sm–η^5(pyrrolide)	2.63_5	2.63_2 and 2.64_3	2.59_2, 2.61_1
Sm–N(amide)	2.327(1)	2.348(5), 2.317(4)	2.292(2)
$\eta^5(pyr)_1$-Sm-$\eta^5(pyr)_2$	140.8_9	140.2_4	141.4_3
O_1-Sm-O_2	107.23(5)	106.21(14)	107.06(8)
pyrrolide tilt	110.4_1	109.1_0, 111.2_5	110.1_3, 110.1_9
furanyl tilt	69.9_5	67.7_0, 69.7_8	68.5_2, 72.9_6
Sm···K(Na)	4.05_5	4.12_5	3.884_1
K(Na)–N(pyr)	2.894(1)	2.941(5), 2.939(5)	2.782(3), 2.787(3)
K(Na)–η^5(furanyl)	3.07_3	3.13_4, 3.05_9	2.97_3, 2.99_4
N-K(Na)-N	89.74(6)	88.09(13)	93.30(8)
$\eta^5(fur)_1$-K(Na)-$\eta^5(fur)_2$	135.7_7	133.2_0	141.4_9

Table 4.2. Summary of important bond lengths and angles of $[(THF)_2K(Et_8N_2O_2)Sm\{N(H)Mes\}_2]$, (**17**), $[\{\mu\text{-}\eta^1\text{:}\eta^3\text{-}\{N(H)Mes\}K(Et_8N_2O_2)SmN(H)Mes\}_n]$, (**18**) and $[(C_6H_5Me)Na(Et_8N_2O_2)Sm\{N(SiMe_3)(SiMe_2CH_2)\}]$, (**XCV**).

4.3. Synthesis of mono(amide) samarium(III) dioxaporphyrinogen complexes.

4.3.1. Synthesis of $[(Et_8N_2O_2)Sm\{N(H)C_6H_2\text{-}2,4,6\text{-}t\text{-}Bu\}]$, (**21**).

The reaction of the orange samarium(III) dinuclear complex $[\{(Et_8N_2O_2)Sm\text{-}(\mu\text{-}I)\}_2]$, (**8**), with the lithium amide $LiN(H)(C_6H_2\text{-}2,4,6\text{-}t\text{-}Bu)$, (**22**), in THF gave a purple solution, which was filtered from a white solid, presumed to be the by-product of the reaction, LiI. Removal of THF *in vacuo* followed by recrystallisation from toluene gave purple crystals of $[(Et_8N_2O_2)Sm\{N(H)C_6H_2\text{-}2,4,6\text{-}t\text{-}Bu\}]$, (**21**) in good yield (61%), as shown in Scheme 4.4.

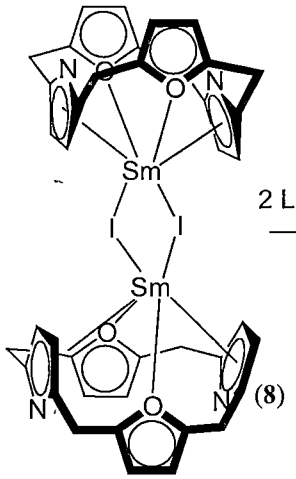

$$\xrightarrow[\text{THF}]{2\ \text{LiN(H)C}_6\text{H}_2\text{-2,4,6-}t\text{-Bu}\ (\mathbf{22})} 2\ [\text{Et}_8\text{N}_2\text{O}_2\text{Sm(N(H)C}_6\text{H}_2\text{-2,4,6-}t\text{-Bu]}\ (\mathbf{21})$$

Scheme 4.4. Synthesis of the purple samarium(III) amide $[(Et_8N_2O_2)Sm\{N(H)C_6H_2$-2,4,6-*t*-Bu$\}]$, (**21**).

Analogous to the synthesis of the bis(amide) complexes $[(THF)_2K(Et_8N_2O_2)Sm\{N(H)Mes\}_2]$, (**17**) and $[\{\mu\text{-}\eta^1\text{:}\eta^3\text{-}\{N(H)Mes\}K(Et_8N_2O_2)SmN(H)Mes\}_n]$, (**18**) the reaction of $[(Et_8N_2O_2)Sm(\mu\text{-I})\}_2]$, (**8**,) with $LiN(H)C_6H_2$-2,4,6-*t*-Bu, (**22**), occurs heterogeneously, with **8** dissolving gradually as the reaction proceeds. The mono(amide) $[(Et_8N_2O_2)Sm\{N(H)C_6H_2$-2,4,6-*t*-Bu$\}]$, (**21**), however, exhibits high solubility in a range of solvents including THF, toluene and petroleum spirits.

$[(Et_8N_2O_2)Sm\{N(H)C_6H_2$-2,4,6-*t*-Bu$\}]$, (**21**) remains the only product of the reaction if the lithium anilide **22** is replaced by the potassium salt $KN(H)C_6H_2$-2,4,6-*t*-Bu, (**23**), in the reaction with $[\{(Et_8N_2O_2)Sm(\mu\text{-I})\}_2]$, (**8**). This suggests that the observed mono(amide) product is favoured over a bis(amide) product analogous to $[\{\mu\text{-}\eta^1\text{:}\eta^3\text{-}\{N(H)Mes\}K(Et_8N_2O_2)SmN(H)Mes\}_n]$, (**18**), due to the increased steric requirements of the tri-*t*-Bu substituted anilide ligand. Consequently, a counter-ion in the base of the macrocyclic cavity is not required, and a stable mononuclear mono-amide complex is observed.

The structural details of $[(Et_8N_2O_2)Sm\{N(H)C_6H_2$-2,4,6-*t*-Bu$\}]$, (**21**) were determined by X-ray crystallography, whilst solution state ^1H and ^{13}C NMR spectroscopy was consistent with the determined structure. The proposed formulation also gave a satisfactory microanalysis.

A schematic three-dimensional representation of the molecular structure of [($Et_8N_2O_2$)Sm{N(H)C_6H_2-2,4,6-*t*-Bu}], (**21**), is shown below in Figure 4.24.

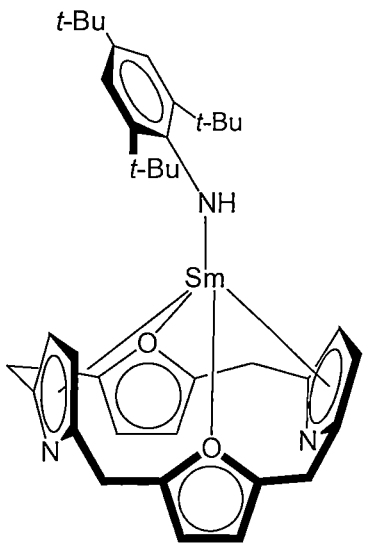

Figure 4.24. Three dimensional representation of the monomeric samarium(III) amide [($Et_8N_2O_2$)Sm{N(H)C_6H_2-2,4,6-*t*-Bu}], (**21**). *Meso*-ethyl substituents omitted for clarity.

4.3.2. NMR spectroscopy of [($Et_8N_2O_2$)Sm{N(H)C_6H_2-2,4,6-*t*-Bu}], (**21**).

The ^1H and ^{13}C NMR resonances of [($Et_8N_2O_2$)Sm{N(H)C_6H_2-2,4,6-*t*-Bu}], (**21**) were able to be fully assigned from gHMQC, gHMBC, gCOSY and NOESY NMR experiments, and are shown in Figure 4.26. Amide **21** exhibits C_2v symmetry in the solution state, suggesting that free rotation of the 2,4,6-tri-*t*-Bu anilide ligand about the Sm–N bond occurs on the NMR timescale.

The ^1H NMR spectrum of the counter-ion free mono(amide) [($Et_8N_2O_2$)Sm{N(H)C_6H_2-2,4,6-*t*-Bu}], (**21**), exhibited a wide chemical shift range of –5.0-25.5 ppm, consistent with the previously discussed understanding that the chemical shift ranges observed in the ^1H NMR spectra of lanthanide complexes of the *trans*-dioxaporphyrinogen ligand are dependent on the presence or absence of a counter-ion in the base of the macrocyclic cavity.

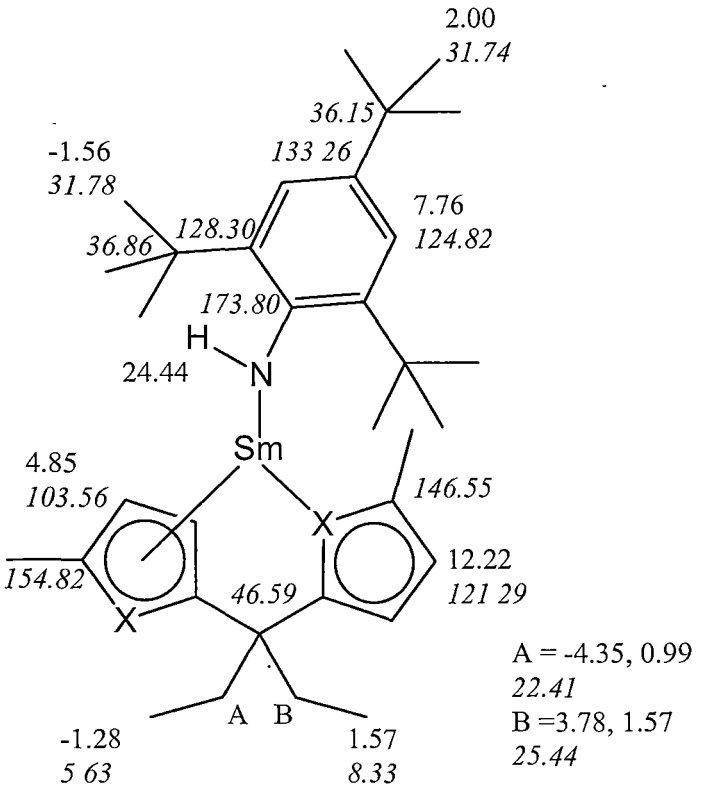

Figure 4.25. Full ^{1}H and ^{13}C NMR assignment of the macrocyclic samarium(III) mono(amide) $[(Et_8N_2O_2)Sm\{N(H)C_6H_2\text{-}2,4,6\text{-}t\text{-}Bu\}]$, (**21**). ^{13}C resonances are italicised.

4.3.3. Molecular structure of $[Et_8N_2O_2Sm\{N(H)C_6H_2\text{-}2,4,6\text{-}t\text{-}Bu\}]$, (**21**).

Purple crystals of $[(Et_8N_2O_2)Sm\{N(H)C_6H_2\text{-}2,4,6\text{-}t\text{-}Bu\}]$.toluene, (**21**) and $[(Et_8N_2O_2)Sm\{N(H)C_6H_2\text{-}2,4,6\text{-}t\text{-}Bu\}]$.THF, (**21**), suitable for single crystal X-ray diffraction studies were grown from a concentrated toluene solution of $[(Et_8N_2O_2)Sm\{N(H)C_6H_2\text{-}2,4,6\text{-}t\text{-}Bu\}]$, (21), left at -17 °C overnight, and from a concentrated THF solution of $[(Et_8N_2O_2)Sm\{N(H)C_6H_2\text{-}2,4,6\text{-}t\text{-}Bu\}]$, (**21**) left overnight at room temperature. The crystals of the toluene solvate were found to belong to the triclinic space group, $P\bar{1}$ (No. 2), a = 11.769(8), b = 13.3342(9), c = 19.2275(14) Å, α = 77.122(2), β = 76.175(2), γ = 66.67(2) °, with 2 molecules in the unit cell, whilst the THF solvate crystals were found to belong to the monoclinic space group, $P21/c$ (No. 14), a = 20.577(6), b = 14.418(7), c = 18.652(16) Å, β = 102.07(5) °, with 4 molecules in the unit cell. The asymmetric unit of the toluene solvate consisted of one molecule of $[(Et_8N_2O_2)Sm\{N(H)C_6H_2\text{-}2,4,6\text{-}t\text{-}Bu\}]$, (**21**) and one non-coordinating molecule of toluene, whilst the asymmetric unit of the

THF solvate consisted of one molecule of $[(Et_8N_2O_2)Sm\{N(H)C_6H_2\text{-}2,4,6\text{-}t\text{-}Bu\}]$, (**21**) and one non-coordinating molecule of THF. The positions of the furanyl O and pyrrolide N atoms in both structures were unambiguously determined *via* significant differences in the refinement model when their positions were transposed. A comparison of the important bond lengths and angles for the two solvates is summarised in Table 4.3. The derived structure of **21** is shown below in Figures 4.26 and 4.27. Further discussion of bond lengths and angles for **21** is based on the THF solvate.

Distance (Å) / Angle (°)	Toluene solvate	THF *solvate*
Sm–O(fur)	2.6633(12), 2.6780(12)	2.660(4), 2.697(4)
Sm–N(pyr)	2.646(14), 2.658(14)	2.642(5), 2.652(4)
Sm–η^5(pyr)	2.53_3, 2.48_6	2.55_8, 2.51_1
Sm–N(amide)	2.2669(14)	2.249(5)
O(1)-Sm(1)-O(2)	125.33(4)	122.34(12)
η^5(pyr)(1)-Sm-η^5(pyr)(2)	164.5_0	163.2_4
Furanyl tilt	66.4_6, 64.0_1	68.9_2, 67.0_4
Pyrrolide tilt	104.9_4, 101.9_3	107.6_7, 103.6_2

Table 4.3. Important bond lengths and angles for the two solvates of $[(Et_8N_2O_2)Sm\{N(H)C_6H_2\text{-}2,4,6\text{-}t\text{-}Bu\}]$, (**21**).

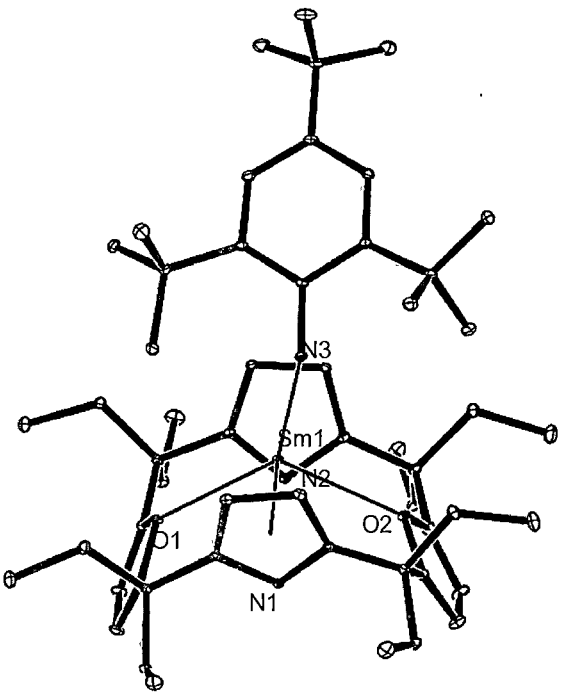

Figure 4.26. Molecular structure of the monomeric samarium(III) mono-amide $[(Et_8N_2O_2)Sm\{N(H)C_6H_2\text{-}2,4,6\text{-}t\text{-}Bu\}]$, (**21**). Thermal ellipsoids are shown at the 20 % level of probability. Protons and a toluene molecule of crystallisation have been omitted for clarity.

$[(Et_8N_2O_2)Sm\{N(H)C_6H_2\text{-}2,4,6\text{-}t\text{-}Bu\}]$, (**21**) forms an unsolvated monomer in the solid state. The samarium centre in **21** is bound to the macrocyclic ligand in the typical $\eta^5:\eta^1:\eta^5:\eta^1$ bonding mode, with the macrocycle adopting the 1,3-alternate conformation. η^5 interactions are again observed between the samarium centre and the pyrrolide rings of the macrocycle, whilst η^1 interactions are formed between the furanyl O atoms and the samarium atom. The coordination sphere of the samarium centre is completed with an η^1 interaction to the N atom of the 2,4,6-tri-*t*-Bu-anilido ligand. The samarium centre in **21** lies much deeper within the macrocyclic cavity than in the bi-metallic, potassium incorporating bis(amide) complexes, $[(THF)_2K(Et_8N_2O_2)Sm\{N(H)Mes\}_2]$, (**17**) and $[\{\mu\text{-}\eta^1:\eta^3\text{-}\{N(H)Mes\}K(Et_8N_2O_2)SmN(H)Mes\}_n]$, (**18**). Consequently, the η^5 Sm-pyrrolide interactions of 2.55_8 and 2.51_1 Å and the η^1 Sm-O (furanyl) interactions of 2.660(4) and 2.697(4) Å in **21** are significantly shorter than those observed in **17** and **18**, which average 2.63_6 and 3.02_7 Å respectively, but are similar to those in the counter-

ion free, samarium(III) iodide [{($Et_8N_2O_2$)Sm(μ-I)}$_2$] (**8**), of 2.51_7 and 2.53_0 Å (Sm-pyrrolide) and 2.660(4) and 2.685(4) Å (Sm-O), respectively. Similarly, the pyrrolide and furanyl tilt angles of **21** which average 105.7_0 and 67.9_8 ° are more consistent with those of **8**, of 106.8_7 and 66.3_2 ° than the counter-ion containing bis(amides), **17** and **18** which average $110._2$ and $69._1$ °.

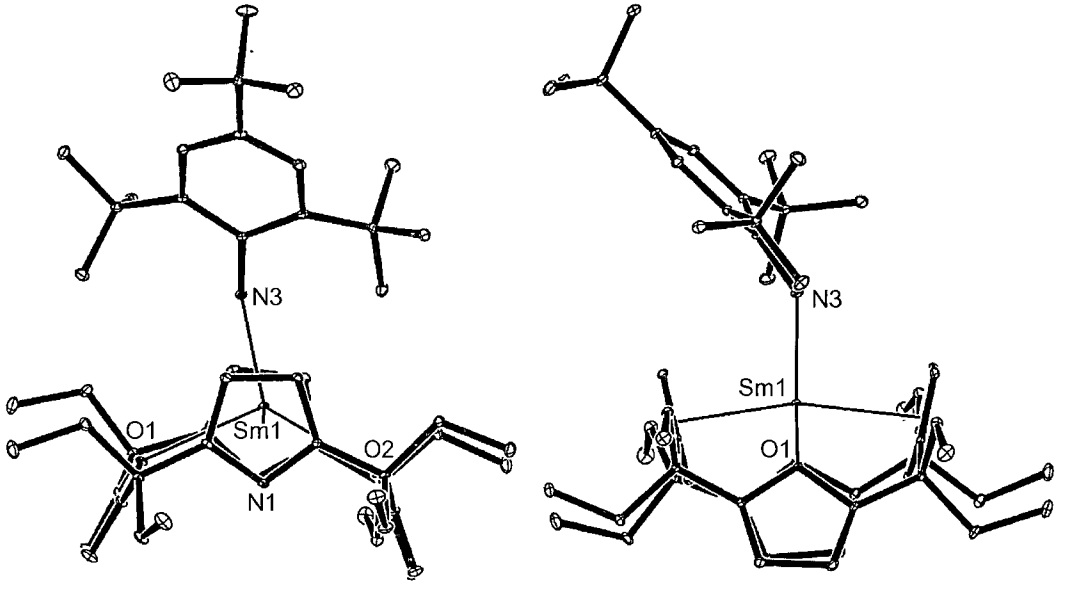

Figure 4.27. Side views of the molecular structure of [($Et_8N_2O_2$)Sm{N(H)C_6H_2-2,4,6-*t*-Bu}], (**21**). Thermal ellipsoids are shown at the 20 % level of probability. Protons and a toluene molecule of crystallisation have been omitted for clarity.

The molecular structure of [($Et_8N_2O_2$)Sm{N(H)C_6H_2-2,4,6-*t*-Bu}], (**21**), exhibits many similarities to the monomeric mono(amide) samarium(III) porphyrinogen complex previously reported by Wang, [($Et_8N_2O_2$)SmN($SiMe_3$)$_2$], (**CXL**).[9] The Sm–O(furanyl) distances of 2.660(4) and 2.697(4) Å in **21** are similar to those of **CXL**, of 2.7029(17) and 2.7181(16) Å, as are the Sm_1–Ct(pyrrolide) distances which average 2.5_3 and 2.5_2 Å for the two complexes, respectively. The Sm–N(amide) distance of 2.254(5) Å in **21** is slightly shorter than those of **CXL** of 2.314(2) Å and the samarocene mono(amide) [(C_5Me_5)$_2$Sm(NHPh)(THF)], (**CXIX**), of 2.331(3),[11] but is similar to the Sm–N(amide) interactions in the only other reported lanthanide(III) amide of the bulky 2,4,6-tri-t-Bu-anilido ligand, [(DippNC(Me)CHC(Me)Ndipp)Sm{N(H)C_6H_2-2,4,6-*t*-Bu}$_2$], (**CLXIV**), (dipp =

diisopropylphenyl), of 2.311(5) and 2.260(5) Å.[8e] The Ln–N(amide) bond in the only lanthanide(II) amide complex of the 2,4,6-tri-t-Bu-anilido ligand, $[(C_5Me_5)Sm\{N(H)C_6H_2\text{-}2,4,6\text{-}t\text{-}Bu\}(\mu\text{-}C_5Me_5)K(THF)_2]$, (**CXLVII**), of 2.47_6 Å is significantly longer than in $[(Et_8N_2O_2)Sm\{N(H)C_6H_2\text{-}2,4,6\text{-}t\text{-}Bu\}]$, (**21**), due to the larger ionic radius of the samarium(II) centre in the former case.[14]

Important bond lengths and angles for the three macrocyclic samarium(III) amide complexes, $[(THF)_2K(Et_8N_2O_2)Sm\{N(H)Mes\}_2]$, (**17**), $[(Et_8N_2O_2)Sm\{N(H)C_6H_2\text{-}2,4,6\text{-}t\text{-}Bu\}]$, (**21**), and $[(Et_8N_2O_2)SmN(SiMe_3)_2]$, (**CXL**), are summarised in Table 4.4.

Distance (Å)/Angle (°)	(**17**)	(**21**), (*C2/c*)	(**CXL**)
Sm–O(fur)	3.036(2)	2.660(4), 2.697(4)	2.7181(16), 2.7029(17)
Sm–η^5(pyrrolide)	2.63_5	2.55_8, 2.51_1	2.52_6, 2.52_9
Sm–N(amide)	2.327(1)	2.254(5)	2.314(2)
$\eta^5(pyr)_1$-Sm-$\eta^5(pyr)_2$	140.8_9	163.2_4	160.5_1
O_1-Sm-O_2	107.23(5)	122.36(12)	121.58(5)
pyrrolide tilt	110.4_1	107.7_7, 103.6_2	106.1_9, 105.63
furanyl tilt	69.9_5	67.0_4, 68.9_2	68.1_7, 69.7_0

Table 4.4. Summary of important bond lengths and angles for $[(THF)_2K(Et_8N_2O_2)Sm\{N(H)Mes\}_2]$, (**17**), $[(Et_8N_2O_2)Sm\{N(H)C_6H_2\text{-}2,4,6\text{-}t\text{-}Bu\}]$, (**21**) and $[(Et_8N_2O_2)SmN(SiMe_3)_2]$, (**CXL**).

4.3.4. Reactivity studies of $[(Et_8N_2O_2)Sm\{N(H)C_6H_2\text{-}2,4,6\text{-}t\text{-}Bu\}]$, (**21**).

The reactivity of $[(Et_8N_2O_2)Sm\{N(H)C_6H_2\text{-}2,4,6\text{-}t\text{-}Bu\}]$, (**21**) towards base was investigated in order to attempt the α-deprotonation of the amide unit to yield an imide complex, as shown in Scheme 4.5.

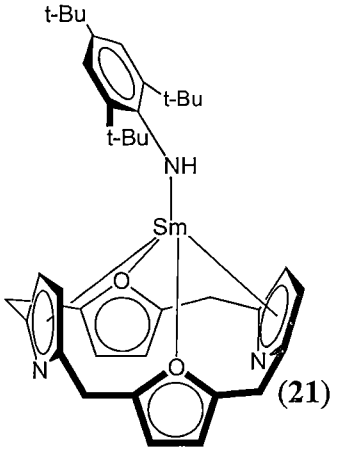

(21)

+ MR ⟶// [$L_xM(Et_8N_2O_2)Sm{=}N(C_6H_2$-2,4,6-*t*-Bu)] + RH

(24)

MR = LiMe, KH
L = THF, toluene

Scheme 4.5. Intended α-deprotonation of the macrocyclic samarium(III) mono(amide) [$(Et_8N_2O_2)Sm\{N(H)C_6H_2$-2,4,6-*t*-Bu}], (**21**). *Meso*-ethyl groups in **21** omitted for clarity.

Addition of MeLi to a THF solution of [$(Et_8N_2O_2)Sm\{N(H)C_6H_2$-2,4,6-*t*-Bu}], (**21**) did not result in any subsequent reactivity. The addition of KH to **21** in THF resulted in a complex mixture of unidentifiable products forming, with the desired α-deprotonation of the amide unable to be confirmed. The lack of desired reactivity of **21** towards base may be rationalised from steric considerations, when the availability of the α-NH proton is considered. Figure 4.28 shows a space filling representation of the molecular structure of **21** with the α-NH proton highlighted. From this structure, it can be seen that the steric bulk of both the macrocyclic and aromatic 2,4,6-tri-*t*-Bu-anilido ligands provide significant steric shielding to the α-NH proton, which may prohibit reactivity at this site. The 2,4,6-tri-*t*-Bu-anilido samarium(III) complex of Arnold *et al.*, [(DippNC(Me)CHC(Me)Ndipp)Sm$\{N(H)(C_6H_2$-2,4,6-*t*-Bu)$\}_2$], (**CLXIV**), also exhibited stability towards excess base, with no α-NH deprotonation observed when $KN(SiMe_3)_2$ was added to a solution of the complex.[8e]

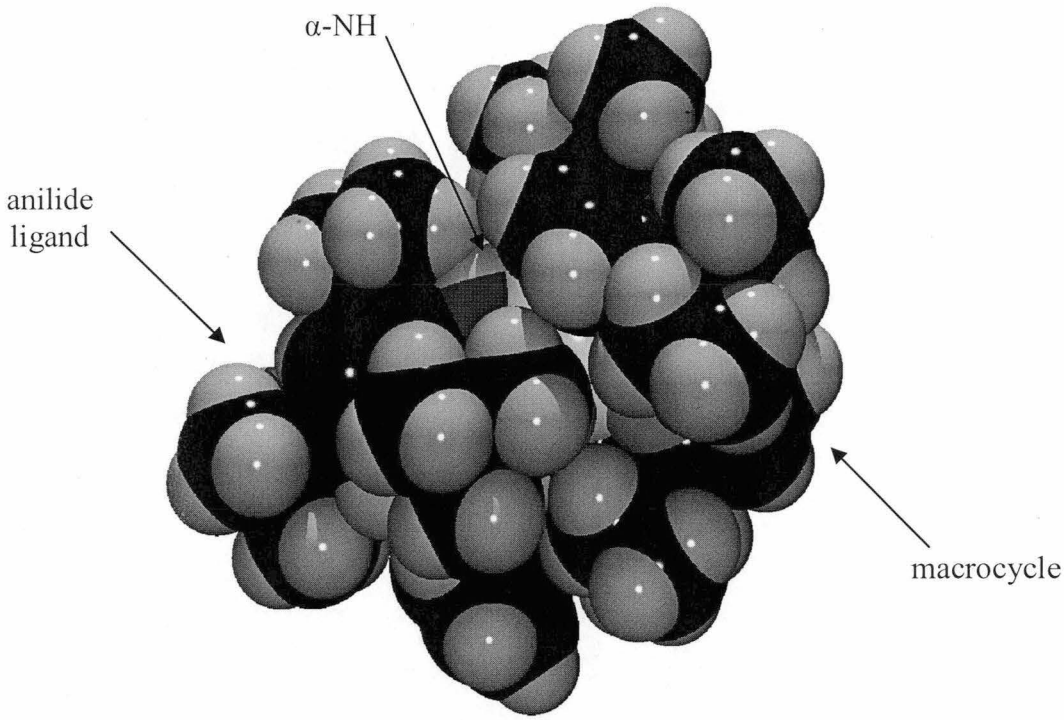

Figure 4.28. Space filling representation of the molecular structure of **21**.

4.3.5. Synthesis and reactivity studies of [{($Et_8N_2O_2$)SmN(H)Mes], (**20**).

The reaction of the orange samarium(III) dinuclear complex [{($Et_8N_2O_2$)Sm(μ-I)}$_2$], (**8**) with the lithium amide LiN(H)Mes, (**25**), in THF also gave a red solution, analogous to the reaction of [{($Et_8N_2O_2$)Sm(μ-I)}$_2$], (**8**), with KN(H)Mes, (**19**). Concentration of the solution *in vacuo* gave crystals of the samarium mono(amide) [($Et_8N_2O_2$)SmN(H)Mes], (**20**), as shown below in Scheme 4.6.

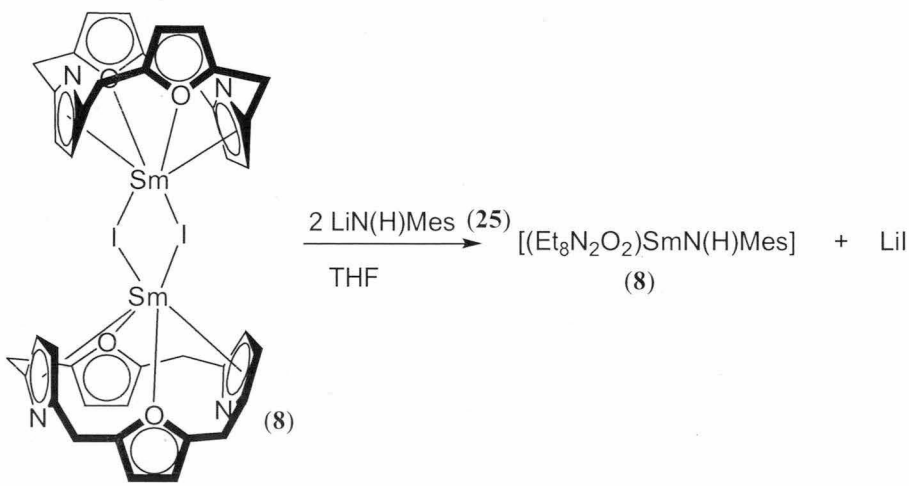

Scheme 4.6. Synthesis of the samarium(III) mono(amide) [($Et_8N_2O_2$)SmN(H)Mes], (**20**). Meso-ethyl substituents in **8** omitted for clarity.

[($Et_8N_2O_2$)SmN(H)Mes], (**20**) exhibits high solubility in THF, benzene and toluene, and moderate solubility in petroleum spirits and was characterised by ^1H and ^{13}C NMR spectroscopy, and microanalysis.

Structural details of [($Et_8N_2O_2$)SmN(H)Mes], (**20**), were confirmed through ^1H, $^{13}C\{^1H\}$, gHMQC, gHMBC, gCOSY and NOESY NMR spectroscopy. Full assignment of the ^1H and ^{13}C NMR resonances of **20** are shown in Figure 4.29, whilst a three dimensional representation of **20** is shown in Figure 4.30. **20** exhibits C_{2v} symmetry in the solution state, analogous to [($Et_8N_2O_2$)Sm{N(H)(C_6H_2-2,4,6-*t*-Bu)}], (**21**), with one amide ligand bound to the samarium(III) centre. The chemical shift range of resonances in the ^1H NMR spectrum of **20** are similar to that of **21**, with resonances ranging from –5.0 to 24.5 ppm. Together, these are similar to previous mononuclear (group 1 metal free) complexes of the metallated dioxaporphyrinogen ligand.

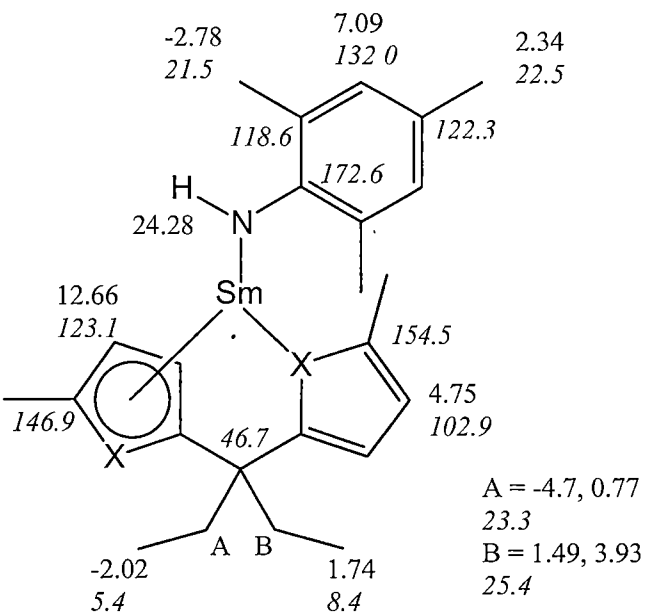

Figure 4.29. Full ^1H and ^{13}C assignment of the NMR resonances of the samarium(III) mono(amide) [($Et_8N_2O_2$)SmN(H)Mes], (**20**).

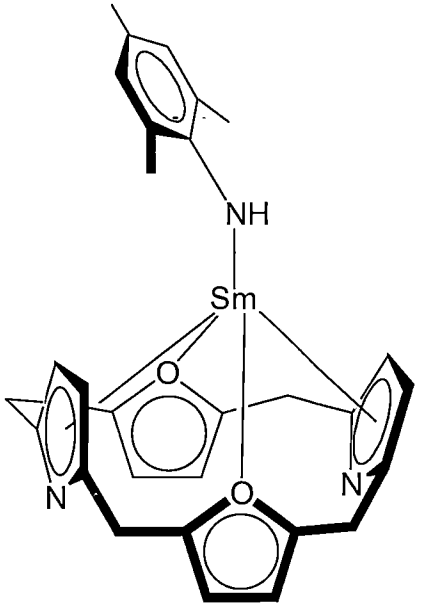

Figure 4.30. Three dimensional representation of the samarium(III) mono(amide) [$(Et_8N_2O_2)$SmN(H)Mes], (**20**). *Meso*-ethyl substituents omitted for clarity.

The observed preference for mono(amide) formation from the reaction of [{$(Et_8N_2O_2)$Sm(μ-I)}$_2$], (**8**), with lithium mesitylamide, LiN(H)Mes, (**25**), as opposed to bis(amide) formation, observed in the reaction of **8** with potassium mesitylamide, KN(H)Mes, (**19**), can be rationalised from an analysis of the differing binding modes observed for Group 1 metal complexes of macrocyclic porphyrinogen ligands. Previously reported Li porphyrinogen structures generally exhibit flattened partial cone conformations,[21] as the small electropositive metal centre seeks strong interactions with the Lewis base donors in the macrocyclic ligand. In contrast, Group 1 metal porphyrinogen complexes of larger K ions favour the 1,3-alternate macrocyclic conformation observed in lanthanide porphyrinogen chemistry, as steric protection, in addition to favourable electronic interactions is afforded by the η^5-bonds. Consequently, the binding of a potassium cation within the macrocyclic cavity of [$(Et_8N_2O_2)$SmN(H)Mes], (**20**), (and subsequent amide anion) which possesses the desired 1,3-alternate conformation is expected to be more favourable than for lithium, which is unable to exploit the full electronic and steric stabilisation afforded by the macrocyclic ligand in the 1,3-alternate macrocyclic conformation.

The reaction of [{$(Et_8N_2O_2)$SmN(H)Mes], (**20**), with base was investigated, analogous to the deprotonation attempts of the lanthanide amide compounds

$[(Et_8N_2O_2)Sm\{N(H)C_6H_2\text{-}2,4,6\text{-}t\text{-}Bu\}]$, (**21**), and $[(THF)_2K(Et_8N_2O_2)Sm\{N(H)Mes\}_2]$, (**17**). However, as observed previously **20** exhibited no reactivity with MeLi, and no reactivity with KH until 2 equivalents of base were added and the mixture heated for an extended period to give the metal exchange product, $[\{(Et_8N_2O_2)K_2(\mu\text{-}\eta^6\text{:}\eta^6\text{-}C_6D_6)\}_n]$, (5), identified by ^1H NMR spectroscopy.

4.4. Further reactions utilising $[\{(Et_8N_2O_2)Sm(\mu\text{-}I)\}_2]$, (8).

4.4.1. Reaction of $[\{(Et_8N_2O_2)Sm(\mu\text{-}I)\}_2]$, (8) with $[\{(THF)MgNPh\}_6]$, (26).

The direct synthesis of a lanthanide imide complex from the samarium(III) dinuclear complex $[\{(Et_8N_2O_2)Sm(\mu\text{-}I)\}_2]$, (**8**), and the known transition metal imidating agent $[\{(THF)MgNPh\}_6]$,[22] (**26**) was also attempted in THF, as shown in Scheme 4.7. However, after prolonged heating at 50 °C, no reaction was evident.

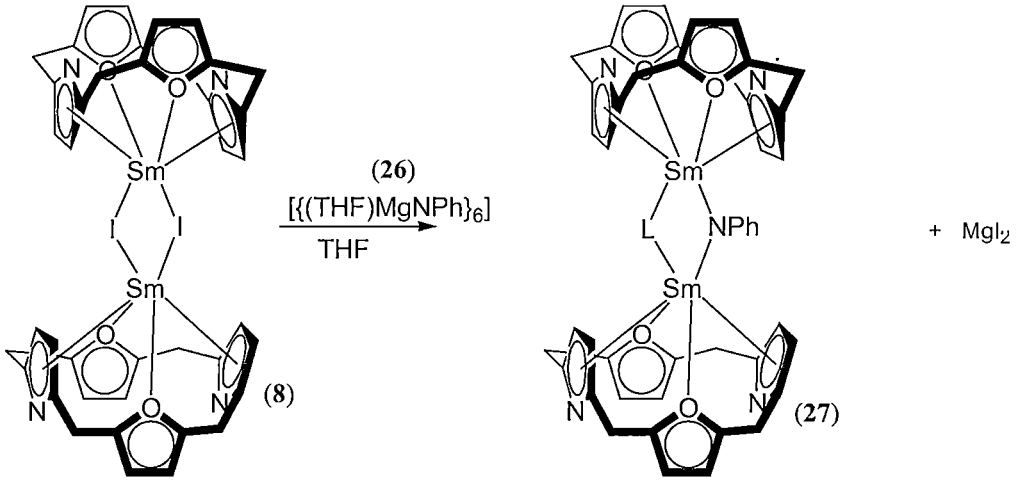

Scheme 4.7. Proposed synthesis of a lanthanide imide complex. Meso-ethyl substituents in **8** and **27** omitted for clarity.

4.4.2. Attempted macrocyclic samarium(III) alkyl syntheses.

The synthesis of a lanthanide alkyl complex, from the samarium(III) and (II) macrocycle complexes, $[\{(Et_8N_2O_2)Sm(\mu\text{-}I)\}_2]$, (**8**) and $[\{(THF)_2K(Et_8N_2O_2)Sm(\mu\text{-}I)\}_2]$, (**6**), which may facilitate the deprotonation of an amide substrate to yield a lanthanide imide species was also attempted, as shown in Scheme 4.8. The metathetical exchange reaction of the dinuclear samarium(III) complex $[\{(Et_8N_2O_2)Sm(\mu\text{-}I)\}_2]$, (**8**), with MeLi in THF was attempted, however no reaction

was observed. Alternatively, the redox reaction between the green heterometallic samarium(II) complex $[\{(THF)_2K(Et_8N_2O_2)Sm(\mu\text{-}I)\}_2]$, (**6**), with the known transition metal methylating agent, $SnMe_4$,[23] was also attempted, however no reaction was observed. These results contrast with those observed for the *N,N'*-dimethyl macrocyclic system, whereby the lanthanide alkyl complexes $[(Et_8N_4Me_2)SmMe]$, (**CLXVIII**), and $[(Et_8N_4Me_2)SmCH_2SiMe_3]$, (**CLXIX**), were synthesised via metathetical exchange between the corresponding macrocyclic samarium(III) chloride and Group 1 alkyl reagent.[24]

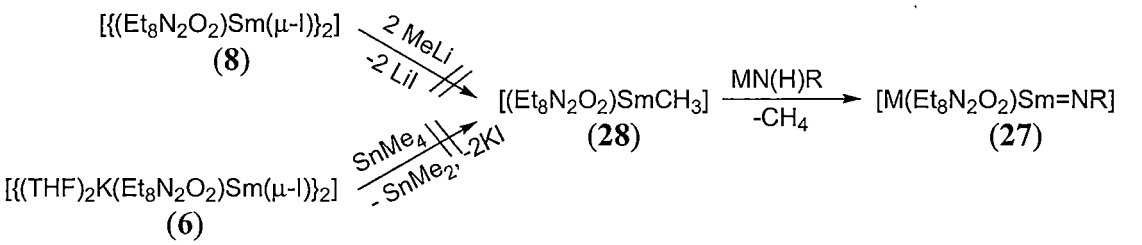

Scheme 4.8. Proposed synthesis of a lanthanide alkyl complex and the intended subsequent formation of a lanthanide imide complex.

4.5. Experimental.

KN(H)Mes, (**19**)

To a stirred suspension of KH (0.65 g, 16.2 mmol) in THF (40 mL) was added 2,4,6-trimethylaniline dropwise (3 mL, 2.85 g, 21 mmol). The solution was stirred for 1 hour before toluene (40 mL) was added and the solution filtered. The resulting orange solution was then concentrated *in vacuo* and cooled to –17 °C overnight yielding orange crystals of $KN(H)C_6H_2Me_3$, (**19**), (1.7 g, 9.8 mmol, 61 %).

^{1}H NMR (THF-d^8, 299.905 MHz, 25 °C, ppm): δ 1.98 (s, 9H, *o*- and *p*-CH_3), 2.81 (s, 1H, NH), 6.36 (s, 2H, *m*-CH).

$^{13}C\{^1H\}$ NMR (THF-d^8, 75.417 MHz, 25 °C, ppm): δ 21.5 (*o*-CH_3), 21.9 (*p*-CH_3), 112.2 (*o*-*C*CH3), 119.2 (*p*-*C*CH3), 130.3 (*m*-CH), 161.8 (C-N).

$[(THF)_2K(Et_8N_2O_2)Sm\{N(H)C_6H_2Me_3\}_2]$, (**17**)

To a stirred flask containing $[\{(Et_8N_2O_2)Sm(\mu\text{-}I)\}_2]$, (**8**), (1.2 g, 0.73 mmol) in THF (100 mL), was added dropwise a solution of $KN(H)C_6H_2Me_3$, (**19**), (0.50 g, 2.9 mmol). The resulting red solutiuon was stirred overnight before being filtered from a white solid (presumably KI). The solution was then concentrated *in vacuo* to 60 mL and left overnight at room temperature to yield **17** as a pure red crystalline solid (1.13 g, 64 %).

^{1}H NMR (THF-d^8, 299.905 MHz, -50 °C, ppm): δ –4.24 (broad, s, 2H, CH_2), -2.62 (broad, m, 2H, CH_2), -1.92 (broad, m, 2H, CH_2), -1.25 (t, 6H, CH_2CH_3), -0.24 (t, 6H, CH_2CH_3), 0.22 (broad, m, 2H, CH_2), 0.88 (t, 6H, CH_2CH_3), 1.64 (s, 6H, *p*-CH_3), 2.22 (t, 6H, CH_2CH_3), 2.28 (s, 6H, *o*-CH_3), 2.36 (s, 6H, *o*-CH_3), 2.51 (broad, m, 2H, CH_2), 3.22 (broad, m, 2H, CH_2), 3.86 (broad, m, 2H, CH_2), 5.02 (broad, m, 2H, CH_2), 7.10 (s, 2H, fur/pyr CH), 7.18 (s, 2H, fur/pyr CH), 7.27 (s, 2H, fur/pyr CH), 7.34 (s, 2H, fur/pyr CH), 9.92 (s, 2H, *m*-CH), 10.21 (s, 2H, *m*-CH). NH resonances not observed.

^{1}H NMR (THF-d^8, 299.905 MHz, 25 °C, ppm): δ –0.22 (broad, s, 8H, CH_2), 1.18 (broad, s, 8H, CH_2), 1.73 (s, 6H, *p*-CH_3), 1.92 (broad, s, 24H, CH_2CH_3), 2.19 (s, 12H, *o*-CH_3), 6.62 (broad, s, 4H, fur/pyr CH), 6.99 (s, 4H, *m*-CH), 7.18 (broad, s, 4H, fur/pyr CH).

$^{13}C\{^1H\}$ NMR (C_6D_6, 75.417 MHz, 25 °C, ppm): 6.02 (CH_2), 7.78 (CH_2), 16.88 (*p*-CH_3), 21.96 (*o*-CH_3), 22.84 (CH_3), 24.02 (CH_3), 46.12 (*meso*-*C*CH_2), 119.46 (α-C

pyr or fur), 126.84 (fur/pyr CH), 130.80 (*m*-CH), 131.86 (fur/pyr CH), 159.20 (α-C pyr or fur).

Anal. Calcd.: C, 65.25; H, 7.96; N, 4.61 ($C_{66}H_{96}N_4O_5SmK$, MW 1214.95) Found: C 65.43; H, 7.75; N, 4.67

[{μ-η^1:η^3-{N(H)Mes}K($Et_8N_2O_2$)SmN(H)Mes}$_n$].THF, (**18**)

To a flask containing [(THF)$_2$K($Et_8N_2O_2$)Sm{N(H)$C_6H_2Me_3$}$_2$], (**17**), (0.10 g, 0.08 mmol) was added benzene (5 mL), and the resulting suspension heated at 50 °C for 5 days to yield dark red crystals of **18** (0.064 g, 0.06 mmol, 80 %).

Anal. Calcd.: C, 65.01; H, 7.40; N, 5.41 ($C_{58}H_{80}KN_4O_3Sm$, MW 998.63) Found: C, 64.56; H, 7.22; N, 5.12

LiN(H)C_6H_2(*t*-Bu)$_3$, (**22**)

To a stirred solution of 2,4,6-tri-*t*-butylaniline (0.50 g, 1.9 mmol) in petroleum spirit 40-60 °C (30 mL), n-BuLi (1.6 M in hexanes, 1.4 mL, 2.2 mmol) was added dropwise, resulting in a white solid immediately precipitating. The resulting suspension was then stirred at room temperature for a further 20 minutes before being filtered, leaving **22** as a pure white solid (0.34 g, 1.3 mmol, 67 %).

^{1}H NMR (C_6D_6, 299.905 MHz, 25 °C, ppm): δ 1.65 (s, 9H, CH_3), 1.72 (s, 9H, CH_3), 1.79 (s, 9H, CH_3), 7.39 (s, 2H, *m*-CH).

[($Et_8N_2O_2$)Sm(N(H)C_6H_2(*t*-Bu)$_3$)], (**21**)

To a flask containing [{($Et_8N_2O_2$)Sm(μ-I)}$_2$], (**8**), (0.10 g, 0.06 mmol) and LiN(H)C_6H_2(*t*-Bu)$_3$, (**22**), (0.030 g, 0.11 mmol), THF (30 mL) was added, and the solution stirred for 2 hours. THF was then removed *in vacuo* leaving a crude purple solid to which toluene (30 mL) was added. The purple solution was then filtered from a white solid (presumably LiI) and concentrated *in vacuo* to 15 mL. Cooling to –17 °C overnight yielded purple crystals of **21**, (0.07 g, 61 %).

^{1}H NMR (C_6D_6, 299.905 MHz, 25 °C, ppm): δ -4.35 (m, 4H, CH_2), -1.56 (s, 18H, *o*-*t*-Bu), -1.28 (t, 12H, CH_3), 0.99 (m, 4H, CH_2), 1.57 (s, 16H, CH_3 + CH_2), 2.00 (s, 9H, *p*-*t*-Bu), 3.78 (m, 4H, CH_2), 4.85 (s, 4H, CH), 7.76 (s, 2H, *m*-CH), 12.22 (s, 4H, CH), 24.44 (broad, s, 1H, NH).

^{13}C{^{1}H} NMR (C_6D_6, 75.417 MHz, 25 °C, ppm): δ 5.63 (CH_3 (-1.28)), 8.33 (CH_3 (1.57)), 22.41 (CH_2, 0.99), 25.44 (CH_2, 3.78), 31.74 (*p*-*t*-Bu-CH_3 (2.00)), 31.78 (*o*-*t*-

Bu-CH_3 (-1.56)), 36.15 (*p*-$C(CH_3)_3$), 36.81 (*o*-$C(CH_3)_3$), 46.59 (*meso*-CCH_2), 103.56 (pyr or fur CH (4.85)), 121.29 (pyr or fur CH (12.22)), 124.82 (*m*-CH (7.76)), 128.30 (*o*-$CC(CH_3)_3$), 133.26 (*p*-$CC(CH_3)_3$), 146.55 (α-C pyr or fur), 154.82 (α-C pyr or fur), 173.80 (C-N).

Anal. Calcd.: C, 70.20; H, 8.31; N, 4.03 ($C_{61}H_{86}N_3O_2Sm$, MW 1043.71)
Found: C, 70.05; H, 8.34; N, 3.68

$LiN(H)C_6H_2Me_3$, (**25**)

To a stirred solution of 2,4,6-trimethylaniline (2 mL, 1.90 g, 14.2 mmol) in petroleum spirit 40-60 °C (40 mL) at 0 °C was added *n*-BuLi (1.6 M in hexanes, 12 mL, 19.2 mmol). The solution was let warm to room temperature and was stirred overnight before being filtered, leaving a white solid which was washed with petroleum spirit 40-60 °C (30 mL) and dried *in vacuo* (1.8 g, 91 %).

$[(Et_8N_2O_2)Sm\{N(H)C_6H_2Me_3\}]$, (**20**)

To a flask containing $[\{(Et_8N_2O_2)Sm(\mu\text{-}I)\}_2]$, (**8**), (0.20 g, 0.12 mmol) and LiN(H)Mes, (**25**), (0.034 g, 0.24 mmol) was added THF (40 mL) and the solution stirred for 12 hours. The resulting red solution was then concentrated in vacuo to approximately 10 ml and cooled to -17 °C for 2 weeks to give **20** as a red crystalline solid, contaminated with LiI, (0.1 g, 50 %).

^{1}H NMR (C_6D_6, 299.905 MHz, 25 °C, ppm): δ -4.71 (m, 4H, CH_2), -2.78 (s, 6H, *o*-CH_3), -2.02 (t, ^{3}J = 12H, CH_3), 0.77 (m, 4H, CH_2), 1.49 (m, 4H, CH_2), 1.74 (t, ^{3}J = 12H, CH_3), 2.34 (s, 3H, *p*-CH_3), 3.93 (m, 4H, CH_2), 4.75 (s, 4H, pyr or fur CH), 7.09 (s, 2H, *m*-CH), 12.66 (s, 4H, pyr or fur CH), 24.28 (broad, s, 1H, NH).

^{13}C{^{1}H} NMR (C_6D_6, 75.417 MHz, 25 °C, ppm): δ 5.4 (CH_3 (-2.02)), 8.4 (CH_3 (1.74)), 21.5 (*o*-CH_3 (-2.78)), 22.5 (*p*-CH_3 (2.34)), 23.4 (CH_2 (0.77)), 23.5 (CH_2 (-4.71)), 25.4 (CH_2 (3.93)), 46.7 (CCH_2), 102.9 (CH (4.75)), 118.6 (*o*-C), 122.3 (*p*-C), 123.1(CH (12.66)), 132.0 (*m*-CH (7.09)), 146.9 (α-C pyr or fur), 154.5 (α-C pyr or fur), 172.6 (C-N).

Anal. Calcd.: C, 62.22; H, 6.96; N, 4.84 ($C_{45}H_{60}N_3O_2Sm$ M.W. 825.34 + 5 %w/w LiI)
Found: C, 62.16; H, 6.52; N, 4.83

[{(THF)MgNPh}$_6$], (**26**)

26 was prepared according to a modified literature procedure.[22]

To a stirred solution of dibutyl magnesium (1 M in heptane, 33 mL, 33 mmol) at 0 °C was added a solution of aniline (3.0 mL, 3.1 g, 33 mmol) in THF (40 mL), and the solution stirred for 4 hours. The solution was then let stand overnight at room temperature affording white crystals of **26** (4.0 g, 64 %).

4.6. References

1. Power, P. P. *J. Organomet. Chem.* **2004**, *689*, 3904.
2. Ghotra, J.D.; Hursthouse, M.B.; Welch, A.J.
   J. Chem. Soc., Chem. Commun. **1973**, 669.
3. a) Hitchcock, P.B.; Hulkes, A.G.; Lappert, M.F.; Li, Z.
   Dalton Trans. **2004**, 129,
   b) Evans, W.J.; Lee, D.S.; Ziller, J.W. *J. Am. Chem. Soc.* **2004**, *126*, 454,
   c) Karl, M.; Seybert, G.; Massa, W.; Agarwal, A.; Greiner, A.; Dehnicke, K.
   Z. Anorg. Allg. Chem. **1999**, *625*, 1405,
   d) Tilley, T.D.; Andersen, R.A.; Zalkin, A. *Inorg. Chem.* **1984**, *23*, 2271,
   e) Boncella, J.M.; Andersen, R.A. *Organometallics* **1985**, *4*, 205,
   f) Karl, M.; Harms, K.; Seybert, G.; Massa, W.; Fau, S.; Frenking, G.;
   Dehnicke, K. *Z. Anorg. Allg. Chem.* **1999**, *625*, 2055,
   g) Berg, D.J.; Gendron, R.A.L. *Can. J. Chem.* **2000**, *78*, 454,
   h) Brady, E.D.; Clark, D.L. Gordon, J.C.; Hay, P.J.; Keogh, D.W.; Poli, R.;
   Scott, B.L. Watkin, J.G. *Inorg. Chem.* **2003**, *42*, 6682,
   i) Hitchcock, P.B.; Hulkes, A.G.; Lappert, M.F. *Inorg. Chem.* **2004**, *43*, 1031,
   j) Niemeyer, M. *Z. Anorg. Allg. Chem.* **2002**, *628*, 647,
   k) Evans, W.J.; Drummond, D.K.; Zhang, H.; Atwood, J.L.
   Inorg. Chem. **1988**, *27*, 575,
   l) Evans, W.J.; Lee, D.S.; Rego, D.B.; Perotti, J.M.; Kozimor, S.A.; Moore,
   E.K.; Ziller, J.W. *J. Am. Chem. Soc.* **2004**, *126*, 14574,
   m) Edelmann, F.T.; Steiner, A.; Stalke, D.; Gilje, J.W.; Jagner, S.;
   Hakansson, M. *Polyhedron* **1994**, *13*, 539,
   n) Heeres, H.J.; Meetsma, A.; Teuben, J.H.; Rogers, R.D.
   Organometallics **1989**, *8*, 2637,
   o) Aspinall, H.C.; Bradley, D.C.; Hursthouse, M.B.; Sales, K.D.; Walker,
   N.P.C.; Hussain, B. *J. Chem. Soc., Dalton Trans.* **1989**, 623,
   p) Evans, W.J.; Zucchi, G.; Ziller, J.W. *J. Am. Chem. Soc.* **2003**, *125*, 10,
   q) Collin, J.; Giuseppone, N.; Jaber, N.; Domingos, A.; Maria, L.; Santos, I.
   J. Organomet. Chem. **2001**, *628*, 271,
   r) Anwander, R.; Runte, O.; Eppinger, J.; Gerstberger, G.; Herdtweck, E.;
   Spiegler, M. *J. Chem. Soc., Dalton. Trans.* **1998**, 847,

s) Rees, W.S. Junior; Just, O.; Van Derveer, D.S.
J. Mater. Chem. **1999**, *9*, 249,
t) Just, O.; Rees, W.S., Junior *Inorg. Chem.* **2001**, *40*, 1751,
u) Eisenstien, O.; Hitchcock, P.B.; Hulkes, A.G.; Lappert, M.F.; Maron, L.
Chem. Commun. **2001**, 1560,
v) Hitchcock, P.B.; Hulkes, A.G.; Lappert, M.F.
Inorg. Chem. **2004**, *43*, 1031,
w) Evans, W.J.; Johnston, M.A.; Clark, R.D.; Anwander, R.; Ziller, J.W.
Polyhedron **2001**, *20*, 2483,
x) Andersen, R.A.; Templeton, D.H.; Zalkin, A. *Inorg. Chem.* **1978**, *17*, 2317,
y) Zhou, S.L.; Wang, S.W.; Yang, G.S.; Liw, X.Y.; Sheng, E.H.; Zhang,
K.H.; Cheng, L.; Huang, Z.X. *Polyhedron* **2003**, *22*, 1019,
z) Schumann, H.; Winterfeld, J.; Esser, L. Kociok-Köhn, G.
Angew. Chem., Int. Ed. Engl. **1993**, *32*, 1208,
aa) Evans, W.J.; Keyer, R.A.; Ziller, J.W. *Organometallics* **1993**, *12*, 2618,
ab) Jank, S.; Hanss, J.; Reddmann, H.; Amberger, H.D.; Edelstein, N.M. *Z.
Anorg. Allg. Chem.* **2002**, *628*, 1355,
ac) Sheng, E.; Wang, S.; Yang, G.; Zhou, S.; Cheng, L.; Zhang, K.; Huang, Z.
Organometallics **2003**, *22*, 684,
ad) Niemeyer, M. *Inorg. Chem.* **2006**, *45*, 9085,
ae) Herrmann, W.A.; Anwander, R.; Munck, F.C.; Scherer, W.; Dufaud, V.;
Huber, N.W.; Artus, G.R.J. *Z. Naturforsch.,B:Chem. Sci.* **1994**, *49*, 1789.

4. Schumann, H.; Palamidis, F.; Loebel, J. *J. Organomet. Chem.* **1990**, *390*, 45.
5. Schumann, H.; Winterfeld, J.; Rosenthal, E.C.E.; Hemling, H.; Esser, L. *Z.
Anorg. Allg. Chem.* **1995**, *621*, 122.
6. Heeres, H.J.; Meetsma, A.; Teuben, J.H.; Rogers, R.D.
Organometallics **1989**, *8*, 2637.
7. Schuetz, S.A.; Day, V.W.; Sommer, R.D.; Rheingold, A.L.; Belot, J.A.
Inorg. Chem. **2001**, *40*, 5292.
8. a) Avent, A.G.; Caro, C.F.; Hitchcock, P.B.; Lappert, M.F.; Li, Z.; Wei, X.H.
Dalton Trans. **2004**, 1567,
b). Vitanova, D.V.; Hampel, F.; Hultzsch, K.C.
J. Organomet. Chem. **2005**, *690*, 5182,
c) Schuetz, S.A.; Day, V.W.; Rheingold, A.L.; Belot, J.A.

Dalton Trans. **2003**, 4303,

d) Schuetz, S.A.; Silvernail, C.M.; Incarvito, C.D.; Rheingold, A.L.; Clark, J.L.; Day, V.W.; Belot, J.A. *Inorg. Chem.* **2004**, *43*, 6203,

e) Cui, C.; Shafir, A.; Schmidt, J.A.R. Oliver, A.G.; Arnold, J. *Dalton Trans.* **2005**, 1387,

f) Schuetz, S.A.; Day, V.W.; Sommer, R.D.; Rheingold, A.L.; Belot, J.A. *Inorg. Chem.* **2001**, *40*, 5292,

g) Schuetz, S.A.; Day, V.W.; Clark, J.L.; Belot, J.A. *Inorg. Chem. Commun.* **2002**, *5*, 706,

h) Yao, Y.; Zhang, Y.; Shen, Q.; Yu, K. *Organometallics* **2002**, *21*, 819,

i) Xue, M.; Yao, Y.; Shen, Q.; Zhang, Y. *J. Organomet. Chem.* **2005**, *690*, 4685,

j) Vitanova, D.V. Hampel, F.; Hultzsch, K.C. *Dalton Trans.* **2005**, 1565,

k) Yao, Y.; Zhang, Z.; Peng, H.; Zhang, Y.; Shen, Q.; Lin, J. *Inorg. Chem.* **2006**, *45*, 2175.

9. Wang, J.; Gardiner, M.G. *Chem. Commun.* **2005**, 1589.
10. Wang, J.; Dick, A.K.J.; Gardiner, M.G.; Yates, B.F.; Peacock, E.J.; Skelton, B.W.; White, A.H. *Eur. J. Inorg. Chem.* **2004**, 1992.
11. Evans, W.J.; Kociok-Köhn, G.; Leong, V.S.; Ziller, J.W. *Inorg. Chem.* **1992**, *31*, 3592.
12. a) Wang, S.; Li, H.W.; Xie, Z. *Organometallics* **2004**, *23*, 2469

b) Chan, H.S.; Li, H.W.; Xie, Z. *Chem. Commun.* **2002**, 652,

c) Giesbrecht, G.R.; Gordon, J.C.; Clark, D.L.; Hay, P.J.; Scott, B.L.; Tait, C.D. *J. Am. Chem. Soc.* **2004**, *126*, 6387,

d) Cameron, T.M.; Gordon, J.C.; Scott, B.L.; Tumas, W. *Chem. Commun.* **2004**, 1398,

e) Cameron, T.M.; Gordon, J.C.; Scott, B.L. *Organometallics* **2004**, *23*, 2995,

f) Giesbrecht, G.R.; Collis, G.E.; Gordon, J.C.; Clark, D.L.; Scott, B.L.; Hardman, N.J. *J. Organomet. Chem.* **2004**, *689*, 2177,

g) Cui, C.; Shafir, A.; Schmidt, J.A.R.; Oliver, A.G.; Arnold, J. *Dalton Trans.* **2005**, 1387,

h) Gordon, J.C.; Giesbrecht, G.R.; Clark, D.L.; Hay, P.J.; Keogh, D.W.; Poli, R.; Scott, B.L.; Watkin, J.G. *Organometallics* **2002**, *21*, 4726,

i) Wang, S.; Li, H.W.; Xie, Z. *Organometallics* **2004**, *23*, 3780,

j) Evans, W.J.; Ansari, M.A.; Ziller, J.W.; Khan, S.I.
Inorg. Chem. **1996**, *35*, 5435,
k) Hou, Z.; Zhang, Y.; Tezuka, H.; Xie, P.; Tardiff, O.; Koizumi, T.; Yamazaki, H.; Wakatsuki, Y. *J. Am. Chem. Soc.* **2000**, *122*, 10533

13. Pi, C.; Zhang, Z.; Pang, Z.; Zhang, J.; Luo, J.; Chen, Z.; Weng, L.; Zhou, X. *Organometallics* **2007**, *26*, 1934.
14. Hou, Z.; Zhang, Y.; Tezuka, H.; Xie, P.; Tardif, O.; Koizumi, T.; Yamazaki, H.; Wakatsuki, Y. *J. Am. Chem. Soc.* **2000**, *122*, 10533.
15. Layfield, R.A.; Bashall, A.; McPartlin, M.; Rawson, J.M.; Wright, D.S.; *Dalton Trans.* **2006**, 1660.
16. a) Wang, S.; Li, H.W.; Xie, Z. *Organometallics* **2004**, *23*, 2469,
b) Wang, S.; Li, H.W.; Xie, Z. *Organometallics* **2004**, *23*, 3780.
17. Click, D.R.; Scott, B.L.; Watkin, J.G. *Chem. Commun.* **1999**, 633.
18. Giesbrecht, G.R.; Gordon, J.C.; Clark, D.L.; Hay, P.J.; Scott, B.L.; Tait, C.D. *J. Am. Chem. Soc.* **2004**, *126*, 6387.
19. Evans, W.J.; Ansari, M.A.; Ziller, J.W.; Khan, S.I.
Inorg. Chem. **1996**, *35*, 5435.
20. Woodman, T.J.; Schormann, M.; Hughes, D.L.; Bochmann, M. *Organometallics* **2003**, *22*, 3028.
21. De Angelis, S.; Solari, E.; Floriani, C.; Chiesi-Villa, A.; Rizzoli, C. *J. Chem. Soc. Dalton Trans.* **1994**, 2467.
22. a) Hascall, T.; Ruhlandt-Senge, K.; Power, P.P.
Angew. Chem. Int. Ed. Engl. **1994**, *33*, 356,
b). Grigsby, W.J.; Olmstead, M.M.; Power, P.P.
J. Organomet. Chem. **1996**, *513*, 173.
23. Herrmann, W. A.; Felixberger, J. K.; Herdtweck, E.; Schaefer, A.; Okuda, J. *Angew. Chem., Int. Ed. Engl.* **1987**, *26*, 466.
24. Wang, J.; Gardiner, M.G.; Skelton, B.W.; White, A.H
Organometallics **2005**, *24*, 815.

Chapter 5 Theoretical studies of lanthanide imides.

5.1. Introduction to theoretical lanthanide investigations

5.1.1. Comment on theoretical studies of the lanthanides.

Synthetic organolanthanide chemistry first attracted large-scale attention during the late 1970s and 1980s when effective synthesis and characterisation methods became more available. Since that time organolanthanide chemistry has experienced tremendous growth. Consequently, theoretical studies of the lanthanide elements have recently received an increasing focus as an understanding of the many unique lanthanide based systems is sought. F-block elements, however, pose many theoretical challenges.

5.1.2. Complications in lanthanide calculations: relativistic effects.

Heavy nuclei such as those of the lanthanide elements enforce large velocities on the surrounding electron cloud, resulting in the core electrons travelling at velocities which are an appreciable fraction of the speed of light. As a consequence, relativistic effects in heavy elements are important. As the effective mass of the electrons increases, the Bohr radius of the atomic orbitals decreases, causing contraction of the core orbitals. This phenomenon extends throughout the atomic orbitals and has a chemically significant effect on the valence atomic orbitals.[1] Necessarily, theoretical calculations involving heavy elements require some treatment of relativistic effects in order to correlate with experiment.

The Dirac-Fock method is the relativistic analogue of the well reported Hartree-Fock method and it has been used well for heavy atoms since the 1970s.[2] This method utilises four-component spinors and is thus referred to as the four-component method. Configuration interaction methods are also available with this method. Calculations utilising this approach are very accurate, however for larger molecules they become too computationally demanding at present and approximate methods are required.[1] Scalar Relativistic Effective Core Potential (RECP) calculations can account for the relativistic contraction of core orbitals, whilst saving computational expense. RECP methods incorporate many of the non-valence electrons into an 'effective core', which accounts for the relativistic contraction of the core orbitals whilst simplifying the calculation by lowering the number of electrons treated

explicitly. Comparisons of RECP methods with four-component methods for simple molecules give good correlation, and good agreement between RECP methods and experiment in larger systems have been shown.[1]

Density Functional Theory (DFT) calculations can incorporate RECPs and are thus highly suited to the lanthanide elements, possessing the required accuracy in dealing with relativistic effects, whilst maintaining feasible computational demands for larger molecules. Both Slater type and Gaussian type basis sets are in common use, most often within the Amsterdam Density Functional (ADF)[3] and Gaussian[4] software packages, respectively. Hybrid Density Functional Theory methods such as B3LYP[5] and B3PW91[6] have been well utilised for the lanthanide elements.

Scalar RECPs are generally regarded as being acceptable for use in lanthanide calculations[7] and several are available for use. The Stuttgart-Dresden (SDD) ECP and associated valence basis set is well regarded for lanthanide systems, as is the CEP sets of Stevens, Cundari and co-workers. The comparison of optimised geometries resulting from either of these basis sets is quite favourable.[8] The SDD and CEP valence sets do, however, differ in the number of electrons incorporated in the ECP.

The lanthanide 4f electrons are generally thought to not participate in bonding,[9-11] and due to the complexity they can add to theoretical studies, they are often incorporated into the ECP. Of common use is the SDD[12] ECP employing a large core ECP, MWB51, with 51 electrons incorporated into the effective core, including the 4f electrons. Conversely, a small core SDD set is also available, MWB28, with 28 electrons in the effective core, which treats 4f electrons explicitly. The CEP-4G[13] set incorporates 42 electrons into the effective core, whilst treating the 4f electrons explicitly, representing a balance between accuracy and speed between the MWB28 and MWB51 basis sets, respectively. However, to minimise computational complexity, the MWB28 and CEP-4G sets are often avoided.

5.1.3. Complications in lanthanide calculations: paramagnetism.

Lanthanide based systems are frequently open shell, with large numbers of unpaired electrons - a direct consequence of the large number of lanthanide valence atomic orbitals that have similar energies. Subsequently, attempts to determine electron wavefunctions in organolanthanide compounds can be quite computationally demanding. This effect may be partly offset *via* the utilisation of a large core effective core potential, which incorporates the unpaired f-electrons into the effective core, at the cost of accuracy in the calculation.

5.1.4. Complications in lanthanide calculations: molecular size.

As discussed in Section 1.2, lanthanide metals generally require bulky ligands to facilitate the isolation of stable mononuclear compounds. However, historically the ligands involved in organolanthanide complexes are often simplified when modelled theoretically to also help minimise computational expense. Early examples of this simplification included the use of Cl ligands to substitute more complex monoanionic cyclopentadienyl ligands. These simplifications based purely on simplistic electronic considerations, however, are not ideal for the lanthanides, whose large coordination spheres are often experimentally satisfied with sterically demanding ligands. Studies of ligand simplification on methane methasis energy barriers have shown that significant energy changes are observed as ligand bulk and electron donating effects change from Cl to C_5Me_5 ligands.[9,14] With careful simplification of ancillary ligands coupled with the use of the previously described basis sets and methods, a number of organolanthanide systems have recently been studied.

5.1.5. Previous theoretical studies of lanthanide systems.

Theoretical studies into carbon-hydrogen bond activation and hydroamination have been successful in organolanthanide systems, and as such have received an intensive theoretical focus.[10] Of particular success has been the study of lanthanide mediated hydroamination which has resulted in the elucidation and refinement of the general catalytic mechanism.[15-17] Further to the thermodynamic studies of this nature, an understanding of organolanthanide bonding has been sought.

Probing the nature of lanthanide – ligand interactions has been a focus of computational studies. Typically this has involved a study of the ionic/covalent nature of lanthanide – ligand bonds and the role of the 4f lanthanide orbitals in bonding.[18]

In order to understand the chemistry of the lanthanide elements, the ionic or covalent nature of organolanthanide bonds has come under scrutiny.[19] The lanthanide 4f orbitals are contracted and are generally thought to have poor overlap with ligand orbitals. The lanthanides are also classified as 'hard acids' characterised by predominantly ionic bonding.[20] Often, atomic charges are considered the best measure of the ionic or covalent nature of lanthanide bonds. In a purely ionic bond, the charge on the constituent atoms is +1 and -1, whereas in a purely covalent bond the charge on each atom is 0.[21] A number of methods exist for determining the atomic charge within a molecule from DFT calculations. These include the classic Mulliken Population Analysis (MPA) atomic charge method, [22] the Natural Bond Order (NBO) method,[23] the Hirshfeld atoms in molecules analysis,[24] and the Voronoi Deformation Density (VDD).[25] Of these methods, the Mulliken definition of atomic charge is most widely recognised. However, in recent years this approach has been criticised for its treatment of complexes containing elements with diffuse basis sets.[21] Theoretical studies of covalency in organolanthanide systems have generally found that orbital overlap between the metal and ligand is restricted to the lanthanide 6s, 6p, and 5d orbitals and ligand s and p orbitals.[9,26,19,11,27-30] Included in studies of this nature are those of Gordon *et al.* who have reported the only theoretical studies of lanthanide imide systems to date.[29,30] To determine the bonding nature of the imide system in this case, the B3LYP functional was used and RECPs which incorporated the 4f orbitals in the effective core were utilised. This was based on the supported assumption that the lanthanide 4f orbitals are too contracted to participate in bonding,[27] as shown in the radial distribution of orbitals in Figure 5.1.

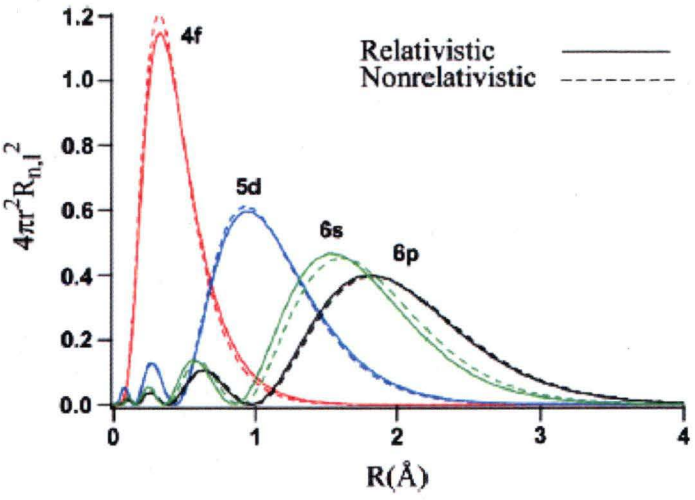

Figure 5.1. Radial contraction of the Lanthanide 4f orbitals.[30]

A Mulliken population analysis of the model imide [{(μ-PhN)Sm(μ-NH_2)(μ-Me)AlH_2}$_2$], (A), showed a significant 5d population of 1.28 electrons/metal, resulting from donation from the nitrogen ligands – both amide and imide. The frontier imide orbitals, consisting of the N $p\pi_\perp$ and N $p\pi_\parallel$ anilide orbitals were also analysed and found to exhibit between 3 and 8% 5d character.

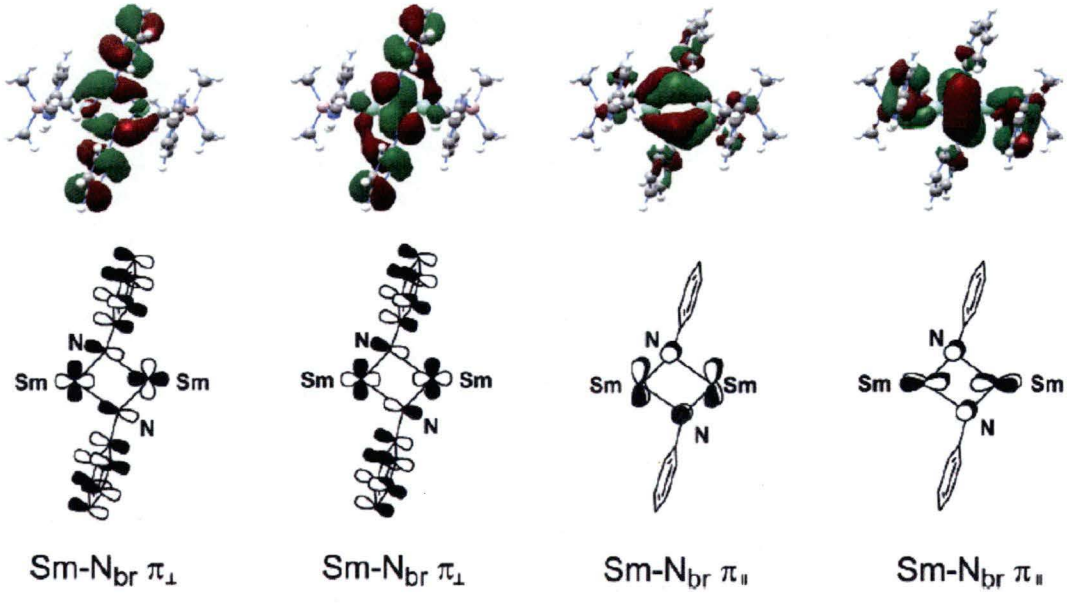

Figure 5.2. Frontier anilide orbitals exhibiting overlap with Sm 5d orbitals in [{(μ-PhN)Sm(μ-NH_2)(μ-Me)AlH_2}$_2$], (A).[30]

The four frontier anilide orbitals contributed almost half of the 1.28 electrons/metal occupying the Sm 5d orbitals. The charge on the Sm centre was also analysed using

both Mulliken and NBO methods, and was found to be 1.20 and 2.61, respectively. The discrepancy between Mulliken and NBO analyses is consistent with other studies of a similar nature, which have suggested that Mulliken analyses overestimate covalency, whilst NBO analyses underestimate covalent interactions.[31] The relative difference in derived NBO or Mulliken charges between molecules provides a more reliable estimate of covalency trends between ligand types.

Organolanthanide compounds are generally accepted to favour ionic bonding, which has been supported by theory in numerous cases.[32] Conversely, recent studies of samarium alkyl, $[Sm\{CH(SiMe_3)_2\}_3]$, (**B**), and amido, $[Sm\{N(SiMe_3)_2\}_3]$, (**C**), complexes have suggested that quite strong covalent interactions are possible for lanthanide compounds, with nuclear charges as low as 0.54 being observed.[33] To date there have been no theoretical studies of the interactions of porphyrinogens, or pyrrolide based ligands with lanthanide elements. Hence the covalent or ionic nature of porphyrinogen and pyrrolide bonding is yet to be determined.

As discussed previously and illustrated in Figure 5.1, the lanthanide 4f orbitals are considered to be too contracted to contribute to bonding. However, there exists both theoretical and experimental evidence to suggest that f orbitals can have a significant contribution in some covalent interactions.[34-36] The current literature debate on the participation or otherwise of lanthanide f orbitals in bonding, coupled with the importance in understanding the role of f orbitals in organolanthanide chemistry suggests that further studies of lanthanide f orbital contributions are required. Previous studies of f orbital interactions have been undertaken utilising small core and large core basis sets, treating f electrons explicitly (in the former case), and as part of the core electrons (in the latter case). In a systematic study of the two methods, lanthanide complexes of simple amide ligands with each lanthanide element were modelled and the electronic and geometric results from each method compared. Little change to either property was observed when the simplified large core system was utilised, highlighting the effectiveness of such a simplification which is far less computationally demanding.[9]

Subsequent reports of lanthanide DFT calculations have drawn on this result in order to apply large core methods to more complex systems, such as that of [{(μ-PhN)Sm(μ -NH_2)(μ-Me)AlH_2}$_2$], (**A**). Caution must be used in this approach, however, as any reaction which results in a change in the formal oxidation state of the lanthanide centre cannot be modelled by a single effective core potential.[9] Furthermore, in determining the bonding nature of novel ligand types such as imido or macrocyclic ligands to lanthanide centres, a thorough investigation open to f-orbital interactions is required.

Results and Discussion.

5.2. General comments on the theoretical method.

In parallel to the synthetic lanthanide imide investigations reported in Chapters 3 and 4, high level DFT calculations on model lanthanide imide complexes have been undertaken to probe the bonding interactions of importance in such complexes. Optimisations of the model systems were performed using the hybrid density functional theory method, UB3LYP.[5] The 28 electron basis set of Stuttgart and Dresden, MWB28,[12] and 42 electron set of Cundari and Stevens, CEP-4G,[13] were employed for the lanthanide centre, each employing a relativistic effective core potential for dealing with relativistic effects. Both basis sets also treat the f-electrons explicitly rather than incorporating them into the effective core. The 6-31G(d)[37] basis set was employed for the remaining elements. The metallated macrocyclic *meso*-octaethyl-*trans*-dioxaporphyrinogen ligand, (**1**), employed in the synthetic studies was modelled by the less computationally demanding *trans*-dioxaporphyrinogen ligand, (**D**), as shown in Figure 5.1.

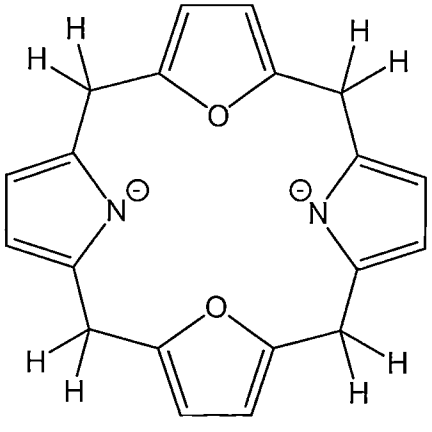

Figure 5.3. The *trans*-dioxaporphyinogen ligand ($H_8N_2O_2$), (**D**), utilised in the theoretical study.

In all cases, the optimised geometries were analysed by frequency calculations to ensure true minima in the potential surface had been identified. Stability calculations on the derived wavefunctions were also performed in order to prevent any confusion in the wavefunction resulting from the numerous lanthanide frontier orbitals of similar energy.

5.3. Geometry and basis set comparison of model macrocyclic amide and imide complexes.

5.3.1. Comparison of amide complexes.

The model lanthanide amide complex $[(H_8N_2O_2)SmN(H)CH_3]$, (**E**), was optimised at the UB3LYP/CEP-4G:6-31G(d) level of theory, whereby the CEP-4G basis set was employed for the samarium centre and the 6-31G(d) basis set was utilised for the remaining elements, giving the optimised geometry shown below in Figure 5.4.

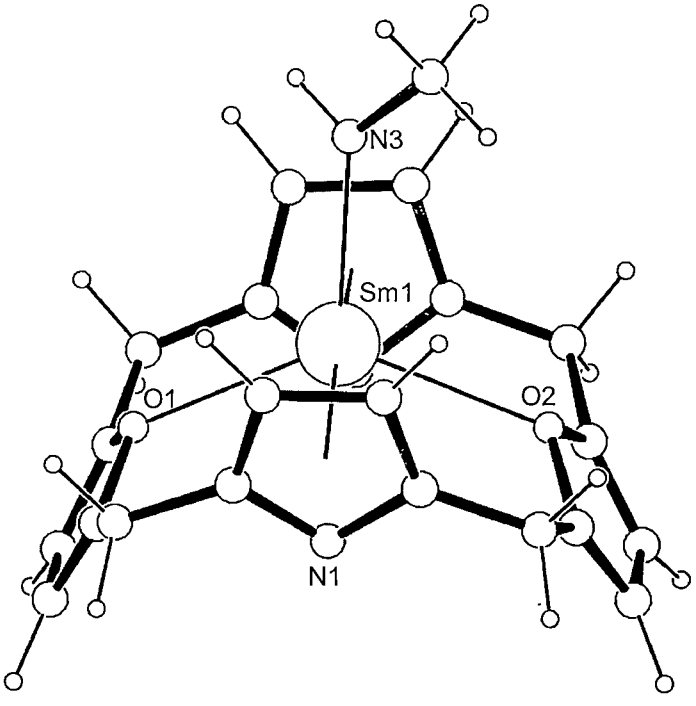

Figure 5.4. Optimised structure of the model macrocyclic mono(amide) complex $[(H_8N_2O_2)SmN(H)CH_3]$, (**E**).

The determined structure of the mono(amide), $[(H_8N_2O_2)SmN(H)CH_3]$, (**E**), utilising the CEP-4G basis set for the samarium centre exhibits reasonable qualitative

correlation with the analogous experimentally observed macrocyclic mono(amide), [($Et_8N_2O_2$)Sm{N(H)C_6H_2-2,4,6-*t*-Bu}], (**21**), with the η^5:η^1: η^5:η^1 samarium-macrocycle binding mode and 1,3-alternate macrocyclic conformation accurately reproduced. Quantitatively, the η^1 Sm–O(furanyl) macrocycle interactions measuring 2.67_5 and 2.67_4 Å for **E** are comparable to those of **21** of 2.660(4) and 2.697(4) Å (Sm–O), however the η^5 Sm–pyrrolide interactions measuring 2.67_1 and 2.64_3 Å for **E** are significantly longer than those for **21** of 2.55_8 and 2.51_1 Å. Similarly, the Sm-N(amide) interaction in **E** of 2.58_4 Å is substantially larger than that observed in **21** of 2.254(5) Å.

Given the large discrepancy between the Sm-N(amide) interactions of the model amide complex, [($H_8N_2O_2$)SmN(H)CH_3], (**E**) utilising the CEP-4g basis set, with the experimentally observed mono(amide), [($Et_8N_2O_2$)Sm{N(H)C_6H_2-2,4,6-*t*-Bu}], (**21**), the structure of **E** was re-optimised using the small core SDD basis set, MWB28, for the samarium centre in order to determine which method gave the most accurate representation of the experimental system.

The determined structure of [($H_8N_2O_2$)SmN(H)CH_3], (**E**), at the UB3LYP/MWB28:6-31G(d) level of theory exhibits the same global geometry to that determined at the UB3LYP/CEP-4G:6-31G(d) level, and shown in Figure 5.4, however the important lanthanide bond lengths of **E** at the MWB28 level exhibit far better correlation with the experimental structure of [($Et_8N_2O_2$)Sm{N(H)C_6H_2-2,4,6-*t*-Bu}], (**21**). The Sm–O(furanyl) interactions of **E** measure 2.66_8 and 2.67_3 Å, whilst the η^5 Sm–pyrrolide interactions measure 2.59_0 and 2.54_9 Å, which correlate well with those for **21** of 2.660(4) and 2.697(4) Å (Sm–O) and 2.55_8 and 2.51_1 Å (Sm–pyrrolide). The key Sm–N(amide) interaction in **E** of 2.22_3 Å also correlates well with that of **21** of 2.254(5) Å.

5.3.2. Comparison of imide complexes.

As for the determination of the geometry of the model amide complex, [($H_8N_2O_2$)SmN(H)CH_3], (**E**), the geometry of the corresponding macrocyclic imide, [K($H_8N_2O_2$)SmN(CH_3)], (**F**) resulting from α-deprotonation of amide **E** and subsequent incorporation of potassium in the macrocyclic cavity was determined at

the UB3LYP/CEP-4G:6-31G(d) and UB3LYP/MWB28:6-31G(d) levels of theory. The calculated geometry of **F** at the UB3LYP/CEP-4G:6-31G(d) level is shown in Figure 5.5.

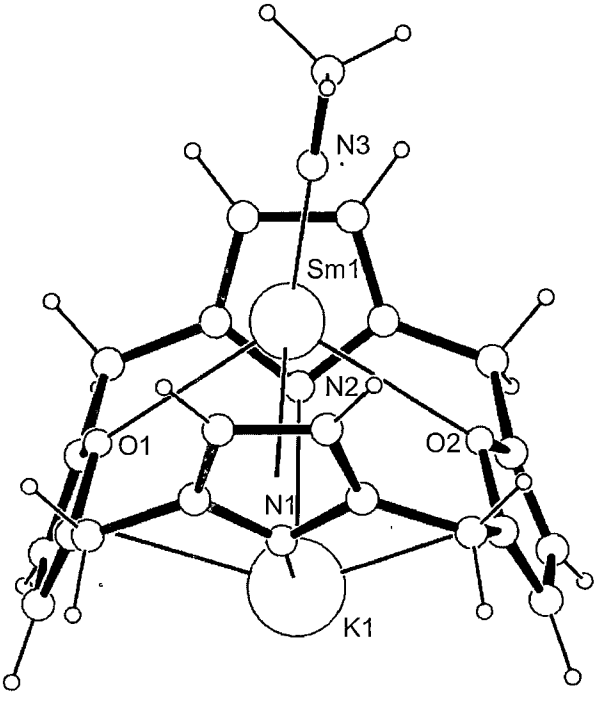

Figure 5.5. Optimised structure of the model macrocyclic lanthanide imide, $[K(H_8N_2O_2)SmN(CH_3)]$, (**F**).

The structure of $[K(H_8N_2O_2)SmN(CH_3)]$, (**F**), at the UB3LYP/CEP-4G:6-31G(d) level shows reasonable correlation with experimentally observed hetero-bimetallic lanthanide/Group 1 macrocycle systems utilising the *meso*-octaethyl-*trans*-dioxaporphyrinogen ligand. The Sm–O (furanyl) distances of 3.06_8, 3.00_0 Å (Sm–O) in the calculated structure are consistent with those of the hetero-bimetallic samarium(III) bis(amide) complex, $[\{\mu\text{-}\eta^1\text{:}\eta^3\text{-}(N(H)Mes)K(Et_8N_2O_2)SmN(H)Mes\}_n]$, (**18**), of 2.944(6) and 3.092(6) Å, however, as observed in the calculated amide structure at the CEP-4G level, the Sm–η^5(pyrrolide) interactions in the calculated model of 2.83_8 and 2.84_0 Å are substantially longer than those of the experimental bis(amide) system of 2.63_2 and 2.64_3 Å. The imide moiety in **F** exhibits a linear Sm-N-C arrangement, though the imide fragment is bent with respect to the C_2 axis of the macrocycle. The key Sm-N(imide) interaction in the CEP-4G structure of $[K(H_8N_2O_2)SmN(CH_3)]$, (F) of 2.290 Å is longer than the previously investigated

bridging imide [{(μ-PhN)Sm(μ-NH_2)(μ-Me)AlH_2}$_2$], (**A**), of 2.220 Å (calculated),[28] suggesting that the CEP-4G basis set does not adequately model the lanthanide–N interaction.

The structure of [K($H_8N_2O_2$)Sm$N(CH_3)$], (**F**) at the UB3LYP/MWB28:6-31G(d)level does, however, give a Sm-N(imide) bond length (2.00_4 Å) more consistent with that expected from the experimentally observed macrocyclic amide, and previously reported dimeric imide structures. The Sm–macrocycle interactions at the MWB28 level are also consistent with expected lengths, and consequently the MWB28 structure is considered to give a more reliable estimate of the bonding present within [K($H_8N_2O_2$)Sm$N(CH_3)$], (**F**). A comparison of the important bond lengths and angles for the amide and imide systems studied at the UB3LYP/CEP-4G:6-31G(d) and UB3LYP/MWB28:6-31G(d) levels is summarised in Table 5.1.

	Counter ion free			Counter ion containing		
Distance/ Angle Å/°	**E**		**21**	**F**		**18**
	CEP-4g	MWB28		CEP-4g	MWB28	
Sm-O(fur)	2.67_5, 2.67_4	2.66_8, 2.67_3	2.660(4), 2.697(4)	3.06_8, 3.00_0	3.07_0, 3.01_2	3.092(5), 2.944(5)
Sm-Ct(pyr)	2.67_1, 2.64_3	2.54_9, 2.59_0	2.55_8, 2.51_1	2.83_8, 2.84_0	2.75_9, 2.75_4	2.63_2, 2.64_3
Sm-N (amide/imide)	2.58_4	2.22_3	2.254(5)	2.29_0	2.00_4	2.292(2)
O-Sm-O	132.3_8	130.2_1	122.36(12)	110.1_6	110.9_3	106.2_1
Ct(pyr)-Sm-Ct(pyr)	167.9_5	167.2_5	163.2_4	153.2_7	154.0_9	140.2_4

Table 5.1. Comparison of geometries for the macrocyclic samarium amide and imide, [($H_8N_2O_2$)Sm$N(H)CH_3$], (**E**) and [K($H_8N_2O_2$)Sm$N(CH_3)$], (**F**) at the UB3LYP/CEP-4G:6-31G(d) and UB3LYP/MWB28:6-31G(d) levels of theory, with the experimental amides, [($Et_8N_2O_2$)Sm{N(H)C_6H_2-2,4,6-*t*-Bu}], (**21**) and [{μ-η^1:η^3-(N(H)Mes)K($Et_8N_2O_2$)Sm$N(H)$Mes}$_n$], (**18**).

5.4. Thermodynamic studies of macrocyclic amide and imide complexes.

5.4.1. Stability of bis(amide) macrocyclic complexes.

In order to rationalise the isolation of the experimentally observed bis(amide) complexes, $[(THF)_2K(Et_8N_2O_2)Sm\{N(H)Mes\}_2]$, (**17**), and $[\{\mu\text{-}\eta^1\text{:}\eta^3\text{-}(N(H)Mes)K(Et_8N_2O_2)SmN(H)Mes\}_n]$, (**18**), the model bis(amide) complex, $[K(H_8N_2O_2)Sm\{N(H)CH_3\}_2]$, (**G**), was optimised at the UB3LYP/CEP-4G:6-31G(d) level of theory, giving the geometry shown in Figure 5.6, and the corresponding energy compared to that of the target imide complex, $[K(H_8N_2O_2)SmN(CH_3)]$, (**F**). The UB3LYP/CEP-4G:6-31G(d) level of theory was utilised for the thermodynamic studies in place of the UB3LYP/MWB28:6-31G(d) level due to complications in modelling the larger molecules at the UB3LYP/MWB28:6-31G(d) level.

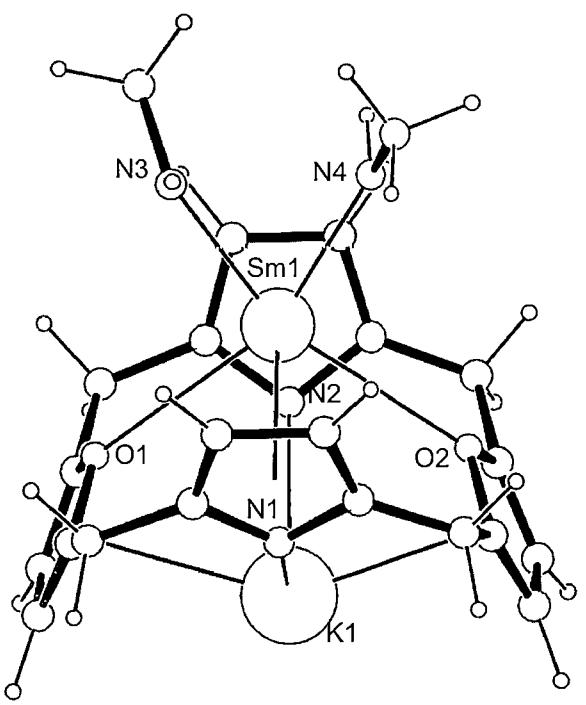

Figure 5.6. Optimised structure of the model macrocyclic lanthanide bis(amide) complex, $[K(H_8N_2O_2)Sm\{N(H)CH_3\}_2]$, (**G**).

The bis(amide) complex, $[K(H_8N_2O_2)Sm\{N(H)CH_3\}_2]$, (**G**) was found to be lower in energy than the imide/free amine system by 88 kJ/mol, at the UB3LYP/CEP-4G:6-31G(d) level of theory, suggesting that bis(amide) formation is favoured over imide

formation, as observed experimentally and described in Section 4.2.1, and shown below in Scheme 5.1.

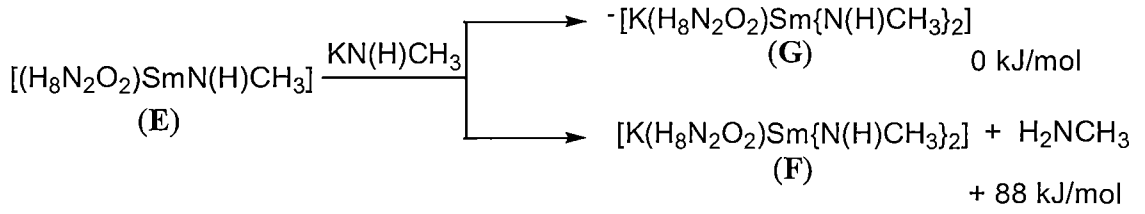

Scheme 5.1. Relative energies of bis(amide) and imide/free amine products from the reaction of the mono(amide) $[(H_8N_2O_2)SmN(H)CH_3]$, (**E**) with the Group 1 amide, $KN(H)CH_3$.

5.4.2. Stability of mixed alkyl/amide macrocyclic systems.

As for the bis(amide) energetic study, the mixed alkyl/amide model complex, $[K(H_8N_2O_2)Sm(CH_3)(N(H)CH_3)]$, (**H**) was optimised at the UB3LYP/CEP-4G:6-31G(d) level of theory, giving the structure shown in Figure 5.7. A comparison of the energy of **H** with that of the corresponding imide, $[K(H_8N_2O_2)SmN(CH_3)]$, (**F**) and free methane showed the imide/methane system to be 31 kJ/mol lower in energy than the corresponding alkyl/amide complex, $[K(H_8N_2O_2)Sm(CH_3)\{N(H)CH_3\}]$, (**H**), at the UB3LYP/CEP-4G:6-31G(d) level of theory, suggesting that the deprotonation of the mono(amide) species is favoured when Group 1 alkyl reagents are used, as shown in Scheme 5.2.

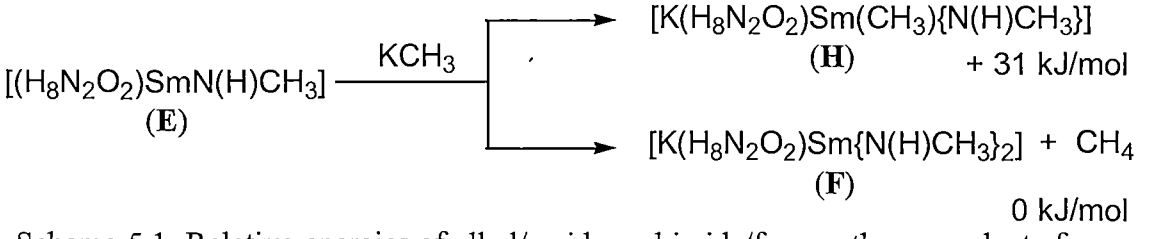

Scheme 5.1. Relative energies of alkyl/amide and imide/free methane products from the reaction of the mono(amide) $[(H_8N_2O_2)SmN(H)CH_3]$, (**E**) with the Group 1 alkyl, KCH_3.

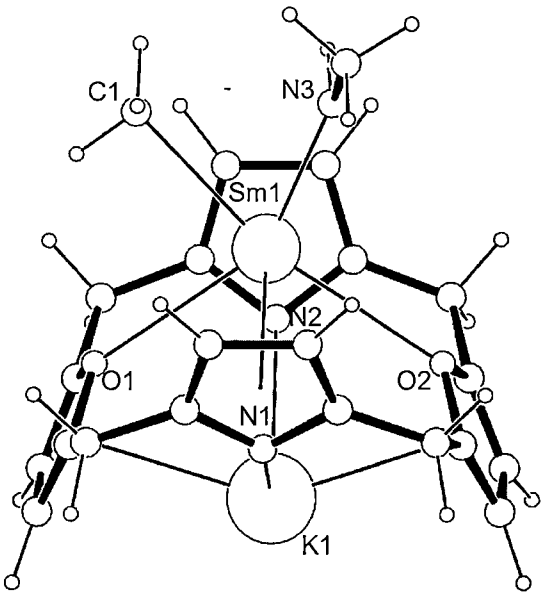

Figure 5.7. Optimised geometry of the macrocyclic alkylamide model, $[K(H_8N_2O_2)Sm(CH_3)\{N(H)CH_3\}]$, (**H**) at the UB3LYP/CEP-4G:6-31G(d) level of theory.

A summary of the determined thermodynamic preferences for imide formation is shown in Scheme 5.3. These results are consistent with the observed reactivity of the mono(amide) complex, $[(Et_8N_2O_2)SmN(H)Mes]$, (**20**), with [KN(H)Mes], (**19**), which gave the bis(amide) complex, $[(THF)_2K(Et_8N_2O_2)Sm\{N(H)Mes\}_2]$, (**17**), and is also consistent with previous postulated synthetic methods for imide formation described by Gordon.[27] These results also suggest that the reaction of the mono(amide) **20** with a Group 1 alkyl reagent favours imide formation, however, this was not observed synthetically, as discussed in Section 4.3.5.

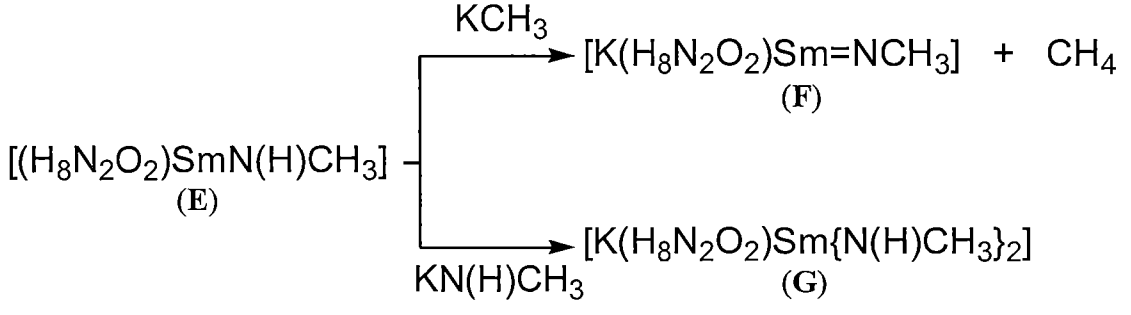

Scheme 5.3. Calculated reactivity preferences for the model macrocyclic lanthanide amide system.

5.5. Imide bond analysis.

5.5.1. Mulliken and Natural Bond Order charge analysis.

The covalent/ionic nature of the Ln-N bond in the macrocyclic lanthanide imide $[K(H_8N_2O_2)SmN(CH_3)]$, (**F**) was thoroughly investigated through analysis of the bonding orbitals, electron occupancies and atomic charges. The Mulliken Population Analysis (MPA)[22] was utilised to determine orbital occupancies within the imide complex, and was compared with the Natural Bond Order (NBO)[23] analysis also available within Gaussian. The occupancies and charges of imide **F** from both the UB3LYP/CEP-4G:6-31G(d) and UB3LYP/MWB28:6-31G(d) optimised structures were determined. The derived charges and occupancies are shown in Table 5.2. For a purely ionic samarium(III) complex, an f occupancy of 5.0 and d occupancy of 0.0 is expected. Electron density excess to these amounts suggests covalent interactions between the samarium centre and surrounding ligands.

	UB3LYP/CEP-4G:6-31G(d)		UB3LYP/MWB28:6-31G(d)	
	MPA	NBO	MPA	NBO
Sm Charge	1.05	1.43	0.68	1.24
N(imide) Charge	-0.57	-0.79	-0.44	-0.94
K Charge	0.53	0.81	0.55	0.83
Sm f occupancy	5.98	5.90	5.56	5.48
Sm d occupancy	0.64	0.40	1.28	0.97

Table 5:2. Atomic charges and orbital occupancies for the model imide, $[K(H_8N_2O_2)SmN(CH_3)]$, (**F**).

From the results of the single point calculations shown in Table 5.2., several comparisons to previously reported lanthanide DFT systems can be made. For both levels of theory, the derived atomic charges are much smaller for the MPA procedure than for the NBO analysis, consistent with previous studies which have suggested that MPA over-estimates covalency in organometallic complexes, whereas the NBO procedure is said to underestimate covalency. Despite the derived NBO charges (1.43 and 1.24 for the CEP-4G and MWB28 calculations, respectively) for the samarium centres being higher than the MPA results (1.05 and 0.68 respectively), they are significantly lower than those reported by Gordon for the model imide, $[\{(\mu\text{-}PhN)Sm(\mu\text{-}NH_2)(\mu\text{-}Me)AlH_2\}_2]$, (**A**) of 2.61. This suggests that the model

macrocyclic imide, $[K(H_8N_2O_2)SmN(CH_3)]$, (**F**) exhibits stronger covalent interactions between the samarium centre and the surrounding ligand environment than that of **A**, but does not represent the most covalent interactions for lanthanide systems reported to-date whereby a charge of 0.54 has been reported in the Mulliken analysis of $[Sm\{CH(SiMe_3)_2\}_3]$, (**B**).[26] As discussed in Section 5.1, previous studies of organolanthanide complexes have highlighted the contracted nature of lanthanide f orbitals and subsequent lack of participation in bonding. In contrast, the macrocyclic lanthanide imide system studied utilising the CEP-4G basis set exhibits significant f-orbital occupancy of the order of 1 extra electron/samarium in both the MPA and NBO analyses, whilst the MWB28 system exhibits f orbital occupancy of approximately 0.5 extra electrons/samarium, suggesting that despite the contracted nature of the f-orbitals, some overlap with the orbitals of the surrounding ligand environment exists. The importance of d-electron acceptance by the lanthanide metal in order to stabilise the imido nitrogen centre has been highlighted in the study of imide **A** where a Mulliken derived 5d electron occupancy of 1.28 electrons/Sm centre was observed. Similarly, a d-type Mulliken electron occupancy of 1.28 electrons is observed for the UB3LYP/MWB28:6-31G(d) system, whilst the NBO calculation also reveals a d-type occupancy of 0.97 electrons. The UB3LYP/CEP-4G:6-31G(d) system exhibits much lower d-type occupancy, partially offset by the higher f-type occupancy to give a similar overall samarium charge to the UB3LYP/MWB28:6-31G(d) system.

The previously reported study of $[\{(\mu\text{-PhN})Sm(\mu\text{-}NH_2)(\mu\text{-Me})AlH_2\}_2]$, (**A**), also proposed delocalisation from the aromatic system of the anilide ring through the imide atom and onto the lanthanide centre. In order to understand the importance of this effect in the macrocyclic imide system reported here, the electron occupancies of the methyl imide, $[K(H_8N_2O_2)SmN(CH_3)]$, (**F**) were compared with those of the corresponding phenyl imide, $[K(H_8N_2O_2)SmN(C_6H_5)]$, (**I**), optimised at the UB3LYP/CEP-4G:6-31G(d) level, and shown in Figure 5.8. The derived electron occupancies are shown in Table 5.3. In this instance, little change to either the d orbital or f orbital occupancies, or the charge of the lanthanide metal were observed, suggesting that delocalisation of the aromatic ring of the imide species is not a significant effect in the macrocyclic system. Furthermore, a slight lengthening of the imide bond from 2.29_0 Å, in the methyl case, to 2.31_0 Å, in the phenyl case, was

observed. Since the substitution of the methyl imide **F** by the phenyl imide **I** at the UB3LYP/CEP-4G:6-31G(d) level did not significantly change the important occupancies and charges within the molecule, the analogous comparison using the more computationally expensive UB3LYP/MWB28:6-31G(d) level of theory was not pursued.

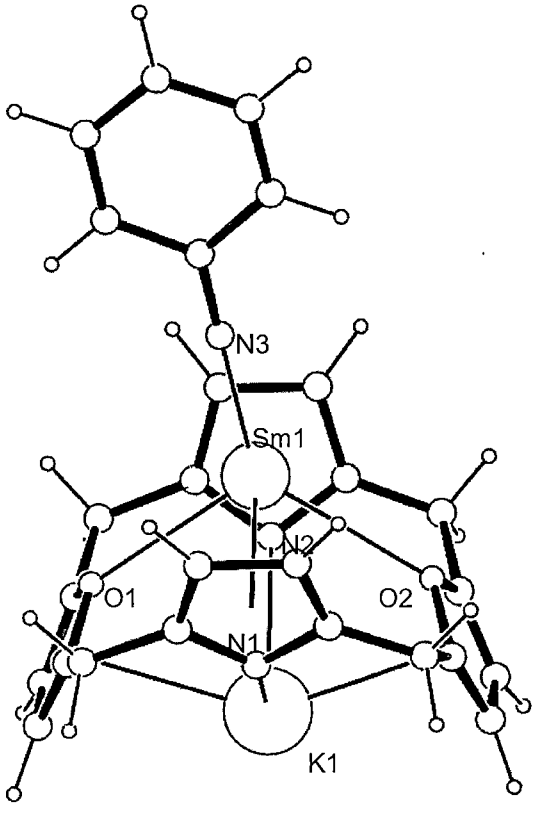

Figure 5.8. Optimised geometry of the model macrocyclic lanthanide imide, $[K(H_8N_2O_2)SmN(C_6H_5)]$, (**I**) at the UB3LYP/CEP-4G:6-31G(d) level of theory.

	UB3LYP/CEP-4G:6-31G(d)	
	$[K(H_8N_2O_2)SmN(C_6H_5)]$, (**I**)	$[K(H_8N_2O_2)SmN(CH_3)]$, (**F**)
Sm Charge	1.06	1.05
N(imide) Charge	-0.68	-0.57
K Charge	0.53	0.53
Sm f occupancy	5.97	5.98
Sm d occupancy	0.59	0.64

Table 5.3. Comparison of MPA populations and charges for the model macrocyclic imides, $[K(H_8N_2O_2)SmN(C_6H_5)]$, (**I**) and $[K(H_8N_2O_2)SmN(CH_3)]$, (**F**).

The low charge on the lanthanide centre, which implies a strong covalent interaction between the lanthanide centre and the surrounding ligands, was further investigated using the Hirschfeld charge analysis procedure.[22] As discussed in Section 5.1, the MPA procedure exhibits a strong basis set dependency and, as such, the reliability of organometallic charge analyses utilising the MPA have been questioned. In order to validate the observed MPA charges, a single point calculation of the optimised UB3LYP/CEP-4G:6-31G(d) geometry of [K($H_8N_2O_2$)SmN(CH_3)], (**F**) was attempted within the ADF package (Relativistic ZORA, TZ2P Basis, 0 electron core) and a Hirshfeld analysis was undertaken. The resulting charge on the lanthanide centre was calculated to be substantially lower than that obtained by the Mulliken analysis, with a samarium charge of 0.05. Such a small charge on the samarium centre suggests that the Hirshfeld procedure is not suited for calculating the lanthanide charge in this case, and suggests that the MPA and NBO methods were more reliable.

5.5.2. Molecular Orbital analysis.

The bonding within [K($H_8N_2O_2$)SmN(CH_3)], (**F**) was investigated *via* analysis of the molecular orbitals present within the complex, from both the UB3LYP/CEP-4G:6-31G(d) and UB3LYP/MWB28:6-31G(d) derived structures. Several occupied orbitals exhibit overlap between the lanthanide centre and both the macrocyclic and imide ligands, resulting in the observed low charge on the lanthanide centre.

5.5.2.1. [K($H_8N_2O_2$)SmN(CH_3)], (F) UB3LYP/CEP-4G:6-31G(d) orbital analysis.

The UB3LYP/CEP-4G:6-31G(d) derived molecular orbitals of [K($H_8N_2O_2$)SmN(CH_3)], (**F**) exhibit significant overlap between the macrocyclic ligand and samarium centre. The HOMO-6 and HOMO-7 (shown in Figure 5.9) represent overlap between the lanthanide f orbitals and the aromatic π electrons of the pyrrolide rings within the macrocyclic ligand. Each of these molecular orbitals exhibit modest f-character (12.6 and 12.3 %, respectively), but contribute 25 % of the excess f-electron density to the samarium centre, and contribute to the relatively high f electron count in the MPA. The observation of f orbital overlap between the samarium centre and macrocyclic ligand is not consistent with much of the previous studies of organolanthanide systems that have deemed the f orbitals to be too

contracted to participate in bonding. However, these results add to the growing body of analyses that suggest that f orbital interactions are important in understanding subtleties in lanthanide bonding.[34-36] Furthermore, it is not surprising that bonding interactions are observed between the f orbitals and the macrocyclic ligand, whose pyrrolide π orbitals possess the correct symmetry to interact with the lanthanide f orbitals.

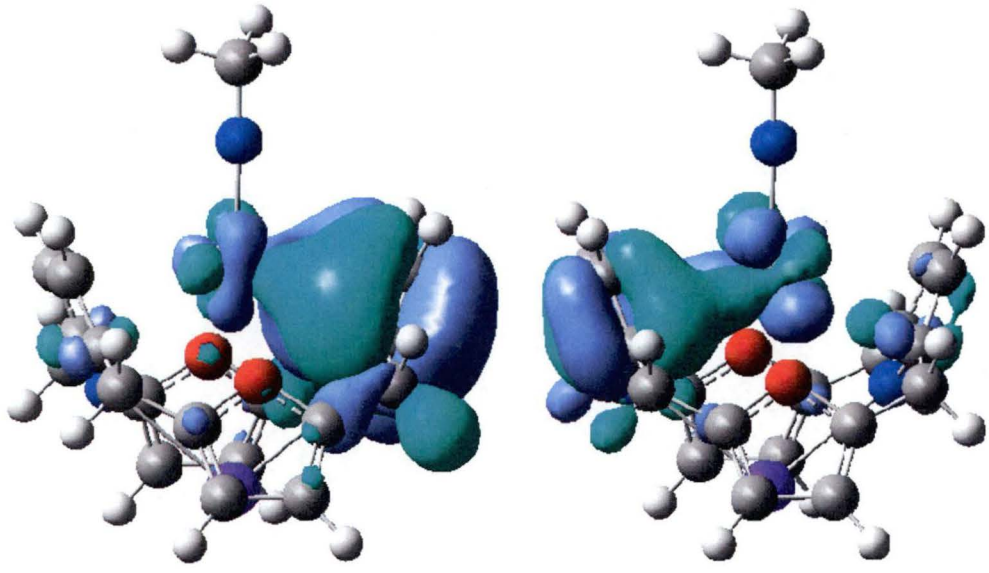

Figure 5.9. HOMO-6(Left) and HOMO-7(Right) of $[K(H_8N_2O_2)SmN(CH_3)]$, (F), at the UB3LYP/CEP-4G:6-31G(d) level, demonstrating f-type overlap between the samarium centre and the η^5-bound pyrrolides of the macrocyclic ligand.

The lanthanide imide model complex also exhibits atomic orbital overlap between the 5d orbitals of the samarium centre and the imide ligand, consistent with previous studies. The ability of the lanthanide centre to accept electron density from the imide ligand has been identified as an important factor in the isolation of lanthanide imide species. In this instance, a total of 0.15 electrons are accepted by the lanthanide d_{xz} and d_{yz} orbitals, which exhibit overlap with the imide ligand, as shown in Figure 5.10. This d- type overlap is significantly less than that observed in the case of $[\{(\mu\text{-PhN})Sm(\mu\text{-}NH_2)(\mu\text{-Me})AlH_2\}_2]$, (**A**), which exhibited a total of 0.54 d-type electrons per samarium atom from imide overlap, but represents 25 % of the total d occupancy of $[K(H_8N_2O_2)SmN(CH_3)]$, (**F**), at the UB3LYP/CEP-4G:6-31G(d) level. The lower d-type occupancy observed for **F** at the UB3LYP/CEP-4G:6-31G(d) level may result from the lower charge on the samarium centre due to acceptance of electron density

from the macrocyclic ligand (into the lanthanide f-orbitals). Consequently, d orbital overlap between the samarium centre and imide ligand is compromised by the lower charge on the samarium centre, which may also account for the long samarium-imide bond length observed for **F** at the UB3LYP/CEP-4G:6-31G(d) level.

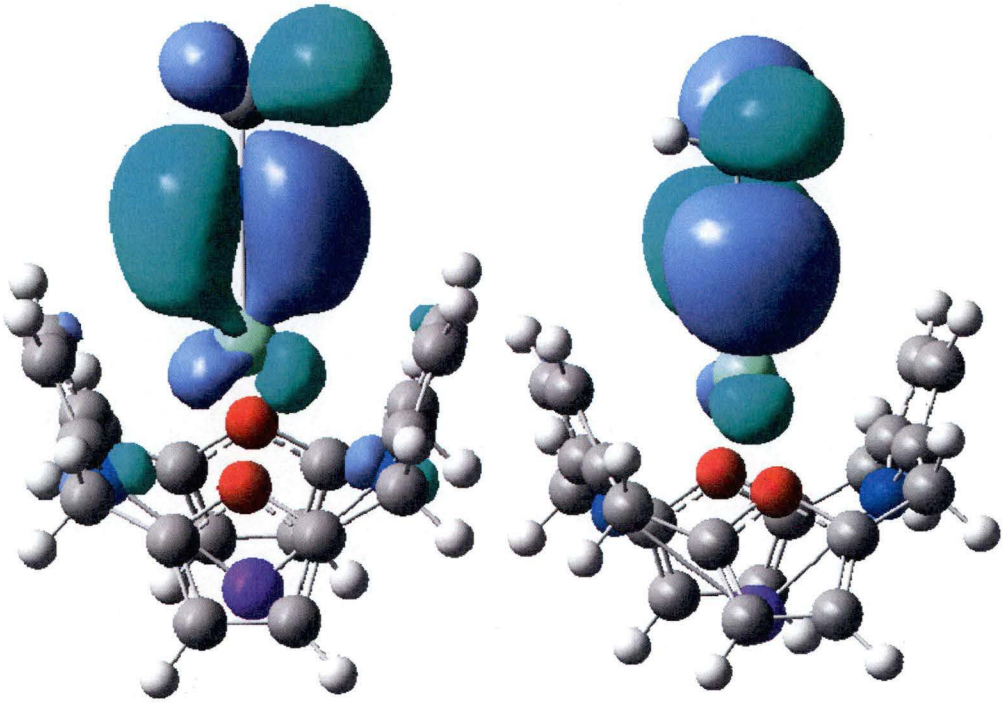

Figure 5.10. α-HOMO(Left) and β-HOMO-1(Right) of [K($H_8N_2O_2$)SmN(CH_3)], (**F**), at the UB3LYP/CEP-4G:6-31G(d) level, demonstrating d-type overlap between the samarium centre and imide ligand.

5.5.2.2. [K($H_8N_2O_2$)SmN(CH_3)], (F) UB3LYP/MWB28:6-31G(d) orbital analysis. A study of the key frontier orbitals of [K($H_8N_2O_2$)SmN(CH_3)], (**F**) at the UB3LYP/MWB28:6-31G(d) level of theory reveals significant overlap between the samarium d and f-orbitals and imide p-orbitals, accounting for much of the d and f orbital occupancy in the MPA analysis. Key orbitals are shown in Figures 5.11. and 5.12. The HOMO exhibits significant overlap between an f-type samarium orbital and p type imide nitrogen orbital, and accounts for 80 % of the 0.56 excess f-type electrons on the samarium centre. The d-type electron occupancy of the samarium centre is shared across a number of molecular orbitals, however the HOMO-1, and HOMO-15 contribute approximately 50 % of the 1.28 d-type electrons, *via* overlap with the p orbital and sp^2 hybrid orbital of the imide nitrogen centre, with the samarium d_{xy} and d_{z2} orbitals respectively. Orbital overlap between the macrocyclic

ligand and the samarium centre is considerably smaller in magnitude than that observed for the imide ligand, with 10 % of the total d-electron density residing in one bonding interaction between the pyrrolide π-cloud and lanthanide d_{xy} orbital, as shown in Figure 5.13. The modest covalent interactions between the samarium centre and macrocyclic ligand at the UB3LYP/MWB28:6-31G(d) level of theory suggests that the macrocycle-samarium interaction in $[K(H_8N_2O_2)SmN(CH_3)]$, (**F**) is predominantly ionic. No Sm-O(furanyl) interactions were observed for **F** at either the UB3LYP/CEP-4G:6-31G(d) or UB3LYP/MWB28:6-31G(d) level of theory, consistent with the long (> 3.0 Å) Sm-O contacts in the derived structures.

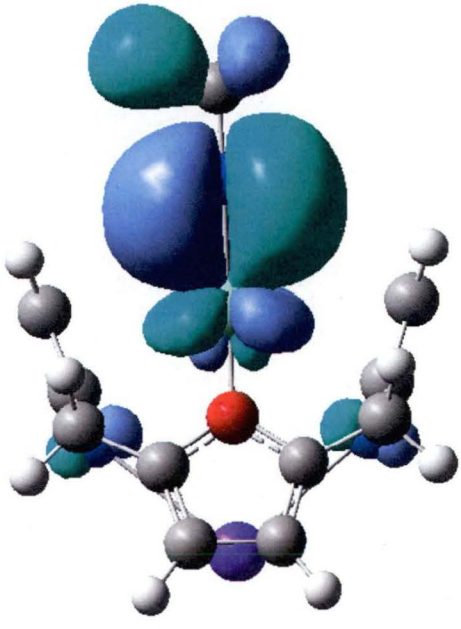

Figure 5.11. HOMO of $[K(H_8N_2O_2)SmN(CH_3)]$, (**F**) at the UB3LYP/MWB28:6-31G(d) level of theory, demonstrating f-type overlap with the imide p orbitals.

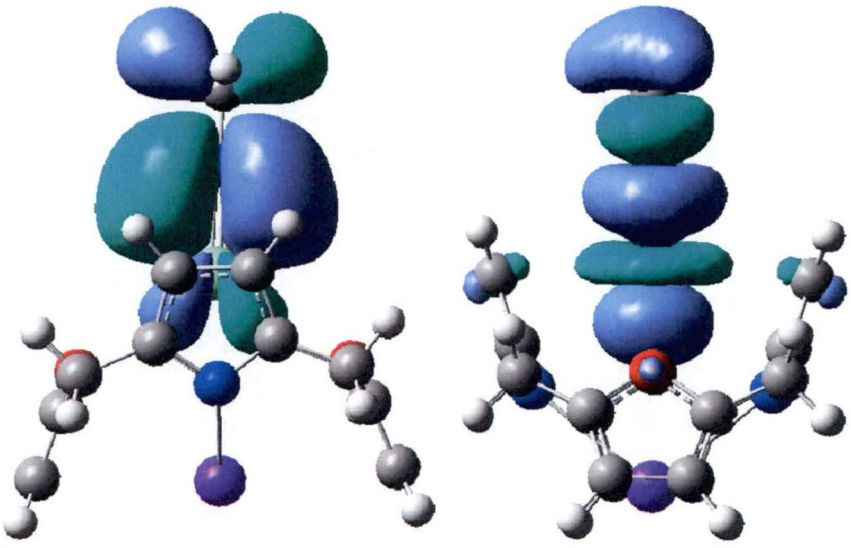

Figure 5.12. HOMO-1(Left) and HOMO-15(Right) of $[K(H_8N_2O_2)SmN(CH_3)]$, (**F**) at the UB3LYP/MWB28:6-31G(d) level of theory, demonstrating d-type overlap with the imide p orbitals.

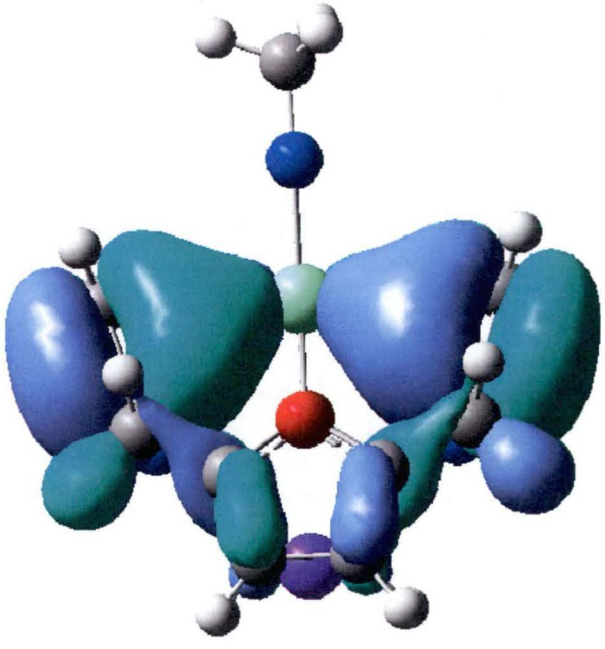

Figure 5.13. HOMO-3(β spin) of $[K(H_8N_2O_2)SmN(CH_3)]$, (**F**) at the UB3LYP/MWB28:6-31G(d) level of theory, demonstrating d-type overlap between the samarium centre and macrocycle.

5.5.3. Comparison of Amide and Imide bonding.

As discussed in Section 5.5.2, significant overlap between the samarium d and f orbitals and the imide nitrogen centre is observed in the analysis of $[K(H_8N_2O_2)SmN(CH_3)]$, (**F**) at both the UB3LYP/CEP-4G:6-31G(d) and UB3LYP/MWB28:6-31G(d) levels of theory. In order to understand the importance of these interactions in stabilising a lanthanide imide complex, the derived orbital occupancies, atomic charges and bond energies of **F** at the UB3LYP/MWB28:6-31G(d) level was compared with that of the model amide, $[(H_8N_2O_2)SmN(H)(CH_3)]$, (**E**). A comparison of the calculated occupancies and charges is summarised in Table 5.4.

	$[(H_8N_2O_2)SmN(H)(CH_3)]$, (E)		$[K(H_8N_2O_2)SmN(CH_3)]$, (F)	
	MPA	NBO	MPA	NBO
Sm charge	0.91	1.32	0.68	1.24
N(a/imide) Charge	-0.40	-0.98	-0.44	-0.94
Sm f occupancy	5.34	5.24	5.56	5.48
Sm d occupancy	1.13	0.98	1.28	0.97

Table 5.4. Comparison of orbital occupancies and atomic charges for the model amide and imide, $[(H_8N_2O_2)SmN(H)(CH_3)]$, (E) and $[K(H_8N_2O_2)SmN(CH_3)]$, (F) at the UB3LYP/MWB28:6-31G(d) level of theory.

From Table 5.4, little change to the charge of the samarium centre is evident between the amide and imide complexes. Similar d-electron occupancies are also observed, with a slight increase in the f-electron density of the imide complex. This suggests that the bonding interactions between the samarium centre and nitrogen centre do not change considerably upon deprotonation of the amide to give the imide complex, which contains a formally dianionic nitrogen centre. The charges of the nitrogen atoms in the amide and imide complexes are also comparable, however, suggesting that electron donation from the imide nitrogen centre to the samarium centre is more prominent than electron donation from the amido nitrogen centre. Inspection of the

bonding molecular orbitals of $[(H_8N_2O_2)SmN(H)(CH_3)]$, (**E**), and MPA populations reveals significant overlap between the samarium d_{xy} and d_{xz}-orbitals with the pyrrolide rings of the macrocyclic ligand, accounting for 40 % of the 1.13 d-electrons as shown in Figure 5.14, whilst only minor overlap between the amide nitrogen centre and samarium d-orbitals is observed. This suggests that in the amide case, significant covalent interactions between the macrocycle and samarium centre exist *via* electron donation from the pyrrolide anions to the samarium d-orbitals. Conversely, the formally dianionic imido nitrogen centre in $[K(H_8N_2O_2)SmN(CH_3)]$, (**F**) out competes the macrocyclic pyrrolide orbitals in donating electron density to the samarium centre, contributing 50 % of the 1.28 d electrons, and the samarium pyrrolide interactions are weakened, contributing only 10 % of the d-electron density.

The NBO analysis of both complexes also demonstrates the differing macrocycle and amide/imide bonding modes. An estimation of the key bonding interactions within a molecule is provided by the NBO package, and a comparison of the relative energies of these interactions reveals further insight into the samarium-nitrogen bonding mode. $[K(H_8N_2O_2)SmN(CH_3)]$, (**F**) possesses two formal nitrogen-samarium bonds in the NBO analysis, providing a stabilisation energy of the order of 700 kJ/mol, resulting predominantly from overlap of the nitrogen based p-orbitals, and samarium based d orbitals. In contrast, $[(H_8N_2O_2)SmN(H)(CH_3)]$, (**E**) exhibits only 1 bonding interaction, which contributes 500 kJ/mol to the stability of the complex. Together, the electron occupancy and NBO analyses of amide **E** and imide **F** suggest that significant covalent interactions are required in stabilising the imide Sm-N bond, and is consistent with the Sm-N(imide) interaction having double bond character.

The second order perturbation theory analysis from the NBO calculations, which gives an estimate of the importance of non-bonding donor-acceptor interactions within a molecule, demonstrates the altered macrocycle bonding between the two complexes. Whilst no formal NBO bonds between the macrocycle and samarium centre are observed in either molecule, the donor-acceptor macrocycle-samarium interactions in $[(H_8N_2O_2)SmN(H)(CH_3)]$, (**E**) are of the order of 2.5 times greater than those in $[K(H_8N_2O_2)SmN(CH_3)]$, (**F**), consistent with the observed d-electron occupancies of the two complexes.

The differing macrocycle-samarium bonding interactions may be related to the samarium-pyrrolide bond lengths for the two model complexes as shown in Table 5.1, whereby the samarium pyrrolide interactions for $[(H_8N_2O_2)SmN(H)(CH_3)]$, (**E**) of 2.54_9 and 2.59_0 Å are significantly shorter than those in $[K(H_8N_2O_2)SmN(CH_3)]$, (**F**) of 2.75_9 and 2.75_4 Å.

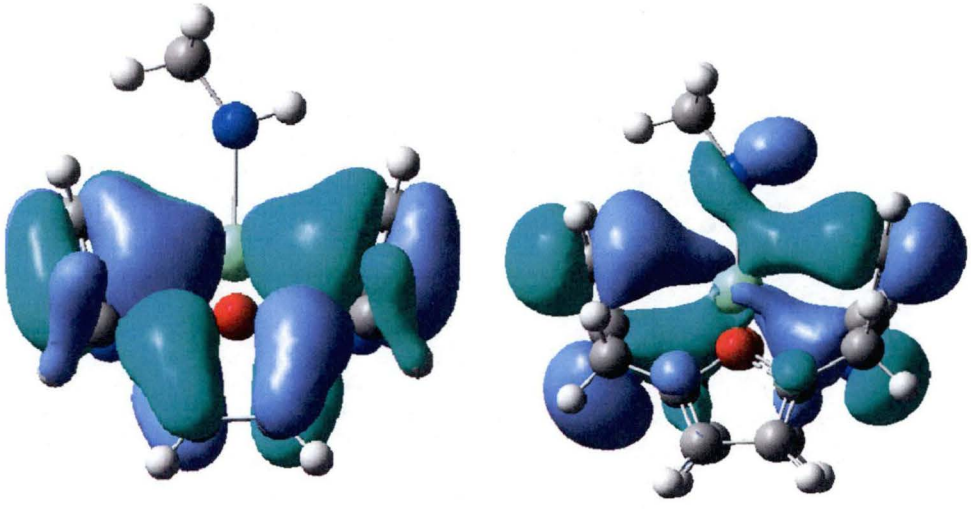

Figure 5.14. HOMO-5(Left) and HOMO-6(Right) of $[(H_8N_2O_2)SmN(H)(CH_3)]$, (**E**) at the UB3LYP/MWB28:6-31G(d) level of theory, demonstrating d-type overlap between the samarium centre and macrocycle.

5.5.4. Summary of theoretical findings.

The structural analysis of the model amides and imides utilising the CEP-4G and MWB28 basis sets and corresponding effective core potentials for the samarium centre have shown both systems to correlate well with experiment. The experimentally observed 1,3-alternate macrocyclic conformation and $\eta^5:\eta^1:\eta^5:\eta^1$ bonding mode was reproduced using both basis sets. Comparison of the derived model amides and imides with the experimentally observed amides, $[(Et_8N_2O_2)Sm\{N(H)C_6H_2\text{-}2,4,6\text{-}t\text{-}Bu\}]$, (**21**), and $[\{\text{-}\mu\text{-}\eta^1:\eta^3\text{-}(N(H)Mes)K(Et_8N_2O_2)SmN(H)Mes\}_n]$, (**18**), suggest that the MWB28 basis set more accurately describes the bonding between the samarium centre and both the macrocycle and amide/imide, with the CEP-4G significantly underestimating the bonding between the samarium centre and the macrocyclic pyrrolides and amido/imido nitrogen moieties.

The thermodynamic studies of the amide/imide system also correlate well with the observed experimental results, correctly predicting the favoured bis(amide) formation observed experimentally. The intramolecular α-deprotonation of the mono(amide) complex by a samarium alkyl species was shown to be favourable, as predicted previously.[27]

From the electronic analysis of the macrocyclic amide and imide systems discussed in Section 5.5, the role of the f-orbitals in bonding appears to be somewhat dependent on the basis set chosen, with the CEP-4G basis set exhibiting significant f-orbital interactions, whilst the f-orbital interactions observed in the SDD derived model complexes are significantly smaller. The poor agreement of the CEP-4G model complexes with experiment however suggests that the CEP-4G description may not be accurate, and the role of f-orbitals may be less important, as shown for the SDD systems. Covalent interactions between the imide ligand and samarium centre have been shown to be important in stabilising the imide complex, resulting predominantly from electron donation from the imide nitrogen centre to the lanthanide d-orbitals, consistent with previous studies. However, these interactions result in the weakening of the covalent samarium pyrrolide interactions, such that the binding of the macrocycle to the lanthanide centre in the imide complex may be considered to be predominantly ionic, whereas the amide complex may be considered to exhibit more covalent macrocycle-samarium interactions. The observed weakening of the macrocycle-samarium interactions resulting from imide formation provides some insight into the isolation of $[(Et_8N_2O_2)K_2(C_6H_5Me)_2]$, (**5**) from the reaction of $[\{(THF)_2K(Et_8N_2O_2)Sm(\mu\text{-}I)\}_2]$, (**6**) with mesityl azide, as discussed in Section 3.3.1.

5.6. References

1. Almlöf, J.; Gropen, O. in *Revs. Comp. Chem.* Lipkowitz, K.B.; Boyd, D.B. **1996**, *8*, 203.
2. Desclaux, J.P. *Comput. Phys. Commun.* **1975**, *9*, 31.
3. a) te Velde, G.; Bickelhaupt, F.M.; van Gisbergen, S.J.A.; Guerra, C.F.; Baerends, E.J.; Snijders, J.G.; Ziegler, T. *J. Comput. Chem.* **2001**, *22*, 931,
   b) Guerra, C.F.; Snijders, J.G.; te Velde, G.; Baerends, E.J. *Theor. Chem. Acc.* **1998**, *99*, 391,
   c) ADF2007.01, SCM, Theoretical Chemistry, Vrije Universiteit, Amsterdam, The Netherlands, http://www.scm.com.
4. Gaussian 03, Revision E.01, Frisch, M. J.; Trucks, G. W.; Schlegel, H. B.; Scuseria, G. E.; Robb, M. A.; Cheeseman, J. R.; Montgomery, Jr., J. A.; Vreven, T.; Kudin, K. N.; Burant, J. C.; Millam, J. M.; Iyengar, S. S.; Tomasi, J.; Barone, V.; Mennucci, B.; Cossi, M.; Scalmani, G.; Rega, N.; Petersson, G. A.; Nakatsuji, H.; Hada, M.; Ehara, M.; Toyota, K.; Fukuda, R.; Hasegawa, J.; Ishida, M.; Nakajima, T.; Honda, Y.; Kitao, O.; Nakai, H.; Klene, M.; Li, X.; Knox, J. E.; Hratchian, H. P.; Cross, J. B.; Bakken, V.; Adamo, C.; Jaramillo, J.; Gomperts, R.; Stratmann, R. E.; Yazyev, O.; Austin, A. J.; Cammi, R.; Pomelli, C.; Ochterski, J. W.; Ayala, P. Y.; Morokuma, K.; Voth, G. A.; Salvador, P.; Dannenberg, J. J.; Zakrzewski, V. G.; Dapprich, S.; Daniels, A. D.; Strain, M. C.; Farkas, O.; Malick, D. K.; Rabuck, A. D.; Raghavachari, K.; Foresman, J. B.; Ortiz, J. V.; Cui, Q.; Baboul, A. G.; Clifford, S.; Cioslowski, J.; Stefanov, B. B.; Liu, G.; Liashenko, A.; Piskorz, P.; Komaromi, I.; Martin, R. L.; Fox, D. J.; Keith, T.; Al-Laham, M. A.; Peng, C. Y.; Nanayakkara, A.; Challacombe, M.; Gill, P. M. W.; Johnson, B.; Chen, W.; Wong, M. W.; Gonzalez, C.; and Pople, J. A.; Gaussian, Inc., Wallingford CT, **2004**.
5. a) Becke, A.D. *J. Chem. Phys* **1988**, *38*, 3098,
   b) Lee, C.; Yang, W.; Parr, R.G. *Phys. Rev. B.* **1988**, *37*, 785.
6. a) Becke, A.D.; *J. Chem. Phys.* **1993**, *98*, 5648,
   b) Perdew, J.P.; Chevary, J.A.; Vosko, S.H.; Jackson, K.A.; Pederson, M.R.; Singh, D.J.; Fiolhais, C.
   Phys. Rev. B: Condens. Matter Mater. Phys. **1992**, *46*, 6671.

7. Adamo, C.; Maldivi, P. *J. Phys. Chem.y A* **1998,** *102*, 6812.
8. Adamo, C.; Barone, V. *J. Comput. Chem.* **2000,** *21*, 1153.
9. Eisenstein, O.; Maron, L. *J. Organomet. Chem.* **2002,** *647*, 190.
10. Hunt, P. A. *Dalton Transactions* **2007,** *18*, 1743.
11. Maron, L.; Eisenstein, O. *J. Phys. Chem. A* **2000,** *104*, 7140.
12. a) Dolg, M.; Stoll, H.; Savin, A.; Preuss, H. *Theor. Chim. Acta* **1989**, *75*, 173,
b) Dolg, M.; Fulde, P.; Kuechle, W.; Neumann, C.-S.; Stoll, H.
J.Chem. Phys. **1991**, *94*, 3011,
c) Dolg, M.; Stoll, H.; Preuss, H. *Theor. Chim. Acta* **1993**, *85*, 441.
13. a) Stevens, W.; Basch, H.; Krauss, J. *J. Chem. Phys.* **1984**, *81*, 6026,
b) Stevens, W.J.; Krauss, M.; Basch, H.; Jasien, P.G.
Can. J. Chem. **1992**, *70*, 612,
c) Cundari, T.R.; Stevens, W.J. *J. Chem. Phys.* **1993**, *98*, 5555.
14. Sherer, E. C.; Cramer, C. J. *Organometallics* **2003,** *22*, 1682.
15. Motta, A.; Lanza, G.; Fragala, I. L.; Marks, T. J.
Organometallics **2004,** *23*, 4097.
16. Tobisch, S. *J. Am. Chem. Soc.* **2005,** *127*, 11979.
17. Tobisch, S. *Chem. - Eur. J.* **2005,** *11*, 6372.
18. Luo, Y.; Parasuraman, S.; Koyama, M.; Momoji, K.; Miyamoto, A.
Chem. Lett. **2004,** *33*, 780.
19. Luo, Y.; Selvam, P.; Ito, Y.; Endou, A.; Kubo, M.; Miyamoto, A.
J. Organomet. Chem. **2003,** *679*, 84.
20. Anwander, R. *Topics in Organometallic Chemistry 2 (Lanthanides)*
1999, 1-61.
21. Guerra, C. F.; Handgraaf, J.-W.; Baerends, E. J.; Bickelhaupt, F. M.
J. Comput. Chem. **2003,** *25*, 189.
22. Mulliken, R. S. *J. Chem. Phys.* **1955,** *23*, 1841.
23. a) Carpenter J.E.; Weinhold, F. *J. Mol. Struct. (Theochem)* **1988**, *169*, 41,
b) Foster, J.P.; Weinhold, F. *J. Am. Chem. Soc.* **1980**, *102*, 7211,
c) Reed, A.E.; Weinhold, F. *J. Chem. Phys.* **1983**, *78*, 4066,
d) Reed, A.E.; Weinstock, R.B.; Weinhold, F. *J. Chem. Phys.* **1985**, *83*, 735.
24. Hirshfeld, F. L. *Theor. Chim. Acta* **1977**, *44*, 129.
25. Guerra, C.F.; Handgraaf, J.W.; Baerends, E.J.; Bickelhaupt, F.M.
J. Comput. Chem. **2003**, *25*, 189.

26. Evans, W. J.; Champagne, T. M.; Ziller, J. W.; Kaltsoyannis, N. *J. Am.Chem. Soc.* **2006,** *128*, 16178.
27. Perrin, L.; Maron, L.; Eisenstein, O. *Faraday Discuss.* **2003,** *124*, 25.
28. Clark, D. L.; Gordon, J. C.; Hay, P. J.; Martin, R. L.; Poli, R. *Organometallics* **2002,** *21*, 5000.
29. Giesbrecht, G. R.; Gordon, J. C. *Dalton Trans.* **2004**, 2387.
30. Gordon, J. C.; Giesbrecht, G. R.; Clark, D. L.; Hay, P. J.; Keogh, D. W.; Poli, R.; Scott, B. L.; Watkin, J. G. *Organometallics* **2002,** *21*, 4726.
31. Brady, E.D.; Clark, D.L.; Gordon, J.C.; Hay, P.J.; Keogh, D.W.;Poli, R.; Scott, B.L.; Watkin, J.G. *Inorg. Chem.* **2003**, *42*, 6682.
32. Perrin, L.; Maron, L.; Eisenstein, O.; Lappert, M.F. *New J. Chem.* **2003**, *27*, 121.
33. Brady, E.D.; Clark, D.L.; Gordon, J.C.; Hay, P.J.; Keogh, D.W.; Poli, R.; Scott, B.L.; Watkin, J.G. *Inorg. Chem.* **2003**, 42, 6682.
34. Anderson, D. M.; Cloke, F. G. N.; Cox, P. A.; Edelstein, N.; Green, J. C.; Pang, T.; Sameh, A. A.; Shalimoff, G. *J. Chem. Soc., Chem. Commun.* **1989**, 53.
35. Depaoli, G.; Russo, U.; Valle, G.; Grandjean, F.; Williams, A. F.; Long, G. J. *J. Am. Chem. Soc.* **1994,** *116*, 5999.
36. Schinzel, S.; Bindl, M.; Visseaux, M.; Chermette, H. *J. Phys. Chem. A* **2006,** *110*, 11324.
37. Rassolov, V.A.; Ratner, M.A.; Pople, J.A.; Redfren, P.C.; Curtiss, L.A. *J. Comp. Chem.* **2001**, *22*, 976.

Chapter 6. Studies of lanthanide alkene interactions.

6.1. Introduction to lanthanide alkenyl complexes

6.1.1. Overview of lanthanide alkene chemistry.

Alkene lanthanide complexes have become established as one of the most important classes of lanthanide compounds, arising from the importance of alkene insertion into Ln-C, Ln-H and Ln-N bonds in catalytic and stoichiometric reactions of the lanthanides.[1] Studies into insertions of this type have yielded numerous catalytic processes, and proven the lanthanide elements to be effective alkene polymerisation catalysts.[2] Consequently, lanthanide alkene polymerisation studies have received tremendous attention in recent times as applications of the unique lanthanide reactivity, which does not suffer from the orbital symmetry constraints that restrict the transition metals, have been sought.

Despite the numerous reports of catalytic processes involving alkene substrates and lanthanide catalysts, very few structural investigations probing the important alkene-metal interaction have been reported. Presumably this is a result of the mis-match of the hard Lewis acidic metal with the soft Lewis basic alkene, compounded by the inability of lanthanide elements to back-donate *d*-electron density to the π^* orbitals of the alkene. [1] Typically, Lewis base solvents are also required, which out compete alkene binding due to these reasons.

6.1.2. Lanthanide-alkene complexes.

The first lanthanide complex of an η^2- bound alkene to be crystallographically authenticated was reported in 1987 by Andersen and Burns.[3] The reaction of [$(C_5Me_5)_2Yb$], (**CLXX**) with the platinum alkene complex $[Pt(\eta^2\text{-}C_2H_4)(PPh_3)_2]$, (**CLXXI**), gave the bimetallic ytterbium(II) adduct $[(C_5Me_5)_2Yb(\mu\text{-}\eta^2\text{:}\eta^2\text{-}C_2H_4)Pt(PPh_3)_2]$, (**CLXXII**), which exhibited a bridging interaction between the alkene ligand and the two metal centres, as shown in Figure 6.1. In this instance, the Lewis basicity of the alkene ligand was increased *via* π donation from the Pt(0) species to the alkene, which allowed the isolation of the complex. Despite the increased basicity of the alkene in this instance, solution state NMR spectroscopic studies of the complex in

toluene-D_8 suggested a dynamic equilibrium of the bimetallic complex with the starting reagents at temperatures as low as –70 °C. In addition, the crystallographically derived alkenyl C–C bond length of 1.436(5) Å did not differ from that observed for [Pt(η^2-C_2H_4)(PPh_3)$_2$], (**CLXXI**) at 1.43(1) Å, also suggesting a weak alkenyl-lanthanide interaction. Consistent with this, the Yb-C(alkenyl) bond lengths were long at 2.770(3) and 2.793(3) Å.

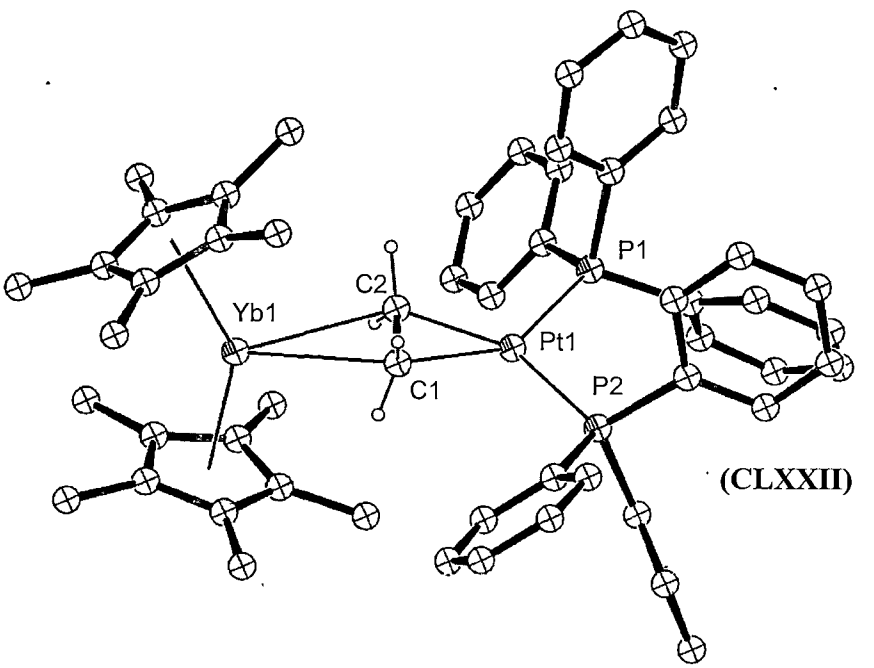

(CLXXII)

Figure 6.1. Molecular structure of [(C_5Me_5)$_2$Yb(μ-η^2:η^2-C_2H_4)Pt(PPh_3)$_2$] (**CLXXII**). Figure generated from CCDC obtained coordinates. Atoms of arbitrary size. Non-alkenyl H atoms are omitted for clarity.

Following the isolation of [(C_5Me_5)$_2$Yb(μ-η^2:η^2-C_2H_4)Pt(PPh_3)$_2$], (**CLXXII**), few reports of coordinated neutral alkene ligands were made for some time. Thermochemical studies of alkene addition reactions have been reported, yielding quantitative data on olefin insertion processes.[4] Studies of alkene complexes of the Group 3 lanthanide analogue complex [{(C_5Me_5)$_2$YH}$_2$], (**CLXXIII**), yielded the first d^0 transition metal mixed alkenyl alkyl complex to be characterised spectroscopically, [(C_5Me_5)$_2$Y$CH_2CH_2C(CH_3)_2CH_2CH$=CH_2], (**CLXXIV**). ^{1}H NMR studies of the complex suggested alkene coordination *via* differences between the chemical shifts of

the alkenyl proton resonances in the alkene reagent and the resulting complex, though this was unable to be crystallographically verified.[5]

The reaction of $[(C_5Me_5)_2Sm]$, (**XI**) with styrene yielded the two electron reduced alkene complex, $[\{(C_5Me_5)_2Sm\}_2(\mu\text{-}\eta^2\text{: }\eta^4\text{-}CH_2CHPh)]$, (**CLXXV**), whereby the alkene ligand bridged each samarium(III) centre in an η^2- fashion, with additional coordination from the *ipso* and *ortho* carbon atoms to one of the samarium centres, as shown in Figure 6.2. **CLXXV** exhibited significant lengthening of the alkene bond arising from strong electron donation from the oxidised Sm(III) centres. Addition of THF to **CLXXV** resulted in the complex decomposing to give $[Sm(C_5Me_5)_2(THF)_2]$, (**XXIV**) and $PhCH{=}CH_2$, which suggests that despite the alkene reduction to give **CLXXV**, only a weak bonding interaction resulted.[6]

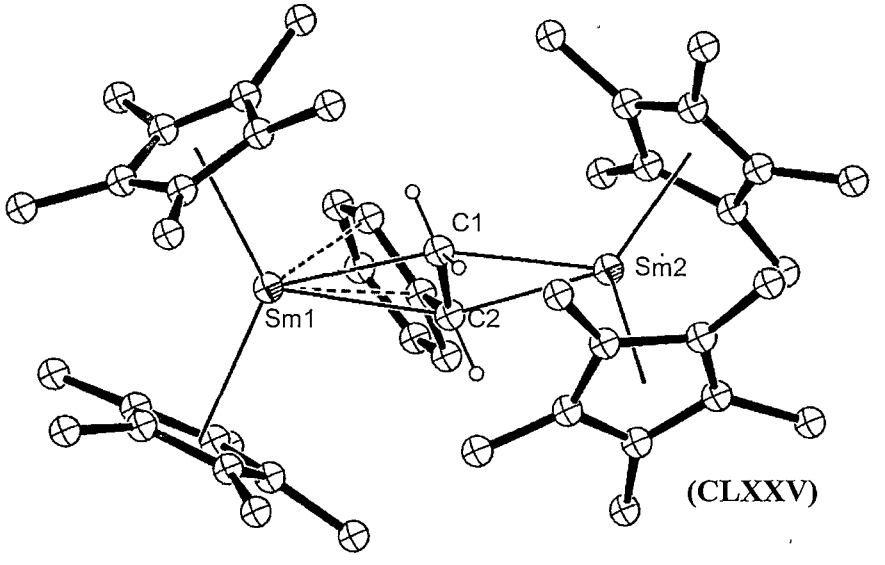

Figure 6.2. Molecular structure of $[\{(C_5Me_5)_2Sm\}_2(\mu\text{-}\eta^2\text{:}\eta^4\text{-}CH_2CHPh)]$, (**CLXXV**). Figure generated from CCDC obtained coordinates. Atoms of arbitrary size. Non-alkenyl H atoms are omitted for clarity

Following the isolation of $[\{(C_5Me_5)_2Sm\}_2(\mu\text{-}\eta^2\text{: }\eta^4\text{-}CH_2CHPh)]$, (**CLXXV**), by Evans in 1990, little progress in probing lanthanide alkene interactions was made for some time. In 1999, the reaction of ethylene with Pr and Nd complexes of the metallated *meso*-octaethylporphyrinogen, in the presence of reducing alkali metals, led to the

isolation of the dianionic reduced ethylene complexes, $[\{(\eta^5{:}\eta^1{:}\eta^5{:}\eta^1\text{-}(Et_8N_4)M\}_2(\mu\text{-}\eta^2{:}\eta^2\text{-}C_2H_4)\{Na(THF)_2\}_2]^{2-}$, M = Nd (**CLXXVI**), Pr (**CLXXVII**), which were balanced by two ligated alkali cations, $[\{Na(THF)(18\text{-crown-}6)\}2(\mu\text{-dioxane})]^{2+}$. The Nd complex, (**CLXXVI**), shown in Figure 6.3. was crystallographically authenticated and found to have a long C–C (ethylene) bond distance of 1.49(2) Å, consistent with the ethylene ligand having been reduced to a 1,2-dimetallated ethane moiety.[7] Thd Nd–C(alkenyl) contacts of 2.497(7) and 2.790(7) Å suggested a $\mu\text{-}\eta^2{:}\eta^2$ bonding motif was present. The inequivalent Nd-C(alkenyl) contacts and skewed ethylene H positions show a strong tendency towards δ M-C bonding.

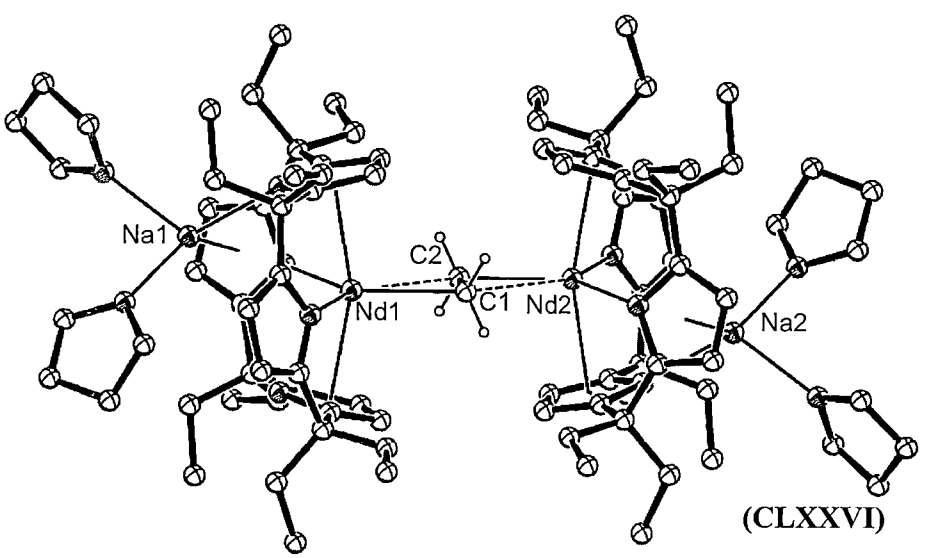

Figure 6.3. Molecular structure of $[\{(\eta^5{:}\eta^1{:}\eta^5{:}\eta^1\text{-}(Et_8N_4)Nd\}_2(\mu\text{-}\eta^2{:}\eta^2\text{-}C_2H_4)\{Na(THF)_2\}_2]^{2-}$ (**CLXXVI**). Figure generated from CCDC obtained coordinates. Atoms of arbitrary size. The $[\{Na(THF)(18\text{-crown-}6)\}_2(\mu\text{-dioxane})]^{2+}$ counterion and non-alkenyl H atoms are omitted for clarity.

Also in 1999, Nd, (**CLXXVIII**) and Gd, (**CLXXIX**) hydroxide/chloride complexes featuring the alkene pendant cyclopentadienyl ligand, $C_5H_4C(CH_3)(C_3H_7)CH_2CH{=}CH_2$, (**CLXXX**), were reported. However, the pendant alkene group did not coordinate to the lanthanide centres.[8] The Nd complex, shown in Figure 6.4, exhibited η^5- bonding to the cyclopentadienyl ligand and retained THF solvated Mg cations and both hydroxide and chloride anions.

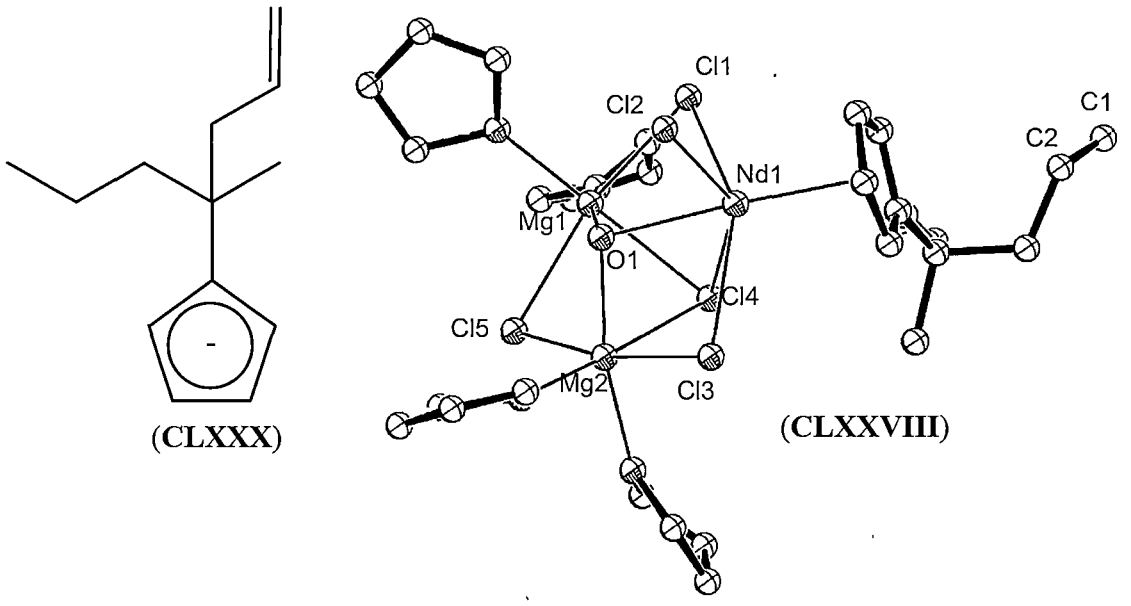

Figure 6.4. Representation of the pendant alkene cyclopentadienyl ligand, (**CLXXX**) (left) used to synthesise the pendant alkenyl cyclopentadienyl Nd oxide [{$C_5H_4C(CH_3)(C_3H_7)CH_2CH{=}CH_2$}Nd(OH)Cl·2$MgCl_2$·4THF], (**CLXXVIII**) (right). Figure generated from CCDC obtained coordinates. Atoms of arbitrary size with alkenyl carbons numbered. H atoms are omitted for clarity.

Following the report of the alkene pendant complexes, **CLXXVIII**, **CLXXIX** and **CLXXX**, Schumann reported the synthesis of a series of lanthanide and alkaline earth complexes bearing related alkene pendant functional groups attached to the ubiquitous cyclopentadienyl ligand.[9] In each case, a tetramethylcyclopentadienyl ligand was substituted with an alkyl chain bearing a pendant alkene group, with variable chain length and alkene substitution in order to promote interactions between the alkene and the metal centres, as shown in Figure 6.5. Despite the variation in chain length, as well as lanthanide size, nō alkenyl-lanthanide interactions were observed, with the lanthanide centres preferentially being stabilised by the formation of alkali metal halide adducts, coordination of additional Lewis basic solvents, or dimerisation.[9a,b] In contrast, alkene binding to alkaline earth metals was observed.[9c]

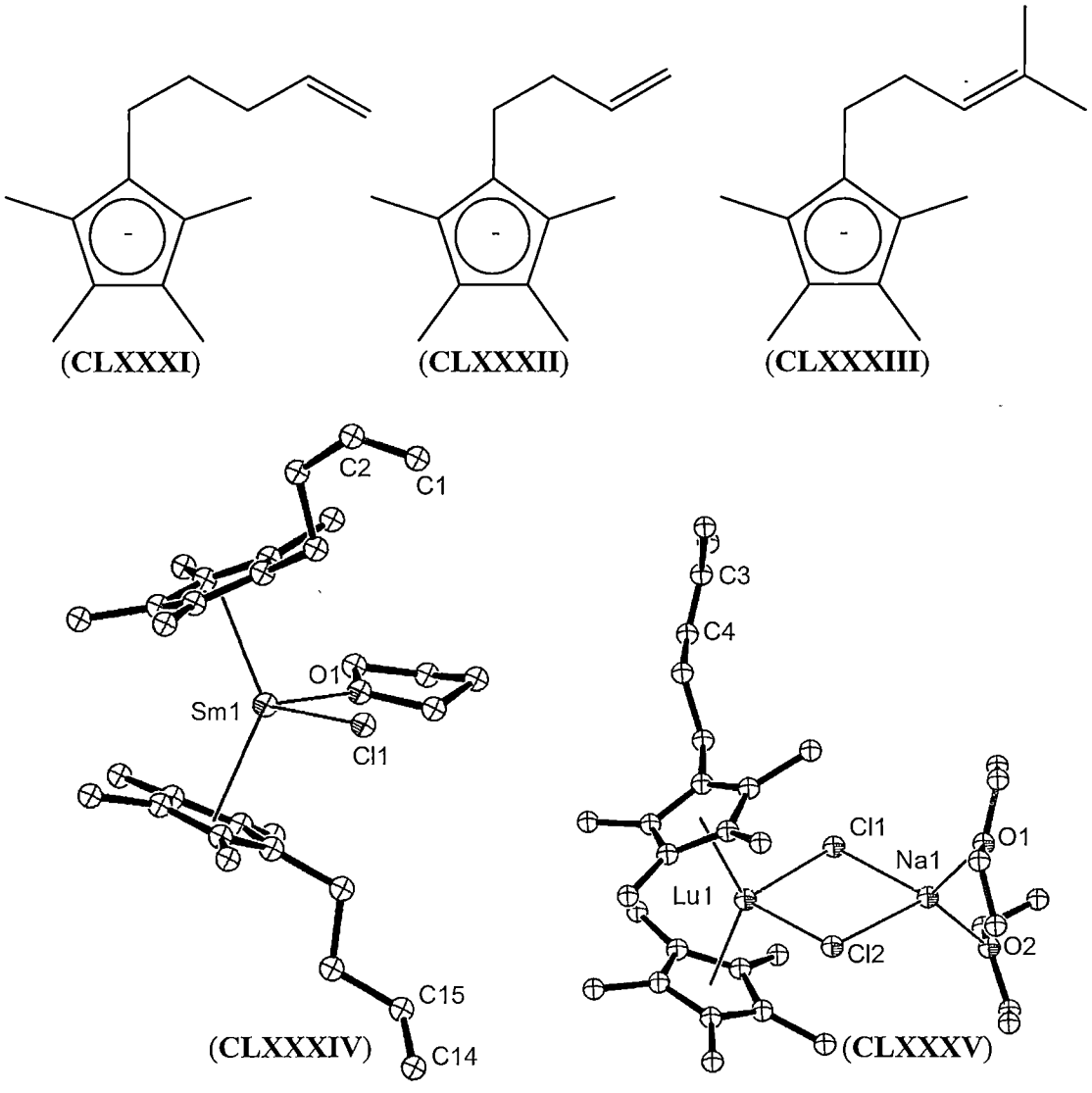

Figure 6.5. Alkene substituted cyclopentadientyl ligands (**CLXXXI** - **CLXXXIII**) used in lanthanide complexation studies (top), and derived Sm, (**CLXXXIV**) (left), and Lu, (**CLXXXV**) (Right), complexes. Figure generated from CCDC obtained coordinates. Atoms of arbitrary size with alkenyl carbons numbered. H atoms are omitted for clarity.

Following the work of Schumann, Evans reported the synthesis of the Sm, (**CLXXXVI**), Eu, (**CLXXXVII**) and Yb, (**CLXXXVIII**) complexes $[\{(C_5Me_4)Si(Me)_2CH_2CH{=}CH_2\}_2Ln]$, also featuring a pendant alkenyl cyclopentadienyl ligand. In these cases, interactions between the lanthanide centres and the pendant alkene groups were observed, as shown for the samarium case in Figure 6.6. Whilst the

binding of the alkene group to the Eu and Yb centres had little effect on the alkene bond length, which measured 1.328(4) and 1.328(5) Å, respectively. The reaction of the Sm complex with $[Ag(BPh_4)]$ to yield the cationic samarium complex, $[\{(C_5Me_4)SiMe_2(CH_2CH{=}CH_2)\}_2Sm][BPh_4]$, (**CLXXXIX**), retained pendant alkene interactions, indicating that olefin complexation was favoured over the binding of $[BPh_4]^-$. Accurate C–C bond lengths for the Sm case were not determined due to large thermal ellipsoids for the alkenyl C atoms. The M–C contacts to the terminal alkenyl C atoms which ranged from 2.905(3) to 3.008(3) Å were shorter than those to the internal C atoms of 3.182(3) to 3.249(4) Å, though these were significantly longer than those observed in $[(C_5Me_5)_2Yb(\mu\text{-}\eta^2{:}\eta^2\text{-}C_2H_4)Pt(PPh_3)_2]$, (**CLXXII**). $[\{(C_5Me_4)SiMe_2(CH_2CH{=}CH_2)\}_2Sm]$, (**CLXXXVI**), also reductively coupled CO_2 to form an oxalate bridged dimeric species, which displaced the pendant alkene groups.[10]

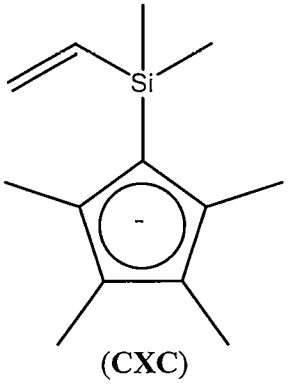

(**CXC**)

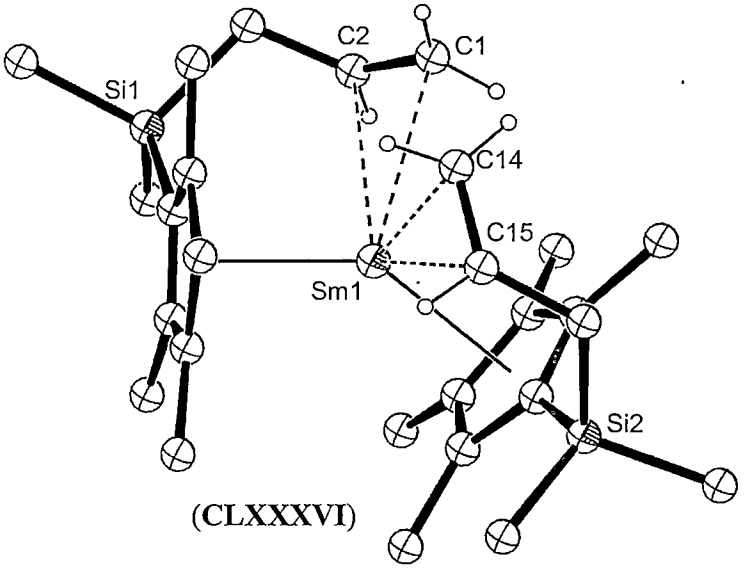

(**CLXXXVI**)

Figure 6.6. Alkene substituted cyclopentadienyl ligand (left), succesful in alkene coordination to samarium (right) $[\{(C_5Me_4)SiMe_2(CH_2CH{=}CH_2)\}_2Sm]$, (**CLXXXVI**). Figure generated from CCDC obtained coordinates. Atoms of arbitrary size with alkenyl carbons numbered. Non-alkenyl H atoms are omitted for clarity.

Recently, Schumann has also reported the synthesis of a tethered alkene cyclopentadienyl compound in which the pendant alkene group interacted with a Yb(II) centre in [{(C_5Me_4)$CH_2CH_2CH{=}CH_2$}$_2$Yb], (**CXCI**), shown in Figure 6.7. In this instance, the C–C (alkene) distances of 1.317(9) and 1.353(8) Å were similar to those of [{(C_5Me_4)Si(Me)$_2CH_2CH{=}CH_2$}$_2$Yb], (**CLXXXVIII**), of 1.328(5) Å. The Yb–C contacts which range from 2.850-3.132 Å were similar to those in **CLXXXVIII** of 2.905-3.182 Å.[11] [($C_5Me_4CH_2CH_2CH{=}CH_2$)$_2$Yb], (**CXCI**), was crystallised from hexane, similar to the crystallisation method of **CLXXXVI**, **CLXXXVII** and **CLXXXVIII**, preventing the competitive binding of Lewis basic solvents to the lanthanide centre as observed for the samarium and lutetium complexes of the same ligand prepared previously.[9a,b]

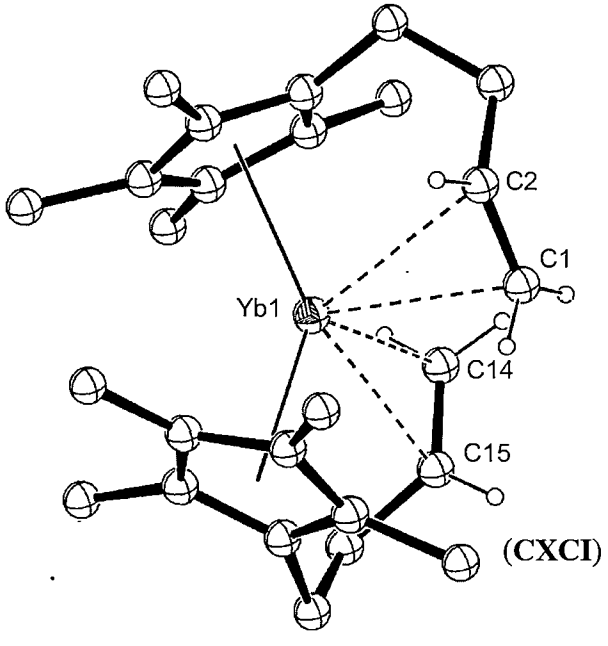

Figure 6.7. Tethered alkene ytterbium complex, [{(C_5Me_4)$CH_2CH_2CH{=}CH_2$}$_2$Yb], (**CXCI**). Figure generated from CCDC obtained coordinates. Atoms of arbitrary size with alkenyl carbons numbered. Non-alkenyl H atoms are omitted for clarity.

The limited number of coordinated neutral alkene complexes of the lanthanides reported to date have primarily relied upon the tethering of an alkene group to substituted cyclopentadienyl ligands in order to promote an alkene-lanthanide interaction. Whilst

these complexes have given some insight into the nature of alkene-lanthanide interactions, the number and type of alkene-lanthanide complexes reported to date require further expansion in order to understand the unique alkene reactivity trends observed with the lanthanide elements. For this to be achieved, it appears that ligand design is of upmost importance. Chelating effects which promote alkene interactions are desirable, whilst the traditional steric and electronic requirements of the lanthanide metal must also be satisfied.

6.2. Strategic alkene functionalised ligand design: tropylidene pendant ligands.

The 5H-dibenzo[a,d]cycloheptene molecule, also known as dibenzotropylidene (tropH), (**CXCII**), was first reported in 1951 from the reduction of dibenzo[a,e]cycloheptatrienone (dibenzosuberenone).[12]

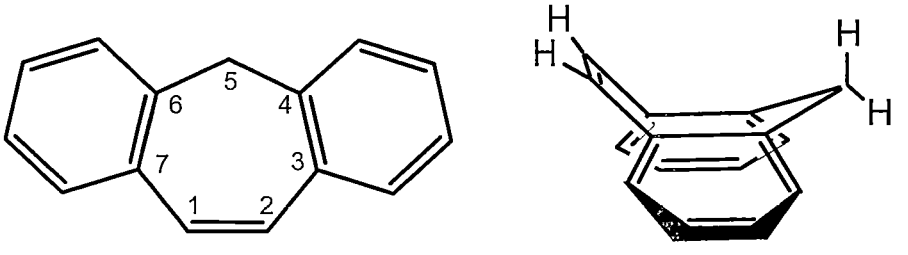

Figure 6.8. Structure and three dimensional representation of dibenzocycloheptene (tropH), (**CXCII**).

Derivatives of the dibenzocycloheptene structure have been reported in abundance since 1913 when dibenzosuberenone was first reported.[13] Many derivatives have been found to have a range of biological activities.[14] The sp^3 hybridised carbon atom of the dibenzotropylidene moiety enforces a non-planar, pseudo-boat conformation of the 7-membered ring. This results in the alkenyl HC=CH plane lying considerably out of the plane of the aromatic substituents, as shown in Figure 6.8. Consequently, the C=C bond length of the tropylidene moiety has been shown to be similar to that of acyclic alkenes, of the order of 1.3 Å, whereas the adjacent tropylidene bond lengths are typically 1.46 Å.[15] Consequently, the tropylidene C=C bond is considered to behave as an isolated olefin. Further to synthetic investigations of tropylidene compounds for biological

activity, a number of organometallic complexes employing the dibenzocycloheptene moiety have been reported.

The first reports of the use of the dibenzotropylidene (trop) ligand framework for the stabilisation of transition metal complexes were made by Jones in 1995,[16] who synthesised the platinum alkyne complex $[\{(C_4H_4)_2C_7O\}Pt(PPh_3)_2]$, (**CXCIII**), from the dehydrogenation/dehalogenation of brominated dibenzosuberenone, (**CXCIV**), as shown in Scheme 6.9. Upon reaction of **CXCIII** with *t*-butylisocyanide, the tropyne fragment reductively coupled to give a strained substituted benzene resulting from the trimerisation of the alkyne.

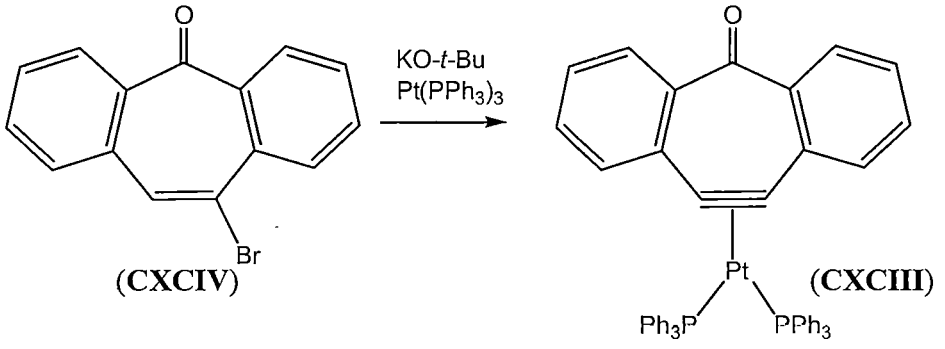

Scheme 6.9. Synthesis of the platinum complex, $[\{(C_4H_4)_2C_7O\}Pt(PPh_3)_2]$, (**CXCIII**).

Following the isolation of $[\{(C_4H_4)_2C_7O\}Pt(PPh_3)_2]$, (**CXCIII**), Tamm reported the isolation of a cationic ruthenium(II) allenylidene complex, $[(C_5H_5)Ru\{([C_4H_4]_2C_7)=C=C=\}(PPh_3)_2]PF_6$, (**CXCV**), shown in Figure 6.10, as part of a series of complexes with differing charge stabilising properties in the range, $[Ru^+]=C=C=CR_2$ to $[Ru]-C\equiv C-CR_2^+$. **CXCV** did not exhibit any interaction between the alkenyl carbon atoms within the tropylidene ligand and the Ru centre due to the end on binding of the metal to the *sp* hybridised substituents at the bridging 5-position carbon atom.[17]

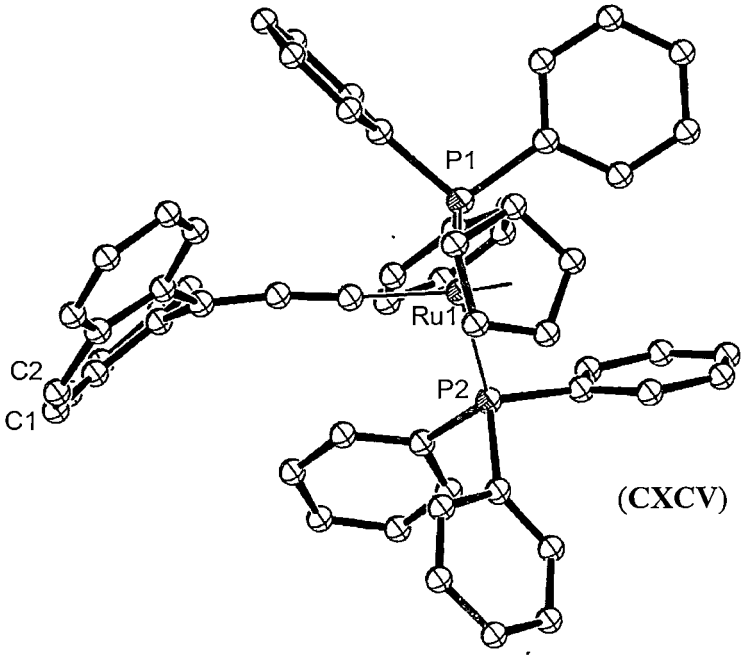

Figure 6.10. Molecular structure of $[(C_5H_5)Ru\{([C_4H_4]_2C_7)=C=C=\}(PPh_3)_2]PF_6$, (**CXCV**).[17] Figure generated from CCDC obtained coordinates. Atoms of arbitrary size with alkenyl carbon atoms numbered. H atoms and $[PF_6]^-$ are omitted for clarity.

The first tropylidene complexes to exhibit binding between a metal centre and the alkenyl carbon atoms were reported in 1998 by Grützmacher.[18] Substitution of the ligand at the bridging 5-position by PPh_2 to give the diphenylphosphine ligand ((5H-dibenzo[a,d]cycloheptene-5-yl)diphenylphosphine), $tropP^{Ph}$, (**CXCVI**), allowed the isolation of a series of rhodium complexes which led to the preparation of the first monomeric d^9-rhodium(0) complex $[Rh(tropP^{ph})_2]$, (**CXCVII**), shown in Figure 6.11. In all instances, the $tropP^{Ph}$ ligand acted as a chelating ligand to the Rh centre, binding in an η^1 fashion through the phosphorous atom and an η^2 fashion through the alkenyl-type C atoms of the tropylidene ring. Analysis of the structures of the rhodium complexes of the $tropP^{Ph}$ ligand showed a significant deviation in the angle of the aryl substituents from the plane of the alkenyl (C_2H_2) group in the dibenzotropyilidene backbone, resulting in the alkenyl fragment bonding to the rhodium centre in an equivalent fashion to a free alkene. Electron donation from the rhodium(0) centre to the alkenyl π^* orbital

resulted in a lengthening of the alkenyl bonds, which measured 1.410(10) and 1.426(9) Å.

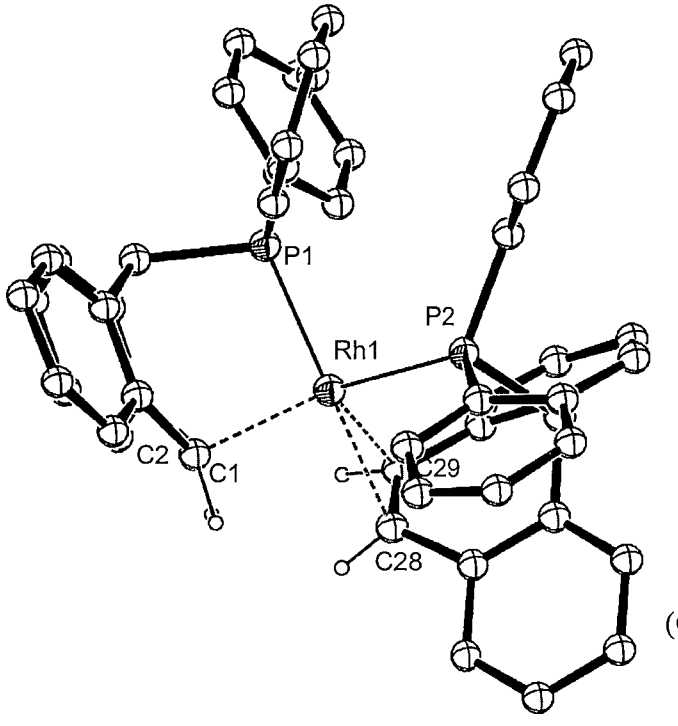

(CXCVII)

Figure 6.11. Molecular structure of the tropylidene ligated Rh(0) complex, $[Rh(tropP^{ph})_2]$, (**CXCVII**).[18] Figure generated from CCDC obtained coordinates. Atoms of arbitrary size with alkenyl carbon atoms numbered. Non-alkenyl H atoms are omitted for clarity.

Since the first reports of the use of the tropylidene system in Rh complexes, numerous ligand types based on the tropylidene framework have been developed and applied to late (Group 9 – 11) transition metals by the group of Grützmacher.[19] Included in these studies is the report of the first stable aminyl radical complex $[\{(C_5H_4N)_2\}Rh(Ntrop_2)]$, (**CXCVIII**), shown in Figure 6.12, which employed the bis(dibenzotropylidene) amine ligand, $trop_2N$, (**CXCIX**).[19n]

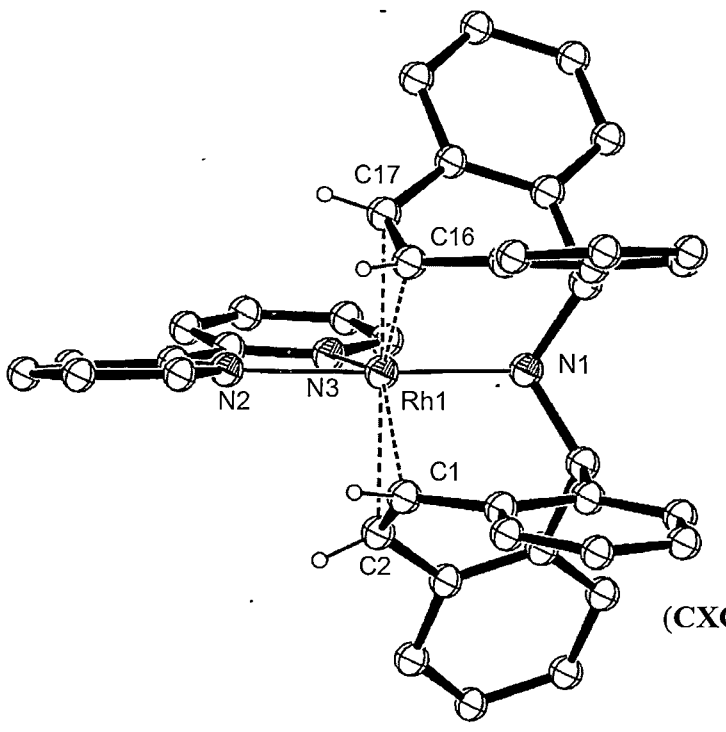

(CXCVIII)

Figure 6.12. Molecular structure of [{$(C_5H_4N)_2$}Rh(Ntrop$_2$)], (**CXCVIII**). Figure generated from CCDC obtained coordinates. Atoms of arbitrary size with alkenyl carbon atoms numbered. Non-alkenyl H atoms are omitted for clarity.

The tropylidene based ligands utilised to date have largely employed tethered pnictogens, which bind to metal centres through neutral Lewis base interactions. Chelating interactions arise from the additional binding of the ligand through the alkenyl atoms of the tropylidene unit. A summary of the tropylidene ligands employed to date is shown in Figure 6.13.

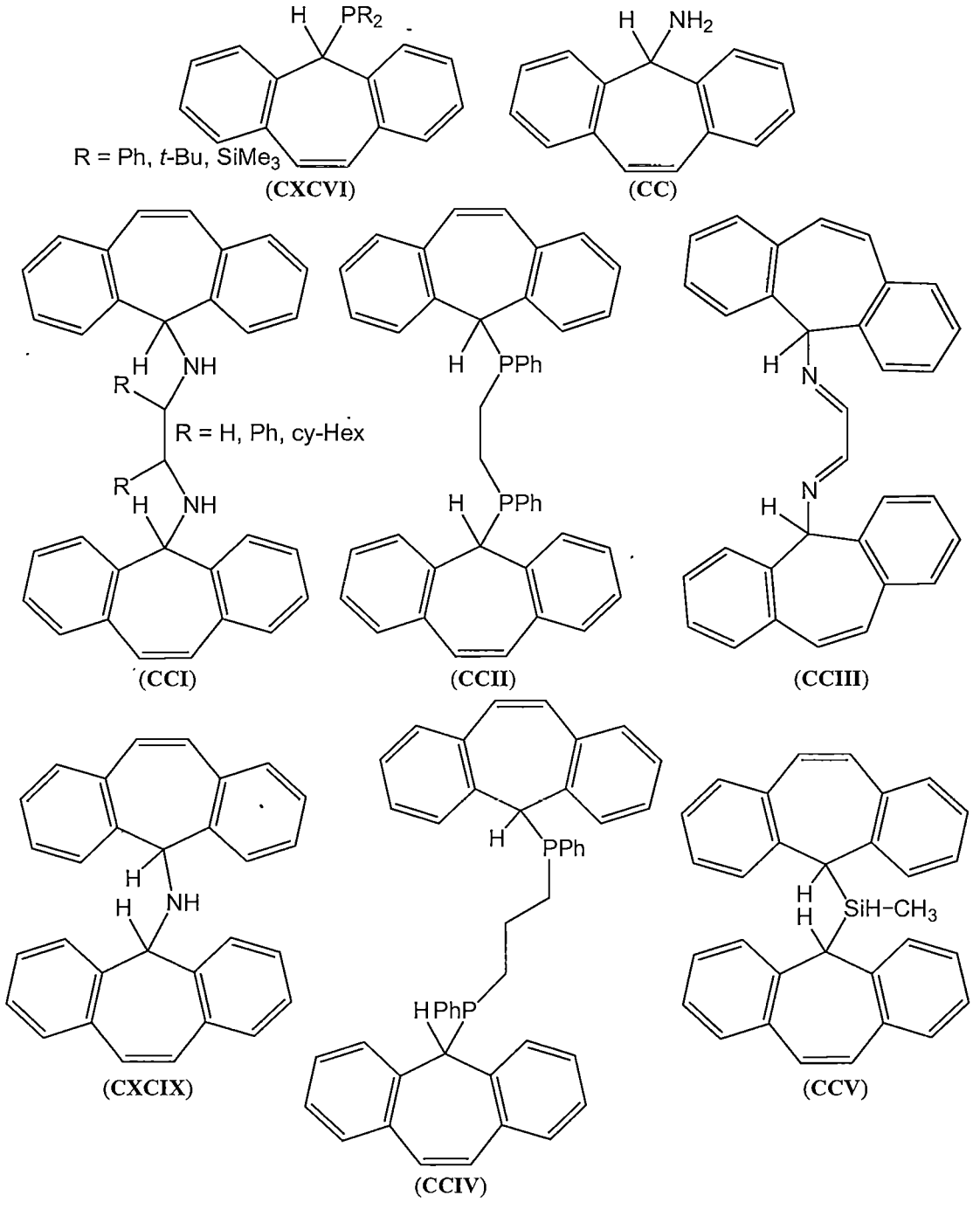

Figure 6.13. Tropylidene based ligands/deprotonated ligands utilised in late transition metal chemistry.[19]

The syntheses of the substituted tropylidene ligands for transition metal chemistry all utilise the tropylidene ketone dibenzosuberenone. The ketone is reduced to the corresponding alcohol, before substitution yields the tropylidene chloride, 5-chloro-5H-dibenzo[a,d]cycloheptene. Subsequent substitution of the chloride to incorporate the required pnictogen and further manipulation gave the targeted compounds.

The ready synthesis of substituted tropylidene compounds, and the alkenyl-type behaviour of the tropylidene double bond suggests that substituted tropylidene complexes suitable for bonding to the lanthanide elements may be readily accessible and useful in probing lanthanide alkene interactions.

Results and Discussion:

6.3. Studies of primary tropylidene amines.

6.3.1. Synthesis of primary tropylidene amines.

The previously reported primary tropylidene amine (5H-Dibenzo[a,d]cyclohepten-5-yl)amine, (**29**), (tropNH$_2$), and the novel N-*t*-Bu substituted tropylidene amine *t*-BuN(H)-(5H-Dibenzo[a,d]cyclohepten-5-yl)amine, (**30**), (tropN(H)-*t*-Bu), were prepared according to a procedure based on the previously reported synthesis of **29** as shown below in Scheme 6.1.[19j]

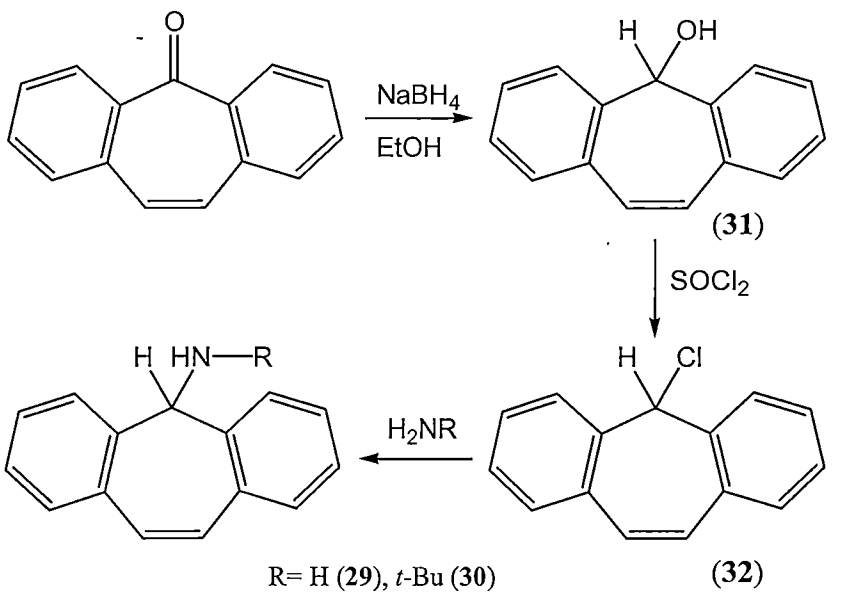

Scheme 6.1. Syntheses of the tropylidene amine compounds, (5H-Dibenzo[a,d]cyclohepten-5-yl)amine, (**29**), ($tropNH_2$) and *t*-BuN(H)-(5H-Dibenzo[a,d]cyclohepten-5-yl)amine, (**30**), (tropN(H)-*t*-Bu).

The commercially available ketone precursor dibenzosuberenone was reduced with $NaBH_4$ to yield the alcohol 5H-Dibenzo[a,d]cyclohepten-5-ol, (31), in 91 % isolated yield. Chlorination of the alcohol **31** with $SOCl_2$ gave the chloride 5-chloro-5H-Dibenzo[a,d]cycloheptene, (**32**), which, due to its instability upon exposure to water, was reacted *in situ* with either ammonia or *t*-butylamine to give the desired amine products (5H-Dibenzo[a,d]cyclohepten-5-yl)amine, (**29**), and *t*-BuN(H)-(5H-Dibenzo[a,d]cyclohepten-5-yl)amine, (**30**), in isolated yields (over 2 steps) of 87 and 83 %, respectively.

The primary amine (5H-Dibenzo[a,d]cyclohepten-5-yl)amine, (**29**) has poor solubility in petroleum spirits, but exhibits high solubility in diethyl ether, THF and toluene. Whereas the secondary amine *t*-BuN(H)-(5H-Dibenzo[a,d]cyclohepten-5-yl)amine, (**30**) is moderately soluble in petroleum spirits and benzene and exhibits high solubility in diethyl ether and THF.

Both amine products **29** and **30** were characterised by ^{1}H and ^{13}C NMR spectroscopy. The proposed formulations also gave satisfactory microanalysis results. tropNH$_2$, (**29**) was also characterised by single crystal X-ray diffraction studies.

6.3.2. ^{1}H NMR spectroscopy of primary tropylidene amines.

The ^{1}H NMR spectra of (5H-Dibenzo[a,d]cyclohepten-5-yl)amine, (**29**) and (tropN(H)-*t*-Bu), (**30**), exhibits two singlet resonances for the tropylidene 5H protons. Similarly, two singlet resonances are observed for the amine *t*-Bu protons of **30** suggesting the presence of two conformers in the solution state, as shown in Figure 6.13. This observation has been reported for a variety of tropylidenes with varying substitution,[20] resulting from the amine substituent occupying the pseudo- axial or equatorial positions of the tropylidene 5 carbon position. Interconversion between the two conformers is not achieved on the NMR timescale allowing for the observation of both conformers. For the tropylidene alkene substituent to achieve metal coordination, the axial conformation is required.

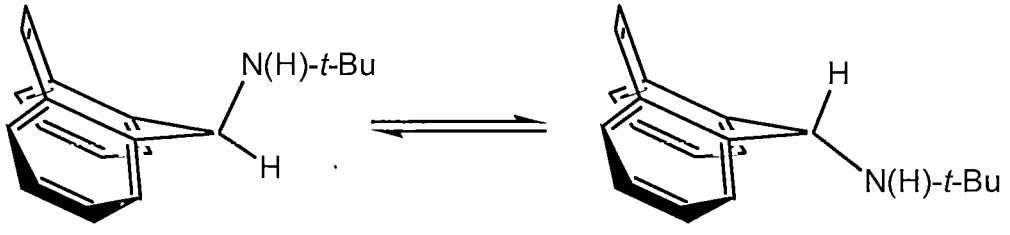

Figure 6.14. Conformers of tropN(H)-*t*-Bu, (**30**), axial (left), equatorial (right), observed by ^{1}H NMR spectroscopy at 25 °C.

6.3.3. Molecular structure of tropNH$_2$, (**29**).

Crystals of tropNH$_2$, (**29**), suitable for single crystal X-ray structural determination studies were grown from a solution of 40-60 °C petroleum spirits and diethyl ether (2:1 v/v). The crystals were found to belong to the monoclinic space group, $P2_1/n$ (No. 14), a = 5.110(3), b = 24.860(11), c = 9.020(2) Å, β = 101.07(3) °, with 4 molecules in the unit cell. The asymmetric unit consisted of one molecule of tropNH$_2$, of approximate (non-crystallographic) *Cs* symmetry. The molecular structure of tropNH$_2$, (**29**), is shown in Figures 6.15.

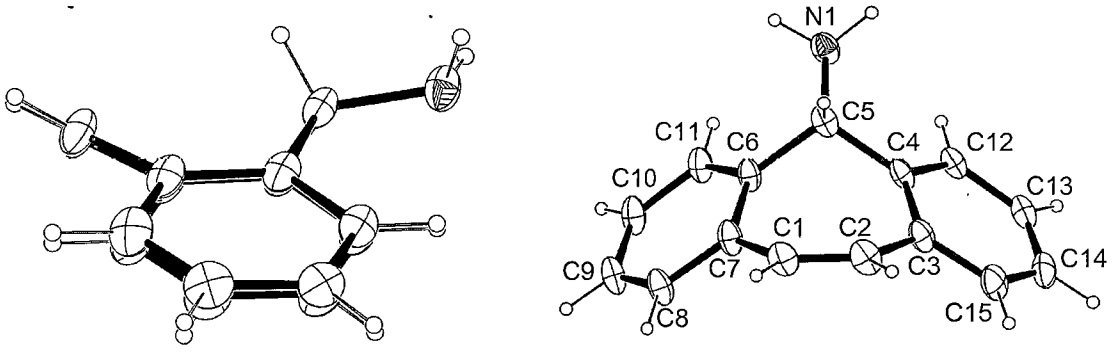

Figure 6.15. Molecular structure of tropNH$_2$, (**29**). Thermal ellipsoids are shown at the 20 % level of probability.

The structure of tropNH$_2$, (**29**), reveals a pseudo boat-type conformation in the seven membered ring, with the amine substituent occupying the *pseudo*-equatorial position. The geometry of the amine substituent is of interest for further studies as the metallation of substituents in this position requires an axial geometry in order to achieve chelation through the alkenyl moiety. The C1-C2 bond length of 1.326(4) Å is characteristic of alkenyl-type C–C bond distances and is significantly shorter than the neighbouring aromatic C3–C4 and C6–C7 aromatic bond lengths of 1.409(4) and 1.407(4) Å, respectively. The C2–C3 and C1–C7 bonds between the alkenyl group and aromatic rings measure 1.464(4) and 1.461(4) Å, which compare with those of the C–C single bond in toluene of 1.50(1) Å.[21] In addition, the least squares plane defined by the alkenyl C_2H_2 moiety lies at an angle of 139.52 ° to the least squares plane defined by the aromatic rings. Consequently, the structure of **29** exhibits bond lengths consistent with those expected for an alkene moiety exhibiting little overlap with the aromatic substituents. No internal H-bonding was observed in the structure of **29**.

Petroleum spirit/diethyl ether solutions of tropNH$_2$, (**29**), exhibit reactivity toward acetone to give the tropylidene imine tropN=C(Me)$_2$, (**33**). Crystals of **33** suitable for single crystal X-ray diffraction studies were grown from a petroleum spirit/diethyl ether solution of **29** left to react with acetone vapour *via* vapour diffusion at -17 °C. The crystals were found to belong to the monoclinic space group *P2/n*, (No. 13), a = 7.6316(15), b = 6.7949(14), c = 13.398(3) Å, β = 95.19(3) °, with 4 molecules in the unit

cell. The iminyl group was observed to occupy the pseudo-equatorial position, analogous to **29**. The determined structure is shown in Figure 6.16.

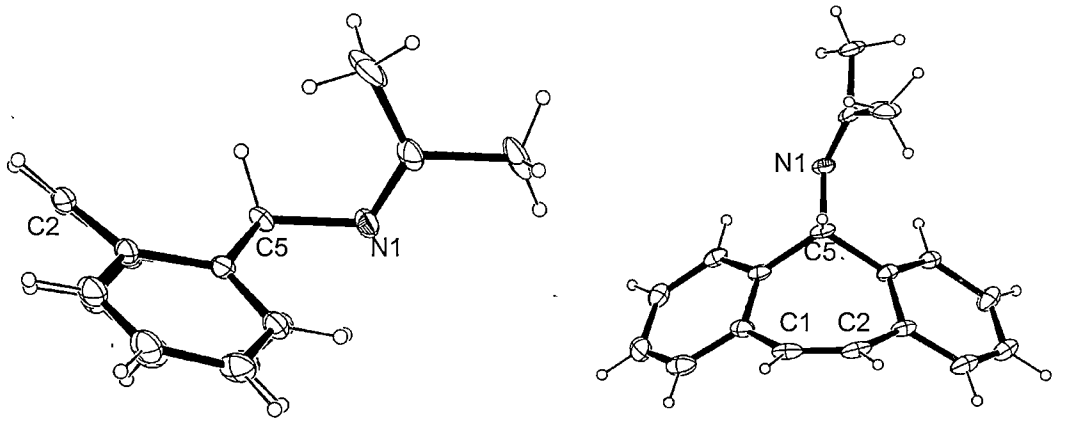

Figure 6.16. Molecular structure of tropN=C(Me)$_2$, (**33**). Thermal ellipsoids are drawn at the 20 % level of probability.

6.3.4. Synthesis of Group 1 metal tropylidene amides.

The reaction of MeLi with the secondary amine tropN(H)-*t*-Bu, (**30**), in diethyl ether gave a dark brown solution, from which red crystals of the metallated tropylidene amide [{tropN(*t*-Bu)Li}$_2$OEt$_2$], (**34**), were isolated in 62 % isolated yield, as shown in Reaction 6.1.

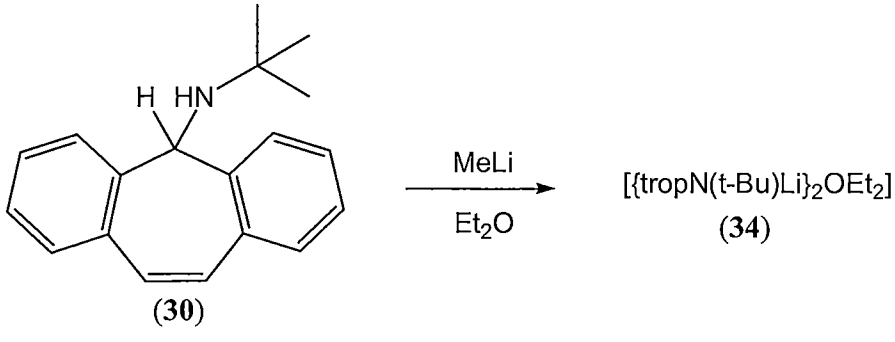

Reaction 6.1. Synthesis of the lithiated tropylidene amide [{tropN(*t*-Bu)Li}$_2$OEt$_2$], (**34**).

The proposed structure of [{tropN(*t*-Bu)Li}$_2$OEt$_2$], (**34**) was confirmed through single crystal X-ray diffraction, whilst ^{1}H and ^{13}C NMR spectroscopic studies were consistent with the solid state structure. The proposed formulation also gave a satisfactory microanalysis.

[{tropN(*t*-Bu)Li}$_2$OEt$_2$], (**34**) is moderately soluble in diethyl ether, THF and benzene. However, **34** exhibits instability in THF, giving a brown oil when left at room temperature for 1 hour. The related lithiation of tropN(H)-*t*-Bu, (**30**) with *n*-BuLi was also attempted, giving a viscous brown solution in petroleum spirit, which, upon quenching with water, gave the tropylidene alkyl compound, trop-*n*-Bu, $C_{19}H_{20}$, (**35**), identified by ^{1}H NMR spectroscopy, and GC-MS studies. The isolation of **35** is presumably a result of initial cleavage of the tropylidene amine C-N bond. The observed instability of this bond upon reaction with *n*-BuLi, provides some insight into the possible degradation pathways for [{tropN(*t*-Bu)Li}$_2$OEt$_2$], (**34**), which likely involves the cleavage of the same C-N bond. Given the stability of the tropylium cation, which forms a planar 6π electron aromatic structure, and hence dibenzotropylium, which forms a 14π electron aromatic structure, the cleavage of tropylidene heteroatom bonds by metallating agents, as observed here, may be rationalised.

The deprotonated N atoms in [{tropN(*t*-Bu)Li}$_2$OEt$_2$], (**34**), bridge two Li centres, resulting in a four-membered Li_2N_2 core, as shown in Figure 6.17. Each of the tropylidene amides act as bidentate chelating ligands to one of the lithium centres through the amido nitrogen atom and a single alkenyl carbon atom of the tropylidene ring. Both tropylidene alkenyl-Li interactions involve a single lithium centre resulting in a four-coordinate Li centre. The second Li centre exhibits interactions with the two bridging N centres and additionally a diethyl ether molecule to give a coordination number of three.

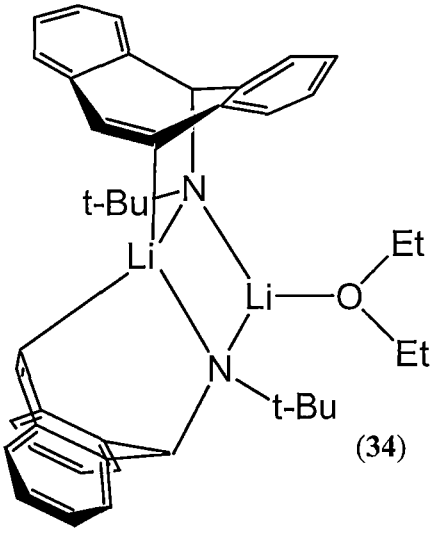

(34)

Figure 6.17. Schematic representation of the molecular structure of the tropylidene lithium amide [{tropN(*t*-Bu)Li}$_2$OEt$_2$], (**34**).

6.3.5. ^{1}H NMR spectroscopic studies of [(tropN(*t*-Bu)Li)$_2$OEt$_2$], (**34**).

The ^{1}H NMR spectrum of [{tropN(*t*-Bu)Li}$_2$OEt$_2$], (**34**), exhibits a range of broad resonances for the aromatic and alkenyl protons, suggesting fluxional processes occurring in the solution state at 25 °C. This possibly results from the dynamic binding of the tropylidene alkenyl group to the Li centres, as well as equilibria between open dimer and closed dimer structures, as shown in Figure 6.18, and observed in solution state studies of similar dimeric lithium complexes.[22]

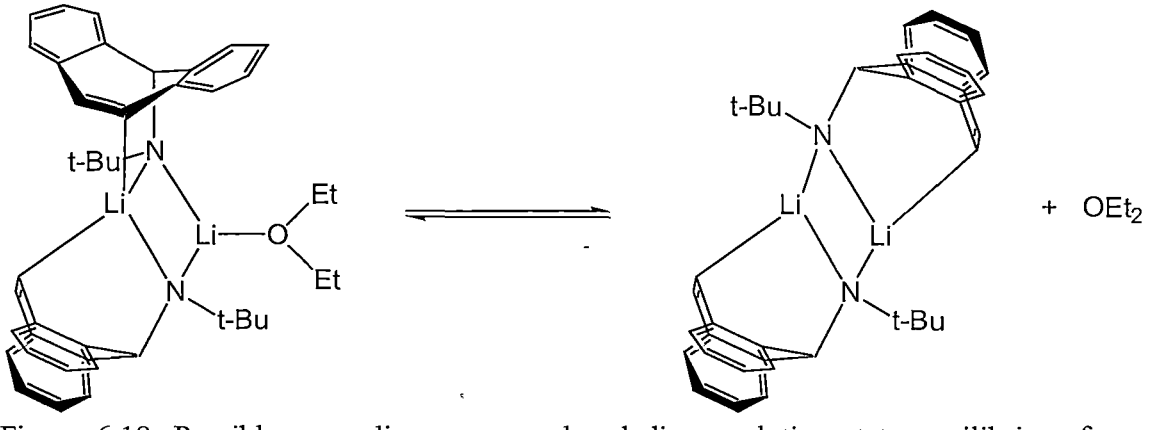

Figure 6.18. Possible open dimer versus closed dimer solution state equilibrium for [{tropN(*t*-Bu)Li}$_2$OEt$_2$], (**34**).

In contrast to the ^{1}H NMR spectrum of the precursor tropN(H)-*t*-Bu, (**30**), [{tropN(*t*-Bu)Li}$_2$OEt$_2$], (**34**), exhibits single proton resonances for the tropylidene 5H proton and the amide *t*-Bu protons, suggesting that despite the fluxional nature of the alkenyl-Li interaction, only one tropylidene conformation is present in solution, in order to cater for the alkenyl-Li interaction, as shown in Figure 6.19.

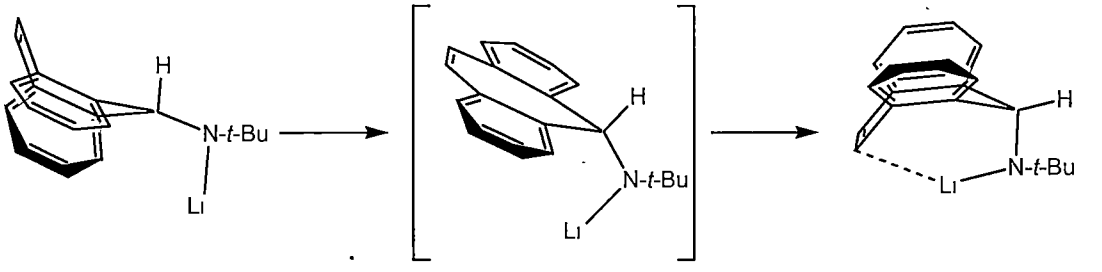

Figure 6.19. Simplified conformational inversion to promote alkenyl-Li interactions, *via* a planar transition state.

6.3.6. Molecular structure of [{tropN(*t*-Bu)Li}$_2$OEt$_2$], (**34**).

Red crystals of [{tropN(*t*-Bu)Li}$_2$OEt$_2$], (**34**), suitable for single crystal X-ray diffraction studies were grown from a concentrated diethyl ether solution of **34** cooled to -17 °C. The crystals were found to belong to the monoclinic space group, $P2_1/c$ (No. 14), a = 10.1130(10), b = 31.433(3), c = 11.7732(11) Å, β = 105.309(2) °, with 4 molecules in the unit cell. The asymmetric unit consists of one molecule of [{tropN(*t*-Bu)Li}$_2$OEt$_2$], (**34**). The structure of **34** is shown in Figure 6.20. **34** represents the first crystallographically authenticated Group 1 metal complex of the dibenzotropylidene moiety.

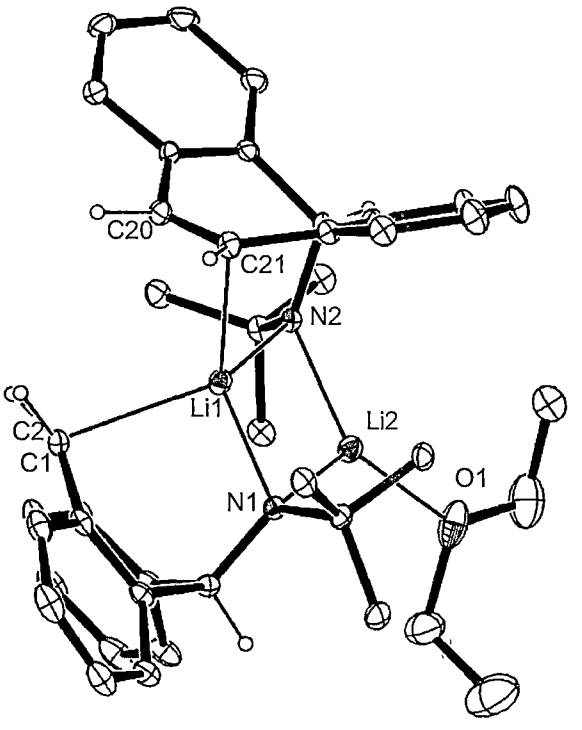

Figure 6.20. Molecular structure of the dimeric tropylidene lithium amide, [{tropN(*t*-Bu)Li}$_2$OEt$_2$], (**34**). Thermal ellipsoids are drawn at the 20 % level of probability. Non-tropylidene H atoms are omitted for clarity.

[{tropN(*t*-Bu)Li}$_2$OEt$_2$], (**34**), adopts a dimeric structure in the solid state of approximate (non-crystallographic) C_2 symmetry. The Li–N bond lengths to the four-coordinate Li centre of 2.033(5), 2.018(5) and to the three-coordinate Li centre of 2.070(5) Å and 2.091(5), are typical of those of lithium centres bound to secondary amides, such as [{Li(N(SiMe$_3$)$_2$)(OEt$_2$)}$_2$], (**CCVI**), which exhibits average Li-N interactions of 2.06(1) Å.[23] The four-coordinate alkene solvated Li centre binds to a single C atom from each alkene unit through interactions measuring 2.511(6) and 2.490(5) Å, with the distances to the non-bonding alkenyl C atoms measuring 2.691(6) and 2.726(5) Å. The alkenyl Li–C interactions are marginally longer than those in the internal alkene solvated allylic polymers, [(CH$_3$OCH$_2$CH$_2$)$_2$NCH$_2$C(CH$_2$)(C(H)SiMe$_3$)Li], (**CCVII**) and [(CH$_3$OCH$_2$)$_2$(CHCH$_2$CH$_2$CH)NCH$_2$C(CH$_2$)(C(H)SiMe$_3$)Li], (**CCVIII**), which exhibited Li-C interactions also to one end of the alkenyl bond of 2.442(5) and 2.48(11)

Å, respectively.[24] The four coordinate alkene solvated Li centre adopts a distorted tetrahedral geometry, with L-Li-L angles ranging between C7-Li1-C27 111.2(2) and N1-Li1-C7 124.1(2) °, with larger angles observed between the Li centre and the N and C atoms within each chelating tropylidene ligand. The Li–O interaction of the three-coordinate Li centre measures 2.046(6) Å, which is longer than the Li–O interactions in the trigonal diethyl ether solvated three-coordinate Li centres of the secondary amide complex [{Li(N(SiMe$_3$)$_2$)(OEt$_2$)}$_2$], (**CCVI**), of 1.961(11) Å. The three-coordinate Li centre adopts a trigonal planar geometry with L-Li-L angles ranging from N2-Li2-N1 107.1(2) to O1-Li2-N1 133.5(3) °. The C=C (alkenyl) interactions in **34** of 1.340(4) and 1.341(4) Å, are comparable to those of the free tropylidene amine ligand tropNH$_2$, (**30**), of 1.326(4) Å, suggesting that the Li–C interactions have little effect on the length of the C=C bonds.

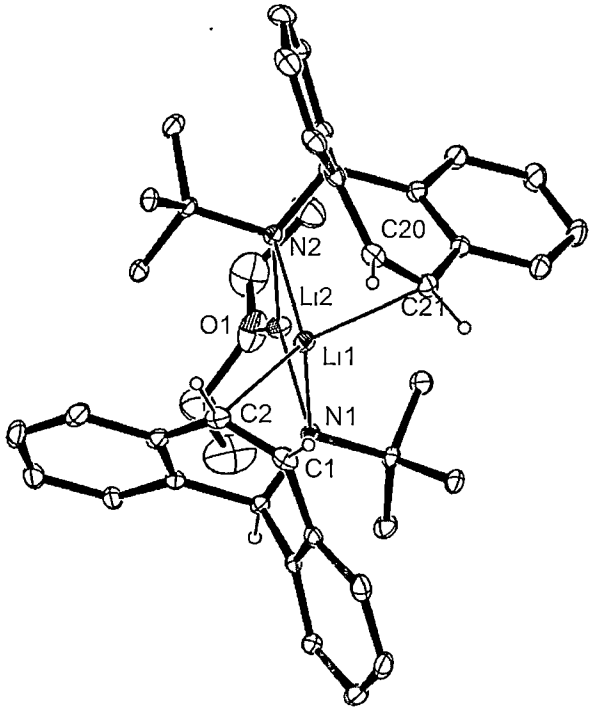

Figure 6.21. Molecular structure of [{tropN(*t*-Bu)Li}$_2$OEt$_2$], (**34**), demonstrating the planar Li$_2$N$_2$ core. Thermal ellipsoids are drawn at the 20 % level of probability. Non-tropylidene H atoms are omitted for clarity.

6.3.7. Reactivity studies of [{tropN(*t*-Bu)Li}$_2$OEt$_2$], (**34**).

The reactivity of [{tropN(*t*-Bu)Li}$_2$OEt$_2$], (**34**), with the lanthanide reagents $SmBr_3$, YbI_2 and SmI_2 was investigated. No organolanthanide compounds were able to be isolated, either from lack of reactivity (for $SmBr_3$) or ligand degradation (SmI_2 and YbI_2). In the case of SmI_2, reductive cleavage of the tropylidene amide C-N bond was observed, yielding the dimeric tropylidene species (trop)$_2$, (**36**), as shown in Reaction 6.2. (trop)$_2$, (**36**), is poorly soluble in a range of solvents including THF, toluene and petroleum spirits, preventing NMR characterisation. The identity of **36** was confirmed through single crystal X-ray diffraction studies. Microanalytic studies were also consistent with the proposed structure. **36** may also be synthesised by the reduction of the tropylidene chloride compound **32** by SmI_2 in THF. The isolation of **36** from **32**, is presumed to occur from the reductive cleavage of the tropylidene chloride bond by SmI_2 to give the corresponding samarium trihalide and **36** *via* the generation of a dibenzotropyl radical. Similarly, the reaction of **34** with SmI_2 presumably proceeds *via* metathetical exchange followed by intramolecular reduction of the tropylidene amide bond by the samarium(II) centre to give **36**.

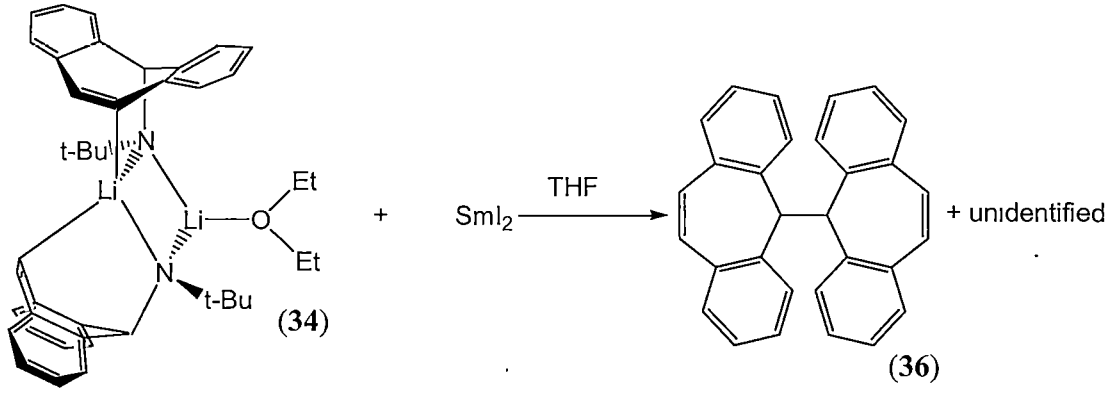

Reaction 6.2. Synthesis of the tropylidene dimer (trop)$_2$, (**36**).

Crystals of (trop)$_2$, (**36**), suitable for single crystal X-ray diffraction studies were grown from a THF solution of [{tropN(*t*-Bu)Li}$_2$OEt$_2$], (**34**), and SmI_2 cooled to -17 °C overnight. The crystals were found to belong to the monoclinic space group, $P2_1/n$, (No. 14), with a = 10.340(5), b = 8.330(3), c = 12.510(4) Å, β = 108.53(3) °, with 2 molecules in the unit cell. The asymmetric unit consisted of one half of a molecule of

$(trop)_2$, (**36**), which lie on inversion centres. ORTEP representations of the molecular structure of **36** are shown in Figure 6.22.

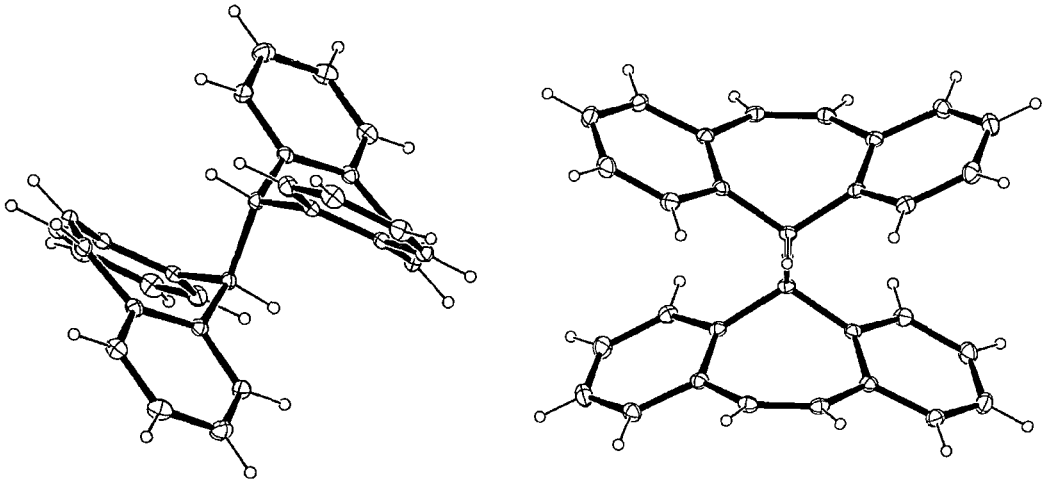

Figure 6.22. Molecular structure of the tropylidene dimer, $(trop)_2$, (36). Thermal ellipsoids are shown at the 20 % level of probability.

6.4. Studies of tropylidene imines.

6.4.1.Synthesis of tropylidene 1,4-diazabuta-1,3-diene and diketiminato ligands.

Given the observed instability of tropN(H)-*t*-Bu, (**30**), towards lithiation and subsequent instability of $[\{tropN(t\text{-}Bu)Li\}_2OEt_2]$, (**34**), coupled with the isolation of $(trop)_2$, (**36**) from metathetical exchange reactions of **34** with lanthanide(II) reagents, the synthesis of the previously reported tropylidene diazadiene tropDAD, (**37**), and the unknown tropylidene β-diketiminate $HC\{C(CH_3)N(trop)\}C(CH_3)(N(H)trop)$, (**38**), was attempted.

The previously reported tropylidene diazadiene tropDAD, (**37**), was synthesised according to a literature method,[19g] *via* the condensation of glyoxal with the tropylidene amine, $tropNH_2$, (**29**), as shown below in Scheme 6.2, giving tropDAD, (**37**), in good (85 %) yield. The analogous reaction of **29** with 2,5-pentanedione following conditions usually suited to the synthesis of β-diketiminates,[25] does not, however, give the corresponding targeted β–diketiminate, (**38**), as shown in Reaction 6.3, but rather the diketone tropacacH, (**39**), shown in Scheme 6.2, in good yield (68 %), presumably

liberating NH_3. When the reaction is carried out under alternative conditions, including using molecular sieves, the diketone **39** remained the only product.

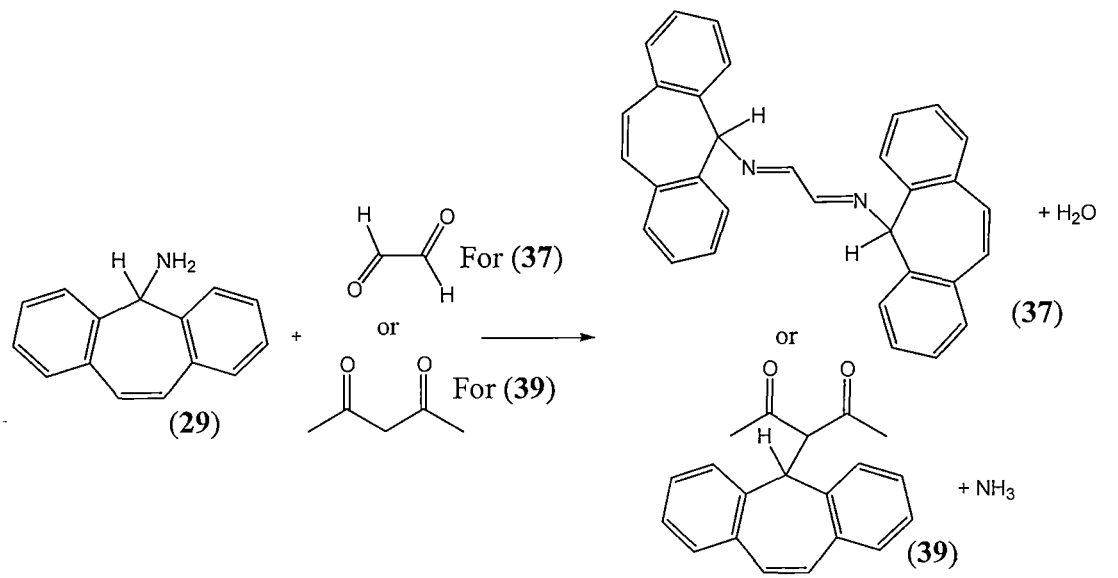

Scheme 6.2. Synthesis of the tropylidene 1,4-diazabuta-1,3-diene **37** and diketone **39**.

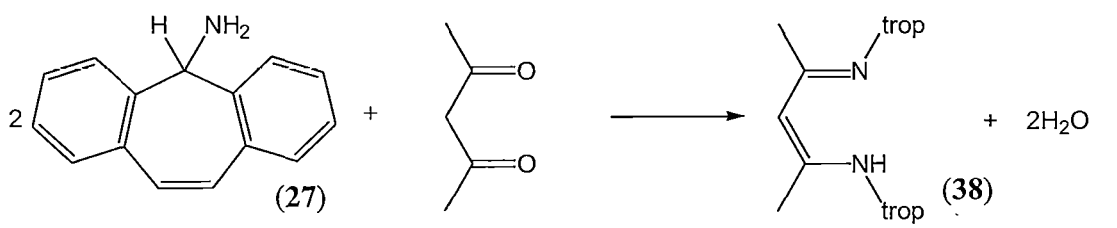

Reaction 6.3. Intended synthesis of the tropylidene β–diketiminate, $HC\{C(CH_3)N(trop)\}C(CH_3)(N(H)trop)$, (**38**).

The diketone tropacacH, (**39**), is moderately soluble in dichloromethane, methanol and benzene. The molecular structure of **39** was confirmed by single crystal X-ray diffraction. ^1H and ^{13}C NMR spectroscopy studies were also consistent with the derived structure, whilst the proposed formulation also gave a satisfactory microanalysis.

6.4.2. Molecular structure of tropacacH, (**39**).

Crystals of tropacacH, (**39**), suitable for X-ray diffraction studies were grown from a solution of **39** in MeOH cooled to -17 °C overnight. The crystals were found to belong to

the orthorhombic space group, $P2_12_12_1$, (No. 19), a = 8.1532(16), b = 10.798(2), c = 18.164(4) Å, with the asymmetric unit consisting of one molecule of tropacacH, (**39**). The molecular structure of tropacacH, (**39**), is shown in Figure 6.23.

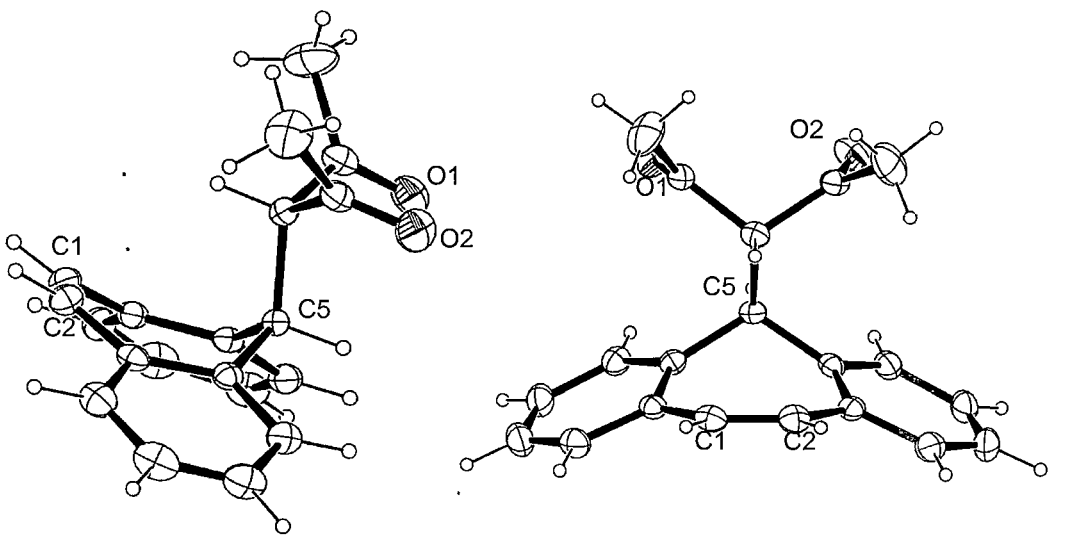

Figure 6.23. Molecular structure of tropacacH, (**39**). Thermal ellipsoids are shown at the 20 % level of probability.

As for the structure of $tropNH_2$, (**29**), the tropylidene ring in tropacacH, (**39**), adopts a *pseudo*-boat conformation. However, in contrast to **29**, the diketone substituent of **39** occupies the *pseudo*-axial position as is required for metal complex studies with internal alkene interactions. However, the remote location of the heteroatoms and the envisaged geometry of the acac unit upon metallation make $(tropacac)^-$ un-suitable for obtaining the desired chelate formation *via* interaction with the pendant alkene moiety. Consequently, the further chemistry of **39** was not pursued.

6.4.3. Reactivity studies of tropDAD, (**37**).

The reactivity of the tropylidene 1,4-diazabuta-1,3-diene tropDAD, (**37**), with the lanthanide(II) reagents SmI_2 and YbI_2 was investigated. Upon addition of THF solutions of the lanthanide(II) substrates to THF solutions of tropDAD, (**37**), immediate colour changes were observed to brown and green, respectively, consistent with the oxidation of the metal species. Colourless crystals of the tropylidene dimer $(trop)_2$, (**36**), were

isolated from the SmI_2 reaction, as observed previously for the reaction of SmI_2 with [{tropN(*t*-Bu)Li}$_2$OEt$_2$], (**34**). In this instance, the generation of the $(trop)_2$ dimer is presumably accompanied by the generation of an unidentified Sm(III) ketimide complex, "Ln(III)N=CC=NLn(III)", (**40**), as shown in Scheme 6.3.

Characterisation of products from the reaction of tropdad, (**37**), with YbI_2 was unable to be achieved, presumably resulting from similar reductive processes forming a complex mixture of products. The formation of $(trop)_2$ again suggests that frailty in the tropylidene-heteroatom bond exists, accentuated by the generation of an anionic heteroatom adjacent to the tropylidene moiety, consistent with the previously observed instability of [{tropN(*t*-Bu)Li}$_2$OEt$_2$], (**34**). Hence, subsequent ligand development has focussed on utilising remote sites for metallation.

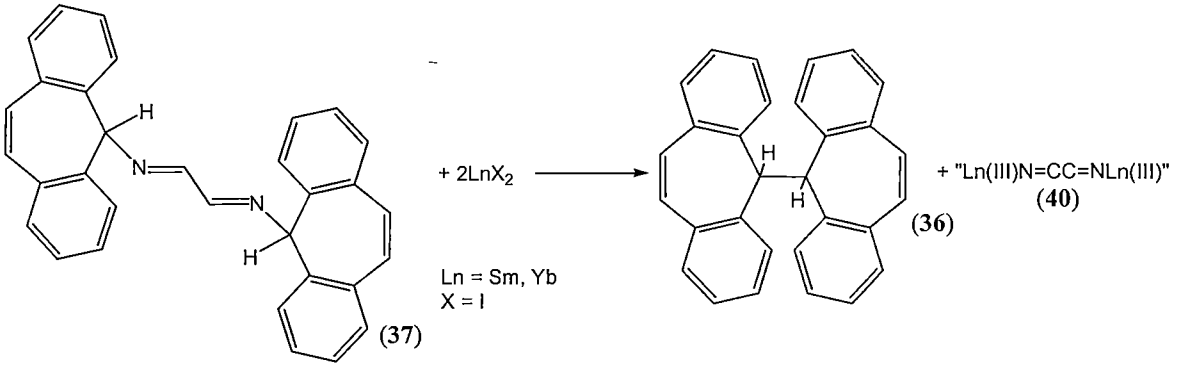

Scheme 6.3. Cleavage of the C–N bond of tropDAD, (**37**), by lanthanide(II) reagents to generate the tropylidene dimer $(trop)_2$, (**36**) and a presumed, unidentified lanthanide(III) ketimide complex, "Ln(III)N=CC=NLn(III)", (**40**).

The reactivity of the tropylidene 1,4-diazabuta-1,3-diene tropDAD, (**37**), with the lanthanide(III) reagent $SmBr_3$ was also investigated in order to generate a coordination compound, thereby avoiding stability issues induced by reductive Ln(II) chemistry. Upon prolonged heating of a THF solution of **37** and $SmBr_3$, orange crystals of the previously reported tetrakis(THF) adduct of $SmBr_3$, [$(THF)_4SmBr_3$], (**CCIX**), were isolated,[26] suggesting that the binding of neutral tropDAD, (**37**), to lanthanide(III) species is weaker than that afforded by solvation by the Lewis basic species.

6.4.4. Synthesis of tropylidene imines.

Following the observed frailty of the tropylidene C-N bond in both amine (tropN(H)-*t*-Bu, (**30**)) and 1,4-diazabuta-1,3-diene (tropDAD, (**37**)) compounds, the synthesis of tropylidene species bearing remote anionic sites was attempted, in order to stave off C-N cleavage.

The yellow tropylidene imine compounds tropNsalOH, (**41**) and tropNsal‡OH, (**42**), (where "salO" = $HC(C_6H_4)$-2-O, sal‡O = $HC(C_6H_2)$-2-O-3,5-*t*-Bu)), were synthesised according to a procedure based on the condensation of primary amines with ketones[27] as shown below in Scheme 6.4. The condensation of the primary tropylidene amine $tropNH_2$, (**29**), with the benzaldehydes, salicylaldehyde and 3,5-di-*tert*-butyl-2-hydroxybenzaldehyde, gave the tropylidene imines tropNsalOH, (**41**), and (tropNsal‡OH), (**42**), in 64 and 86 % isolated yields, respectively.

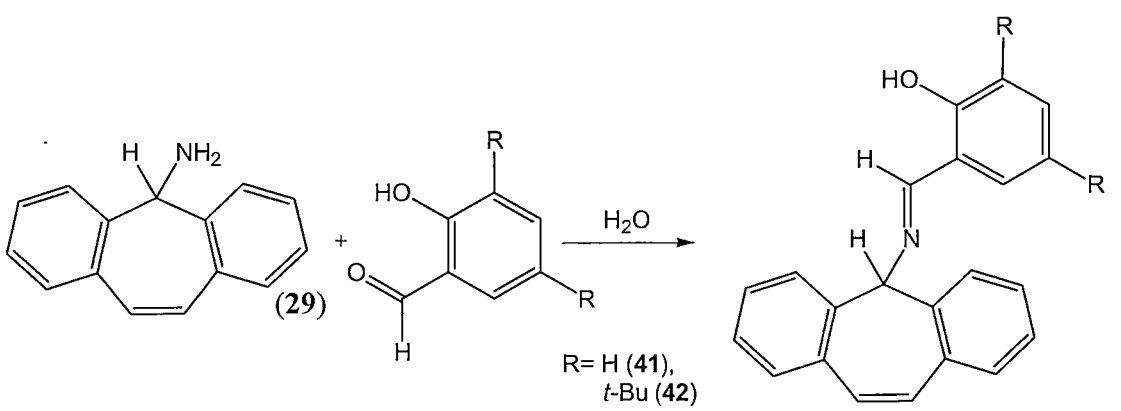

Scheme 6.4. Synthesis of the tropylidene imine compounds tropNsalOH, (**41**), and tropNsal‡OH, (**42**).

tropNsalOH, (**41**), is moderately soluble in polar solvents such as methanol, diethyl ether and tetrahydrofuran, but has poor solubility in petroleum spirits. tropNsal‡OH, (**42**), exhibits high solubility in polar solvents and is moderately soluble in petroleum spirits. Due to the higher solubility and crystallinity of **42** than **41**, further reactivity studies were focussed on **42**.

tropNsalOH, (**41**), and tropNsal‡OH, (**42**), were characterised by ^{1}H and ^{13}C NMR spectroscopic studies, whilst the molecular structure of **42** was also confirmed through a single crystal X-ray diffraction study. Both compounds also gave satisfactory microanalyses.

6.4.5. Molecular structure of tropNsal‡OH, (**42**).

Crystals of tropNsal‡OH, (**42**), suitable for single crystal X-ray diffraction studies were grown from a petroleum spirit solution of **42** left to evaporate slowly at room temperature over a period of 2 days. The yellow crystals were found to belong to the triclinic spacegroup, $P\bar{1}$ (No. 2), a = 9.7604(33), b = 11.2904(93), c = 12.2546(57) Å, α = 84.98(5) β = 74.80(3) γ = 69.08(4) °, with 2 molecules in the unit cell. The asymmetric unit consisted of one molecule of tropNsal‡OH, (**42**). ORTEP representations of the molecular structure of **42** are shown in Figure 6.24.

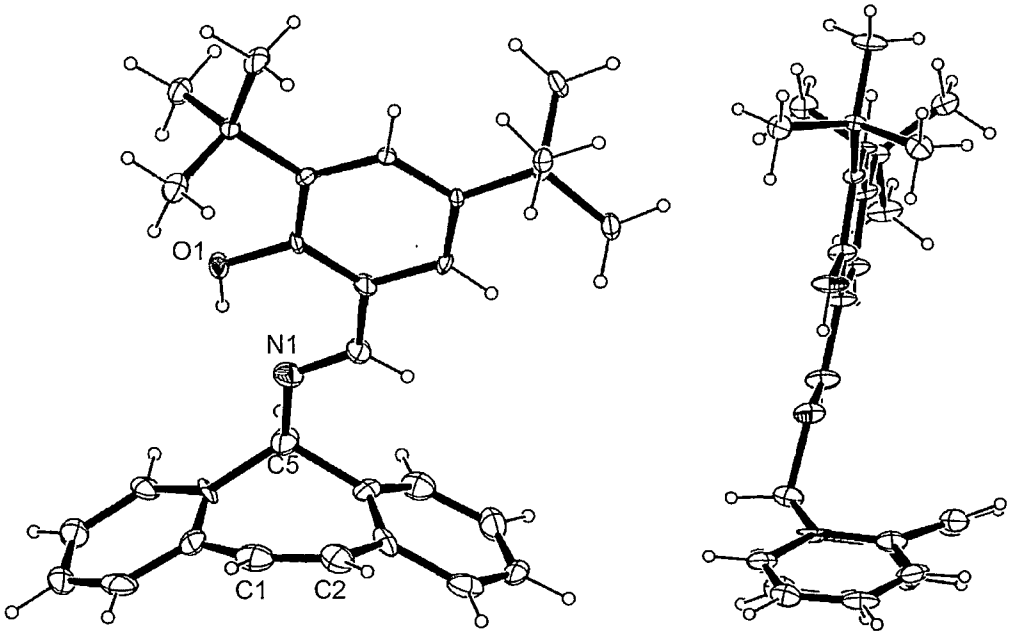

Figure 6.24. Molecular structure of the tropylidene imine, tropNsal‡OH, (**42**). Thermal ellipsoids are shown at the 20 % level of probability. H atoms have been omitted for clarity.

The tropylidene ring in tropNsal‡OH, (**42**), also adopts a pseudo-boat conformation as observed previously for tropNH$_2$, (**29**), and tropacacH, (**39**), with the NSal‡OH substituent adopting the *pseudo*-axial position needed for coordination of the pendant alkene to a metal centre in a chelation mode. tropNsal‡OH, (**42**), exhibits a similar alkenyl C_1=C_2 bond length (1.327(13) Å) to that in **29** (1.326(4) Å) and **39** (1.333(6) Å). tropNsal‡OH, (**42**), also exhibits an intramolecular H-bond between the imine N atom and the phenolic H atom.

6.4.6. Synthesis of Group 1 metal complexes of tropylidene imines.

The reaction of yellow tropNsal‡OH, (**42**), with white lithium diisopropylamide (LDA) in diethyl ether gave a dark red solution, from which colourless crystals of the lithium aryloxide, [(tropNsal‡OLi)$_2$], (**43**), were isolated in 57 % yield, as shown below in Reaction 6.4. [(tropNsal‡OLi)$_2$], (**43**), exhibits moderate solubility in the aromatic solvents, benzene and toluene, and high solubility in the Lewis basic solvents diethyl ether and THF.

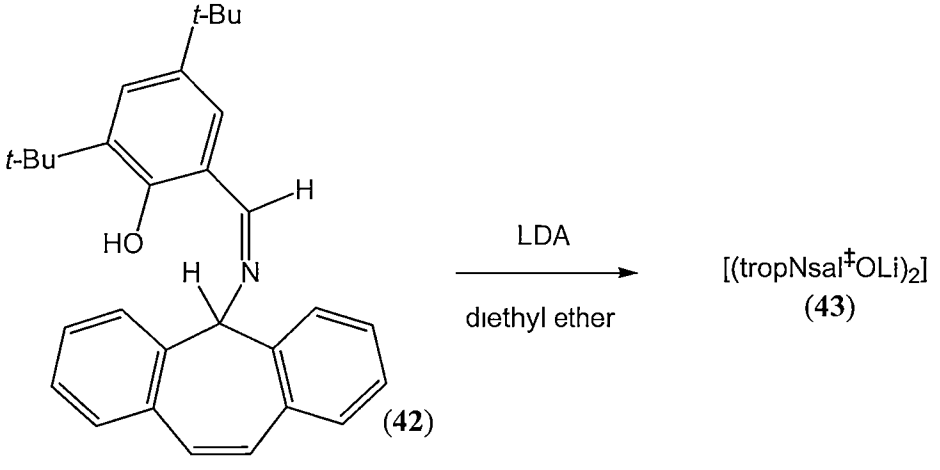

Reaction 6.4. Synthesis of the lithiated tropylidene dimer, [(tropNsal‡OLi)$_2$], (**43**).

The molecular structure of [(tropNsal‡OLi)$_2$], (**43**), was determined *via* single crystal X-ray diffraction, whilst ^{1}H and ^{13}C NMR spectroscopic studies were consistent with the solid-state structure. The proposed formulation also gave a satisfactory microanalysis.

[(tropNsal‡OLi)$_2$], (**43**), adopts an unsolvated closed dimer form in the solid state *via* bridging of the phenolic O centres. The complex features a butterflied square Li_2O_2 core, with each ligand binding to the Li atoms through the phenolic O atom, the imino N atom and one of the alkenyl C atoms. The tropylidene ligands form a *syn* arrangement with respect to the Li_2O_2 plane. Unlike the majority of lithium alkoxides, which form tetramers and hexamers, and sometimes dimers with external Lewis basic solvation,[28] [(tropNsal‡OLi)$_2$], (**43**) forms a dimer with internal imine nitrogen coordination, observed recently in a limited number of cases.[28] A schematic representation of the molecular structure of **43** is shown in Figure 6.25.

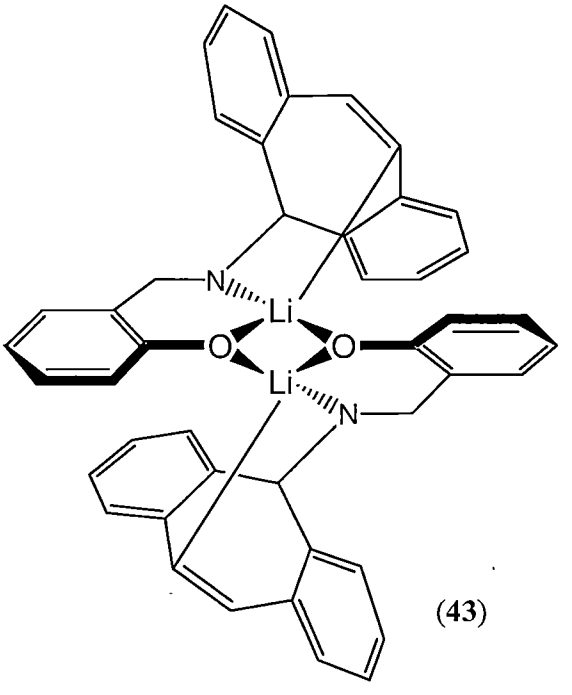

(**43**)

Figure 6.25. Schematic representation of the molecular structure of the lithiated tropylidene, [(tropNsal‡OLi)$_2$], (**43**). 3,5-*t*-Bu substituents from each phenol have been omitted for clarity.

^{1}H NMR spectroscopic studies of [(tropNsal‡OLi)$_2$], (**43**), suggest that fluxional processes within the molecule occur on the NMR timescale, analogous to [{tropN(*t*-Bu)Li}$_2$OEt$_2$], (**34**), with each resonance exhibiting broad peak shapes. This is consistent with dynamic processes in the solution state, possibly involving the weak interactions between the Li centres and the tropylidene alkenyl group. Inversion of the *pseudo*-axial

tropylidene heteroatom bond to the pseudo-equatorial position, or dynamic equilibria between closed/open dimeric structures as for [(tropN(*t*-Bu)Li)$_2$OEt$_2$], (**34**) may be operative.

6.4.7. Molecular structure of [(tropNsal‡OLi)$_2$], (**43**).

Crystals of [(tropNsal‡OLi)$_2$], (**43**) suitable for single crystal X-ray diffraction studies were grown from a solution of **43** in diethyl ether left to stand at room temperature overnight. The crystals were found to belong to the triclinic space group, $P\bar{1}$ (No. 2), a = 12.550(4), b = 12.600(4), c = 17.770(7) Å, α = 73.53(3), β = 81.24(9), γ = 69.21(9) ° with 2 dimers in the unit cell. The asymmetric unit consisted of one molecule of the dimeric complex, [(tropNsal‡OLi)$_2$], (**43**). The structure of **43** is shown in Figures 6.26 and 6.27.

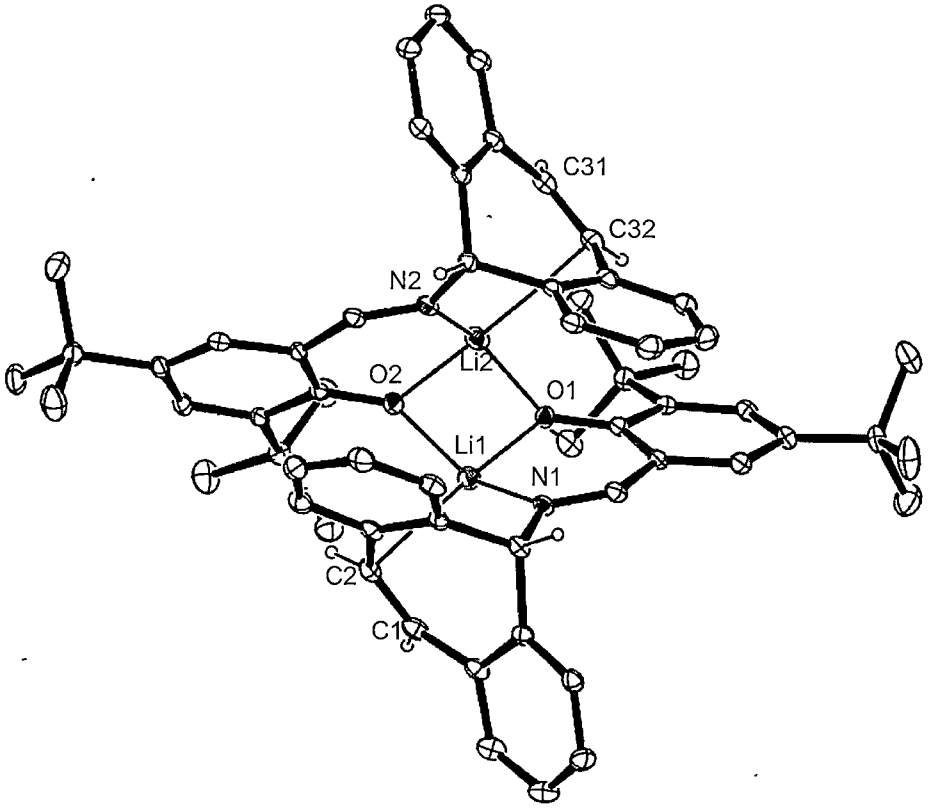

Figure 6.26. Molecular structure of [(tropNsal‡OLi)$_2$], (**43**). Thermal ellipsoids are drawn at the 20 % level of probability. Non-tropylidene H atoms are omitted for clarity.

[(tropNsal‡OLi)$_2$], (**43**), forms an unsolvated dimer in the solid state, with the phenolic O atoms from each trop ligand bridging the two metal centres. The four Li–O bond lengths are not significantly different, ranging from 1.857(7) to 1.906(7) Å, consistent with the Li–O bond lengths in the Li_2O_2 core of other dimeric mixed imine phenoxide complexes.[28,29] The core, however, exhibits significant puckering along the Li···Li vector, with an O1-Li1-Li2-O2 dihedral angle of 126.$_3$ °. Consequently, the internal angles of the Li–O core deviate from 90 °, with the largest deviation observed in the Li–O–Li angles, which measure 78.5(3) and 78.0(3) °.

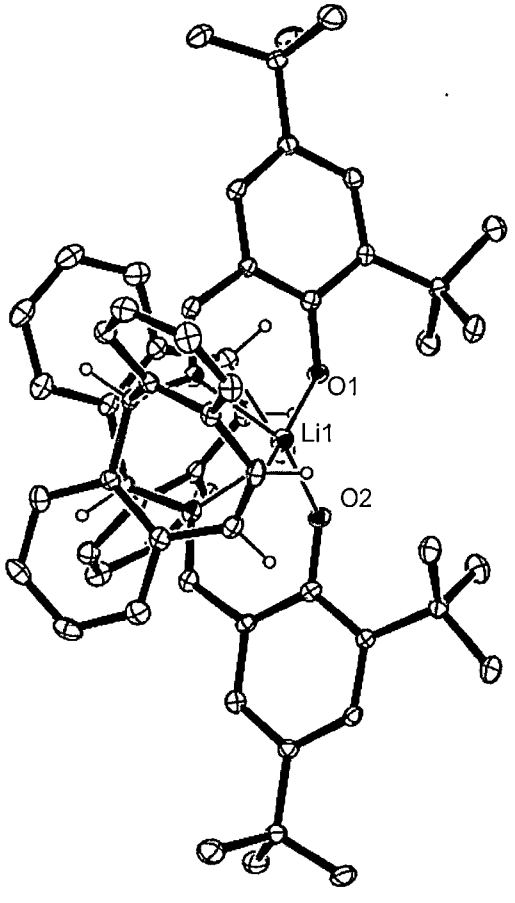

Figure 6.27. Side view of the molecular structure of [(tropNsal‡OLi)$_2$], (**43**), demonstrating the puckered Li_2O_2 core. Thermal ellipsoids are shown at the 20 % level of probability. Non-tropylidene H atoms are omitted for clarity.

The tropylidene ligands bind to each Li atom in a *mer*-type arrangement such that each Li atom has a coordination number of 4, resulting from the tridentate tropylidene ligand and the bridging interaction with the O atom of the neighbouring tropylidene ligand. In order to facilitate the distrorted tetrahedral Li binding mode, the *t*-Buphenol ring has rotated through 90 ° compared to the structure of the free ligand. The tetrahedral tendency of the Li centres result in the tropylidene ligands chelating through the imine N atom above the plane of the Li_2O_2 core, rather than in the plane, which would result in a square-planar Li coordination geometry.

The steric bulk of the dibenzotropylidene and 3,5-di-*t*-Buphenol rings provides steric shielding to the Li_2O_2 core, as shown in Figure 6.28. This prevents the binding of solvent molecules to the lithium centres, resulting in the observed unsolvated dimeric structure. Consequently, the binding of the Lewis basic diethyl ether solvent molecules can be concluded to be less beneficial than the chelating alkene interaction observed in $[(tropNsal^{\ddagger}OLi)_2]$, (**43**).

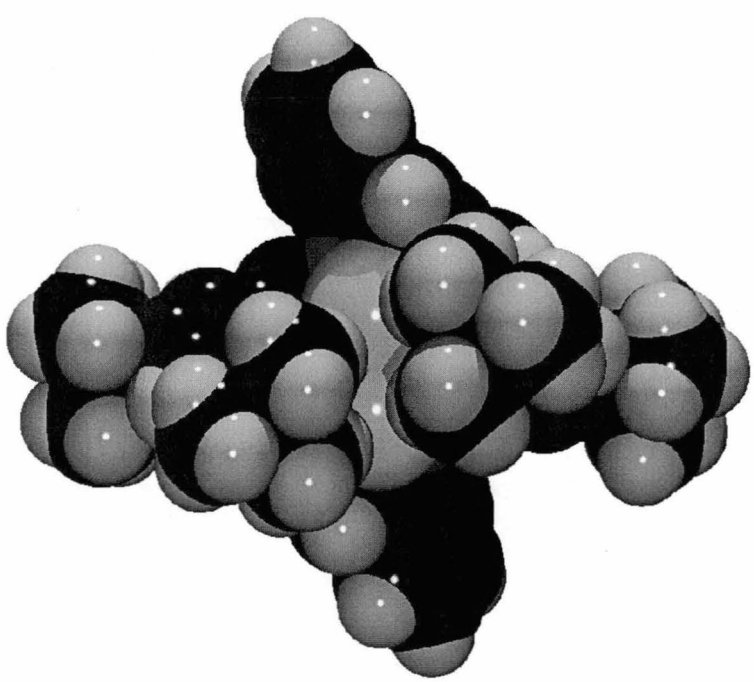

Figure 6.28. Space-filling representation of the dimeric lithiated tropylidene $[(tropNsal^{\ddagger}OLi)_2]$, (**43**), viewed perpendicular to the Li_2O_2 plane.

The Li–N(imine) distances in [(tropNsal‡OLi)$_2$], (**43**), of 2.010(7) and 2.008(7) Å, are consistent with those of other dimeric mixed imine/phenoxide complexes such as [{*i*-Pr-NCMeCHCMeOLiOP(NMe$_2$)$_3$}$_2$], (**CCX**), of 2.026(5) Å.[29a] The tropylidene alkenyl C–Li interactions exhibit significantly different lengths of 2.582(7) (Li1–C2) and 2.695(7) (Li2–C32) Å (one end of each of the two Li bound alkenyl units), presumably as a result of crystal packing effects and are significantly longer than those observed in [{tropN(*t*-Bu)Li}$_2$OEt$_2$], (**34**), of 2.511(6) and 2.490(5) Å. The non-bonding Li–C(alkenyl) interactions are significantly longer, measuring 2.801 (Li1–C1) and 2.922 (Li2–C32) Å.

6.4.8. Reactivity studies of [(tropNsal‡OLi)$_2$], (**43**).

The reactivity of [(tropNsal‡OLi)$_2$], (**43**), with the lanthanide(II) substrates, SmI_2 and YbI_2 was investigated *via* addition of THF solutions of the lanthanide reagents to THF solutions of **43**. In both cases, rapid colour changes were observed to orange (for SmI_2) and dark green (for YbI_2), consistent with the oxidation of each metal, presumably resulting from reduction of the imine moiety in the deprotonated ligand following metathetical exchange. The observed colour changes were coupled with the precipitation of a white solid. Over a period of 6 hours, the green ytterbium complex subsequently decomposed to give a yellow solution with a large amount of a colourless precipitate forming, identified by single crystal X-ray diffraction to be (trop)$_2$, (**36**), as observed for the (tropN-*t*-Bu)$^-$, and tropDAD, (**37**), systems in their SmI_2 reactions. Whilst the identification of **36** from the SmI_2 reaction was not able to be confirmed, ^{1}H NMR spectroscopy of the reaction mixture was consistent with that for the YbI_2 case, suggesting that reductive cleavage of the tropylidene ligand had also occurred.

In order to avoid the reduction of the imine bond in [(tropNsal‡OLi)$_2$], (**43**), the reaction of the milder lanthanide(II) reagent EuI_2 with **43** was also attempted. However, as for the SmI_2 and YbI_2 reactions, a rapid colour change to orange was observed, followed by precipitation of a colourless solid, consistent with ligand reduction. ^{1}H NMR spectroscopy of the resulting solution was devoid of tropylidene proton resonances suggesting that the formation of insoluble (trop)$_2$, (**36**), had occurred.

The reaction of the lanthanide(III) reagent $SmBr_3$ with $[(tropNsal^{\ddagger}OLi)_2]$, (**43**), was also attempted. In this instance however, no reaction was observed after prolonged heating of a THF solution of $SmBr_3$ and $[(tropNsal^{\ddagger}OLi)_2]$, (**43**).

The reaction of $tropNsal^{\ddagger}OH$, (**42**), with *n*-BuLi in diethyl ether also gives $[(tropNsal^{\ddagger}OLi)_2]$, (**43**), in 90 % isolated yield when the reaction is carried out at -15 °C and *n*-BuLi is added dropwise. If the lithiation of $tropNsal^{\ddagger}OH$, (**42**), with *n*-BuLi is carried out at room temperature, a mixture of $[(tropNsal^{\ddagger}OLi)_2]$, (**43**), and a product of addition of *n*-BuLi across the imine C=N bond, $[\{tropN(H)(n\text{-}Bu)sal^{\ddagger}OLi\}_2]$, (**44**), results, as shown in Figure 6.29.

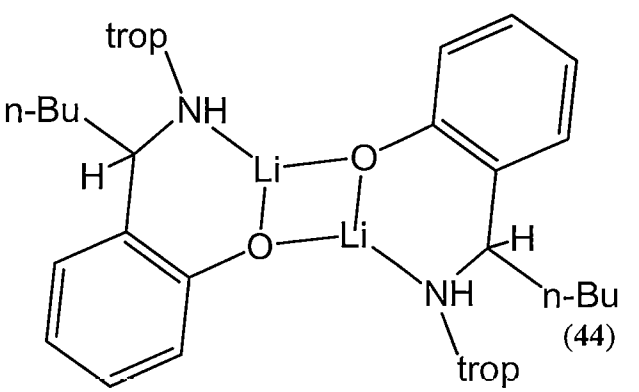

Figure 6.29. Two dimensional representation of the lithiated tropylidene $[\{tropN(H)(n\text{-}Bu)sal^{\ddagger}OLi\}_2]$, (**44**).

The isolation of $[\{tropN(H)(n\text{-}Bu)sal^{\ddagger}OLi\}_2]$, (**44**), possibly arises from lithiation of the phenol group followed by addition across the imine group and subsequent protonation by unreacted $tropNsal^{\ddagger}OH$, (**42**), assuming the phenol group is more reactive towards *n*-BuLi than the imine group, as shown in Scheme 6.5.

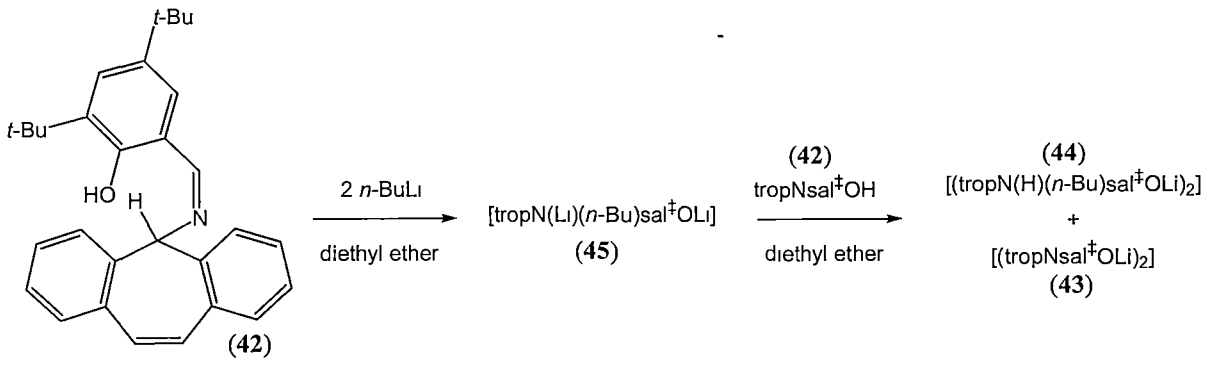

Scheme 6.5. Di-lithiation of tropNsal‡OH, (**42**), and proposed subsequent protonation to give the reduced lithiated tropylidene [{tropN(H)(*n*-Bu)sal‡OLi}$_2$], (**44**).

6.4.9. Molecular structure of [{tropN(H)(*n*-Bu)sal‡OLi}$_2$], (**44**).

Crystals of [{tropN(H)(*n*-Bu)sal‡OLi}$_2$], (**44**) suitable for single crystal X-ray diffraction studies were grown from a solution of **44** and [(tropNsal‡OLi)$_2$], (**43**), in 40-60 °C petroleum spirits left to stand at room temperature overnight. The crystals were found to belong to the triclinic space group, $P\bar{1}$ (No. 2), a = 11.41(1), b = 11.52(1), c = 13.18(1) Å, α = 96.51(5), β = 114.26(6), γ = 105.47(9) ° with 1 dimeric complex in the unit cell. The asymmetric unit consisted of one half of the dimeric [{tropN(H)(*n*-Bu)sal‡OLi}$_2$], (**44**). The molecular structure is shown in Figure 6.30.

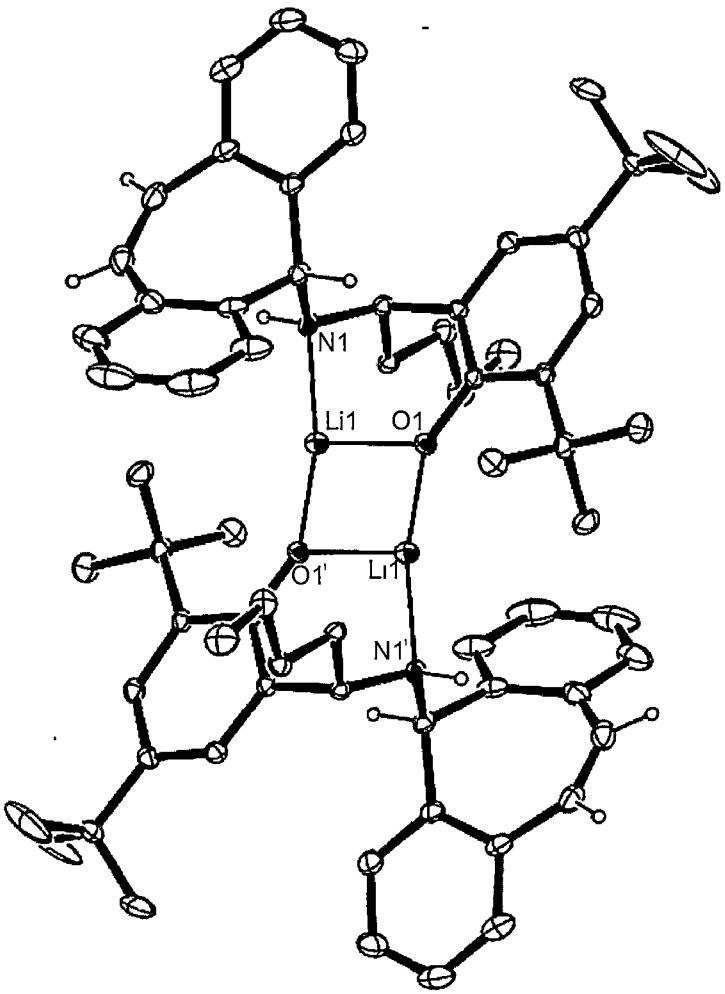

Figure 6.30. Molecular structure of the dimeric lithiated tropylidene [{tropN(H)(*n*-Bu)sal‡OLi}$_2$], (**44**). Thermal ellipsoids are shown at the 20 % level of probability. Only tropylidene and amine H atoms shown for clarity.

Analogous to [(tropNsal‡OLi)$_2$], (**43**), [{tropN(H)(*n*-Bu)sal‡OLi}$_2$], (**44**), forms an unsolvated dimer in the solid state, with a central Li_2O_2 core. However, the molecular structure of **44** differs substantially from **43** *via* the lack of any interaction between the alkenyl carbon atoms of the trop units and the lithium centres. The Li_2O_2 core in **44** differs from the butterflied Li_2O_2 core of **43**, by exhibiting a planar geometry with more obtuse Li–O–Li angles of 80.4(3) °, compared to those of **43** of 78.5(3) and 78.0(3) °, as shown in Figure 6.31. The Li1–O1' and Li–O1 interactions of **44** measuring 1.817(7) and 1.841(8) Å, respectively, are significantly shorter than those in **43** which range from

1.857(7) to 1.906(7) Å, as is expected for the 3-coordinate Li centres in **44**. The Li1-N1 interactions in **44** of 2.024(7) Å are consistent with those observed in **43** of 2.010(7) and 2.008(7) Å. The addition of the *n*-Bu substituent to the imine bond prevents the tropylidene moiety from binding with the Li centres through the alkenyl C atoms, as a *mer*-type arrangement as observed in **43** is not possible due to the sp^3 hybridisation of the N centres forcing the tropylidene unit away from the central Li_2O_2 core in order to facilitate chelation through the N centres. Consequently, the lower coordination number of the lithium centres in **44** results in a short Li···Me contact to the *t*-butyl substituent *ortho*- to the C–O bond of the aryloxide moiety (Li1···C(24)/H(24A) = $3.15_2/2.24_4$ Å respectively, H centre in calculated position), as the Li centres seek coordinative saturation. The C_1=C_2 bond length in **44** of 1.324(7) Å is consistent with that of the precursor ligand, tropNsal‡OH, (**42**), of 1.327(13) Å, and is again similar to that expected for an isolated alkene, as discussed in Section 6.1.3 and 6.3.3.

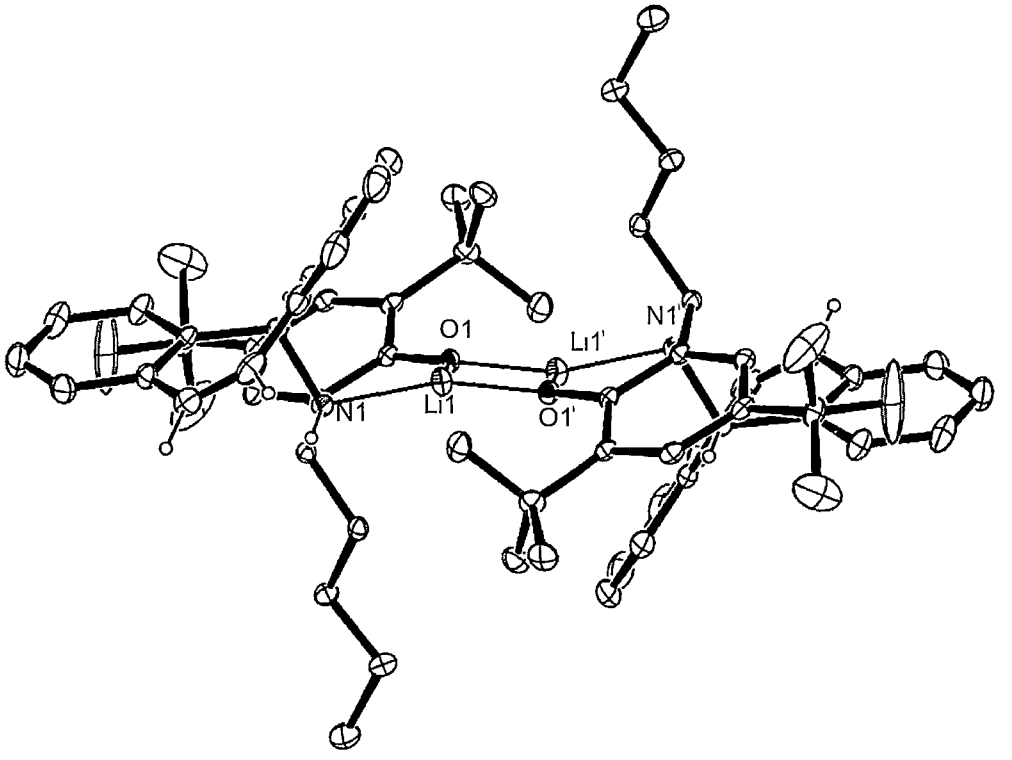

Figure 6.31. Molecular structure of [{tropN(H)(*n*-Bu)sal‡OLi}$_2$], (**44**). Side view demonstrating the planar Li_2O_2 core and arrangement of the *n*-Bu substituents. Thermal ellipsoids are shown at the 20 % level of probability. Only tropylidene and amine H atoms shown for clarity.

6.5. Experimental

tropOH, (**31**)

tropOH, (**31**), was prepared according to a modified literature procedure.[30]

$NaBH_4$ (2.08 g, 55.0 mmol) was added to a stirred solution of dibenzosuberenone (10.0 g, 48.5 mmol) in methanol (600 mL) under argon. The solution was left stirring for 14 hours, before 10 mL H_2O was added. MeOH and H_2O were removed *in vacuo* to leave a crude white solid which was extracted with diethyl ether (350 mL). The ethereal extract was then washed with saturated NaCl(*aq*) and dried with Na_2CO_3. The solution was then concentrated to 100 mL and an equal volume of petroleum spirit was added. Cooling to -17 °C yielded needles of **31** (9.16 g, 91 %).

^{1}H NMR ($CDCl_3$, 299.905 MHz, 25 °C, ppm):δ 2.54 (s, 1H, 5-CH), 5.41 (s, 1H, 5-CH), 7.11 (s, 2H, HC=), 7.22-7.42 (m, 6H, Ar-CH), 7.65 (d, 2H, Ar-CH)

tropCl, (**32**)

tropCl, (**32**) was prepared according to a modified literature procedure.[31]

$SOCl_2$ (6 mL) was added dropwise to a stirred flask containing 5H-dibenzo[a,d]cyclohepten-5-ol, (**31**) (2.75 g, 13.2 mmol). The resulting red solution was refluxed for 40 minutes before $SOCl_2$ was removed *in vacuo* to leave **32** as a crude white solid, which was washed with 40-60 °C petroleum spirits and dried *in vacuo* to give **32** as a pure white solid, 2.20 g, 74 %.

tropNH$_2$, (**29**)

tropNH$_2$, (**29**) was prepared according to a modified literature procedure.[19k]

To a flask containing 5-chloro-5H-dibenzo[a,d]cycloheptene, (**32**), at –78 °C, $NH_3(g)$ was condensed to give 10 mL of $NH_3(l)$. The resulting solution was then stirred at –78 °C for 2 hours before being left to warm to room temperature, liberating excess NH_3. 5H-Dibenzo[a,d]cyclohepten-5-yl)amine, (**29**), was then dissolved in diethyl ether, (100 mL), and filtered from NH_4Cl. Solvent was then removed *in vacuo* to leave 20 mL of a concentrated solution to which petroleum spirit 40-60 °C (100 mL) was added. Cooling to –10 °C for 12 hours gave **29** as a crystalline light brown solid (3.6 g from 4.14 g of alcohol precursor (**31**), 87 %).

^{1}H NMR ($CDCl_3$, 299.905 MHz, 25 °C, ppm):δ 4.58 (broad, s, 1H, trop-5-CH), 5.08 (broad, s, 1H, trop-5-CH), 7.06 (s, 4H, Ar-CH), 7.20-7.65 (m, 6H, Ar-CH and HC=).

Anal. Cald.: C, 86.92; H, 6.32; N, 6.76 ($C_{15}H_{13}N$, MW 207.27)
Found: C, 86.66; H, 6.62; N, 6.65

tropN(H)-*t*-Bu, (**30**)

t-butyl amine, (18 mL, 0.17 mol) was added dropwise with stirring to a flask containing tropCl, (32), (6.0 g, 27 mmol). The resulting suspension was stirred for 2 hours before excess *t*-butyl amine was removed *in vacuo*. tropN(H)-*t*-Bu, (**30**), was then extracted with diethyl ether (3 x 50 mL), and filtered from *t*-$BuNH_3Cl$ before diethyl ether was removed *in vacuo* to leave **30** as a crude yellow oil. Recrystallisation from petroleum spirit 40-60 °C at –17 °C gave **30** as a pure white solid (6.38 g from 6.09 g of alcohol precursor (**31**), 83 %).

^{1}H NMR ($CDCl_3$, 299.905 MHz, 25 °C, ppm): δ 0.91 (s, 9H, CH_3 (73% isomer), 1.03 (s, 9H, CH_3 (27% isomer), 4.21 (s, 1H, trop-5-CH (27% isomer), 5.07 (s, 1H, trop-5-CH(73% isomer), 7.08 – 7.70 (m, 10H, Ar-CH and HC=).

^{13}C{^{1}H} NMR ($CDCl_3$, 75.417 MHz, 25 °C, ppm): δ 30.04 (73% CH_3), 30.25 (27% CH_3), 54.96 (CCH_3), 64.40 (trop-5-CH), 122.81 (Ar-CH), 125.39 (Ar-C), 127.40 (Ar-C), 129.03 (Ar-C), 130.02 (Ar-C), 131.17 (Ar-CH), 131.43 (Ar-CH), 133.67 (Ar-C).

Anal. Calcd.: C, 86.65; H, 8.04; N, 5.32 ($C_{19}H_{21}N$, MW 263.38)
Found: C, 86.48; H, 8.11; N, 5.14

tropDAD, (**37**)

tropDAD, (**37**), was prepared according to a modified literature procedure.[19g]

To a stirred flask containing $tropNH_2$, (**29**), (3.48 g, 17 mmol) and glyoxal (0.9 mL of 40 % aqueous solution) in ethanol (5 mL), was added formic acid, (3 drops). The resulting suspension was stirred for 12 hours before being filtered to give **37** as a crude white solid. Recrystallisation from toluene (250 mL) gave **37** as a crystalline white solid (3.14 g, 85 %)

^{1}H NMR (C_6D_6, 299.905 MHz, 25 °C, ppm): δ 4.77 (broad, s, 2H, CH=N), 6.88 (s, 4H, =CH), 6.93-7.4 (m, 16H, Ar-CH), 7.83 (broad, s, 2H, N=CH).

tropacacH, (**39**)

To a stirred flask containing tropNH$_2$, (**29**), (0.40 g, 1.9 mmol) and 2,4-pentanedione (0.25 mL, 2.4 mmol) in ethanol, (4 mL) was added concentrated HCl(*aq*) (2 drops). The resulting solution was then refluxed for 72 hours before ethanol was removed *in vacuo* to leave **39** as a crude white solid. Dichloromethane (5 mL) was added and the resulting solution washed with saturated NaHCO$_3$(*aq*). Dichloromethane was removed *in vacuo* before **39** was recrystallised from methanol to yield white crystals of **39**, (0.38 g, 68 %).

^{1}H NMR ($CDCl_3$, 299.905 MHz, 25 °C, ppm): δ 1.83 (s, 6H, CH_3), 4.76 (d, 1H, ac-CH), 4.87 (d, 1H, trop-5-CH), 7.04 (s, 2H, HC=), 7.23 – 7.34 (m, 8H, Ar-H).

^{13}C{^{1}H} NMR ($CDCl_3$, 75.417 MHz, 25 °C, ppm): δ 30.58 (CH_3), 53.89 (trop-5-CH), 65.98 (ac-CH), 127.36 (Ar-CH), 129.38 (Ar-CH), 129.97 (Ar-CH), 130.70 (Ar-CH), 131.49 (CH=CH), 134.30 (Ar-C), 136.53 (Ar-C), 202.72 (C=O).

Anal. Calcd.: C, 82.73; H, 6.25; N, 0.0 ($C_{20}H_{18}O_2$, MW 290.36)
Found: C, 82.49; H, 6.45; N, 0.0

tropNsalOH, (41)

To a stirred flask containing tropNH$_2$, (**29**), (3.0 g, 14.6 mmol) in water (50 mL) was added 1-hydroxybenzaldehyde (1.5 mL, 1.83 g, 15 mmol). The resulting suspension was then stirred at room temperature for 2 hours before the resulting yellow precipitate was extracted in diethyl ether. The ethereal extract was then dried over Na_2CO_3 and filtered before ether was removed *in vacuo*. Recrystallisation from methanol:diethyl ether, 50:50 gave **41** as a yellow solid (2.9 g, 64 %).

^{1}H NMR ($CDCl_3$, 299.905 MHz, 25 °C, ppm): δ 4.98 (broad, s, 1H, trop-5-CH), 6.83 (broad, s, 2H, HC=), 7.07 – 7.47 (broad, m, 10H, Ar-H), 7.55 (broad, d, 2H, Ar-H), 8.38 (broad, s, 1H, HC=N).

tropNsal‡OH, (**42**)

To a stirred flask containing tropNH$_2$, (**29**), (1.2 g, 5.8 mmol) in water (50 mL) was added 1-hydroxy-2,4-di-*t*-butylbenzaldehyde, (1.37 g, 5.8 mmol). The resulting suspension was then stirred at 60 °C for 4 hours before the resulting yellow solid was

extracted in petroleum spirits 40-60 °C, (20 mL). **42** was then isolated as a crystalline yellow solid *via* slow evaporation of solvent at room temperature (2.1 g, 86 %).

^{1}H NMR ($CDCl_3$, 299.905 MHz, 25 °C, ppm): δ 1.27 (s, 9H, CH_3), 1.50 (s, 9H, CH_3), 5.06 (broad, s, 1H, trop-5-H), 7.04 (s, 2H, HC=), 7.14 (s, 2H, Ar-H), 7.27 (m, 2H, Ar-H), 7.37 (m, 4H, Ar-H), 7.56 (broad, s, 2H, Ar-H), 8.39 (broad, s, 1H, HC=N).

^{13}C{^{1}H} NMR ($CDCl_3$, 75.417 MHz, 25 °C, ppm): δ 29.70 (CH_3), 29.95 (CCH_3), 31.56 (CH_3), 35.35 (CCH_3), 118.80 (trop-5-CH), 127.33 (Ar-*C*CH), 127.59 (Ar-CH), 127.91 (Ar-CH), 128.23 (Ar-CH), 128.96 (Ar-*C*CH), 131.47 (Ar-CH) 169.60 (C=N).

Anal. Calcd.: C, 85.06; H, 7.85; N, 3.31 ($C_{30}H_{33}NO$ MW 423.59)

Found: C, 84.91; H, 7.95; N, 3.31

$(trop)_2$, (**36**)

To a stirred flask containing SmI_2 (0.1 M in THF, 80 mL, 8.0 mmol), a solution of tropCl, (**32**), (1.81 g, 8.0 mmol) in THF (30 mL), was added dropwise resulting in a distinct colour change from blue to orange. Water (5 mL) was added and the resulting white precipitate was collected by filtration. Sublimation at 3.1 x 10^{-2} Torr and 130 °C yielded white crystals of **32** (1.13 g, 74 %).

Anal. Calcd.: C, 94.20; H, 5.80 ($C_{30}H_{22}$, MW 382.50)

Found: C, 93.63; H, 6.08

[{tropN(*t*-Bu)Li}$_2$OEt$_2$], (**34**)

To a stirred flask containing tropN(H)-*t*-Bu, (**30**), (5.0 g, 19 mmol) in diethyl ether, (100 mL) was added a solution of MeLi (1.4 M in diethyl ether, 16 mL, 22 mmol). The solution was then stirred for 5 hours before being cooled to –17 °C overnight to yield **34** as a crystalline red solid, 3.6 g, 62 %.

^{1}H NMR (C_6D_6, 299.905 MHz, 25 °C, ppm): δ 0.47 (s, 18H, CH_3), 1.05 (t, 6H, Et_2O CH_3), 3.20 (q, 4H, Et_2O CH_2), 5.48 (s, 2H, trop 5-CH), 6.8-7.4 (broad, m, 20H, Ar-CH).

^{13}C{^{1}H} NMR (C_6D_6, 75.417 MHz, 25 °C, ppm): δ 15.28 (Et_2O CH_3), 32.13 (CH_3), 53.32 (CCH_3), 72.57 (trop-5-CH), 125.53 (Ar-CH), 129.12 (Ar-CH), 129.88 (Ar-CH), 130.14 (Ar-CH), 130.92 (Ar-C), 131.24 (Ar-C).

Anal. Calcd.: C, 82.33; H, 8.22; N, 4.57(MW 423.59, $C_{42}H_{50}N_2Li_2O$)

Found: C, 81.37; H, 8.44; N, 4.27

[(tropNsal‡OLi)$_2$], (**43**)

To a stirred solution of tropNsal‡OH, (**42**), (0.522 g, 1.2 mmol) in diethylether (15 mL) at 0 °C, was added dropwise, a suspension of lithiumdiisopropylamide (0.132 g, 1.2 mmol) in diethylether (10 mL). The resulting solution was then allowed to warm to room temperature and was stirred for a further 3 hours before being let stand overnight, after which time white crystals of **43** had precipitated from the red solution. The ethereal solution was removed *via* cannula, and the white crystals were washed with petroleum spirit 40-60 °C (2 x 5 mL) and dried in *vacuo* (0.45 g, 86 %).

^{1}H NMR (C_6D_6, 299.905 MHz, 25 °C, ppm): δ 1.37 (s, 9H, CH_3), 1.41 (s, 9H, CH_3), 5.05 (s, 1H, trop-5-CH), 6.50 (broad, s, 1H, =CH), 6.56 (broad, s, 1H, =CH) 6.85 (broad, s, 2H, Ar-H), 6.92 (m, 3H, Ar-H), 7.03, (d, ^{2}J = 12 Hz, 2H, Ar-H), 7.12, (broad, s, 2H, Ar-H), 7.56 (d, 1H, Ar-H), 8.00 (s, 1H, N=CH).

^{13}C{^{1}H} NMR (C_6D_6, 75.417 MHz, 25 °C, ppm): δ 31.91 (*C*CH_3), 128.89 (Ar-*C*CH), 129.04 (Ar-CCH), 131.54 (Ar-*C*CH), 133.88 (Ar-C), 139.93 (Ar-*C*), 140.47 (Ar-*C*CCH_3).

Anal. Calcd: C, 83.89; H, 7.51; N, 3.26 (MW 859.04, $C_{60}H_{64}Li_2N_2O_2$)
Found: C, 82.92; H, 7.88; N, 3.16

[{tropN(H)(*n*-Bu)sal‡OLi}$_2$], (**44**)

To a stirred flask containing tropNsal‡OH, (**42**), (0.70 g, 1.6 mmol) in petroleum spirit 40-60 °C (30 mL) was added dropwise *n*-BuLi (1.6 M in hexanes, 1.1 ml, 1.8 mmol). The solution was then stirred at room temperature for 30 minutes before being let stand for 72 hours, after which period white crystals of a mixture of **43** and **44** were isolated (0.55 g). ^{1}H NMR showed a product ratio of 6:1, [(tropNsal‡OLi)$_2$], (**43**) to [{tropN(H)C(*n*-Bu)sal‡OLi}$_2$], (**44**).

^{1}H NMR (C_6D_6, 299.905 MHz, 25 °C, ppm): δ 0.81 (t, 3H, CH_3), 1.14-1.62 (broad, m, 9H, n-Bu), 1.42 (s, 9H, CH_3), 1.52 (s, 9H, CH_3), 4.90 (s, 1H, trop-5-CH), 6.40-7.06 (m, Ar-CH), 7.52 (s, 1H, Ar-H).

6.6. References

1. Deacon, G.B.; Shen, Q. *J. Organomet. Chem.* **1996**, *511*, 1.
2. a) Watson, P.L.; Parshall, G.W. *Acc. Chem. Res.* **1985**, *18*, 51,
   b) Cornehl, H.H.; Heinemann, C.; Schröder, D.; Schwarz, H.
   Organometallics **1995**, *14*, 992,
   c) Evans, W.J.; Coleson, K.M.; Engerer, S.C. *Inorg. Chem.* **1981**, *20*, 4320,
   d) Evans, W.J.; Bloom, I.; Hunter, W.E.; Atwood, J.L.
   J. Am. Chem. Soc. **1981**, *103*, 6507,
   e) Evans, W.J.; DeCoster, D.M.; Greaves, J. *Organometallics* **1996**, *15*, 3210,
   f) Evans, W.J.; DeCoster, D.M.; Greaves, J. *Macromolecules* **1995**, *28*, 7929,
   g) Jeske, G.; Schock, L.E.; Swepstone, P.N.; Schumann, H.; Marks, T. J.
   J. Am. Chem. Soc. **1985**, *107*, 8103,
   h) Evans, W. J.; Ulibarri, T.A.; Chamberlain, L.R.; Ziller, J.W.; Alvarez, D.,
   Junior *Organometallics* **1990**, *9*, 2124,
   i) Yasuda, H.; Ihara, E. *Adv. Polym. Sci.* **1997**, *133*, 53,
   j) Boffa, L.S.; Novak, B.M. *Macromolecules* **1997**, *30*, 3494,
   k) Evans, W.J.; Giarikos, D.G.; Ziller, J. W. *Organometallics* **2001**, *20*, 5751.
3. Burns, C.J.; Andersen, R.A. *J. Am. Chem. Soc* **1987**, *109*, 915.
4. Nolan, S.P.; Stern, D.; Marks, T.J. *J. Am. Chem. Soc.* **1989**, *111*, 7844.
5. Casey, C.P.; Hallenbeck, S.L.; Pollock, D.W.; Landis, C.R.
   J. Am. Chem. Soc. **1995**,*117*, 9770.
6. Evans, W.J.; Ulibarri, T.A.; Ziller, J.W. *J. Am. Chem. Soc.* **1990**, *112*, 219.
7. Campazzi, E.; Solari, E.; Scopelliti, R.; Floriani, C. *Chem. Commun.* **1999**, 1617.
8. Lin, J.; Wang, Z. *J. Organomet. Chem.* **1999**, *589*, 127.
9. a) Schumann, H.; Heim, A.; Demtschuk, J.; Mühle, S.H.
   Organometallics **2002**, *21*, 3323,
   b) Schumann, H.; Heim, A.; Demtschuk, J.; Mühle, S.H.
   Organometallics **2003**, *22*, 118,
   c) Schumann, H.; Schutte, S.; Kroth, H.-J.; Lentz, D.
   Angew. Chem. Int. Ed. Engl. **2004**, *43*, 6208.

10. Evans, W.J.; Perotti, J.M.; Brady, J.C.; Ziller, J.W.
J. Am. Chem. Soc. **2003**, *125*, 5204.
11. Schumann, H.; Heim, A.; Schutte, S.; Lentz, D. *Z.*
Anorg. Allg. Chem. **2006**, *632*, 1939.
12. Treibs, W.; Klinkhammer, H. J. *Chem. Ber.* **1951**, *84*, 671.
13. Weitzenbock, R. *Monatshefte fuer Chemie* **1913**, *34*, 193.
14. Missir, A.; Limban, C.; Stecoza, C.; Morusciag, L.; Chirita, I.
Farmacia (Bucharest) **1998**, *46*, 17.
15. Thomaier, J.; Boulmaáz, S.; Schönberg, H.; Rüegger, H.; Currao, A.;
Grützmacher, H.; Hillebrecht, H.; Pritzkow, H. *New J. Chem.* **1998**, 947.
16. Klosin, J.; Abboud, K.A.; Jones, W.M. *Organometallics* **1995**, *14*, 2892.
17. Tamm, M.; Jentzsch, T.; Werncke, W. *Organometallics* **1997**, *16*, 1418.
18. Schönberg, H.; Boulmaâz, S.; Wörle, M.; Liesum, L.; Schweiger, A.;
Grützmacher, H. *Angew. Chem. Int. Ed.* **1998**, *37*, 1423.
19. a) Boulmaâz, S.; Mlakar, M.; Loss, S.; Schönberg, H.; Deblon, S.; Wörle, M.;
Nespera, R.; Grützmacher H. *Chem. Commun.* **1998**, 2623.
b) Liedtke, J.; Loss, S.; Alcaraz, G.; Gramlich, V.; Grützmacher, H.
Angew. Chem. Int. Ed. **1999**, *38*, 1623.
c) Liedtke, J.; Loss, S.; Widauer, C.; Grützmacher, H.
Tetrahedron **2000**, *56*, 143.
d) Deblon, S.; Rüegger, H.; Schönberg, H.; Loss, S.; Gramlich, V.; Grützmacher,
H. *New J. Chem.* **2001**, *25*, 83.
e) Deblon, S.; Liesum, L.; Harmer, J.; Schönberg, S.; Schweiger, A.;
Grützmacher, H. *Chem. Eur. J.* **2002**, *8*, 601.
f) Laporte, C.; Böhler, C.; Schönberg, H.; Grützmacher, H.
J. Organomet. Chem. **2002**, *641*, 1.
g) C. Böhler, D. Stein, N. Donati, H. Grützmacher,
New. J. Chem. **2002**, *26*, 1291.
h) Geier, J.; Frison, G.; Grützmacher, H. *Angew. Chem. Int. Ed.* **2003**, *42*, 3955.
i) Breher, F.; Böhler, C.; Frison, G.; Harmer, J.; Liesum, L.; Schweiger, A.;
Grützmacher, H. *Chem. Eur. J.* **2003**, *9*, 3859.

j) Laporte, C.; Breher, F.; Geier, J.; Harmer, J.; Schweiger, A.; Grützmacher, H. *Angew. Chem. Int. Ed.* **2004**, *43*, 2567.

k) Büttner, T.; Breher, F.; Grützmacher, H. *Chem. Commun.* **2004**, 2820.

l) Breher, F.; Rüegger, H.; Mlakar, M.; Rudolph, M.; Deblon, S.; Schönberg, H.; Boulmaáz, S.; Thomaier, J.; Grützmacher, H. *Chem. Eur. J.* **2004**, *10*, 641.

m) Laporte, C.; Büttner, T.; Rüegger, H.; Geier, J.; Schönberg, H.; Grutzmacher, H. *Inorg. Chim. Acta* **2004**, *357*, 1931.

n) Maire, P.; Breher, F.; Schönberg, H.; Grützmacher, H. *Organometallics* **2005**, *24*, 3207.

o) Büttner, T.; Geier, J.; Frison, G.; Harmer, J.; Calle, C.; Schweiger, A.; Schönberg, H.; Grützmacher, H. *Science* **2005**, *307*, 235.

p) Maire, P.; Breher, F.; Grützmacher, H. *Angew. Chem. Int. Ed.* **2005**, *44*, 6325.

20. Hjelmencrantz, A.; Friberg, A.; Berg, U. *Perkin 2* **2000**, 1293.
21. Ibberson, R.M.; David, W.I.F.; Prager, M. *J. Chem. Soc., Chem. Commun.* **1992**, 1438.
22. Romesberg, F.E.; Gilchrist, J.H.; Harrison, A.T.; Fuller, D.J.; Collum, D.B. *J. Am. Chem. Soc.* **1991**, *113*, 5751.
23. Lappert, M.F.; Slade, M.J.; Singh, A.; Atwood, J.L.; Rogers, R.D.; Shakir, R. *J. Am. Chem. Soc.* **1983**, *105*, 302.
24. Fraenkel, G.; Chow, A.; Fleischer, R.; Liu, H. *J. Am. Chem. Soc.* **2004**, *126*, 3983
25. Stender, M.; Wright, R.J.; Eichler, B.E.; Prust, J.; Olmstead, M.M.; Roesky, H.W.; Power, P.P. *J. Chem. Soc., Dalton Trans.* **2001**, 3465.
26. Petricek, S. *Polyhedron* **2004**, *23*, 2293.
27. Simion, A.; Simion, C.; Kanda, T.; Nagashima, S.; Mitoma, Y.; Yamada, T.; Mimura, K.; Tashiro, M. *J. Chem. Soc., Perkin Trans.* **2001**, 2071.
28. Ball, L.J.; Dickie, A.P.; Mair, F.S.; Middleton, D.A.; Pritchard, R.G. *Chem. Commun.* **2003**, 744.
29. a) Brehon, M.; Cope, E.K.; Mair, F.S.; Nolan, P.; O'Brien, J.E.; Pritchard, R.G.; Wilcock, D.J. *J. Chem. Soc. Dalton Trans.* **1997**, 3421,

b) Wang, Z.G.; Sun, H.M.; Yao, H.S.; Yao, Y.M.; Shen, Q.; Zhang, Y.

J. Organomet. Chem. **2006**, *691*, 3383,

c) Ghazar, A.; Gambarotta, S.; Yap, G.P.A. *Private Communication* **2000**, CCDC 140579.

30. Pavia, M. R. *Eur. Pat. Appl.* **1989**, 346927.
31. Arya, V. P.; David, J.; Fernandes, F.; Gorhe, D. S.; Grewal, R. S.; Oza, S. D.; Shenoy, S. J. *Indian J. Chem.* **1978**, *16B*, 220.

Chapter 7. Conclusion

7.1. Concluding remarks.

7.1.1. Overview

The work described in this thesis constitutes the most exhaustive study of synthetic routes to monomeric lanthanide imides reported, with numerous complexes of the deprotonated *meso*-octaethyl-*trans*-dioxaporphyrinogen ligand synthesised and characterised by single crystal X-ray diffraction, ^{1}H and ^{13}C NMR spectroscopy and microanalytic studies. The theoretical studies of the macrocyclic imide and amide model complexes extend the previous limited study of lanthanide imides, and represents the first report of theoretical studies of the bonding present in lanthanide pyrrolide complexes. The synthesis of numerous dibenzotropylidene based compounds and their subsequent lithiated complexes has demonstrated the limited applicability of this ligand type in organolanthanide chemistry.

7.1.2. Macrocyclic samarium(II) based reductions.

Chapter 2 described the synthesis of the samarium(II) complex, $[\{(C_6H_5Me)K(Et_8N_2O_2)Sm(\mu\text{-}I)\}_2]$, (**7**), and the samarium(III) complexes, $[\{(Et_8N_2O_2)Sm(\mu\text{-}I)\}_2]$, (**8**), and $[\{(Et_8N_2O_2)Sm(\mu\text{-}Br)\}_2]$, (**9**). Each complex exhibited different structural features in the solid state, with the samarium(II) complex incorporating KI to form an iodide bridged dimeric structure. The samarium(III) complexes **8** and **9** both formed halide bridged, Group 1 metal free dimeric structural motifs, however, the smaller bridging bromide centres in **9** enforced an offset geometry in the opposing macrocyclic ligands in order to minimise steric interactions. The synthesis of $[\{(Et_8N_2O_2)Sm(\mu\text{-}Br)\}_2]$, (**9**), from the metathesis reaction of $[\{(Et_8N_2O_2)K_2(C_6H_5Me)\}_n]$, (**5**) with $SmBr_3$ represents the first direct synthesis of a lanthanide(III) complex of this ligand from a lanthanide(III) reagent and suggests that the range of lanthanide complexes available to the *meso*-octaethyl-*trans*-dioxaporphyrinogen ligand may be extended in future studies.

The reactivity of $[\{(C_6H_5Me)K(Et_8N_2O_2)Sm(\mu\text{-}I)\}_2]$, (**7**), with numerous dinitrogen containing substrates are described in Chapter 3. These have demonstrated the differing reactivity trends observed between the macrocyclic samarium(II) system and the ubiquitous decamethylsamarocene. The reduced azo complexes

$[(Et_8N_2O_2)Sm\{\eta^2\text{-}N_2(Mes)_2\}]$, (**10**), and $[(Et_8N_2O_2)Sm(\eta^2\text{-}N_2Ph_2)]$, (**12**), exhibited similar solid-state structures with η^2 bonding observed between the samarium centre and azo ligands. Further reduction of the azo moiety in either complex to form a bridging dianion was not observed, which allows a comparison of the available coordination sphere of the samarium centre in complexes of the macrocyclic porphyrinogen system to that with the ubiquitous bis(pentamethylcyclopentadienyl) ligand set.[1] ^{1}H NMR spectroscopy of each azo complex was able to be achieved despite the radical nature of the reduced azo ligand. The differing steric bulk of the two azo moieties in **10** and **12** resulted in substantial differences in the resulting NMR spectra, with the mesityl complex **12** exhibiting a decrease in macrocyclic symmetry with respect to the phenyl complex **10** from C_{2v} to C_2 on the NMR time scale.

7.1.3. Macrocyclic samarium(III) amides.

The synthesis and characterisation of the bis(amide) complexes, $[(THF)_2K(Et_8N_2O_2)Sm\{N(H)Mes\}_2]$, (**17**), and $[\{\text{-}\mu\text{-}\eta^1\text{:}\eta^3\text{-}\{N(H)Mes\}K(Et_8N_2O_2)SmN(H)Mes\}_n]$, (**18**), described in Chapter 4 revealed differing structural motifs dependent on the presence of a Lewis base solvent to coordinate with the potassium counter-ion in the base of the macrocyclic cavity. In the absence of Lewis basic solvents, a polymeric bridging interaction in the solid state was favoured over the terminal binding of an aromatic solvent molecule to the Group 1 cation analogous to $[\{(C_6H_5Me)K(Et_8N_2O_2)Sm(\mu\text{-}I)\}_2]$, (**7**). The ^{1}H NMR spectra of **17** exhibited fluxionality in the solution state, which upon cooling to -50 °C, allowed the observation of symmetry loss in the complex to C_2, analogous to the mesityl substituted azo complex, $[(Et_8N_2O_2)Sm\{\eta^2\text{-}N_2(Mes)_2\}]$, (**10**).

The observed preference for bis(amide) formation in the reaction of $[\{(Et_8N_2O_2)Sm(\mu\text{-}I)\}_2]$, (**8**), with Group 1 metal amides was observed to be dependent on both the steric bulk of the amide substrate and the size of the Group 1 metal used. Hence, the directed synthesis of the mono(amide) complexes $[(Et_8N_2O_2)Sm\{N(H)(C_6H_2\text{-}2,4,6\text{-}t\text{-}Bu)\}]$, (**21**), and $[\{(Et_8N_2O_2)SmN(H)Mes]$, (**20**) was able to be achieved utilising the greater steric bulk of the 2,4,6-tri-*t*-Bu-anilide ligand as compared to the mesityl amide ligand for the former complex, and the

smaller size of the Li counter-ion in place of K in the Group 1 mesityl amide reagent for the latter complex.

The reactivity of the mono- and bis(amide) complexes **21**, **20**, **17** and **18** towards base did not yield the targeted imido species, with the metal exchange product $[(Et_8N_2O_2)K_2(solvent)_n]$ observed in all cases.

^1H and ^{13}C NMR spectroscopy of complexes **8** to **21** was able to be achieved in spite of the paramagnetic nature of the samarium(II) and (III) centres present in each complex. The observed chemical shift range of the ^1H resonances of the samarium complexes of the *meso*-octaethyl-*trans*-dioxaporphyrinogen ligand was found to be dependent on the presence or absence of a Group 1 metal cation in the base of the macrocyclic cavity.

7.1.4. Theoretical studies.

DFT studies of the model amide and imide complexes in Chapter 5 have revealed significant covalent interactions involving the samarium centre which supports recent studies into covalency in lanthanide amide and imide interactions. The theoretical method was shown to accurately reproduce the experimental geometries of synthetic amide and imide complexes and also accurately predicted the stability of bis(amide) complexes over imide formation.

The stabilisation of the imido nitrogen centre in the model imide complex has been shown to involve samarium 5d orbitals, at the expense of interactions between the macrocycle and samarium centre. Coupled with the isolation of $[\{(Et_8N_2O_2)K_2(C_6H_5Me)\}_n]$, (**5**), from the reaction of $[(THF)_2K(Et_8N_2O_2)Sm(N(H)Mes)_2]$, (**6**), with mesityl azide, as described in Chapter 3, the weakening of the macrocycle-samarium interactions in the model imide complex suggest that some of the difficulties observed in the isolation of a terminal lanthanide imide complex stabilised by the macrocyclic porphyrinogen ligand may be due to ligand displacement resulting from the competitive stabilisation of the imido nitrogen centre. This result provides some insight into the problems faced by lanthanide elements in stabilising terminal imide moieties and is consistent with

experimental observations of lanthanide imides requiring (to date) bridging μ^2-μ^4 interactions with multiple metal centres stabilising the imido nitrogen centre.[2]

7.1.5. Tropylidene chemistry.

The synthesis of the novel dibenzotropylidene ligands tropN(H)-*t*-Bu, (**30**), tropNsalOH, (**41**), and tropNsal‡OH, (**42**), and characterisation of these and other related tropylidenes *via* single crystal X-ray diffraction, NMR spectroscopic and microanalytic studies was achieved. The subsequent Group 1 chemistry of these compounds was explored yielding the lithiated dimeric complexes of tropylidene substituted amide and aryloxide, [(tropN(*t*-Bu)Li)$_2$OEt$_2$], (**34**), and [(tropNsal‡OLi)$_2$], (**43**), which were able to be isolated and characterised by single crystal X-ray diffraction, NMR spectroscopic and microanalytic studies. The tropylidene ligand in both complexes exhibited a chelating binding mode with interactions observed between the Li centres and the alkenyl carbon atoms of the tropylidene ligand, demonstrating the suitability of the tropylidene ligand for promoting alkenyl interactions. The lithiated tropylidene [{tropN(H)(*n*-Bu)sal‡OLi}$_2$], (**44**), was also observed, presumably resulting from the addition of *n*-BuLi across the imine bond. Alkenyl-Li interactions were not observed in the solidstate structure of **44**, resulting from the sp^3 hybridisation of the former imine N centre. Instability in the C-N bond off the 5-position of the tropylidene unit was observed in the Group 1 metal studies of a number of the tropylidene ligands and was found to be accentuated by reaction with lanthanide(II) reagents, limiting the suitability of these tropylidene based ligands in further organolanthanide studies.

^{1}H NMR spectroscopy of the metallated tropylidenes revealed fluxional processes on the NMR timescale, consistent with previous studies of dimeric lithium complexes which exhibited equilibria between open and closed dimeric structures.[3] The hetero-atom in each tropylidene ligand was observed to adopt the *pseudo*-axial position in solution when metallated, in order to facilitate metal-alkenyl interactions.

7.2. References

1. Evans, W.J.; Drummond, D.K.; Chamberlain, L.R.; Doedens, R.J.; Bott, S.G.; Zhang, H.; Atwood, J.L. *J. Am. Chem. Soc.* **1988**, *110*, 4983.
2. a) Emel'Yanova, N.S.; Bochkarev, M.N.; Schumann, H.; Loebel, J.; Esser, L. *Koord. Khim.* **1994**, *20*, 789,
   b) Trifonov, A.A.; Bochkarev, M.N.; Schumann, H; Loebel, J. *Angew. Chem., Int. Ed. Engl.* **1991**, *30*, 1149,
   c) Xie, Z.; Wang, S.; Yang, Q.; Mak, T. *Organometallics* **1999**, *18*, 1578,
   d) Wang, S.; Yang, Q.; Mak, T.; Xia, Z. *Organometallics* **1999**, *18*, 5511,
   e) Cui, D.; Nishiura, M.; Hou, Z. *Angew. Chem. Int. Ed.* **2005**, *44*, 959,
   f) Gordon, J.C.; Giesbrecht, G.R.; Clark, D.L.; Hay, P.J.; Keogh, D.W.; Poli, R.; Scott, B.L.; Watkin, J.G. *Organometallics* **2002**, *21*, 4726,
   g) Chan, H.S.; Li, H.W.; Xie, Z. *Chem. Commun.* **2002**, 652.
3. Romesberg, F.E.; Gilchrist, J.H.; Harrison, A.T.; Fuller, D.J.; Collum, D.B. *J. Am. Chem. Soc.* **1991**, *113*, 5751.

A1 Synthetic Considerations

Unless otherwise stated all manipulations were caried out under an argon atmosphere (high puriity) using standard Schlenk techniques. Solvents used in the preparation of complexes were of analytical grade and were dried over Na or Na/K or by an Innovative Technologies solvent purification system employing activated alumina, copper catalyst or molecular sieve purification cartridges. Storage and preparation of complexes for analyses were undertaken using a dry atmosphere glove box (Innovative Technologies) fitted with O_2 (CuO), H_2O (molecular sieve) and solvent (activated charcoal) removal columns, filled with a pre-dried, recirculating atmosphere of high purity nitrogen. All chemicals used in the preparation of organic pre-cursors were used as received from Aldrich.

NMR spectra were recorded in $CDCl_3$ or appropriately dried C_6D_6, THF-d^8 or toluene-d^8 using a Varian Gemini Mercury Plus spectrometer operating at 299.905 Hz. GC/MS spectra were performed using a Varian 3800 gas chromatograph equipped with a Varian 1200 quadrupole MS. Elemental analyses were performed by the Central Science Laboratory, University of Tasmania using a Thermo Finnigan EA 1112 Series Flash Elemental Analyser.

A2 Collection And Treatment of X-Ray Crystallographic Data

The general experimental and computational procedures which were adopted in the X-ray crystal structure determinations of the compounds described in this thesis are detailed here.

Crystallographic Information Files (CIFs) for each structure may be found in the attached CD-ROM. Where possible, data collection was undertaken using an Enraf-Nonius turbo CAD4 diffractometer by either Dr Michael Gardiner or Mr Adam James and the resulting structures solved by the author. When small crystal size or poor diffraction intensity prevented this treatment, data collection was performed on a Bruker X8 Apex CCD diffractometer and refinement performed by either Dr Matthias Hilder or Dr Craig Forsyth, Monash University. Conditions for the Enraf-Nonius turbo CAD4 diffractometer are outlined below.

Due to the instability of the compounds on exposure to the atmosphere, the crystals were mounted in oil on glass fibers and cooled to 173 °K. Where possible a morphological axis was aligned close to the fiber axis.

Cell determinations and data acquisitions were carried out using an Enraf-Nonius turbo CAD4 diffractometer with a graphite single crystal monochromated molybdenum radiation source, with λ assumed to be 0.71073 Å (K_α). Unit cell calibrations were carried out by using 25 reflections well separated in reciprocal space.

Three, approximately orthogonal, standard reflections were measured every one hour of exposure time, which were then used to scale the data and correct for any variation in crystal position, instrumental fluctuation or deterioration of the crystal. The same three standard reflections were measured every four hundred reflections as a check for reorientation.

The reflection intensities were then corrected for Lorentz and polarisation effects. Extinction effects were not significant and were not applied. Neutral atom scattering factors[1] were corrected for anomalous dispersion ($\Delta f'$ and $\Delta f''$)[2], mass absorption coefficients were taken from the same reference.

Solution of the crystal structures was by direct method routines, which located the position of most of the non-hydrogen atoms in the structures which were then used to phase subsequent Fourier maps. After initial phasing, successive use of three-dimensional Fourier maps was used to locate all of the remaining light, non-hydrogen atoms in the structure refinement. Full matrix refinement of the structures was carried out. Most non-hydrogen atoms were refined with anisotropic temperature factors of the form,

$$\exp\left(-2\pi^2\left[h^2(a^*)^2U_{11} + k^2(b^*)^2U_{22} + l^2(c^*)^2U_{33} + 2hka^*b^*U_{12} + 2hla^*c^*U_{13} + 2klb^*c^*U_{23}\right]\right)$$

Refinements were against F^2, $\Sigma w\left|\,|F_o| - |F_c|\,\right|^2$, which was minimised using full least-squares using the weighting scheme given below. Reflections with $F < 4\sigma(F)$ were not used in the calculations. Damping factors were sometimes required for convergence in the least squares refinement. All parameter shifts were less than 0.001 σ at convergence. Residuals quoted are,

$$R_1 = \Sigma\left|\,|F_o| - |F_c|\,\right| / \Sigma|F_o|$$

$$wR_2 = [\Sigma w\left|\,|F_o|^2 - |F_c|^2\,\right|^2 / \Sigma w|F_o^2|^2]^{1/2}$$

$$w = 1 / [\sigma^2(F_o)^2 + (aP)^2 + bP], \text{ where } P = [F_c^2 + \text{Max}(F_o^2,0)]/3$$

$$s = [\Sigma\left|\,|F_o|^2 - |F_c|^2\,\right| / (n-p)]^{1/2}$$

Computation for data collection, semi-empirical absorption correction, cell refinement, data reduction, structure solution and refinement was carried out using CAD4 Express,[3] WinGX,[4] XCAD4,[5] PsiScans,[6] Shelxs97,[7] and Shelxl97[7] program systems implemented on a PC running Windows 2000.

Tables of atomic coordinates, temperature factors, interatomic distances, bond angles, and structure factor amplitudes are available on request from Dr. Michael G. Gardiner, University of Tasmania.

X-Seed[8] and ORTEP3 for Windows[9] computer packages were used for the molecular structure and unit cell diagrams shown in this thesis.

References for A2

1. *International Tables for Crystallography*, Hahn, Ed., Kluwer Academic Publishers, Dordrecht, The Netherlands, **1995**.
2. Cromer, D. T.; Liberman, D. *J. Chem. Phys.* **1970**, *53*, 1891.
3. *CAD4 Express Software*, 1994, Enraf-Nonius, Delft, The Netherlands.
4. Farrugia, L.J. *J. Appl. Crystallogr.* **1999**, *32*, 837.
5. K. Harms and S. Wocadlo, *XCAD4, CAD4 Data Reduction*, University of Marburg, **1995**.
6. North, A. C. T.; Phillips, D.C.; Mathews, F.S. *Acta. Crystallogr. Sect A*, **1968**, *24*, 351.
7. G.M. Sheldrick, *Shelx97, Programs for Crystal Structure Analysis,* University of Göttingen, **1997**.
8. Barbour, F.S. *X-Seed - A software tool for supramolecular crystallography*", *J. Supramol. Chem.*, **2001**, *1*, 189.
9. Farrugia, L. J. *J. Appl. Crystallogr.* **1997**, *30*, 565.

A3 Theoretical Considerations

Unless otherwise stated, all calculations were performed using the Gaussian 03 Revision E.01 software package[1] employing the UB3LYP functional.[2] Tables of XYZ coordinates for each structure may be found on the attached CD-ROM.

Initially, single point calculations using the 6-31G(d) basis set[3] for non-lanthanide elements and either the CEP-4g[4] or MWB28[5] basis sets with the corresponding Effective Core Potential for the lanthanide elements were undertaken on the original input geometries in order to generate stable wavefunctions. Geometry optimisations were then performed at the appropriate theoretical level, and frequency analyses were applied to the optimised structures to ensure true geometric minima were obtained. Single point calculations were then undertaken on the optimised structure and population analyses performed with either the NBO[6] or MPA[7] methods. Molecular orbitals from these calculations were visualized with Gaussview.[8]

References for A3

1. Gaussian 03, Revision E.01, Frisch, M. J.; Trucks, G. W.; Schlegel, H. B.; Scuseria, G. E.; Robb, M. A.; Cheeseman, J. R.; Montgomery, Jr., J. A.; Vreven, T.; Kudin, K. N.; Burant, J. C.; Millam, J. M.; Iyengar, S. S.; Tomasi, J.; Barone, V.; Mennucci, B.; Cossi, M.; Scalmani, G.; Rega, N.; Petersson, G. A.; Nakatsuji, H.; Hada, M.; Ehara, M.; Toyota, K.; Fukuda, R.; Hasegawa, J.; Ishida, M.; Nakajima, T.; Honda, Y.; Kitao, O.; Nakai, H.; Klene, M.; Li, X.; Knox, J. E.; Hratchian, H. P.; Cross, J. B.; Bakken, V.; Adamo, C.; Jaramillo, J.; Gomperts, R.; Stratmann, R. E.; Yazyev, O.; Austin, A. J.; Cammi, R.; Pomelli, C.; Ochterski, J. W.; Ayala, P. Y.; Morokuma, K.; Voth, G. A.; Salvador, P.; Dannenberg, J. J.; Zakrzewski, V. G.; Dapprich, S.; Daniels, A. D.; Strain, M. C.; Farkas, O.; Malick, D. K.; Rabuck, A. D.; Raghavachari, K.; Foresman, J. B.; Ortiz, J. V.; Cui, Q.; Baboul, A. G.; Clifford, S.; Cioslowski, J.; Stefanov, B. B.; Liu, G.; Liashenko, A.; Piskorz, P.; Komaromi, I.; Martin, R. L.; Fox, D. J.; Keith, T.; Al-Laham, M. A.; Peng, C. Y.; Nanayakkara, A.; Challacombe, M.;

Gill, P. M. W.; Johnson, B.; Chen, W.; Wong, M. W.; Gonzalez, C.; and Pople, J. A.; Gaussian, Inc., Wallingford CT, **2004**.

2. a) Becke, A.D. *J. Chem. Phys.* **1988**, *38*, 3098,
   b) Lee, C.; Yang, W.; Parr, R.G. *Phys. Rev. B.* **1988**, *37*, 785.
3. Rassolov, V.A.; Ratner, M.A.; Pople, J.A.; Redfren, P.C.; Curtiss, L.A. *J. Comp. Chem.* **2001**, *22*, 976.
4. a) Stevens, W.; Basch, H.; Krauss, J. *J. Chem. Phys.* **1984**, *81*, 6026,
   b) Stevens, W.J.; Krauss, M.; Basch, H.; Jasien, P.G. *Can. J. Chem.* **1992**, *70*, 612,
   c) Cundari, T.R.; Stevens, W.J. *J. Chem. Phys.* **1993**, *98*, 5555.
5. a) Dolg, M.; Stoll, H.; Savin, A.; Preuss, H. *Theor. Chim. Acta* **1989**, *75*, 173,
   b) Dolg, M.; Fulde, P.; Kuechle, W.; Neumann, C.-S.; Stoll, H. *J.Chem. Phys.* **1991**, *94*, 3011,
   c) Dolg, M.; Stoll, H.; Preuss, H. *Theor. Chim. Acta* **1993**, *85*, 441.
6. a) Carpenter J.E.; Weinhold, F. *J. Mol. Struct. (Theochem)* **1988**, *169*, 41,
   b) Foster, J.P.; Weinhold, F. *J. Am. Chem. Soc.* **1980**, *102*, 7211,
   c) Reed, A.E.; Weinhold, F. *J. Chem. Phys.* **1983**, *78*, 4066,
   d) Reed, A.E.; Weinstock, R.B.; Weinhold, F. *J. Chem. Phys.* **1985**, *83*, 735.
7. Mulliken, R. S. *J. Chem. Phys.* **1955,** *23*, 1841.
8. GaussView, Version 3.09, Dennington II, R.; Keith, T.; Millam, J.; Eppinnett, K.; Hovell, W. L.; Gilliland, R. Semichem, Inc., Shawnee Mission, KS, **2003**.